2014-01-01

Natural Selectivity of Nickel and Vanadium in Crude Oil

Olienka P. De La O Fernandez
University of Texas at El Paso, olienkadf@gmail.com

NATURAL SELECTIVITY OF NICKEL AND VANADIUM IN CRUDE OIL

OLIENKA PATRICIA DE LA O FERNANDEZ

Materials Science and Engineering

APPROVED:

Russell R. Chianelli, Ph.D., Chair

Lawrence E. Murr, Ph.D.

Tunna Baruah, Ph.D.

Jorge A. Lopez, Ph.D.

Keith Pannell, Ph.D.

Bess Sirmon-Taylor, Ph.D.
Interim Dean of the Graduate School

Dedication

I dedicate this work to my family, boyfriend and all my friends for all of their support throughout this intense journey, my Ph.D. Specially to my mother, sister and grandmother for their overwhelming, unconditional and immense love and support; your words of encouragement, and your life inspiration have been my support and force every day and when I needed them the most. I love you very much. Also I dedicate it to my boyfriend for all his support, knowledge and comprehension throughout the last few years. Finally to every one of my friends that have been my second family during all this time outside of my home, thank you very much for your friendship and support.

Without all of you this would have never been possible

Thank you very much

NATURAL SELECTIVITY OF NICKEL AND VANADIUM IN CRUDE OIL

by

OLIENKA PATRICIA DE LA O FERNANDEZ, M.S.

DISSERTATION

Presented to the Faculty of the Graduate School of

The University of Texas at El Paso

in Partial Fulfillment

of the Requirements

for the Degree of

DOCTOR OF PHILOSOPHY

Materials Science and Engineering

THE UNIVERSITY OF TEXAS AT EL PASO

May 2014

Acknowledgements

I am very grateful to Dr. Chianelli for the opportunity of having been part of his group.

I would like to acknowledge all of the people that helped me in this project either by aiding with analysis, providing chemicals or just provided friendly advice; Dr. Pannell, Dr. Baruah, Dr. Noveron and their group, Dr. Brenda Torres, Dr. Maryam Zarei, M.S. Hugo Alarcon, Dr. Renzo Arias, Dr. Brenda Porta, Emmanuel Zubia, Dr. Echegoyen and his group. I would like to thank all the people in Dr. Chianelli's group.

I would like to acknowledge especially to Dr. Jorge A. Lopez who brought me to UTEP, and has been a very good guide and friend not only during my Masters in Physics as my Advisor, but until now.

Without the financial support and help of the Program Director of Materials Science and Engineering Dr. Lawrence E. Murr, Consejo Nacional de Ciencia y Tecnologia (CONACYT) and El Paso Community College – Physics Department this project would not have come to realization, so thank you very much. I would also like to acknowledge the Chemistry and Materials Science and Engineering departments and its entire faculty for their advice and help. All research in this thesis was conducted in Dr. Chianelli, Dr. Pannell and Dr. Noveron's laboratory as well in the facilities and labs of Chemistry and Materials Science and Engineering Departments at the University of Texas at El Paso.

Abstract

Nickel and Vanadium have always been found in crude oil all around the world. The metal content is found mainly in porphyrin structures in the asphaltene fraction of the petroleum. In order to determine the reason for this natural preference, a set of experiments testing thermodynamics, kinetics, and other factors were performed. Candidate metalloporphyrins containing Vanadyl, Chromium, Iron, Nickel, Copper and Zinc were analyzed through chemical reactions characterized using Silica Column Chromatography, HPLC, MS and UV-Visible. Theoretical analysis of the stability of metalloporphyrins was conducted using DFT/NRLMOL for computational calculation. The analysis of all factors leads us to conclude that the presence of Nickel and Vanadium in petroleum depend on different factors, not only on the stability of the structures, but mainly on abundance in the medium rising from biological processes.

Table of Contents

List of Tables

List of Figures

List of Graphs

Chapter 1: Introduction

1.1 Porphyrin molecule

Porphyrins are biochemically important, medically useful, and synthetically interesting compounds. Porphyrins that occur naturally play a major role in the life sustaining biochemical reactions. They are a ubiquitous class of compounds with many important biological representatives including hemes, chlorophylls, myoglobins, cytochromes, catalases, peroxidases, and several others. Used by nature in the most important processes of photosynthesis and solving transport and other problems in living systems, these compounds have been described as "pigments of life" (1). Their aromatic character, inner chelating pocket and varying peripheral carbon chains have allowed scientists to discover new and unique chemical reactions. Porphyrins and their metal complexes have also stirred interdisciplinary interest due to a multitude of their intriguing physical, chemical and biological properties (2).

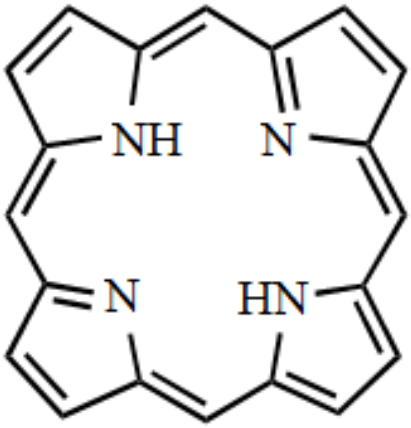

Figure 1.1: Porphyrin macrocycle

The porphyrin macrocycle (Figure **1.1**), consists of four pyrrole rings joined by four interpyrrolic methine bridges to give a highly conjugated macrocycle. The aromaticity of porphyrins has been well established both by its chemical and physical properties (3). These tetrapyrrolic systems have a closed loop of edgewise overlapping p orbitals which interact favorably to stabilize the olefins; the 22 π electrons available in porphyrins make up six different 18e-delocalization pathways (53)(56), (Figure 1.2**)** which follow Huckel's 4n + 2 rule for aromaticity

X-ray crystallography supports this model and shows that the porphyrin ring consists of four pyrrole rings joined by methine bridges. The molecule is considered to be planar but flexible, but meso-substituted porphyrins display less planarity (4). Heat of combustion gives evidence of resonance energy, as such the molecule is susceptible to electrophilic aromatic substitution reaction in the periphery. These substitution reactions can occur both on the porphyrin and metalloporphyrin derivatives; typical examples are halogenations, sulfonation, nitration, and acylation (5).

Porphyrins and their derivatives are highly colored absorbing strongly in the visible region near 400 nm, which is consistent with conjugation and it also displays weaker absorption bands between 450-700 nm. In the spectra of porphyrins the most intense band is called the *Soret* band, named after the biochemist who first observed it in hemoglobin (6). Chemical modification of the porphyrin system usually results in the change in the spectra of the ring. A disrupted porphyrin leads to the disappearance of the *Soret* band (7). Porphyrin molecules are different changing changes in absorption and emission properties giving heme centers a red color, while chlorines are green to blue in color. The absorbance of porphyrin varies depending on chelation, pH, and substitution of the parent ring.

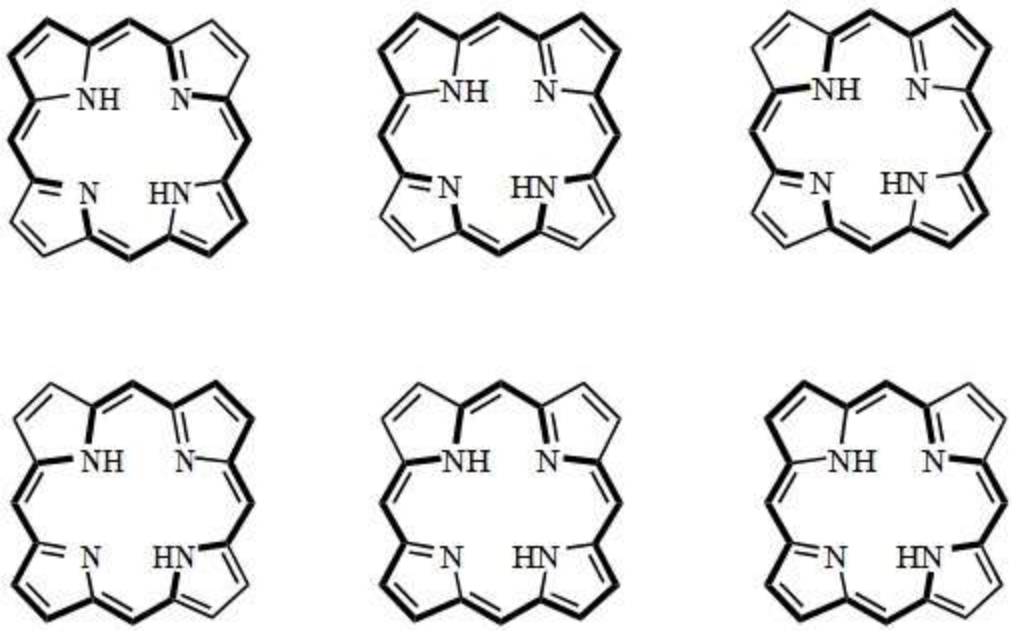

Figure 1.2: 18 pi-electron pathways which make up the aromatic character of the porphyrin ring system

The porphyrin molecules and its derivatives are amphoteric and so they can behave as both as acids and bases. The nitrogen core of the molecule can acts as bases due to the lone pair of electrons on the nitrogen, while rising from resonance imine can increase acidity of the nitrogens bounded to hydrogen.

1.1.1 Porphyrin Syntheses

The porphyrin synthesis began while trying to synthesize large classes of pyrroles. Early work was conducted by Fischer in Germany, and led to the synthesis of a wide array of porphyrins molecules (8). Due to this reason Fisher is consider to be the grandfather of porphyrin chemistry whose work inspired many scientists that built upon his synthesis. In general, you can synthesize porphyrin following different routes. One of the methods used deals with the transformation of porphyrin from natural sources like chlorophyll a, bacteriaphyll, and hemin, which are modified to give the desired porphyrin. Another method is total synthesis starting with individual pyrrole rings.

1.1.2 Porphyrins from Tetramerization

Porphyrins as already mentioned can be prepared linking individual pyrrole rings through methine bridges (9). This method can yield two types of porphyrins the first one is called ß substituted and the second meso substituted porphyrins. The meso substituted porphyrins are acquired by 2,5-unsubstituted condensation of pyrrole rings in the presence of a providing reagent like benzaldehyde and with the help of an acid (10).

1.2 Crude oil

Petroleum (crude oil) has Greek roots meaning “oil from rock,” this is a viscous liquid that is generated in natural formation on earth, which is refined into several types of fuels. Fossil fuels are so important for the development of the society; they are extracted from underground deposits of decaying organic matter. Crude oil is extracted from shale rocks that are formed by the deposition of organic matter and minerals (85). The maturation process of crude starts with the death of organisms and their accumulation in subsequent layers of sand that over time compress over millions of years. As these organisms die they mix with mud, sand, and clay those results in the formation of different types of organic rocks. Through the passage of time this sediments travel deep into the earth and the temperature and pressure in which they are subjected causes their chemical modification. This combination of increased

temperature and pressure changes organic matter in rocks into crude oil, gas, and finally into graphite(85).

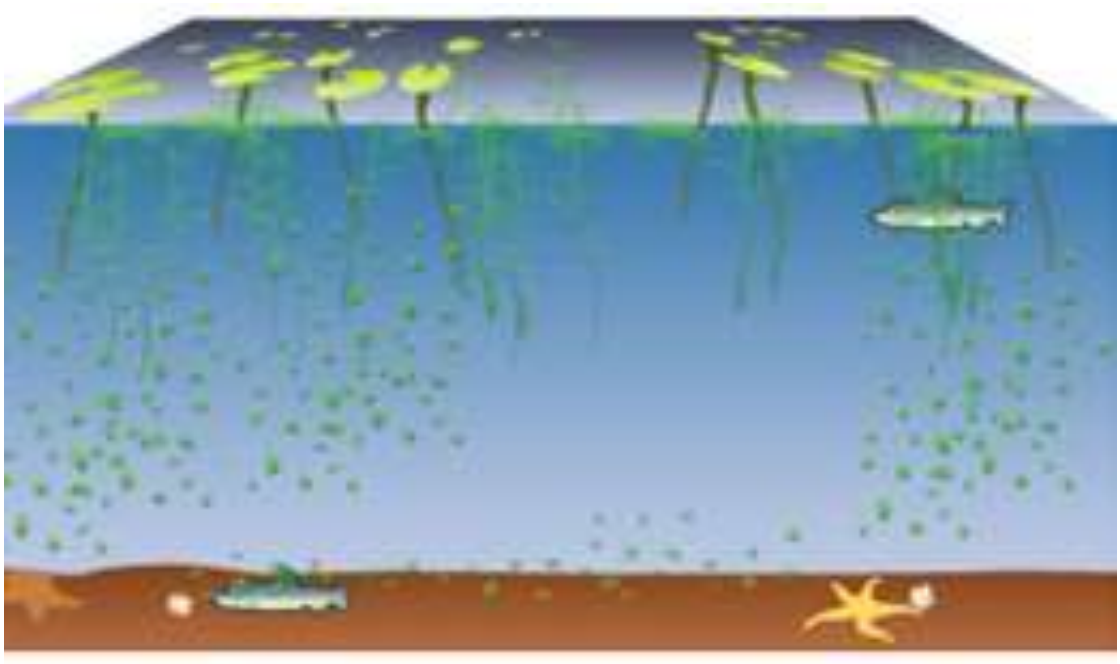

Figure 1.3: Organic matter sedimentation

Through the action of microbial digestion and chemical cracking crude maturation yields crude oil, asphaltenes, methane, along with other hydrocarbons. Carbon-hydrogen bonds disassociate at higher temperatures causing formation of branched alkanes and aromatic molecules. The dark viscous liquid that is used as the primary source of energy around the world is composed of medium size hydrocarbons chains.(86)

Crude composition varies depending on the stage of maturation in which this is extracted from the reservoir. Through microbial action the essential biopolymers loose heteroatoms like phosphorous, sulfur, and nitrogen to yield a new kind of polymer called humic acids. Through the process crude migration due to sedimentation the high temperatures removes oxygen from humics to yields hydrocarbons. Increased temperature and pressure causes carbon-hydrogen rupture and radical formation yielding branches alkanes and aromatic molecules.(87)

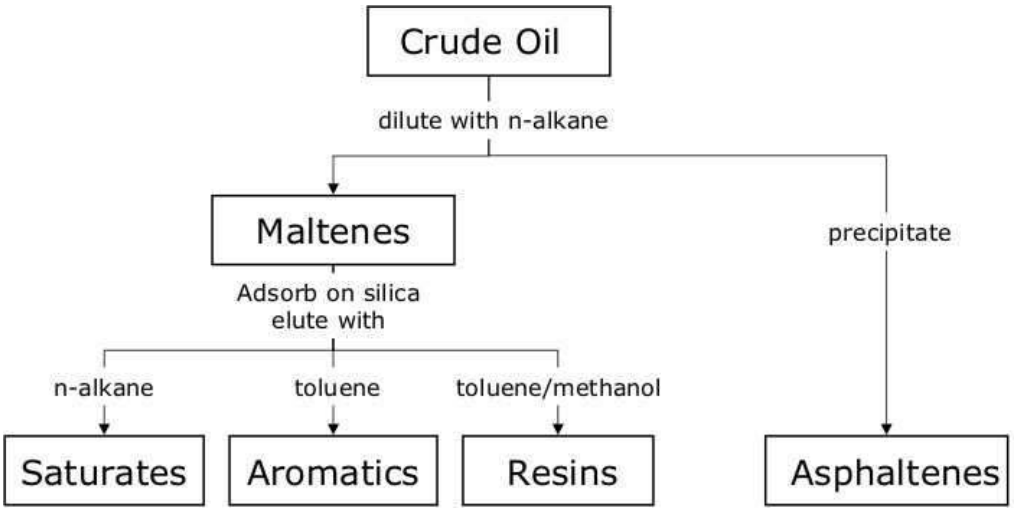

Figure 1.4: Crude oil components and their methods of separation in the laboratory

Crude oil is typically composed of hydrocarbon at a H/C ratio of 1.5 with a greater aliphatic carbon. Large molecular weight chains in called paraffins and rings called naphtalenes, as well as aromatic hydrocarbons are present in the crude. The abundance of each of the components depends on the type of crude. An average was given for more than 500 crude samples where 58% of the crude was made up of saturated hydrocarbons, 29% of aromatic hydrocarbons, and 14% of polar compounds (30, 42). Sulfur content when crude is extracted is usually 0.1-5%. Crude organic molecules are biodegradable for the most part for the exception of hopane molecules (Prince & Atlas, 2005).

1.2.1 Crude oil formation and metalloporphyrin relationship

Organic matter from decaying organisms is processed thorugh the action of biological and chemical processes. Through the action of microbial oxidation heteroatoms are mineralized with the exception of oxygen. Migration of the crude to deeper level expose the organic matter to higher temperatures that cause cracking of hydrocarbons generating branched alkanes and at higher temperature and pressures hydrogen is lost generating aromatic moelucles. As in the figure below.

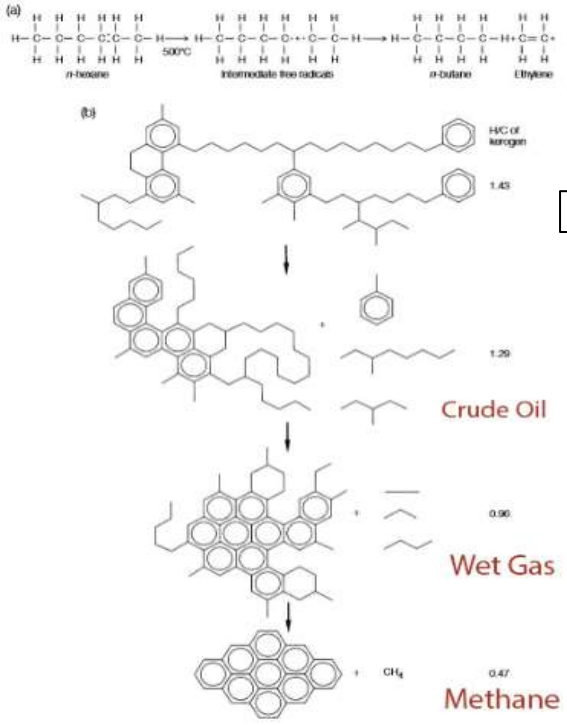

BOND	kcal/mol	kJ/mol
C – H	96 - 99	401 - 414
C – C	83 - 85	347 - 356
C – N	69 - 75	289 - 314
C – O	85 - 91	356 - 381
C – S	66	276
C = C	146 - 151	460 - 464
N – H	93	389
S – H	82	343

Figure 1.5: Cracking process of hydrocarbons in crude oils and energy bonds

The Kerogen only has single bonds between carbon atoms and the energy needed to break this bond is around 83-85 kcal/mol, however the energy needed to break a double bond between carbons is bigger 146-151 kcal/mol.

Then what is happening during the thermal process all these bonds will be very susceptible to break so all this bonds will be aromatized because they going to be losing or they will be separated from the free radicals, then here we will have more aromatization

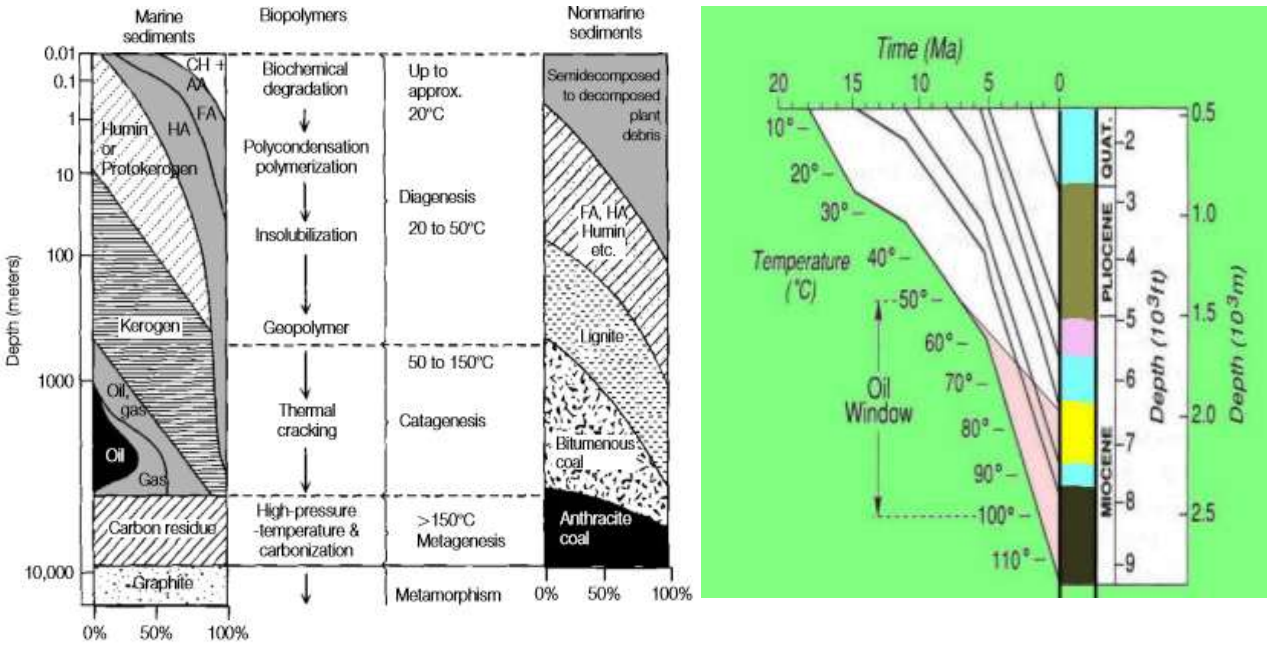

(A) (B) (C)

CH, Chlorophyll AA, Amino Acids FA, Fulvic Acids HA, Humic Acids

Figure 1.6: Oil maturation process[12]

One can see that organic sediments from marine origin forms kerogen that develops into oil and gas, while sediments of non-marine origin does not generate oil instead forms lignite and coal. There are two types of kerogen one of marine origin with high proportion of vanadyl porphyrins and a terrestrial kerogen with no vanadyl porphyrins (31).

One can see from the figure above that the diagenesis temperature window ranges from 20-50 ^{o}C while catagenesis exposes shale rocks up to 150 ^{o}C that transforms kerogen into oil (11). Finally, in the metagenesis stage at higher temperatures organic matter turn into graphite.

One can also appreciate the amount of time the millions of years that it takes for these processes to occur. In the case of metalloporphyrins they are subjected as seen in the oil window at temperatures as high as 100 ^{o}C and the chemical equilibrium that they are at is maintained for a long time.

Starting with marine sediments then going deep we have chlorophyll, amino acids, fulvic acids, humic acids, then humin or protokerogen, then kerogen, then at around 1Km it will start to cook the shale rock or kerogen into oil gas, carbon residue, graphite (12). Then here we will have the nonmarine sediments that basically they will decompose into coal where the presence of the biopolymers is crucial because the entire microorganism it will help to decompose or to transform from 1 state to another the organic matter to creates carbonates to mineralized metals.

1.3 Vanadyl and nickel in crude oil

1.3.1 Metal ions in environment and metalloporphyrins

Important factors for the chelation of porphyrins include availability of efficient metal carriers, abundance of elements, stability of M-N bond in the complex, stability of M-N bond in the environment, and the lability of meso positions (35). There is an dominance of vanadyl and nickel porphyrins in crude oil samples, while there are samples in the world that deviate from this like an anomalous abundance (4000 ppm) of the kerogen Cu^{2+}-porphyrins, but this arises from unusual circumstances (36). In the environment metalloporphyrins have been identified in nature as important enzyme cofactors (45-52).

1.3.1.1 Metal abundance in sea levels

One of the factors that could explain the abundance of NiTPP and VOTPP found in crude around the world is abundance of metal ions in the aquatic environments where petroleum matures. The table below enlists the most abundant ions measured in parts per million found in sea water.

Table 1.1: Sea water metal concentrations[82]

Element Symbol	Name	Sea water metal concentration in ppm
Si	Silicon	2
Zn	Zinc	0.005
As	Arsenic	0.002
Al	Aluminum	0.001
Zr	Zirconium	0.001
V	Vanadium	0.001
Ni	Nickel	0.00048
Cr	Chromium	0.00033
Sb	Antimony	0.0002
Cu	Copper	0.00012
Tl	Thallium	0.00012
Au	Gold	0.00011
Fe	Iron	0.00004
Ga	Gallium	0.000015
Y	Yttrium	0.000013
Mo	Molybdenum	0.00001
Mn	Manganese	0.00001
Bi	Bismuth	0.00001
Hf	Hafmium	0.000008
Ge	Germanium	0.000005
Ce	Cerium	0.000004
La	Lanthanum	0.000004
Nd	Neodymium	0.000004

In order to determine which metalloporphyrins can occur in nature Quirke considered the most abundant elements found in sea water and shale rocks for chelation with geoporphyrins (13). One of the important factors in the determination of stability of metalloporphyrins is the ionic radius of the coordinated metal. Therefore, in sea water the potential candidates for chelation of free based porphyrins would have to be abundant elements that have the smallest radii. Using the information provided in the table one can select silicon, zinc, arsenic, aluminum, nickel, chromium, copper, and iron as the potential metal candidates. Other abundant metals like zirconium, antimony, thalium, and gold can be ruled out due to the increased radii in comparison with the selected candidates.

1.3.1.2 Metal abundance in shale rock

Table 1.2: Shale metal concentrations[83]

Element Symbol	**Name**	**Shale metal concentration in ppm**
Si	Silicon	238000
Al	Aluminum	92000
Fe	Iron	47000
Ti	Titanium	4500
Mn	Manganese	850
Zr	Zirconium	180
V	Vanadium	130
Cr	Chromium	100
Ni	Nickel	80
Ce	Cerium	70
Cu	Copper	50
La	Lanthanum	40
Y	Yttrium	35
Nd	Neodymium	30
Ga	Gallium	25
Co	Cobalt	20

Nb	Niobium	15
As	Arsenic	10
Pr	Praseodymium	9
Sm	Samarium	7
Gd	Gadolium	6
Sn	Tin	6
Dy	Dysprosium	5
Hf	Hafmium	4
Er	Erbium	3.5
Yb	Ytterbium	3.5
Mo	Molybdenum	2
Ta	Tantalum	2
W	Tungsten	1.8
Ge	Germanium	1.5
Ho	Holmium	1.5
Eu	Europium	1.4

In order to account for any unforeseen factors the same analysis as the ion concentration in sea water will be conducted for the relative abundance of ions in shale rock. In shale rock the potential candidates for chelation of free based porphyrins would have to be abundant elements that have the smallest radii. Using the information provided in table two silicon, aluminum, iron, titanium, vanadium, chromium, nickel, and copper. Other abundant metals like zirconium, cerium, and lanthanum can be ruled out due to the increased radii in comparison with the selected candidates.

Relative abundance of elements in sea water and shale rocks, as well as their atomic radii was used to select potential candidates for geoporphyrin formation. Using the information on both tables one can see that silicon, zinc, arsenic, aluminum, nickel, chromium, copper, titanium, vanadium, and iron are the potential metal candidates for chelation with free base porphyrins.

1.4 Metalloporphyrin stability and selection of metal candidates

The metal ions in solution, could chelate with porphyrins, forcing more metal ion into solution until the porphyrins were completely chelated. In addition could be important to consider the nature of the metal prior to chelation and the stability of the metalloporphyrins after chelation. Even though assuming that the different skeletal types of porphyrins will behave similarly in the chelation process, although the absolute rates of chelation may differ for each skeletal type of porphyrins (13).

There are some factors which influence the chelation of the metals predominantly nickel and vanadium within the porphyrins, those are:

1. The abundance of the elements (metals)
- Sea water concentration
- Shale rocks concentration

2. The availability of efficient metal ion carrier

3. The stability of the structures
- The stability of the metal-nitrogen bond in the porphyrin complex
- The stability of the metal-nitrogen bond in porphyrins in the geological environment

1.4.1 Carrier stability

The availability of efficient metal ion carrier is of primary importance because if the metals are in very stable forms it will be very difficult to remove the metal from the carrier and then the insertion it in the TPP will be very hard. In other words very stable ion carriers are very inefficient reagents for the metallation of the porphyrins.

1.4.1.1 Ionic Radii

Porphyrin tend to form more stable complexes in general with smaller elements, because the sizes and energy differences between the orbitals of these smaller elements and the p-orbitals in the amino groups (N) in the center of the ring are less than with bigger elements.

Table 1.3: Ionic radii of some +2 oxidation ions

Bivalent Cations	Ionic Radii of Metal (angstroms)
V^{++}	0.88
$ScOH^{++}$	0.81
Mn^{++}	0.80
Fe^{++}	0.74
Zn^{++}	0.74
VOH^{++}	0.74
Co^{++}	0.72
Cu^{++}	0.72
Ni^{++}	0.69
VO^{++}	0.63

1.4.1.2 Oxidation state

Since stability relates to the N-M bond and the ionic radius of the coordinated atom, then higher oxidation state ions would form more stable complexes. One must keep in mind that really high oxidation state metals rarely occur. Although natural high oxidated metals are rare they do occur like in the case of Ti^{4+} but is tightly hydrated and is underactive (14). Therefore, high oxidation metals require high energy to become disassociated from their carriers. At the normal reduction potential of the environment oxidation states from 1-4 exist for most metals ranging depending on the metal. Still ions with a charge of +1 are bigger than higher oxidations states and therefore less stable. In nature you find metals in the oxidation state of +3 like iron, but +2 ions are more common. As such in order to try and determine the stability of each MTPP complex all +2 salts were chosen for experimentation.

1.4.2 Metal natural oxidation states and other factors for selection of study metals

The following section will present literature evidence regarding the most abundant elements found in sea water and shale stone and how they occur to determine parameters that helped narrow the candidates selected for this dissertation. Porphyrins have been coordinated with a wide array of metals in the laboratory like Cu, Zn, Ga, Fe, Co, among many others (58-78).

One can see in the tables 1.1 and 1.2 the dominant element in sea is Silicon. Nonetheless, natural porphyrin derivative of silicon are not found since most silicon is trapped as silica polymer (15). The same case happens with aluminum which is associated as a polymer and therefore is not available for chelation in nature (15).

In the case of arsenic there have been theoretical calculations determining the superior stability of arsenic (V) porphyrin complex. The problem is that this oxidation state does not occur naturally and the oxidation states available in nature form an unstable porphyrin complex (16).

As explained earlier high oxidation ions generate more stable complexes, although they are hard to come by in the environment. In the case of titanium you find a high oxidation state ion (Ti^{4+}) in nature, but is tightly hydrated and is underactive (14).

Hodson and Peake studies showed that copper (II) porphyrins undergo transmetallation with vanadyl and nickel ions in the presence of clays that are widespread all around (17). Still some samples have been found to contain copper porphyrins and the explanation for the dominant vanadyl and nickel porphyrins would be explained if clay was present in all reservoirs. The relative proportion of nickel (Ni^{2+}) and vanadyl (VO^{2+}) ions is in part controlled by the redox conditions in the environment where Ni^{2+} and VO^{2+} ions compete for chelation with the free porphyrin bases. A predominance of VO species may be indicative of anoxic conditions where sulphate reducing bacteria generate hydrogen sulphide, causing Ni^{2+} to precipitate as nickel sulphide (34).

Based on stability index Iron (III) is stable enough to be considered a candidate, unfortunately under the reducing environments in which crude is found is not expected to find it in this higher oxidation state. The greatest evidence of this is found in a paper by Bonnett, et al in which they found that Fe(III) is abundant in coal that it's been found is a much less strong reducing environment (18).

Chromium (III) is a very stable compound, but has a very stable carrier. As such only Cr (I) and (II) would be candidates. Chromium (III) is readily reduced to Chromium (II) in crude oil environment, Cr (II) is not as stable as Cr (III) (19).

1.5 Porphyrins in crude oil

Animal sources of porphyrin include plants and animals. Porphyrin molecules are associated with proteins responsible for metabolic processes. In the case of plants porphyrins are found in chlorophyll which is responsible for photosynthesis. Chlorophyll active site is a coordinated porphyrin ring with magnesium ion. In the case of animals porphyrins are found associated with the active heme site group of hemoglobin. The reason why blood is red is due to the presence of the porphyrin active site.

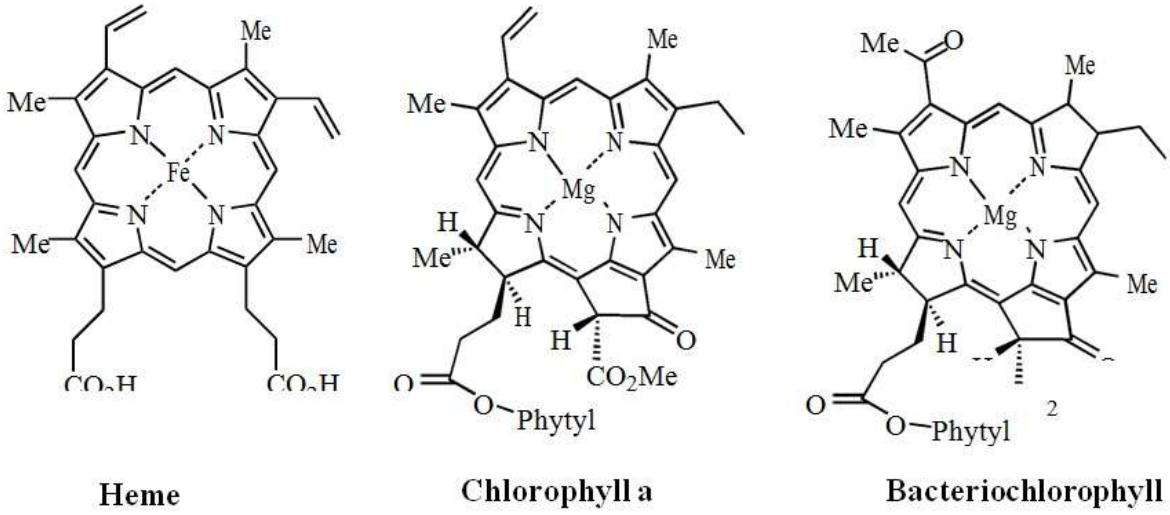

Figure 1.7: Some porphyrin derivatives found in nature

1.6 Crude oil maturation

There are three stages in the formation and maturation of petroleum called diagenesis, catagenesis, and metagenesis. The main differences between them are the chemical and biological changes happening in them due to pressure and temperature at which crude is subjected due to the progressive burial of reservoirs. Crude starts when where vast quantities of organic matter settle on the bottom of the sea or lakes, mixing with sediments starting a process called sedimentation (20).

These stages are:

- Diagenesis
- Catagenesis
- Metagenesis

Diagenesis starts with living organisms that are composed of organic polymers like carbohydrates, proteins, lipids, and nucleic acids. Once massive amounts of organic matter are deposited on the bottom of a water body organics undergo microbial degradation and form fulvic acids, humic acids or humin. Pavle described a high abundance of metals in soils associated with the humin in the diagenesis process (36). This means the degradation of the organic matter, and what these organisms will do is the removal of all the heteroatoms for the living organisms or the organic matter (20).

After they form or the organic matter decompose into these acids they will continue in the diagenesis and increasing the temperature so the organic matter will mix with sediments like clay, sand and other sediments then they will form what is called kerogen which is the last step of diagenesis.

Diagenesis starts when organic matter die and finish with Kerogen formation. And that is also what the geologist called lithification or sedimentation process. Catagenesis is the next step in the maturation process of the crude oil, we will have that the Kerogen form hydrocarbons with low or medium molecular weights and here is when we will have what is called the oil window

then here we will have crude oil, and some gas. But if we continue increasing temperature and pressure it will start the oil to crack so that means we will have methane and light hydrocarbons.

The last step is metagenesis we finish with the zone of gas formation then we will have carbon residue and or graphite

In the step where the hydrocarbons are formed in the crude oil, the shale rocks that are already formed in this step they will migrate to the reservoirs, then from her they will migrate up forming the petroleum deposits.

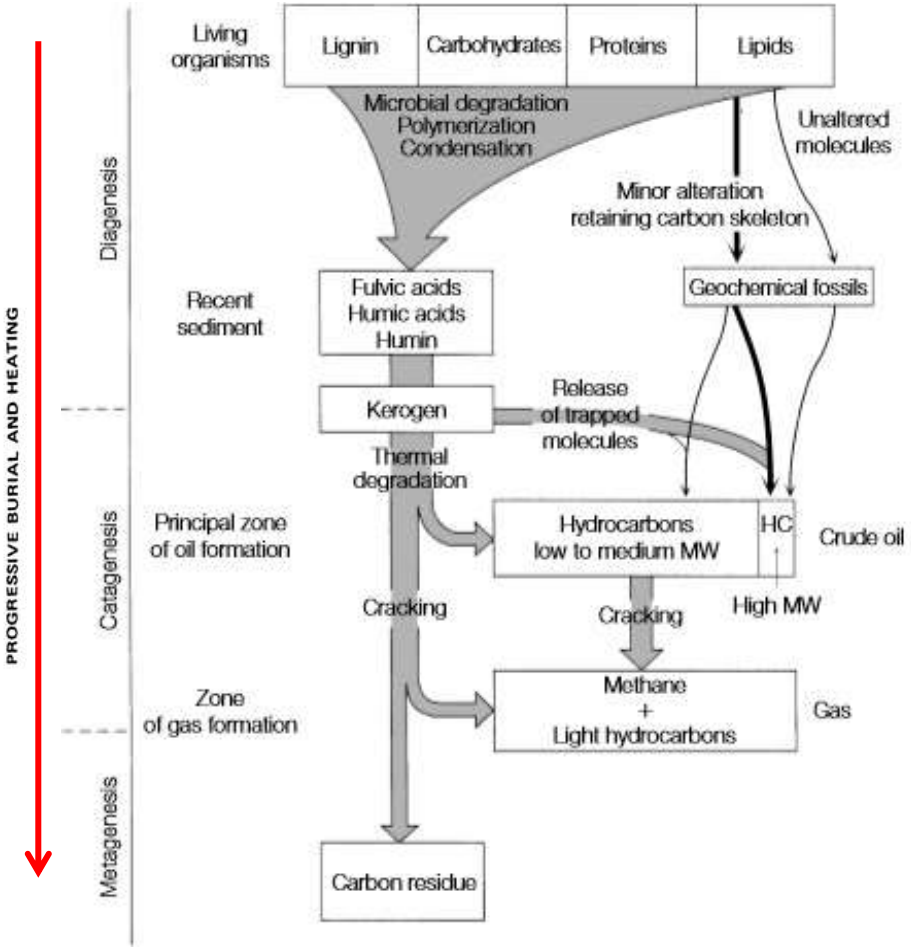

Figure 1.8: Petroleum formation[84]

1.6.1 Diagenesis

One of the early stages of crude maturation where temperatures have still not risen to cause break apart all aliphatic hydrocarbons into aromatics and methane is called diagenesis. The stages of diagenesis known as eodiagenesis, mesodiagenesis, and Telodiagenesis will be introduced in order to determine to try to understand the factors that influence metalloporphyrin selection in crude oil. It's important to notice that organic sedimentation in rock or lithification can be of three types depending on the grain size of the silica sedimented along with organics. When small particle clay get associated with organic matter they form shale rocks from which usually crude oil is extracted. On the other hand when the organics are sedimented with medium sized particles or sand the rocks are called sandstones, which are usually used as building and pavement materials. The other type of rock form by the sedimentation of organic material and the largest particles of silica or gravel are called conglomerates.

Figure 1.9: Sedimentary Rocks

Sedimentary rocks with organic material and mud (left), sand (middle), and gravel (right). Left: shale rock, middle; sandstone rock, and right; conglomerate rock

1.6.1.1 Porphyrin formation in diagenesis

Source of porphyrin ring in crude as previously discussed come from active sites of enzymes of animal and vegetable origin. In the case of crude oil formation the content of the organic material is marine and vegetable and so chlorophyll becomes the primary source of porphyrin. It is generally agreed that crude oil arose from aquatic algae with some terrestrial organic material while terrestrial plants gave rise to coal reserves. The average age of crude oil is about 100 million years (71% between 180-85 million years) (38). Nonetheless, the chelate molecules in chlorophyll are precursor of porphyrin that is not aromatic. Phorbide molecules are

very similar to porphyrins with the difference that one of the pyrrole rings in the porphyrin molecule lacks one double bond and so the phorbides are not aromatic (Figure 56). The chlorophyll molecule loses the phytyl side chain and loses the magnesium ion as it precipitates as carbonate through microbial action. Interestingly enough copper, nickel, and V_xO_y replaces magnesium and acts as hydrogen acceptors of the phorbide molecule generating the fourth pyrrole ring and turning phorbide into porphyrin (11, 32). The copper metalloporphyrin formed by the formation of porphyrins gets demetallated in the presence of clays to generate free base porphyrin ready for chelation (21). Palmer found <1ppm copper porphyrins in very immature sedimentary rocks (31). Nonetheless, metalloporphyrin formation in later stage of the kerogen maturation is not favored since Buchler determined that Cu-porphyrin is exceedegly labile under anoxic conditions (33).

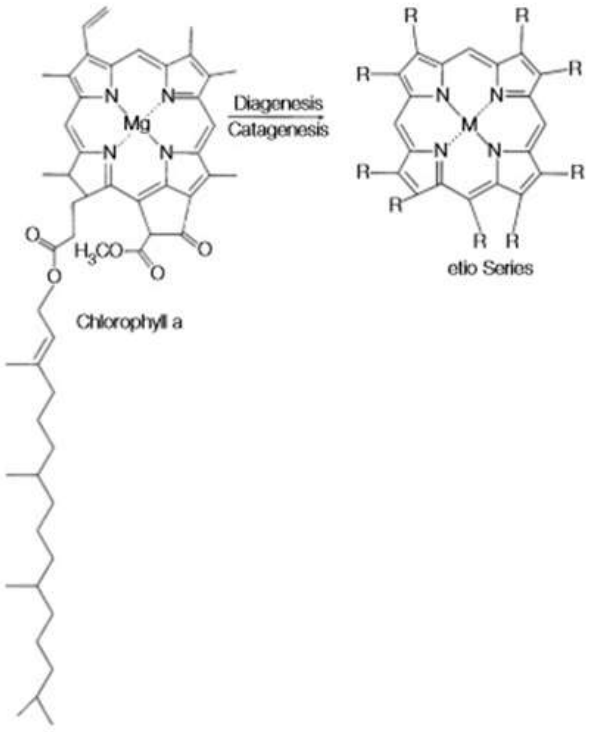

Figure 1.10: Reaction of chlorophyll a (phorbide) with copper ion for the formation of porphyrin ring

1.6.1.2 Eodiagenesis

The earliest stage of petroleum diagenesis is called eodiagenesis. This phase takes place at very shallow depths where dead organism deposit and begin to sediment in the bottom of a water body. This stage is important in the formation of sedimentary rocks as even in these early stages disturbances by organisms (bioturbation) of organic layer can cause crack in the sedimented rocks.

Through the action of bacteria heteroatoms are removed from carbohydrates, proteins, nucleic acids, and fatty acids. These heteroatoms are oxidized and transformed into highly oxidized species like nitrates, sulfates, phosphates, and carbonates. At this stage most heteroams except oxygen are removed from crude oil and introduced in the water column as ions. The leftover organic molecules are known as fulvic and humic acids, which are polymers with carboxylic acids, aldehyde, ketone, and alcohol groups. Fulvic acids are lower molecular weight and higher oxygen content than humic acids. Oxygen based functional groups in humic acids like alcohols and carboxylic acids have the ability to coordinate with available ions such as magnesium, calcium, copper as well as others in diagenesis (40, 41).

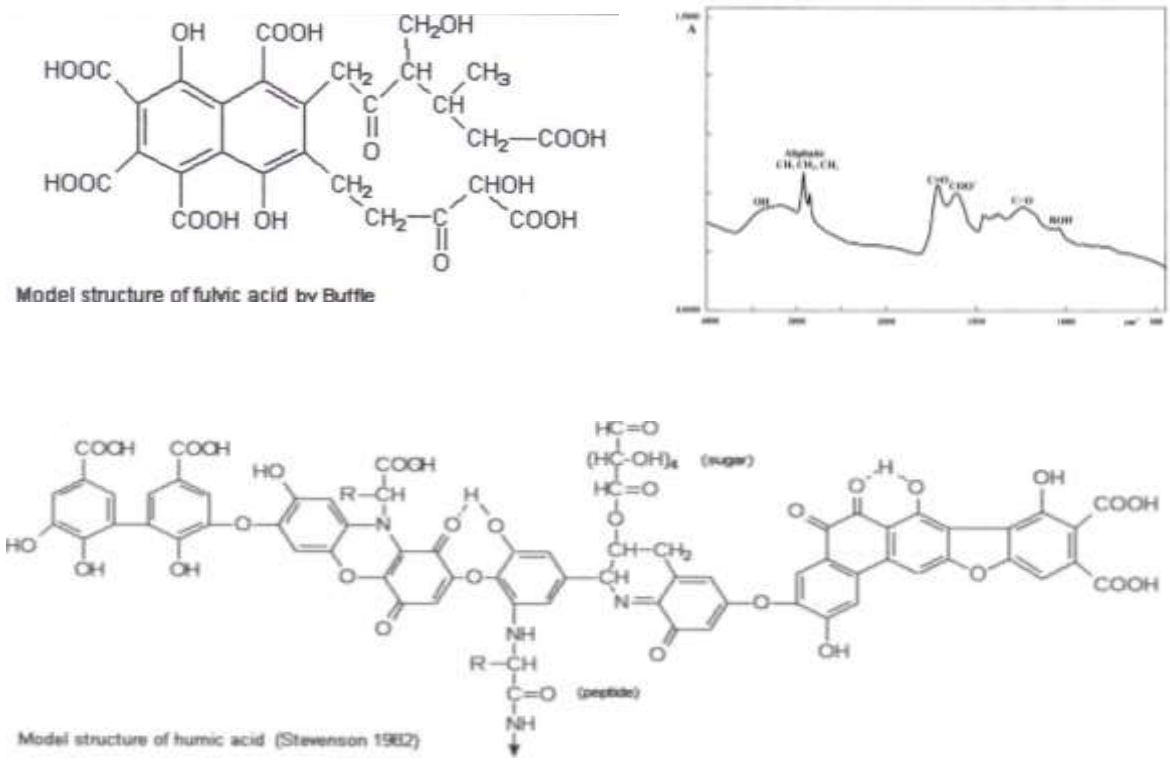

Figure 1.11: Proposed structure of fulvic acids (top left) and humic acids (bottom), as well as spectroscopic evidence that shows that these early polymers contain OH, CO, COO, and ROH groups.

1.6.1.3 Mesodiagenesis

In mesodiagenesis organic matter is isolated somewhat from the surface in a process known as cementation. Due to the oxidation of organic matter in carbonates by the action of cyanobacteria you form insoluble salts that precipitate on top of organic matter (chemical compaction). The subsequent sedimentation on top of organic matter and carbonate components increase pressure and reduce porosity of the organic layer (physical compaction). Over time this generates a dense physical barrier on the organic layer sediment protecting the organics from issues like bioturbation. Cementation is vital in the maturation of crude as its isolation allows for bacterial digestion and also limits oxygen in the water column.

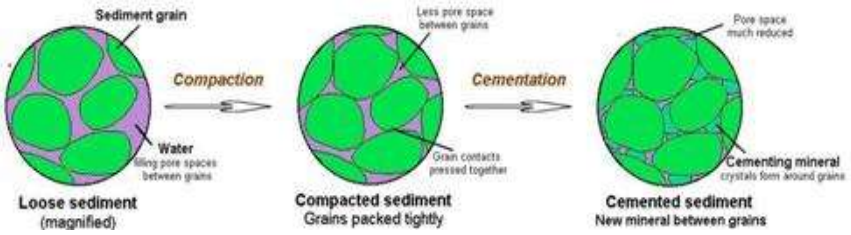

Figure 1.12: Physical and chemical effects in sediments

Shows a theoretical sediment grain and the effect of physical and chemical compaction on the reduction of the porosity of the sediment grain, also known as cementation.

Metal availability in different regions of the water column depend on the type of counterions available. Therefore, early in eodiagenesis metals become insoluble due to their mineralization with carbonates, while in later stages equilibrium is established where some ions fall back into solution as nitrate compounds. Therefore throughout the migration of shale rocks they experience authigenesis reactions in which some minerals present solubilize while other precipitate back changing the mineral composition of rocks.

Through the process of cracking sedimented matter is modified into high molecular weight component called kerogen and a lower molecular weight component called bitumen. Crude oil is extracted from leaching of kerogen and bitumen upon cooking of the shale rocks.

1.6.1.4 Telodiagenesis

Rocks that have gone through deep burial may be uplifted due to erosion or mountain building activities so rocks may move from reservoirs. Shale rocks present are rich in organic matter 0.5 % - 2% by weight. Most of the material encounter is from marine origin although you can have some land based organic material. There is an abundant input of porphyrin-precursor (chlorophylls) to the organic matter derived from algae and bacteria, in marine source rocks. These conditions favor both nickel and vanadium incorporation into porphyrins (22).

1.7 Microbiological influence on metal abundance

Fate of metalloporphyrin formation depends on chemical factors like thermodynamic stability of the complexes, as well as the natural availability of ions for coordination, and the type of ion carriers. Nonetheless, biological events seem to be just as important in determining metal availability for the formation of metalloporphyrins. In this section the most important microbes involved in crude metal availability will be described.

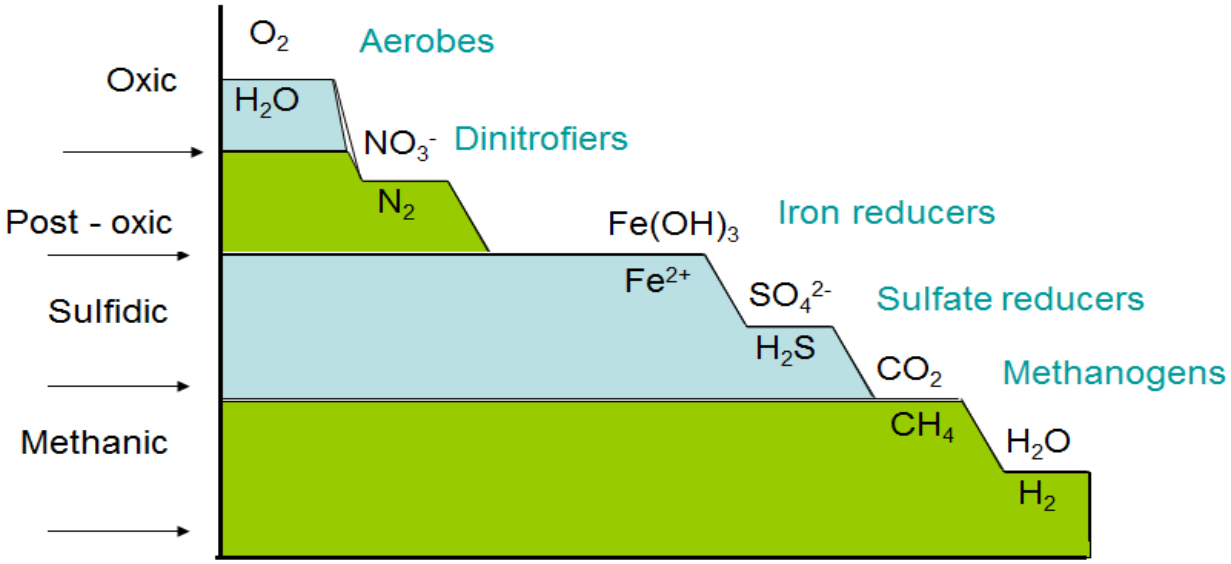

Figure 1.13: Important microorganism in the life cycle of crude oil at the different sediment layers in the formation process.

Petroleum's formation involves several microbiological processes aside from chemical reactions. From all of the microorganisms involved in this process there are microbial organisms that are key for this transformation as shown in the figure above. When organisms die and settle, at the beginning of crude maturation, these sediments are still exposed to oxygen (oxic boundary) where aerobe microbes are responsible organic matter oxidation causing water oxygen depletion and carbon mineralization.

While sedimentation and compaction increases over time the mixture of organics burrow deeper into oxygen depleted regions (anoxic environments) where bacteria use nitrate ions as electron acceptors in their metabolic processes.

Another microbial family that is important in crude formation and more than anything metal fate in the maturing crude is the sulfate reducing bacteria.

Finally, in the later stages of crude maturation methagenic bacteria aid in the formation of natural gas, although this are not essential for the purposes of this research. Therefore the reduction potential in the water column at a certain depth depends on the type of bacteria thriving and their metabolites.

1.7.1 Carbon fixation and mineralization

In the early stages of crude maturation when the organic mixture still has not sedimented into rocks and it's close to the surface microbes transform carbon into carbonate ions. The main groups of microorganisms that can induce the carbon mineralization as carbonate are photosynthetic microorganisms such as sulfate-reducing bacteria and cyanobacteria (23).

Cyanobacteria are also involved in the reduction of nitrogen in ammonia that also plays a role in salt formation under aerobic conditions. Photosynthetic Cyanobacteria takes water of Hydrogen Sulfide as electron donors and produces oxygen as a by-product, as such H_2S produced by purple reducing bacteria in the anoxic layer gets used by cyanobacteria in the oxic layer for carbon fixation (24).

These bacteria play an important role due to the availability of metals in solution available for chelation. Microbial induced carbonate formation causes the precipitation of lots of metal ions as carbonate salts into the sediment and provide for a mineral rich shale rocks. Furthermore, in this layer hydroxide, nitrate, and sulfate salts maintain a chemical equilibrium between ions in solution and in the precipitated in the sediment. Cyanobacteria nitrogen reduction also allows for the formation of soluble ammonium salts in the oxic/anoxic boundary.

Once cementation takes place and oxygen gets restricted to the crude you encounter microbial fermentation, where organic material is transformed into carbon dioxide and methane gas that work as metabolites for other bacteria (24).

This sort of transformation is achieved by anaerobic bacteria close to the oxic layer. Since methane is insoluble in water you can in these initial stage methane bubbles rise to the water surface like in swamps today.

$$\underset{\text{organic matter}}{2\,CH_2O} \xrightarrow{\text{bacteria}} CH_4 + CO_2$$

1.7.2 Nitrogen oxidation and importance in crude maturation

Through the action of bacterial action nitrogen also plays an important role in the maturation of crude oil. Nitrogen capture and reduction by the action of Cyanobacteria generates ammonia as a byproduct of metabolism, introducing nitrogen in the water column, used by other species of bacteria for the maturation process of the crude.

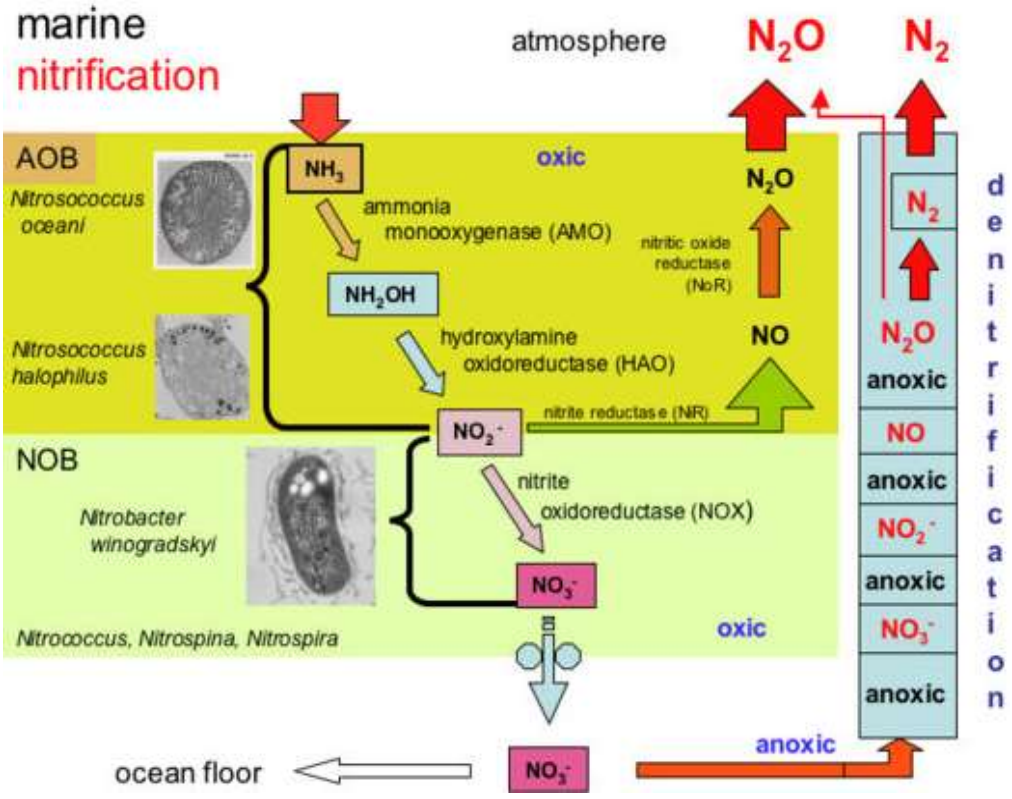

Figure 1.14: Bacteria important in the nitrogen cycle and their nitrogen use and metabolites[25].

In the figure above you can see the nitrogen life cycle and the metabolites associated with different nitrifier bacteria (25). Nitrogen reduction from Nitrococcus oceani uses ammonia in the water column to generate hydroxylamine. Nitroscoccus halophilus uses hydroxylamine to generate nitrite that in turn is used by Nitrobacter windodrasky to generate nitrate ions that are important as electron acceptors for other bacteria species.

It will reduce ammonia to nitrate, it is an aerobic bacteria and it doesn't live in anaerobic conditions however here in the anaerobic conditions there is another bacteria that is Nitrobacter winogradskyi which will help in the reduction of the nitrate, from nitrite to nitrate.

Upon oxygen depletion by the action of organic matter oxidation, nitrogen based molecules become electron acceptors in the metabolism of bacterial species close to the oxic/anoxic layer. Formation of nitrate ions where these bacteria resides increases metal availability due to the formation of soluble nitrate salts. Nonetheless, deeper into the water column sulfur bacteria mass produce sulfide insoluble salts.

1.7.3 Sulfur oxidation and mineralization

Sulfate-reducing bacteria are microorganisms that gather their energy by oxidizing organic compounds while reducing sulfate ions (SO_4^{2-}) in solution to hydrogen sulfide (H_2S)(1). In other words they use sulfate ions as electron acceptors in their electron transport chain metabolic processes (3), so in a sense they breathe sulfate in a form of anaerobic respiration. There are four types of bacteria that undergo anaerobic photosynthesis: purple bacteria, green sulphur bacteria, green sliding bacteria and gram positive bacteria (43, 44). Most sulfate reducing bacteria are anaerobes so they use sulfate ions from the oxic layer carried by the water column.

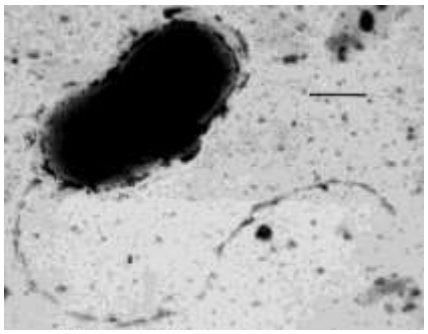

Figure 1.15: Desulfovibrio vulgaris

These bacteria breathe large amounts of sulfate to generate copious amounts of their hydrogen sulfide waste. Most bacteria are also able to reduce other sulfur compounds like

thiosulfate, sulfite, or even elemental sulfur to sulfide and hydrogen sulfide. In addition, there can reduce nitrate, nitrite, and iron Fe(III) (26).

In the stages of crude maturation sulfate reducing bacteria are introduces in the mesodiagenesis stage of diagenesis due to the time it takes for the migration of the crude to the anoxic layer. Much of the hydrogen sulfide generated by these bacteria reacts with soluble ions to produce insoluble sulfide salts. Therefore, availability of metal ions for chelation reaction with free base porphyrins gets dramatically decreased due to formation of sulfide minerals like Pyrite (ferrous sulfide) (27). Therefore initial abundance of metals in the environment becomes a primordial factor for natural metalloporphyrin abundance.

Sulfur cycle is completed by purple sulfur bacteria that take the waste of sulfate reducing bacteria and generate elemental sulfur. These anaerobic bacteria are found in places where hydrogen sulfide accumulates. In the figure below you can observe bacteria involved in the sulfur cycle where some thrive in hydrogen sulfide rich waters, while others do better at lower concentrations. Equilibrium is kept between highly oxidized sulfate ions in the oxic layer and hydrogen sulfide in the anoxic layer by cyanobacteria and sulfate reducing bacteria.

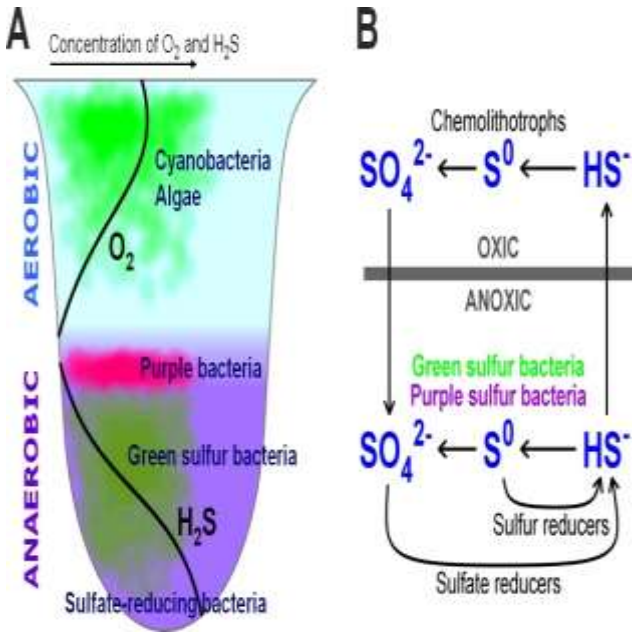

Figure 1.16: Relevant bacteria in the sulfur cycle and their metabolites

Molecules and ions available at the oxic boundary contain molecules with atoms at their highest oxidation states, while in the anoxic boundary these atoms are reduced. Due to the action of bacteria organic matter is oxidized, using oxygen as an electron acceptor, and progressively diminishing its abundance the farther from the surface. At the anoxic layer the reduction potential increases significantly as such counterions and molecules found at these depth usually contain atoms with lower oxidation states.

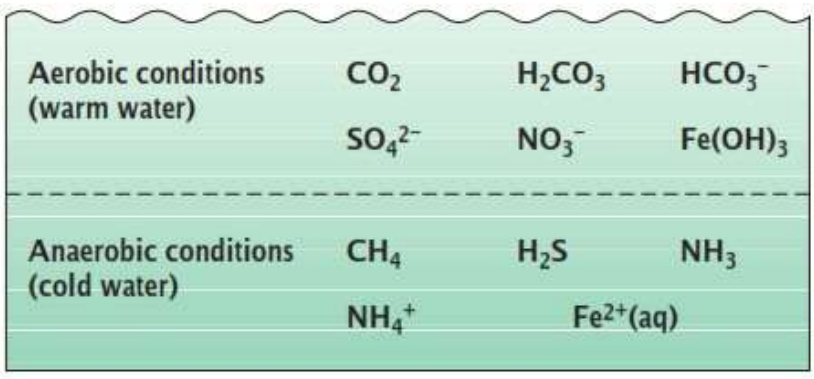

Figure 1.17: Molecules and ions in the oxic and anoxic layers important in the metal fate in crude oil[1]

Oxic Layer atomic oxidation states

- Carbon, with an oxidation number of +4, as CO_2, H_2CO_3 or HCO_3^-
- Sulfur, with an oxidation number of +6, as SO_4^{2-}
- Nitrogen, with an oxidation number of +5, as NO_3^-
- Iron, as Fe(III), in the form of insoluble $Fe(OH)_3$

Anoxic layer atomic reduction

- Carbon, with an oxidation number of -4, as CH_4
- Nitrogen, with an oxidation number -3, as NH_4 and NH_4^+
- Sulfur, with an oxidation number of -2, as H_2S
- Iron, as Fe(II), in the form of soluble Fe^{2+}

Metals may also experience oxidations in anaerobic environments due to the reducing conditions caused by oxygen depletion. Metals like Iron that are widely available in the oxic boundary in a +3 oxidation state very quickly reduce to +2 due to the ion's reduction potential.

The variation of all the chemical species previously mentioned are distributed to the crude through the water column. Therefore, there is equilibrium of the molecules found in the oxic and anoxic layers. As such counterions with higher oxidation states are at higher concentrations close to the surface, while lower oxidized counterions are found in greater quantities at the anoxic layer. This constantly changes the availability of carriers for metals in the water column based on the reducing or oxidizing potential of those waters. Since one of the determining factors in the formation of metalloporphyrins is the disassociation with carriers it's important to notice that Nickel and Vanadyl abundance on crude may have to do with the timing at which free base porphyrins become available for chelation.

Microbe oxygen depletion of the water at certain depths causes a change in reducing potential (pE) of that environment. Similar to in nature to pH, pE measures the available electrons in an environment and as such it can measure can reducing it can be. Reducing potential depend on the proton concentration in solution as well as the partial pressure of oxygen dissolved in the water. As such in the water column the deeper you go the less oxygen you will find due to microbial action.

$$\begin{aligned} \mathrm{pE} &= 20.75 + \log([\mathrm{H^+}]\, P_{\mathrm{O_2}}{}^{1/4}) \\ &= 20.75 - \mathrm{pH} + \tfrac{1}{4}\log(P_{\mathrm{O_2}}) \end{aligned}$$

Since different metals have different reduction windows each metal can tolerate a different reducing potential stress before actually being reduced. As such you can find in the oxic layer Iron (III) and Cu (II) ions while in the anoxic layer you find these species as Iron (II) and Cu(I).

1.8 Selection of metal candidates for experimentation

In order to determine if the natural abundance of nickel and vanadyl arises from the stability of their respective metalloporphyrin complexes, experiments were conducted comparing metals with the same oxidation state. In order to eliminate any kinetic factors the source of all metals for experimentations came from salts containing the same sulfate ion.

1.8.1 Iron (II) ion selection

Iron is very abundant in the environment and forms really stable complexes with porphyrin due to the ion's size. Iron forms more stable porphyrin complex in its +3 oxidation state, although the oxidation state in anoxic environment where chelation of free base porphyrin occurs is +2. Furthermore carriers of the ion at the time of chelation allow this ion to be a potential candidate for chelation. In the later stages of mesodiagenesis where rocks in the water column are subjected at a high concentration of hydrogen sulfide a fraction of free ions are trapped into pyrite (FeS_2) reducing availability of free ions for coordination.

Figure 1.18: Pyrite mineral compose of FeS_2 yielded from the reaction of +2 Iron ions and the bimolecular sulfide ion ($S\text{-}S^{2-}$).

1.8.2 Zinc (II) ion selection

Zinc is very abundant in both sea water and shale rock and in the environment is found in an oxidation state of +2 making it a potential candidate since the carriers associated with it can yield free ion in solution for coordination. In the later stages of mesodiagenesis where rocks in the water column are subjected at a high concentration of hydrogen sulfide a fraction of free ions are trapped into Sparelite (ZnS) minerals reducing availability of free ions for coordination.

Figure 1.19: Sphalerite mineral compose of ZnS yielded from the reaction of +2 iron ions and hydrogen sulfide in anoxic environments.

1.8.3 Copper (II) ion selection

Although there are literature evidences previously discussed as why copper is not a great candidate for metalloporphyrin formation, the vital importance of this ion and the need for comparison with the other candidate motivated the use of this metal in the study of this dissertation. Ionic radius and therefore M-N bond relates to the energy of the metalloporphyrin, in anoxic conditions copper reduces to +1 oxidation state and therefore metalloporphyrins formed with this ion would be unstable compare to other +2 candidates.

Copper has been shown to be essential in the transformation of phorbides into porphyrins and its demetallation in diagenesis causes most crudes in the world to be free of copper. Furthermore, copper (I) ion also precipitates in the presence of hydrogen sulfite in the mineral known as Chalcocite (Cu_2S) decreasing its abundance in the water column.

Figure 1.20: Mineral formed by the reaction of Cu (I) ion and H2S, also known as Chalcocyte (Cu_2S).

1.8.4 Nickel (II) ion selection

Nickel ion was selected not only due to its abundance in sea water and shale rocks, but also due to its oxidative stability under oxic and anoxic conditions. Since the oxidation state for this ion in both oxidative environments is +2 it remains capable of binding on the porphyrin pocket freely without distorting the porphyrin ring. Millerite is the mineral that is formed in the presence of hydrogen sulfide as NiS.

Figure 1.21: Millerite (NiS) mineral from the precipitation reaction between nickel (II) ion and H_2S

1.8.5 Vanadyl ion selection

Vanadium ions in oxic conditions get readily oxidized as Vanadate ion where vanadium holds a +5 oxidation state, while in anoxic environments vanadyl is found as vanadyl where vanadium holds a +4 oxidation state. In the analysis of crude sample around the world vanadium coordinates to porphyrins as vanadyl ions. Due to the increased oxidation state of the vanadium in this ion is expected to generate very stable metalloporphyrin complexes.

Vanadium sources are plentiful since this metal has a marine origin (28). Organism like annelids, phytoplankton, and Ascidian organisms contain high concentrations of vanadium. Since phytoplankton is so abundant in the sea this might be a determining factor in the formation of NiTPP and VOTPP complexes in crude oil.

Extensive research was conducted to try and find the sulfide mineral formed when the ion becomes exposed to hydrogen sulfide in diagenesis, but to no success. Nonetheless, a mineral called Patronite ($V(S_2)_2$) made from the reaction of $S\text{-}S^{2-}$ ion and vanadyl 4+ ion was found in the literature (29). Nonetheless, in anoxic conditions as previously stated vanadium if found as the oxidized vanadyl ion.

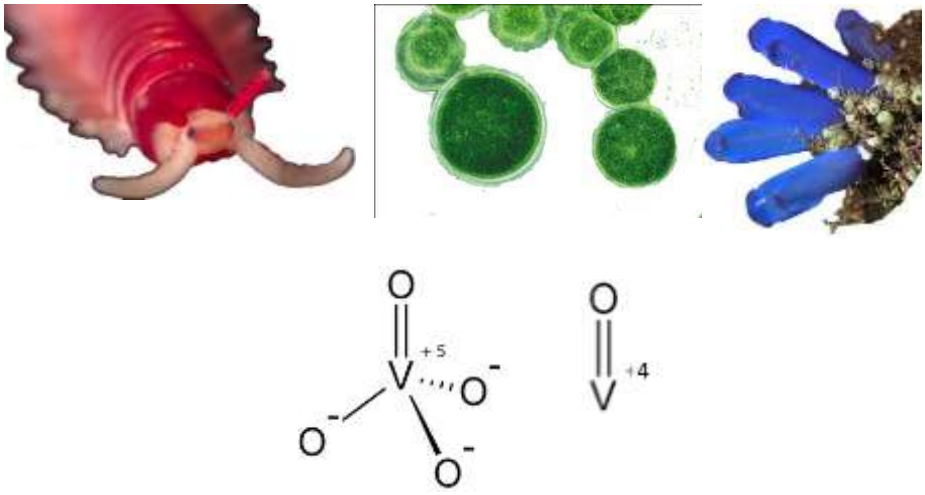

Figure 1.22: From right to left; vanadate ion, vanadyl ion, annelid organism, phytoplankton, and ascidian organism

1.8.6 Chromium (II) ion selection

Chromium ion was selected not only due to its abundance in sea water and shale rocks, but also due to the fact that the ion is present as +2 in anoxic conditions. Although chromium is also found as +3 in the environment this is tightly bound to carrier and quickly reduces to +2 in diagenesis.

1.9 Hypothesis

Although there are several factors to consider in the formation of metalloporphyrins in crude oil, I hypothesize that natural selection of vanadyl and nickel porphyrins is due to the combination of abundance, metal redox potential, and metalloporphyrin stability factors. Therefore in this work Cu^{2+}, Cr^{2+}, Ni^{2+}, Fe^{2+}, Zn^{2+} and Vanadyl ions are selected for the study of the metalloporphyrin complexes.

1.10 References Chapter 1

1. Battersby, A. R.; Fookes, C. J. R.; Matcham, G. W. J.; McDonald, E. Nature, 1980, 285, 17.
2. Falk, J. E. Porphyrins and Metalloporphyrins Elsevier: Amsterdam, 1964
3. Kuster, W. Z. Physiol. Chem. 1912, 82, 463
4. Smith, K. M. 1975; J. Am. Chem. Soc. 1967, 9
5. Boucher, L. J.; Katz, J. J. J. Am. Chem. Soc. 1967, 89, 4703
6. Soret, J. L. Compt. Rend. 1883, 97, 1267
7. Weiss, C., Jr. J. Mol. Spectrosc. 1972, 44, 37
8. Chaundry, I. A.; Clezy, P. S.; Mizra, A. H. Aust. J. Chem. 33, 1980, 1035
9. Smith, K. M. in "Porphyrins and Metalloporphyrins", Smith, K. M. Ed., Elsevier, Amsterdam (1975), p. 32
10. Adler, A. D.; Longo, F. R.; Finarelli, J. D.; Goldmacher, J.; Assour, J.; Korsakoff, L. J. Org. Chem. 32, 1967, 476
11. Hunt, J. M. (1996) Petroleum Geochemistry and Geology, 2nd Ed. W. H. Freeman and Co., New York, p. 208
12. After Tissot, B. P. and D. H. Welte (1978). Petroleum Formation and Ocurrence: A new Approach to Oil and Gas Exploration, 2nd Ed. Springer-Verlag, Heidelberg, Germany, p. 70
13. Quirke J. M. E.; J. Am. Chem. Soc.; 1987, 74-83
14. Van de Velde, G. M. H. Harkema, S.; Gellings, P. J.; Inorg. Nucl. Chem. Lett. 1973, 9, 1169 – 1173.
15. Buchler J. W. Smith, K. M.; Ed. Elsevier; Amsterdam, 1975, p. 157
16. Treibs, A. Ann. Chem. 1969, 728, 115-148
17. Hodgson, G.W.; Baker, B. L. and Peake, E.; Nagy, B.; Colombo, V.; Ed. Elsevier: Amsterdam, 1967; p. 170.
18. Bonnett, R.; Czechowski, F. Phil. Trans. Roy. Soc. Lond., Ser. A 1981, 300, 51 – 63.
19. Buchler J. W. ; Smith, K. M.; Ed. Elsevier; Amsterdam, 1975, p. 157
20. Tissot, B. P., and D.H. Welte (1978). Petroleum Formation and Occurrence: A new Approach to Oil and Gas Exploration, Springer-Verlag, p. 93.
21. Zelmer, P. Pamela. (1983) Organic geochemistry. Vol 5. 43-49
22. Lewan, M. D. Geochim. Cosmochim. Acta 1984,48,2231-2238

23. Ariyanti, D., Handayani, N.A., Hadiyanto (2011). An overview of biocement production from microalgae. Internat. J. od Sci. and Eng. 2(2), 30-33.
24. Cohen Y, Jørgensen BB, Revsbech NP, Poplawski R (1986). "Adaptation to hydrogen sulfide of oxygenic and anoxygenic photosynthesis among Cyanobacteria". Appl. Environ. Microbiol. 51 (2): 398–407.
25. Belser LW (1979). "Population ecology of nitrifying bacteria". Annu. Rev. Microbiol. 33: 309–333.
26. Muyzer, G. and Stams, A. J. (June 2008). "The ecology and biotechnology of sulphate-reducing bacteria". Nature Reviews Microbiology 6: 441–454.
27. Ernst-Detlef Schulze, Harold A. Mooney (1993), Biodiversity and ecosystem function, Springer-Verlag, pp. 88–90
28. Costigan, M and Dobson, S. Vanadium pentoxide and other inorganic vandium compounds. 2001 WHO
29. Vaughan, D. J.; Craig, J. R. “Mineral Chemistry of Metal Sulfides" Cambridge University Press, Cambridge: 1978.
30. Tissot B. P., Welte D.H. (1978) Petroleum formation and occurrence, a new approach to oil and gas exploration, Spriger
31. E.W. BAKER and S.E. Palmer. (1987), Geochemistry of Porphyrins
32. Zelmer, P. Pamel, et al. (1983). Organic Geochemistry, Vol 5 No. 1 43-49
33. Buchler J.W. (1975) In porphyrins and metalloporphyrins. Elsevier, Amsterdam p 157
34. Lewan M.D. (1984) Geochim. Cosmochim. Acta 48, 2231-2238.
35. Quirke J. M. E.; J. Am. Chem. Soc.; 1987, 74-83
36. Pavle I. Premovic, et al. (2000). Earth and Planetary Science Letters 177, 105-118
37. M. Escobar, et al. (2012) Fuel 97 186–196
38. Tissot & Welte. (1984) Petroleum formation and occurrence
39. F.J. Stevenson (1994). Humus Chemistry: Genesis, Composition, Reactions. John Wiley & Sons, New York.
40. Ghabbour, E.A.; Davies, G. (Editors) (2001). Humic Substances: Structures, Models and Functions. Cambridge, U.K
41. Tipping, E (1994). Computers and Geosciences **20** (6): 973–1023.
42. Speight, J. G., Handbook of Petroleum Analysis. John Wiley and Sons, Inc.: New York, 2001.

43. Blankenship, R. E.; Madigan, M. T.; Bauer, C. E.; Editors **1995**, 1331
44. Gust, D.; Moore, T. A.; Moore, A. L. Pure Appl. Chem. **1998**, 70, 2189-2200.
45. D. Dolphin (Ed.), The Porphyrins, vols. I–VII, Academic, New York, 1978.
46. A.B.P. Lever, H.B. Gray (Eds.), Iron Porphyrin, Addison-Wesley Publishing Company, Inc., Reading, MA, 1983.
47. K.M. Kadish, K.M. Smith, R. Guilard (Eds.), The Porphyrin Handbook, Academic Press, San Diego, CA, 2000.
48. H.A.O. Hill, P.J. Sadler, A.J. Thomson (Eds.), Metal Sites in Proteins and Models, Iron Centres, Springer-Verlag, Berlin, Heidelberg, Germany, 1997.
49. I. Bertini, H.B. Gray, S.J. Lippard, J.S. Valentine, Bioinorganic Chemistry, University Science Book, CA, 1994.
50. S. Severance, I. Hamza, Trafficking of heme and porphyrind in metazoa, Chem. Rev. 109 (2009) 4596–4616. and references therein.
51. K. Kitanishi, J. Igarashi, K. Hayasaka, et al. Biochemistry 47 (2008) 6157–6168.
52. S.M. Mense, L. Zhang. Cell. Res. 16 (2006) 681–692Blankenship, R. E.; Madigan, M. T.; Bauer, C. E.; Editors **1995**, 1331
53. Y. Zhu, R.B. Silverman, Electronic effects of peripheral substituents at porphyrin meso positions, J. Org. Chem. 72 (2007) 233–239.
54. N. Jux, The porphyrin twist: Hückel and Möbius aromaticity, Angew. Chem. Int. Ed. 47 (2008) 2543–2546.
55. T.M. Krygowski, M.K. Cyranski, Structural aspects of aromaticity, Chem. Rev. 101 (2001) 1385–1420.
56. M.K. Cyranski, T.M. Krygowski, et al. Chem. Int. Ed. 37 (1998) 177–180.
57. F. Feixas, M. Sola, M. Swart, Chemical bonding and aromaticity in metalloporphyrins, Can. J. Chem. 87 (2009) 1063–1073.
58. D.E. Bikiel, F. Forti, L. Boechi, M. Nardini, F.J. Luque, M.A. Marti, D.A. Estrin. J. Phys. Chem. B 114 (2010) 8536–8543.
59. J.A. Shelnutt, Molecular simulations and normal-coordinate structural analysis of porphyrins and heme proteins, in: K.M. Kadish, K.M. Smith, R. Guilard (Eds.), The Porphyrin Handbook, vol. 7, Academic Press, San Diego,

CA, 2000, pp. 167–224.
60. W. Jentzen, J.-G. Ma, J.A. Shelnutt, Conservation of the conformation of the porphyrin macrocycle in heme proteins, Biophys. J. 74 (1998) 753–763.
61. W. Jentzen, M.C. Simpson, J.D. Hobbs, et al. J. Am. Chem. Soc. 117 (1995) 11085–11097.
62. W. Jentzen, X.Z. Song, J.A. Shelnutt. J. Phys. Chem. B 101 (1997) 1684–1699.
63. W.R. Scheidt, Systematic of stereochemistry of porphyrins and metalloporphyrins, in: K.M. Kadish, K.M. Smith, R. Guilard (Eds.), The Porphyrin Handbook, vol. 3, Academic Press, San Diego, CA, 2000, pp. 49–112.
64. F.A. Walker. Chem. Rev. 104 (2004) 589–616.
65. S. Neya, M. Suzuki, T. Hoshino, et al. Biochemistry 49 (2010) 5642–5650.
66. M. Nakamura, Y. Ohgo, A. Ikezaki, Electronic ground states of low-spin iron(III) porphyrinoids, J. Inorg. Biochem. 102 (2008) 433–445.
67. M. Nakamura, Electronic structures of highly deformed iron(III) porphyrin complexes, Coord. Chem. Rev. 250 (2006) 2271–2294.
68. J. Shao, E. Steene, B.M. Hoffman, et al. J. Inorg. Chem. (2005) 1609–1615.
69. Patra, A. Chaudhury, S.K. Ghosh, S.P. Rath. Chem. 47 (2008) 8324–8335. S.K. Ghosh, R. Patra, S.P. Rath. Inorg. Chem. 47 (2008)
70. R. Patra, S. Bhowmik, S.K. Ghosh, S.P. Rath. Eur. J. Inorg. Chem. (2009) 654–665.
71. S.K. Ghosh, R. Patra, S.P. Rath. Chem. 47 (2008) 10196–10198.
72. M.D. Liptak, X. Wen, K.L. Bren. J. Am. Chem. Soc. 132 (2010) 9753–9763.
73. J.A. Shelnutt, X.Z. Song, J.-A. Ma, S.-J. Jia. Chem. Soc. Rev. 27 (1998) 31–41.
74. J.L. Hoard, Stereochemistry of hemes and other metalloporphyrins, Science 174 (1971) 1295–1302.
75. J.L. Hoard, Some aspects of metalloporphyrin stereochemistry, Ann. N.Y. Acad. Sci. 206 (1973) 18–31.

76. J.L. Hoard, Stereochemistry of porphyrins and metalloporphyrins, in: K.M. Smith (Ed.), Porphyrins and Metalloporphyrins, Elsevier, Amsterdam, 1975, pp. 317–380.
77. M.O. Senge, Exercises in molecular gymnastics – bending, stretching and twisting porphyrins, Chem. Commun. (2006) 243–256.
78. B. Röder, M. Büchner, I. Rückmann. Photochem. Photobiol. Sci. 9 (2010) 1152–1158.
79. R. Bonnett. (1996). International journal of coal geology 32, 137-149.
80. P.I. Premovic, et al. Fuel 79 (2000) 813–819
81. Earl, W. Baker and J. William Louda. (1984). Organic Geochemistry Vol 6, pp 183-192
82. Quinby-Hunt, M. S. and Turekian, K. K.; *Trans. Amer. Geophys. Union*, **1983**, 64, 130
83. Krauskopf, K. B. *"Introduction to Geochemistry"*; 2nd Ed. McGraw Hill: New York, **1979**,
84. Sweeney et al., 1987 Tissot, B. P., and D.H. Welte (1978). Petroleum Formation and Occurrence: A new Approach to Oil and Gas Exploration, Springer-Verlag, p. 93.
85. Hyne, Norman J. (2001). Nontechnical Guide to Petroleum Geology, Exploration, Drilling, and Production. PennWell Corporation. ISBN 0-87814-823-X.
86. Speight, James G; Ancheyta, Jorge, ed. (2007). Hydroprocessing of Heavy Oils and Residua. CRC Press. ISBN 0-8493-7419-7.
87. Speight, James G. (1999). The Chemistry and Technology of Petroleum. Marcel Dekker. ISBN 0-8247-0217-4.

Chapter 2

The focus of this chapter is the understanding of the basics of Density Functional Theory, Basis Sets, Geometry Optimization and Binding Energy. In order to calculate the binding energies of different metalloporphyrins with V, Cr, Fe, Ni, Cu and Zn as the metals used in the tetraphenylporphyrins (TPP) to analyze their stabilities and determine if the most stable ones theoretically correspond to the most abundant Metalloporphyrins (V and Ni) found in the asphaltene fraction of the crude oil in the world.

2.1 Density Functional Theory (DFT)

Density Functional Theory it was develop in 1964 by Walter Kohn and it is a computational quantum mechanical modelling method used in physics, chemistry and materials science to investigate the electronic structure (principally the ground state) of many-body systems, in particular atoms, molecules, and the condensed phases. With this theory, the properties of a many-electron system can be determined by using functionals, i.e. functions of another function, which in this case is the spatially dependent electron density. Hence the name density functional theory comes from the use of functionals of the electron density. DFT is among the most popular and versatile methods available in condensed-matter physics, computational physics, and computational chemistry.[6]

In general, density functional theory finds increasingly broad application in the chemical and material sciences for the interpretation and prediction of complex system behavior at an atomic scale. Specifically, DFT computational methods are applied for the study of systems exhibiting high sensitivity to synthesis and processing parameters. In such systems, experimental studies are often encumbered by inconsistent results and non-equilibrium conditions. Examples of contemporary DFT applications include studying the effects of dopants on phase transformation behavior in oxides, magnetic behavior in dilute magnetic semiconductor materials

and the study of magnetic and electronic behavior in ferroelectrics and dilute magnetic semiconductors.[6][7]

Figure 2.1: Walter Kohn.[33]

Although density functional theory has its conceptual roots in the Thomas–Fermi model, DFT was put on a firm theoretical footing by the two Hohenberg–Kohn theorems (H–K).[8] The original H–K theorems held only for non-degenerate ground states in the absence of a magnetic field, although they have since been generalized to encompass these.[9][10]

The first H–K theorem demonstrates that the ground state properties of a many-electron system are uniquely determined by an electron density that depends on only 3 spatial coordinates. It lays the groundwork for reducing the many-body problem of N electrons with 3N spatial coordinates to 3 spatial coordinates, through the use of functionals of the electron density.[11]

Within the framework of Kohn–Sham DFT (KS DFT), the intractable many-body problem of interacting electrons in a static external potential is reduced to a tractable problem of non-interacting electrons moving in an effective potential. The effective potential includes the external potential and the effects of the Coulomb interactions between the electrons, e.g., the exchange and correlation interactions. [12]

In practice, Kohn–Sham theory can be applied in several distinct ways depending on what is being investigated. In molecular calculations, a huge variety of exchange-correlation functionals have been developed for chemical applications. Some of these are inconsistent with the uniform electron gas approximation; however, they must reduce to LDA in the electron gas limit. Among physicists, probably the most widely used functional is the revised Perdew–Burke–Ernzerhof (PBE) exchange model (a direct generalized-gradient parametrization of the free electron gas with no free parameters). In the chemistry community, one popular functional is known as BLYP (from the name Becke for the exchange part and Lee, Yang and Parr for the correlation part). Even more widely used is B3LYP which is a hybrid functional in which the exchange energy, in this case from Becke's exchange functional, is combined with the exact energy from Hartree–Fock theory. Along with the component exchange and correlation functionals, three parameters define the hybrid functional, specifying how much of the exact exchange is mixed in.[13]

2.1.1 DFT DERIVATION AND FORMALISM

As usual in many-body electronic structure calculations, the nuclei of the treated molecules or clusters are seen as fixed (the Born–Oppenheimer approximation), generating a static external potential V in which the electrons are moving. A stationary electronic state is then described by a wave function $\Psi(\vec{r}_1, \ldots, \vec{r}_N)$ satisfying the many-electron time independent Schrödinger equation

$$\hat{H}\Psi = \left[\hat{T} + \hat{V} + \hat{U}\right]\Psi = \left[\sum_{i}^{N}\left(-\frac{\hbar^2}{2m_i}\nabla_i^2\right) + \sum_{i}^{N} V(\vec{r}_i) + \sum_{i<j}^{N} U(\vec{r}_i, \vec{r}_j)\right]\Psi = E\Psi$$

where, for the N-electron system, $\hat{H}$ is the Hamiltonian, E is the total energy, $\hat{T}$ is the kinetic energy, $\hat{V}$ is the potential energy from the external field due to positively charged nuclei, and $\hat{U}$ is the electron-electron interaction energy. The operators $\hat{T}$ and $\hat{U}$ are called universal

operators as they are the same for any N-electron system, while $\hat{V}$ is system dependent. This complicated many-particle equation is not separable into simpler single-particle equations because of the interaction term $\hat{U}$.**[14]**

There are many sophisticated methods for solving the many-body Schrödinger equation based on the expansion of the wavefunction in Slater determinants. While the simplest one is the Hartree–Fock method, more sophisticated approaches are usually categorized as post-Hartree–Fock methods. However, the problem with these methods is the huge computational effort, which makes it virtually impossible to apply them efficiently to larger, more complex systems.

Here DFT provides an appealing alternative, being much more versatile as it provides a way to systematically map the many-body problem, with $\hat{U}$, onto a single-body problem without $\hat{U}$. In DFT the key variable is the particle density $n(\vec{r})$, which for a normalized Ψ is given by

$$n(\vec{r}) = N \int \mathrm{d}^3 r_2 \int \mathrm{d}^3 r_3 \cdots \int \mathrm{d}^3 r_N \Psi^*(\vec{r}, \vec{r}_2, \ldots, \vec{r}_N) \Psi(\vec{r}, \vec{r}_2, \ldots, \vec{r}_N).$$

This relation can be reversed, i.e. for a given ground-state density $n_0(\vec{r})$ it is possible, in principle, to calculate the corresponding ground-state wave function $\Psi_0(\vec{r}_1, \ldots, \vec{r}_N)$. In other words, Ψ is a unique functional of n_0,**[15]**

$$\Psi_0 = \Psi[n_0]$$

and consequently the ground-state expectation value of an observable $\hat{O}$ is also a functional of n_0

$$O[n_0] = \left\langle \Psi[n_0] \middle| \hat{O} \middle| \Psi[n_0] \right\rangle .$$

In particular, the ground-state energy is a functional of n_0

$$E_0 = E[n_0] = \left\langle \Psi[n_0] \middle| \hat{T} + \hat{V} + \hat{U} \middle| \Psi[n_0] \right\rangle$$

where the contribution of the external potential $\left\langle \Psi[n_0] \middle| \hat{V} \middle| \Psi[n_0] \right\rangle$ can be written explicitly in terms of the ground-state density n_0

$$V[n_0] = \int V(\vec{r}) n_0(\vec{r}) \mathrm{d}^3 r.$$

More generally, the contribution of the external potential $\left\langle \Psi \left| \hat{V} \right| \Psi \right\rangle$ can be written explicitly in terms of the density n,

$$V[n] = \int V(\vec{r}) n(\vec{r}) \mathrm{d}^3 r.$$

The functionals $T[n]$ and $U[n]$ are called universal functionals, while $V[n]$ is called a non-universal functional, as it depends on the system under study. Having specified a system, i.e., having specified $\hat{V}$, one then has to minimize the functional

$$E[n] = T[n] + U[n] + \int V(\vec{r}) n(\vec{r}) \mathrm{d}^3 r_{\text{[16]}}$$

with respect to $n(\vec{r})$, assuming one has got reliable expressions for $T[n]$ and $U[n]$. A successful minimization of the energy functional will yield the ground-state density n_0 and thus all other ground-state observables.

The variational problems of minimizing the energy functional $E[n]$ can be solved by applying the Lagrangian method of undetermined multipliers. First, one considers an energy functional that doesn't explicitly have an electron-electron interaction energy term,

$$E_s[n] = \left\langle \Psi_s[n] \left| \hat{T} + \hat{V}_s \right| \Psi_s[n] \right\rangle$$

where $\hat{T}$ denotes the kinetic energy operator and $\hat{V}_s$ is an external effective potential in which the particles are moving, so that $n_s(\vec{r}) \stackrel{\text{def}}{=} n(\vec{r})$.

Thus, one can solve the so-called Kohn–Sham equations of this auxiliary non-interacting system,

$$\left[-\frac{\hbar^2}{2m} \nabla^2 + V_s(\vec{r}) \right] \phi_i(\vec{r}) = \epsilon_i \phi_i(\vec{r})$$

which yields the orbitals ϕ_i that reproduce the density $n(\vec{r})$ of the original many-body system

$$n(\vec{r}) \stackrel{\text{def}}{=} n_s(\vec{r}) = \sum_i^N |\phi_i(\vec{r})|^2 .$$

The effective single-particle potential can be written in more detail as

$$V_s(\vec{r}) = V(\vec{r}) + \int \frac{e^2 n_s(\vec{r}\,')}{|\vec{r} - \vec{r}\,'|} \mathrm{d}^3 r' + V_{\mathrm{XC}}[n_s(\vec{r})]$$

where the second term denotes the so-called Hartree term describing the electron-electron Coulomb repulsion, while the last term V_{XC} is called the exchange-correlation potential. Here, V_{XC} includes all the many-particle interactions. Since the Hartree term and V_{XC} depend on $n(\vec{r})$, which depends on the ϕ_i, which in turn depend on V_s, the problem of solving the Kohn–Sham equation has to be done in a self-consistent (i.e., iterative) way. Usually one starts with an initial guess for $n(\vec{r})$, then calculates the corresponding V_s and solves the Kohn–Sham equations for the ϕ_i. From these one calculates a new density and starts again. This procedure is then repeated until convergence is reached. A non-iterative approximate formulation called Harris functional DFT is an alternative approach to this.**[16]**

2.1.2 Approximations (exchange-correlation functionals)

The major problem with DFT is that the exact functionals for exchange and correlation are not known except for the free electron gas. However, approximations exist which permit the calculation of certain physical quantities quite accurately. In physics the most widely used approximation is the local-density approximation (LDA), where the functional depends only on the density at the coordinate where the functional is evaluated:

$$E_{\mathrm{XC}}^{\mathrm{LDA}}[n] = \int \epsilon_{\mathrm{XC}}(n) n(\vec{r}) \mathrm{d}^3 r.$$

Generalized gradient approximations (GGA) are still local but also take into account the gradient of the density at the same coordinate:

$$E_{XC}^{\mathrm{GGA}}[n_\uparrow, n_\downarrow] = \int \epsilon_{XC}(n_\uparrow, n_\downarrow, \vec{\nabla} n_\uparrow, \vec{\nabla} n_\downarrow) n(\vec{r}) \mathrm{d}^3 r.$$

Using the latter (GGA) very good results for molecular geometries and ground-state energies have been achieved.**[17]**

2.1.3 Kohn – Sham equations

In physics and quantum chemistry, specifically density functional theory, the Kohn–Sham equation is the Schrödinger equation of a fictitious system (the "Kohn–Sham system") of non-interacting particles (typically electrons) that generate the same density as any given system of interacting particles.[18][19] The Kohn–Sham equation is defined by a local effective (fictitious) external potential in which the non-interacting particles move, typically denoted as $v_s(r)$ or $v_{eff}(r)$, called the Kohn–Sham potential. As the particles in the Kohn–Sham system are non-interacting fermions, the Kohn–Sham wave function is a single Slater determinant constructed from a set of orbitals that are the lowest energy solutions to

$$\left(-\frac{\hbar^2}{2m}\nabla^2 + v_{\text{eff}}(\mathbf{r})\right)\phi_i(\mathbf{r}) = \varepsilon_i\phi_i(\mathbf{r})$$

This eigenvalue equation is the typical representation of the Kohn–Sham equations. Here, ε_i is the orbital energy of the corresponding Kohn–Sham orbital, φ_i, and the density for an N-particle system is

$$\rho(\mathbf{r}) = \sum_i^N |\phi_i(\mathbf{r})|^2.$$

The Kohn–Sham equations are named after Walter Kohn and Lu Jeu Sham, who introduced the concept at the University of California, San Diego in 1965.

2.1.4 Kohn–Sham potential

In density functional theory, the total energy of a system is expressed as a functional of the charge density as

$$E[\rho] = T_s[\rho] + \int d\mathbf{r}\; v_{\text{ext}}(\mathbf{r})\rho(\mathbf{r}) + V_H[\rho] + E_{\text{xc}}[\rho]$$

where T_s is the Kohn–Sham kinetic energy which is expressed in terms of the Kohn–Sham orbitals as

$$T_s[\rho] = \sum_{i=1}^N \int d\mathbf{r}\; \phi_i^*(\mathbf{r})\left(-\frac{\hbar^2}{2m}\nabla^2\right)\phi_i(\mathbf{r}),$$

v_{ext} is the external potential acting on the interacting system (at minimum, for a molecular system, the electron-nuclei interaction), V_H is the Hartree (or Coulomb) energy,

$$V_H = \frac{e^2}{2} \int d\mathbf{r} \int d\mathbf{r}' \, \frac{\rho(\mathbf{r})\rho(\mathbf{r}')}{|\mathbf{r} - \mathbf{r}'|}.$$

and E_{xc} is the exchange-correlation energy. The Kohn–Sham equations are found by varying the total energy expression with respect to a set of orbitals to yield the Kohn–Sham potential as

$$v_{\text{eff}}(\mathbf{r}) = v_{\text{ext}}(\mathbf{r}) + e^2 \int \frac{\rho(\mathbf{r}')}{|\mathbf{r} - \mathbf{r}'|} d\mathbf{r}' + \frac{\delta E_{\text{xc}}[\rho]}{\delta \rho(\mathbf{r})}.$$

where the last term

$$v_{\text{xc}}(\mathbf{r}) \equiv \frac{\delta E_{\text{xc}}[\rho]}{\delta \rho(\mathbf{r})}$$

is the exchange-correlation potential. This term and the corresponding energy expression are the only unknowns in the Kohn–Sham approach to density functional theory. An approximation that does not vary the orbitals is Harris functional theory.[18][19]

Naval Research Laboratory Molecular Orbital Library (NRLMOL) is a massively parallel code for electronic structure calculations on large molecules and clusters. It solves the electronic systems following Kohn-Sham formulations of density functional theory and presents the Kohn-Sham orbitals as a linear combination of Gaussian orbitals. [20]

In computational chemistry and molecular physics, Gaussian orbitals (also known as Gaussian type orbitals, GTOs or Gaussians) are functions used as atomic orbitals for the representation of electron orbitals in molecules and numerous properties that depend on these.[21]

The principal reason for the use of Gaussian basis functions in molecular quantum chemical calculations is the 'Gaussian Product Theorem', which guarantees that the product of two GTOs centered on two different atoms is a finite sum of Gaussians centered on a point along the axis connecting them. In this manner, four-center integrals can be reduced to finite sums of two-center integrals, and in a next step to finite sums of one-center integrals.

For reasons of convenience, many quantum chemistry programs work in a basis of Cartesian Gaussians even when spherical Gaussians are requested, as integral evaluation is much easier in the cartesian basis, and the spherical functions can be simply expressed using the cartesian functions.[22]

The Gaussian basis functions obey the usual radial-angular decomposition

$$\Phi(\mathbf{r}) = R_l(r)Y_{lm}(\theta, \phi),$$

where $Y_{lm}(\theta, \phi)$ is a spherical harmonic, l and m are the angular momentum and its z component, and r, θ, ϕ are spherical coordinates.

For Gaussian primitives the radial part is

$$R(r) = B(l, \alpha)r^l e^{-\alpha r^2},$$

where $B(l, \alpha)$ is the normalization constant corresponding to the Gaussian.

The exponents are reported in atomic units. There is a large library of published Gaussian basis sets optimized for a variety of criteria available at the EMSL basis set exchange

2.2 Density Basis Set

A **basis set** in theoretical and computational chemistry is a set of functions (called basis functions) which are combined in linear combinations (generally as part of a quantum chemical calculation) to create molecular orbitals. For convenience these functions are typically atomic orbitals centered on atoms, but can theoretically be any function; plane waves are frequently used in materials calculations.[23]

In modern computational chemistry, quantum chemical calculations are typically performed using a finite set of basis functions. In these cases, the wave functions of the system in question are represented as vectors, the components of which correspond to coefficients in a linear combination of the basis functions in the basis set used. The operators are then represented as matrices, (rank two tensors), in this finite basis. The basis function and atomic orbital are sometimes used interchangeably, although it should be noted that these basis functions are usually not actually the exact atomic orbitals, even for the corresponding hydrogen-like atoms, due to approximations and simplifications of their analytic formulas.[24]

Today, there are hundreds of basis sets composed of Gaussian-type orbitals (GTOs). The smallest of these are called minimal basis sets, and they are typically composed of the minimum number of basis functions required to represent all of the electrons on each atom. The largest of

these can contain literally dozens to hundreds of basis functions on each atom.

A minimum basis set is one in which, on each atom in the molecule, a single basis function is used for each orbital in a Hartree–Fock calculation on the free atom.

The most common addition to minimal basis sets is probably the addition of polarization functions, denoted (in the names of basis sets developed by Pople) by an asterisk, *. Two asterisks, **, indicate that polarization functions are also added to light atoms (hydrogen and helium). These are auxiliary functions with one additional node. For example, the only basis function located on a hydrogen atom in a minimal basis set would be a function approximating the 1s atomic orbital. When polarization is added to this basis set, a p-function is also added to the basis set. This adds some additional needed flexibility within the basis set, effectively allowing molecular orbitals involving the hydrogen atoms to be more asymmetric about the hydrogen nucleus. This is an important result when considering accurate representations of bonding between atoms, because the very presence of the bonded atom makes the energetic environment of the electrons spherically asymmetric. Similarly, d-type functions can be added to a basis set with valence p orbitals, and f-functions to a basis set with d-type orbitals, and so on. Another, more precise notation indicates exactly which and how many functions are added to the basis set, such as (d, p).

Another common addition to basis sets is the addition of diffuse functions, denoted in Pople-type sets by a plus sign,+, and in Dunning-type sets by "aug" (from "augmented"). Two plus signs indicate that diffuse functions are also added to light atoms (hydrogen and helium). These are very shallow Gaussian basis functions, which more accurately represent the "tail" portion of the atomic orbitals, which are distant from the atomic nuclei. These additional basis functions can be important when considering anions and other large, "soft" molecular systems.[23][24]

2.2.1 Minimal Basis Sets

The most common minimal basis set is STO-nG, where n is an integer. This n value represents the number of Gaussian primitive functions comprising a single basis function. In these basis sets, the same number of Gaussian primitives comprise core and valence orbitals. Minimal basis sets typically give rough results that are insufficient for research-quality publication, but are much cheaper than their larger counterparts. Commonly used minimal basis

sets of this type are:

- STO-3G
- STO-4G
- STO-6G
- STO-3G* - Polarized version of STO-3G

2.2.2 Split – valence Basis Sets

During most molecular bonding, it is the valence electrons which principally take part in the bonding. In recognition of this fact, it is common to represent valence orbitals by more than one basis function (each of which can in turn be composed of a fixed linear combination of primitive Gaussian functions). Basis sets in which there are multiple basis functions corresponding to each valence atomic orbital are called valence double, triple, quadruple-zeta, and so on, basis sets (zeta, ζ, was commonly used to represent the exponent of an STO basis function[25]). Since the different orbitals of the split have different spatial extents, the combination allows the electron density to adjust its spatial extent appropriate to the particular molecular environment. Minimum basis sets are fixed and are unable to adjust to different molecular environments.

2.3 Pople basis sets

The notation for the split-valence basis sets arising from the group of John Pople is typically X-YZg.[26] In this case, X represents the number of primitive Gaussians comprising each core atomic orbital basis function. The Y and Z indicate that the valence orbitals are composed of two basis functions each, the first one composed of a linear combination of Y primitive Gaussian functions, the other composed of a linear combination of Zprimitive Gaussian functions. In this case, the presence of two numbers after the hyphens implies that this basis set is a split-valence double-zetabasis set. Split-valence triple- and quadruple-zeta basis sets are also used, denoted as X-YZWg, X-YZWVg, etc. Here is a list of commonly used split-valence basis sets of this type:

- 3-21G

- 3-21G* - Polarized
- 3-21+G - Diffuse functions
- 3-21+G* - With polarization and diffuse functions
- 4-21G
- 4-31G
- 6-21G
- 6-31G
- 6-31G*
- 6-31+G*
- 6-31G(3df, 3pd)
- 6-311G
- 6-311G*
- 6-311+G*

The 6-31G* basis set (defined for the atoms H through Zn) is a valence double-zeta polarized basis set that adds to the 6-31G set six d-type Cartesian-Gaussian polarization functions on each of the atoms Li through Ca and ten f-type Cartesian Gaussian polarization functions on each of the atoms Sc through Zn. Some other split-valence (SV) basis sets are[27]:

- SV(P)
- SVP
- DZV - Valence double-zeta
- TZV - Valence triple-zeta
- TZVPP - Valence triple-zeta plus polarization
- QZVPP - Valence quadruple-zeta plus polarization

2.4 Geometry Optimizations

Implicit the idea of a molecule is the concept of molecular structure. That is, a molecule is not only a collection of atoms but is a collection of atoms in a particular set of locations in space.

Often, the structure of a molecule is of interest and also most important molecular properties are structurally dependent. Determining molecular structures is therefore a very important aspect of physics and chemistry. In the area of computational physics-chemistry, structure determination is achieved through a geometry optimization.[28]

The energy of a collection of atoms as a function of their internal degrees of freedom is known as a potential energy surface (PES). Molecular structures correspond to minima on this surface. The function of a geometry optimization is therefore to find a minimum in the potential energy surface.

Once a molecular structure is obtained, it is often necessary to derive quantitative values of important parameters such as certain Bond Lengths, Binding Energies and Angles from the structure.

The first step in a computational study is usually a geometry optimization to obtain an accurate structure of the molecule(s) of interest. The simple building and cleanup process is unlikely to give a geometry accurate enough for use in further studies especially if heavier elements are involved.[28]

2.4.1 Binding Energy

Binding energy represents the mechanical work that must be done against the forces which hold an object together, disassembling the object into component parts separated by sufficient distance that further separation requires negligible additional work.

At the atomic level the **atomic binding energy** of the atom derives from electromagnetic interaction and is the energy required to disassemble an atom into free electrons and a nucleus. Electron binding energy is a measure of the energy required to free electrons from their atomic orbits. This is more commonly known as ionization energy.[29]

At the nuclear level, binding energy is also equal to the energy liberated when a nucleus is created from other nucleons or nuclei.[30][31] This nuclear binding energy (binding energy of nucleons into a nuclide) is derived from the nuclear force (residual strong interaction) and is

the energy required to disassemble a nucleus into the same number of free, unbound neutrons and protons it is composed of, so that the nucleons are far/distant enough from each other so that the nuclear force can no longer cause the particles to interact.[32] The larger the binding energy the most stable a complex is.

In order to determine the binding energies and therefore their stabilities of a set of metallo-porphyrin complexes (where M = VO, Cr, Fe, Ni, Cu or Zn) (Fig. 1) Naval Research Laboratory Molecular Orbital Library (NRLMOL) spin polarized/DFT was used to calculate the full optimized geometry, of the above complexes. In these calculations the default basis set PBE for exchange-correlation functional was used.

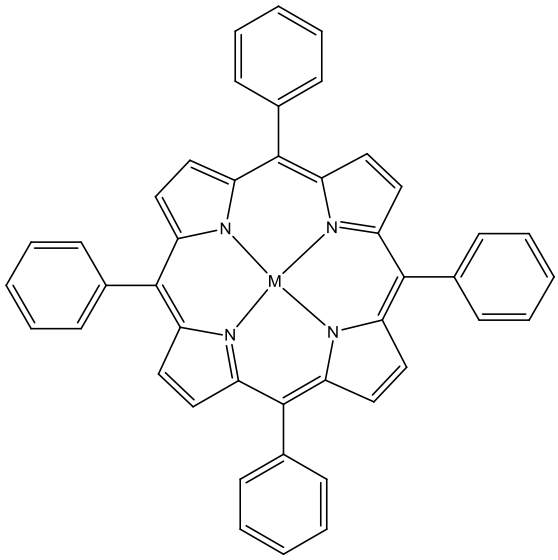

Figure 2.2: Structure of the organometallic tetraphenylporphyrin complex studied.

2.5 Tetraphenylporphyrin and Metalloporphyrin optimization results

The metalloporphyrins were optimized using the luit.utep.edu it was a linux cluster of 100 cores. It was decommissioned about 2 years ago.

The calculations were done using DFT/NRLMOL at the all-electron level using generalized gradient approximation by Perdew-Burke-Ernzerhof (PBE). The basis set used was triple zeta.

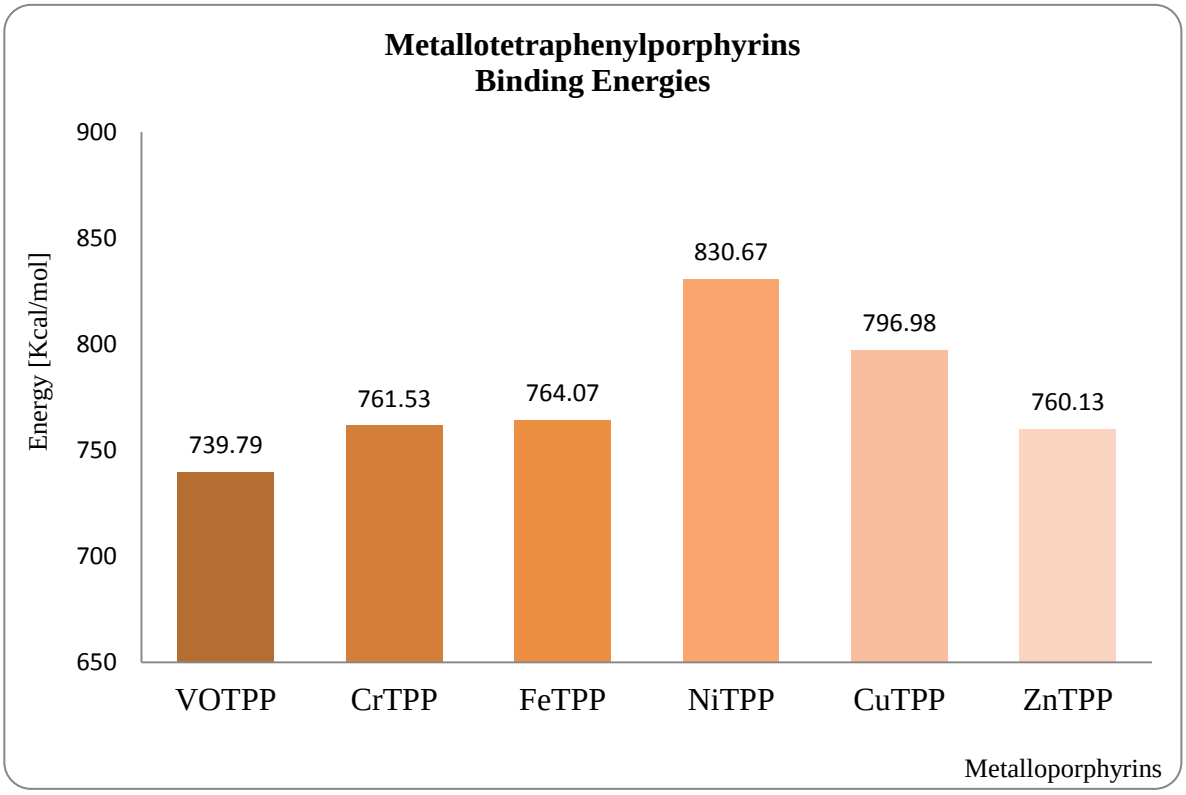

GRAPH 2.1: Optimization results of different metalloporphyrin molecules showing the binding energy in kcal/mol.

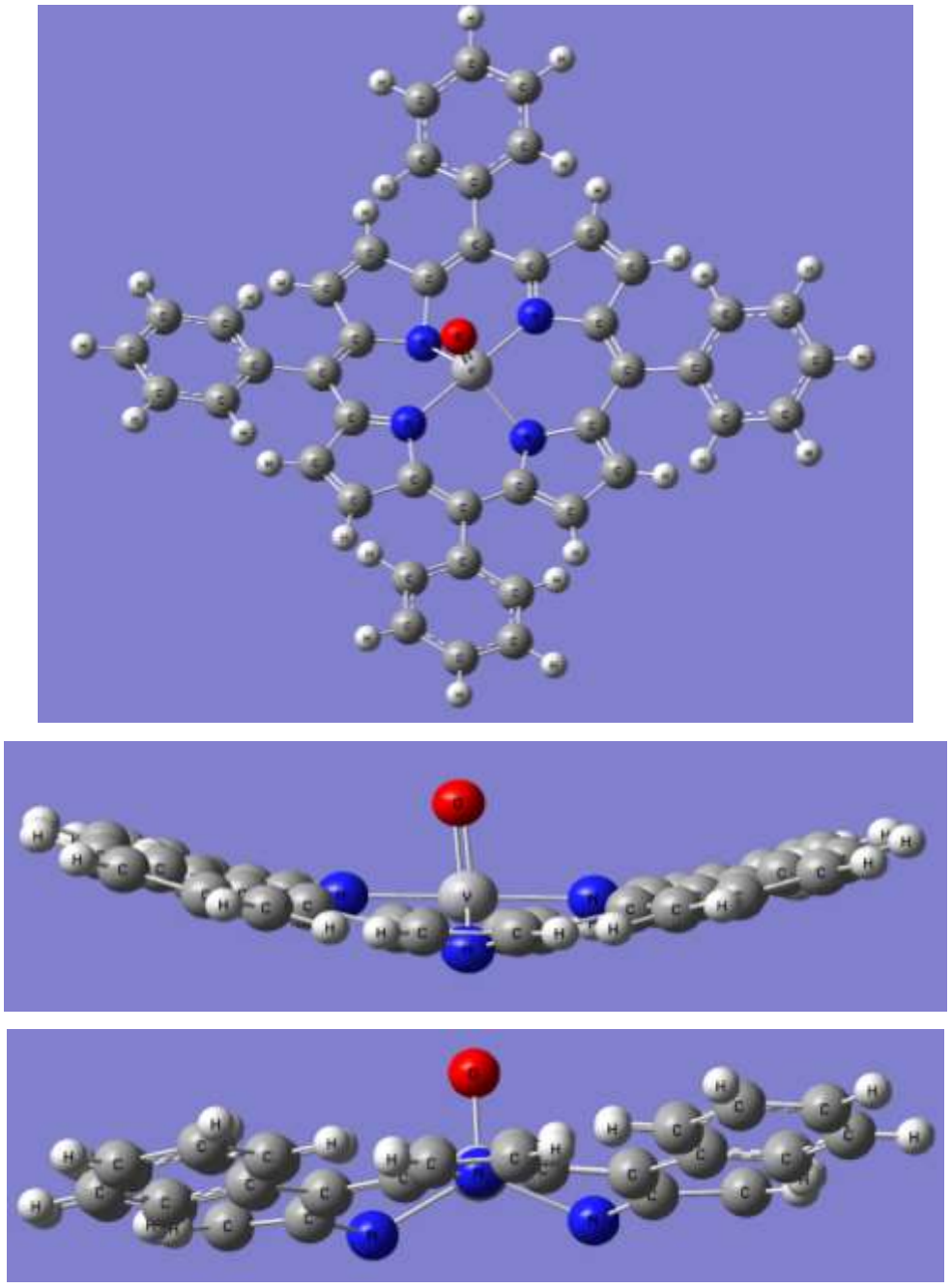

Figure 2.3: Vanadyl Tetraphenylporphyrin (VOTPP)

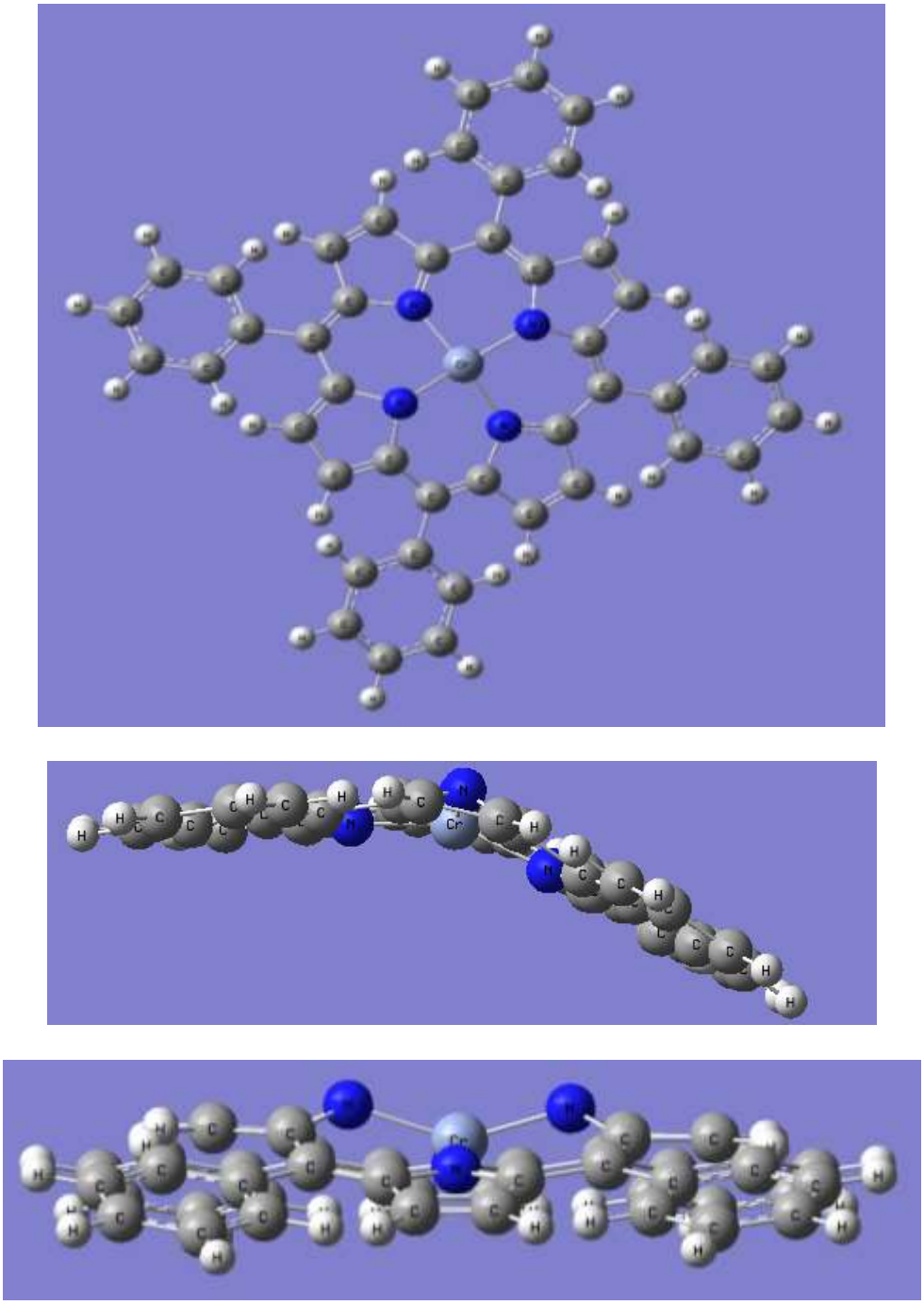

Figure 2.4: Chromium Tetraphenylporphyrin (CrTPP)

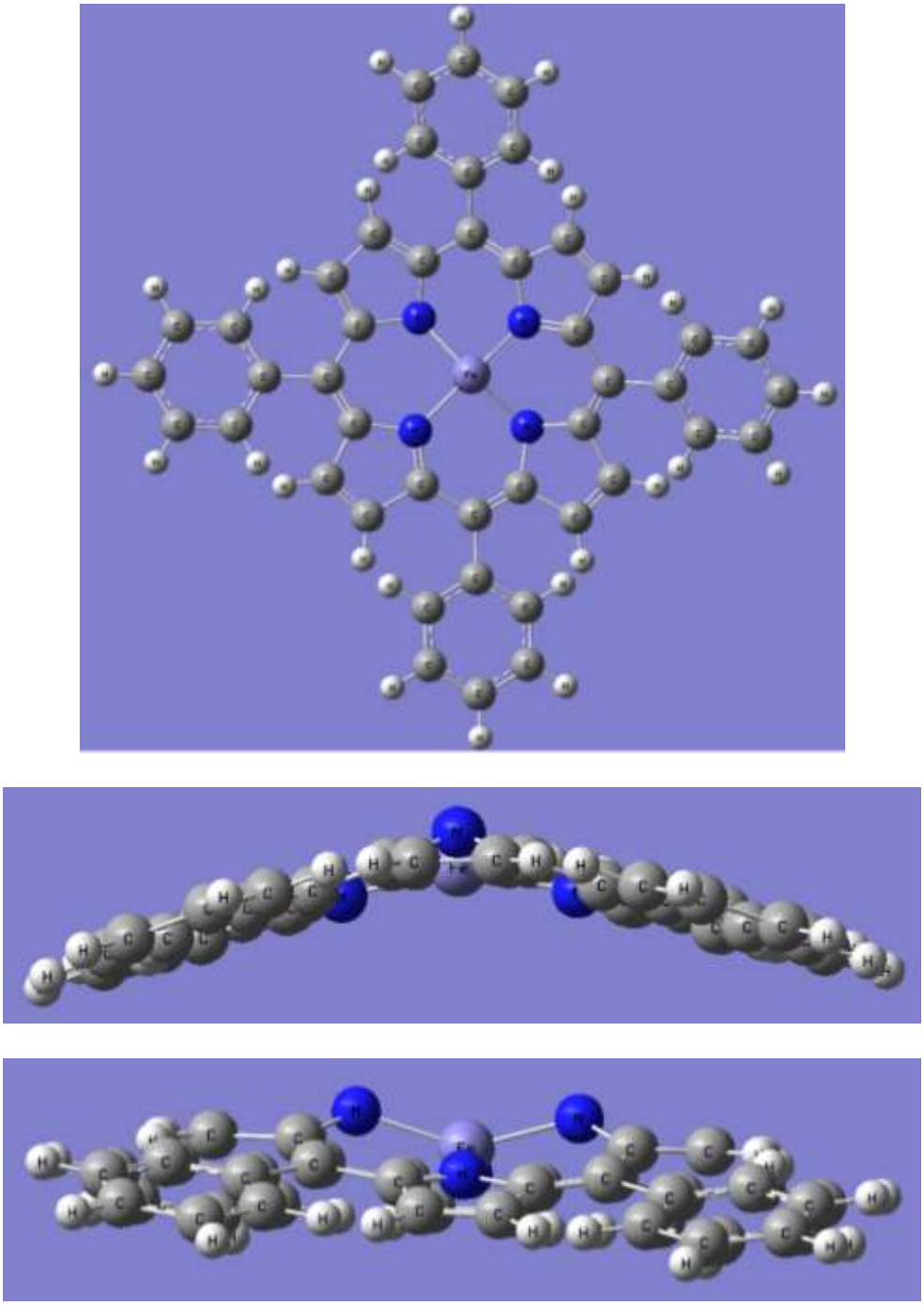

Figure 2.5: Iron Tetraphenylporphyrin (FeTPP)

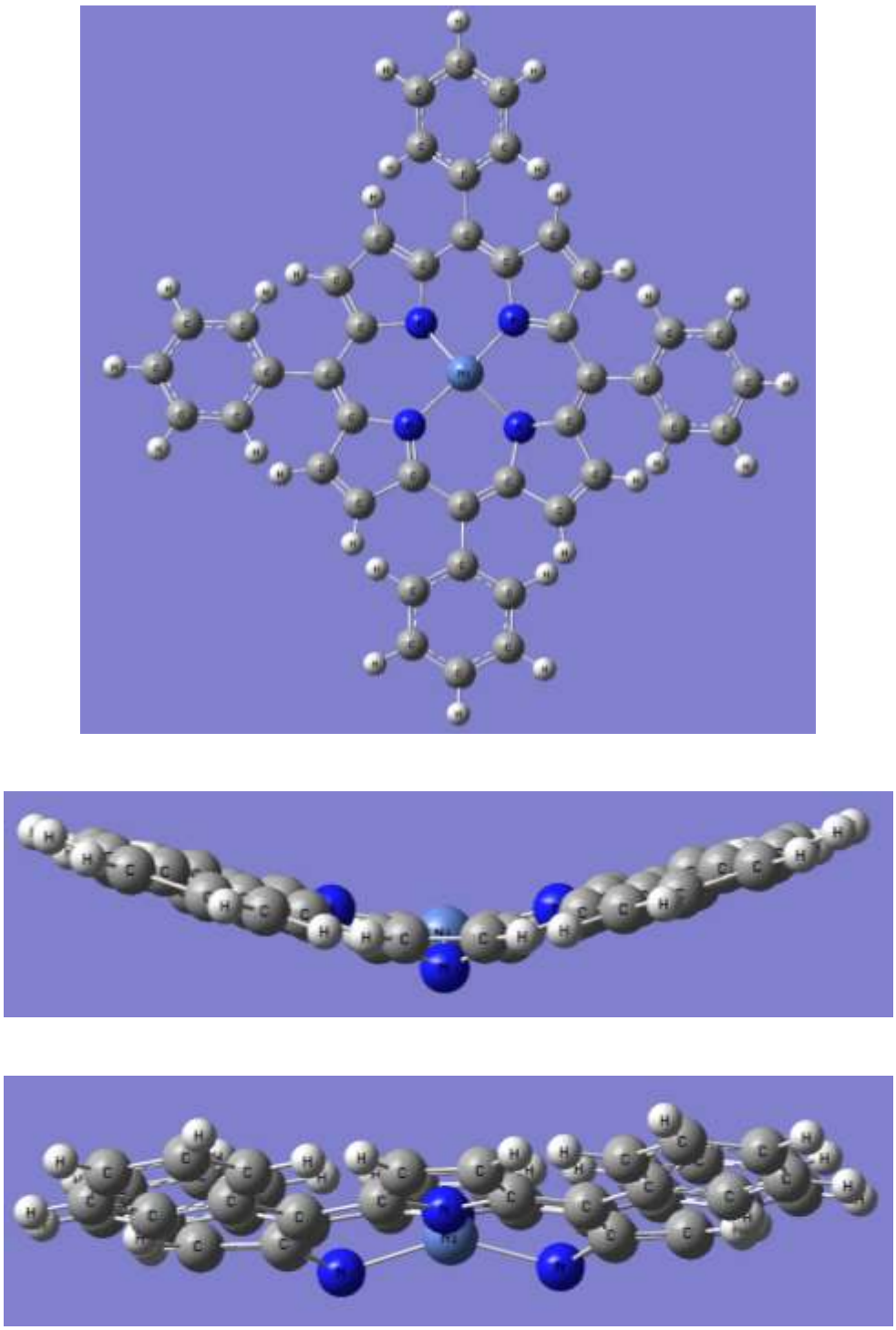

Figure 2.6: Nickel Tetraphenylporphyrin (NiTPP)

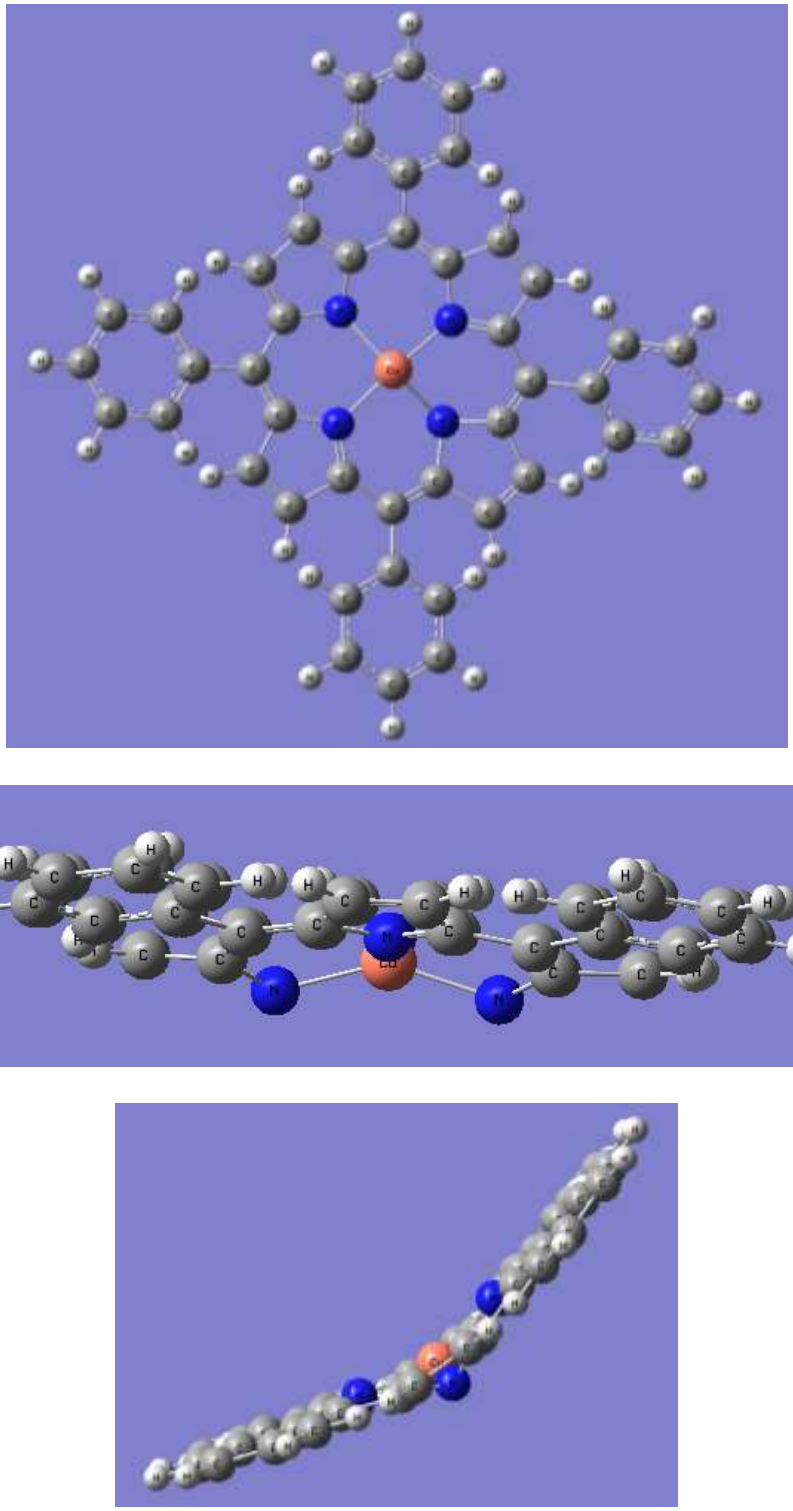

Figure 2.7: Copper Tetraphenylporphyrin (CuTPP)

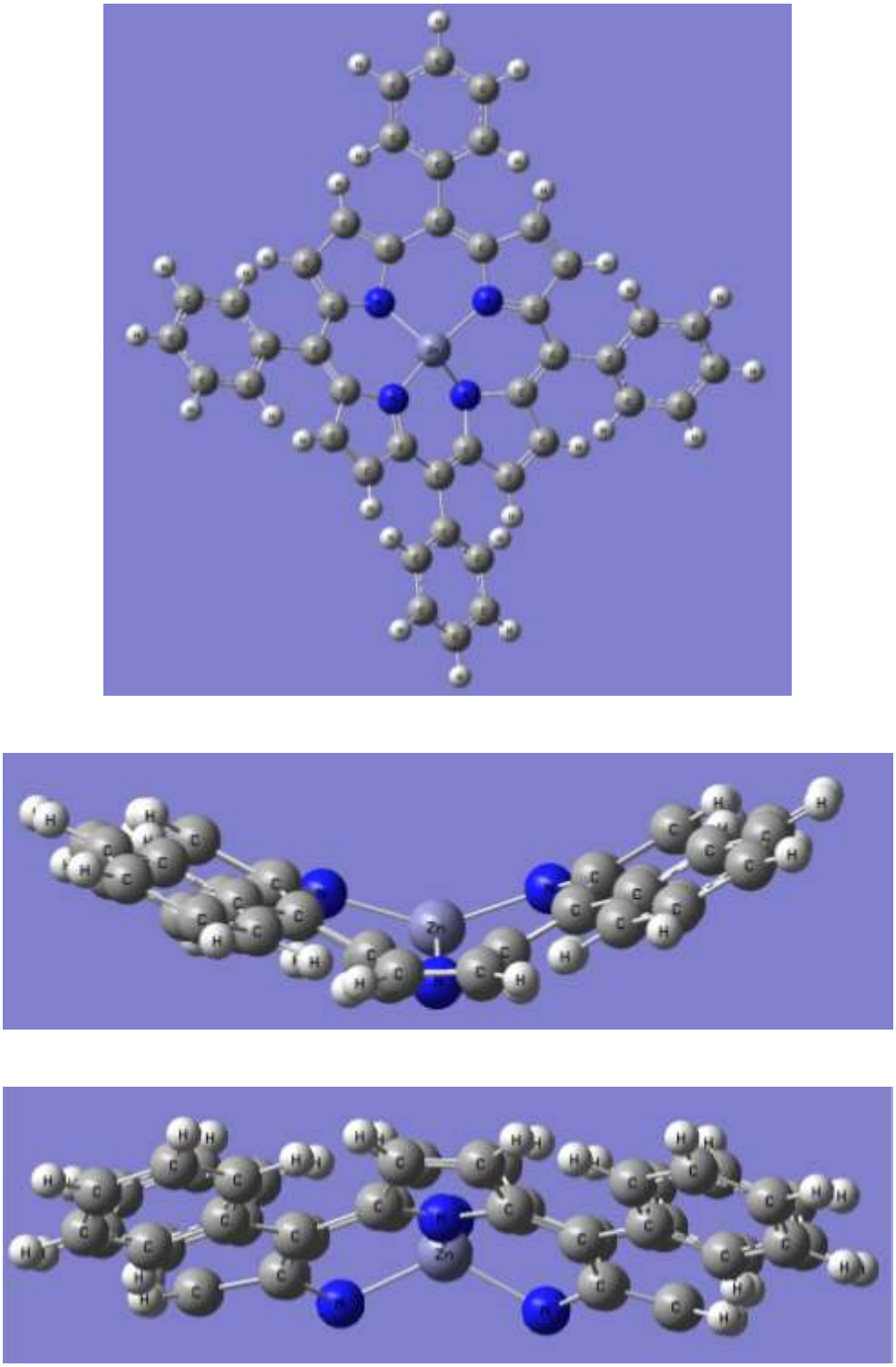

Figure 2.8: Zinc Tetraphenylporphyrin (ZnTPP)

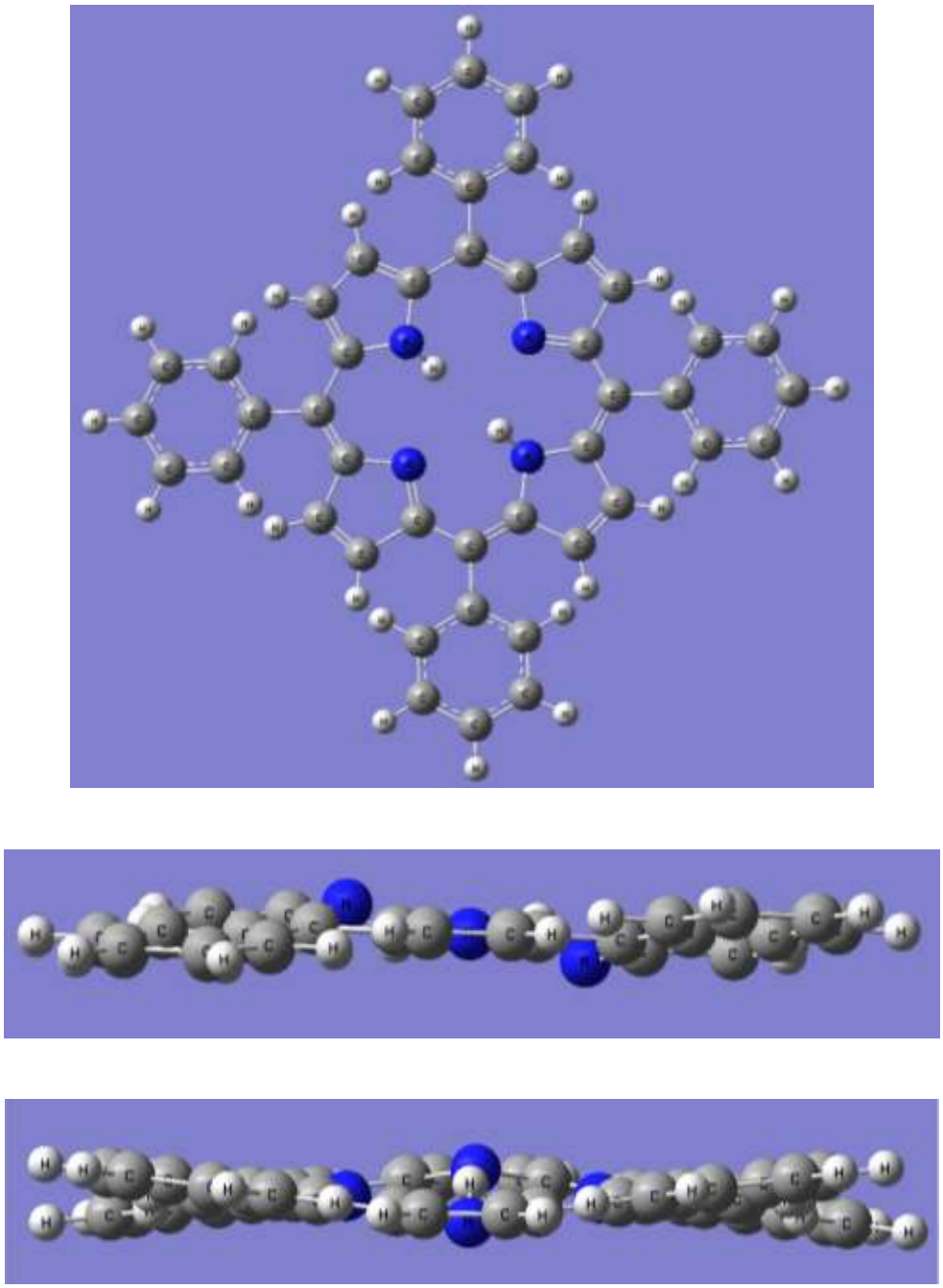

Figure 2.9: Tetraphenylporphyrin (TPP)

2.6 References Chapter 2

(1) Nalwaya, V.; Tangtayakom, V.; Chavadej, S.; Fogler, S. Studies on Asphaltenes Through Analysis of Polar Fractions. Ind. Eng. Chem.Res. 1999, 38, 964-972.

(2) Fish, R. H.; Reynolds, J. G.; Gallegos, E. J. MetGl Complexes in Fossil Fuels, ACS Symposium Series 344; American Chemical Society: Washington, DC, 1987; pp 332-349.

(3) Baker and Hodgson, 1968; Shiobara and Taguchi, 1975

(4) Constantinides et al., 1959

(5) Brunnock et al., 1968;Davis and Gibbs, 1975

(6) Segall, M.D.; Lindan, P.J (2002). "First-principles simulation: ideas, illustrations and the CASTEP code". Journal of Physics: Condensed Matter 14 (11): 2717.

(7) "Ab initio study of phase stability in doped TiO2". Computational Mechanics 50 (2): 185–194. 2012. doi:10.1007/s00466-012-0728-4.

(8) Hohenberg, Pierre; Walter Kohn (1964). "Inhomogeneous electron gas". Physical Review136 (3B): B864–B871.Bibcode:1964PhRv..136..864H.doi:10.1103/PhysRev.136.B864.

(9) Levy, Mel (1979). "Universal variational functionals of electron densities, first-order density matrices, and natural spin-orbitals and solution of the v-representability problem". Proceedings of the National Academy of Sciences (United States National Academy of Sciences) 76 (12): 6062–6065.Bibcode:1979PNAS...76.6062L.doi:10.1073/pnas.76.12.6062.

(10) Vignale, G.; Mark Rasolt (1987). "Density-functional theory in strong magnetic fields". Physical Review Letters (American Physical Society) 59 (20): 2360–2363.Bibcode:1987PhRvL..59.2360V.doi:10.1103/PhysRevLett.59.2360.PMID 10035523

(11) Viraht, Xiao-Yin (2012). "Hohenberg-Kohn theorem including electron spin". Physical Review A 86. Bibcode:1994PhRvA.86.042502.doi:10.1103/PhysRevA.50.3089.

(12) March, N. H. (1992). Electron Density Theory of Atoms and Molecules. Academic Press. p. 24. ISBN 0-12-470525-1.

(13) Parr, R. G.; Yang, W. (1989). Density-Functional Theory of Atoms and Molecules. New York: Oxford University Press. ISBN 0-19-504279-4.. ISBN 0-19-509276-7 (paperback)

(14) Tkatchenko, Alexandre; Scheffler, Matthias (2009). "Accurate Molecular Van Der Waals Interactions from Ground-State Electron Density and Free-Atom Reference Data". Physical Review Letters 102(7): 073005. Bibcode:2009PhRvL.102g3005T.doi:10.1103/PhysRevLett.102.073005. PMID 19257665.

(15) Viraht, Xiao-Yin (2012). "Hohenberg-Kohn theorem including electron spin". Physical Review A 86. Bibcode:1994PhRvA.86.042502.doi:10.1103/PhysRevA.50.3089.

(16) Kohn, W.; Sham, L. J. (1965). "Self-consistent equations including exchange and correlation effects". Physical Review 140 (4A): A1133–A1138. Bibcode:1965PhRv..140.1133K.doi:10.1103/PhysRev.140.A1133.

(17) Viraht, Xiao-Yin (2012). "Hohenberg-Kohn theorem including electron spin". Physical Review A 86. Bibcode:1994PhRvA.86.042502.doi:10.1103/PhysRevA.50.3089.

(18) Kohn, Walter; Sham, Lu Jeu (1965). "Self-Consistent Equations Including Exchange and Correlation Effects". Physical Review 140 (4A): A1133–A1138. Bibcode:1965PhRv..140.1133K.doi:10.1103/PhysRev.140.A1133.

(19) Parr, Robert G.; Yang, Weitao (1994). Density-Functional Theory of Atoms and Molecules. Oxford University Press. ISBN 978-0-19-509276-9.

(20) http://quantum.utep.edu/nrlmol/nrlmol.html

(21) Gill, Peter M.W. (1994). "Molecular integrals Over Gaussian Basis Functions". Advances in Quantum Chemistry 25: 141–205. Bibcode:1994AdQC...25..141G. doi:10.1016/S0065-3276(08)60019-2. Retrieved 17 June 2011.

(22) Schlegel, H.; Frisch, M. (1990). "Transformation between Cartesian and pure spherical harmonic Gaussians".International Journal of Quantum Chemistry 54 (2): 83–87. doi:10.1002/qua.560540202.

(23) Dunning, Thomas H. (1989). "Gaussian basis sets for use in correlated molecular calculations. I. The atoms boron through neon and hydrogen". J. Chem. Phys. 90 (2): 1007–1023. Bibcode:1989JChPh..90.1007D. doi:10.1063/1.456153.

(24) Roman M. Balabin (2010). "Intramolecular basis set superposition error as a measure of basis set incompleteness: Can one reach the basis set limit without extrapolation?". J. Chem. Phys. 132 (21): 211103. Bibcode:2010JChPh.132u1103B. doi:10.1063/1.3430647. PMID 20528011.

(25) Davidson, Ernest; Feller, David (1986). "Basis set selection for molecular calculations". Chem. Rev. 86 (4): 681–696. doi:10.1021/cr00074a002.

(26) Ditchfield, R; Hehre, W.J; Pople, J. A. (1971). "Self-Consistent Molecular-Orbital Methods. IX. An Extended Gaussian-Type Basis for Molecular-Orbital Studies of Organic Molecules". J. Chem. Phys. 54 (2): 724–728. Bibcode:1971JChPh..54..724D. doi:10.1063/1.1674902.

(27) Moran, Damian; Simmonett, Andrew C.; Leach, Franklin E.; Allen, Wesley D.; Schleyer, Paul v. R.; Schaefer, Henry F. (2006). "Popular Theoretical Methods Predict Benzene and Arenes To Be Nonplanar". Journal of the American Chemical Society 128 (29): 9342–3.doi:10.1021/ja0630285. PMID 16848464.

(28) http://www.cobalt.chem.ucalgary.ca/ziegler/Chem575

(29) IUPAC, Compendium of Chemical Terminology, 2nd ed. (the "Gold Book") (1997). Online corrected version: (2006–) "Ionization energy".

(30) Britannica Online Encyclopedia - "nuclear binding energy". Accessed 8 September 2010.http://www.britannica.com/EBchecked/topic/65615/binding-energy

(31) Nuclear Engineering - "Binding Energy". Bill Garland, McMaster University. Accessed 8 September 2010.http://www.nuceng.ca/igna/binding_energy.htm

(32) Atomic Alchemy: Nuclear Processes - "Binding Energy". About. Accessed 7 September 2010.http://library.thinkquest.org/17940/texts/binding_energy/binding_energy.html
(33) http://gabriel.physics.ucsb.edu/~kohn/

Chapter 3: Experimental Procedures

3.1 MATERIALS AND METHODOLOGY

This Chapter describes the materials, conditions and methodologies of each procedure used for the completion of this dissertation.

The procedures are:

- Chemical Reactions
- Characterizations
    - Thin Layer Chromatography (TLC)
    - Ultra Violet Spectroscopy (UV-Vis)
    - Silica Column Chromatography
    - Mass Spectrometry (MS)
    - High Performance Liquid Chromatography (HPLC)

3.1.1 Porphyrin derivatives

Tetraphenylporphyrin, Zinc (II) tetraphenylporphyrin, Copper (II) tetraphenylporphyrin, Iron (II) tetraphenylporphyrin, Vanadyl tetraphenylporphyrin, Nickel (II) tetraphenylporphyrin and Chromium (II) tetraphenylporphyrin reagents were purchased in high purity above 95% from Sigma-Aldrich. Samples were stored in a nitrogen glove box to prevent decomposition.

3.2 CHEMICAL REACTIONS

3.2.1 Chemical Reactions Stages

All the chemical reactions experiments were categorized in two main sections:

- Competitions
- Transmetallations.

At the same time there are different stages in each section which reflects the conditions of the reactions: Open System, Under Nitrogen, Reactions with Sodium Sulfide Na_2S.

The next tables are showing a more comprehensive relation between conditions and reactants used in each stage.

Table 3.1 Sample Relation

STAGE1 OPEN SYSTEM			Experiment #
A	$VOSO_4$ + TPP +	$ZnSO_4$	1
		$CuSO_4$	2
		$CrSO_4$	3
		$NiSO_4$	4
		$FeSO_4$	4_1
B	$NiSO_4$ + TPP +	$ZnSO_4$	5
		$CuSO_4$	6
		$CrSO_4$	7
		$FeSO_4$	7_1

STAGE 4 UNDER NITROGEN			Experiment #
A	$VOSO_4$ + TPP +	$ZnSO_4$	22
		$CuSO_4$	23
		$CrSO_4$	24
		$NiSO_4$	25
		$FeSO_4$	26
B	$NiSO_4$ + TPP +	$ZnSO_4$	27
		$CuSO_4$	28
		$CrSO_4$	29
		$FeSO_4$	30

STAGE 2 OPEN SYSTEM			Experiment #
A	$VOSO_4$ +	ZnTPPP	8
		CuTPP	9
		CrTPP	10
		NiTPP	11
B	$NiSO_4$ +	ZnTPPP	12
		CuTPP	13
		CrTPP	14
		VOTPP	15

STAGE 5 UNDER NITROGEN			Experiment #
A	$VOSO_4$ +	ZnTPPP	31
		CuTPP	32
		CrTPP	33
		NiTPP	34
B	$NiSO_4$ +	ZnTPPP	35
		CuTPP	36
		CrTPP	37
		VOTPP	38

STAGE 3 OPEN SYSTEM			Experiment #
A	VOTPP +	$ZnSO_4$	16
		$CuSO_4$	17
		$CrSO_4$	18
B	NiTPP +	$ZnSO_4$	19
		$CuSO_4$	20
		$CrSO_4$	21

STAGE 6 UNDER NITROGEN			Experiment #
A	VOTPP +	$ZnSO_4$	39
		$CuSO_4$	40
		$CrSO_4$	41
B	NiTPP +	$ZnSO_4$	42
		$CuSO_4$	43
		$CrSO_4$	44

STAGE 7 with Sodium Sulfide			Experiment #
A	$VOSO_4$ + TPP + Na_2S +	$ZnSO_4$	45
		$CuSO_4$	46
		$CrSO_4$	47
		$NiSO_4$	48
		$FeSO_4$	49
B	$NiSO_4$ + TPP + Na_2S +	$ZnSO_4$	50
		$CuSO_4$	51
		$CrSO_4$	52
		$FeSO_4$	53

3.2.2 Competition reactions between $VOSO_4/NiSO_4$ and MSO_4 for the coordination of free base TPP in the presence of oxygen, STAGE 1

Figure 3.1 Set up of Chemical Reaction in reflux with DMF

Reactions were run in Dimethylformamide (DMF) as solvent, at 130 ^{o}C for 24 hrs, using the same molar equivalents for $VOSO_4/NiSO_4$, MSO_4, and TPP. The reactions were placed under refluxing DMF in an open system, and the reaction was tracked for completion using TLC.

3.2.3 Competition reactions between $VOSO_4/NiSO_4$ and MSO_4 for the coordination of free base TPP in the absence of oxygen, STAGE 4

Reactions were refluxed with DMF at 130 ^{o}C for 24 hrs and constantly checked for completion using TLC. The reactants for this competition reaction were introduced with the same molar quantities.

The setup of the reaction was done to try to assimilate a closed system as close as possible in the absence of oxygen.

In order to accomplish this, solvent was gassed in cycles with nitrogen in order to remove dissolved oxygen. Upon addition of the chemicals the reflux system was protected with rubber stoppers and system pressure was regulated with needles using low pressure nitrogen gas.

3.2.4 Transmetallation/demetallation reaction between $VOSO_4/NiSO_4$ and MTPP and VOTPP/NiTPP and MSO_4 in the presence of oxygen. STAGE 2 and STAGE 3 respectively.

Reaction was conducted in the same condition as in the competition reactions in the presence of oxygen. The reactants were mixed in the same molar proportions to be able to quantify any behavior observed.

3.2.5 Transmetallation/demetallation reaction between $VOSO_4/NiSO_4$ and MTPP and VOTPP/NiTPP and MSO_4 in the absence of oxygen. STAGE 5 and STAGE 6 respectively.

Closed system was constructed as in the nitrogen competition reactions by using rubber stoppers, solvent degassing, and constant nitrogen flow to prevent reintroduction of oxygen into the reaction vessel. In this reaction setting same mole content of each reactant was used in the reaction using DMF as solvent at 130 ^oC for 24 hrs.

3.2.6 Competition reactions between $VOSO_4/NiSO_4$ and MTPP in the presence of sulfides. STAGE 7.

Closed system was constructed as in the nitrogen competition reactions by using rubber stoppers, solvent degassing, and constant nitrogen flow to prevent reintroduction of oxygen into the reaction vessel. In this reaction setting excess of ten equivalents of Na_2S and the same mole content of each of the remaining reactant was used in the reaction using DMF as solvent at 130^oC for 24 hrs.

3.2.7 Isolation of products from reactions

Reaction mixtures were removed of DMF by rotovaporation. The resulting product mixture was redissolved in chloroform and washed in water to remove salts used in the reaction. Upon washing of the chloroform solution several times, the wet chloroform was dry up over magnesium sulfate for 1hr. The powder was removed by filtration of the solution and the organic product mixture was stored dried capped for later characterization.

3.2.8 Porphyrin Ultraviolet-Visible characterization

All samples were characterized using the solvent system selected for chromatography in order to determine the exact peak shifts. In order to record spectra at appropriate absorbance ranges the sample concentrations were kept at 1E-3 g/ml at room temperature. Samples were solubilized and filtered just before characterization to prevent any decomposition. UV-VIS spectra were recorded on a Perkin Elmer Lambda spectrometer using WinLab software to process the spectra. Scan parameters were set to record absorbance from 200-800 nm. The samples were measured using a one centimeter quartz cuvette. Before any measurements a background correction was performed using the 75% ethyl acetate/25% toluene mixture.

3.3 CHARACTERIZATION OF REACTION PRODUCTS

3.3.1 Column Chromatography of TPP and MTPP

Thin layer chromatography was conducted on all commercial TPP/MTPP to determine solvent conditions for separation in column chromatography. Retention factor of the samples were very similar due to the sticking similarities in molecular structure. Silica was used for the separation of the product mixture at room temperature. Solvent selection was limited due to the poor solubility of the porphyrin derivatives. The solvent system that proved to be more efficient in the separation of TPP and the different MTPP samples was a mixture of 75% ethyl acetate and 25% toluene. Fractions collected were spotted by using TLC and fractions were isolated for their analysis.

3.3.2 High Performance Liquid Chromatography (HPLC) conditions

Selections of some absorption peaks from the characterization of the samples in UV-VIS were used in the HPLC for detection; 420, 526, 546, 560, and 600 nm. Pure samples were run in the system, with 75% ethyl acetate and 25% toluene, in order to determine the flow rate that gave the best time gaps between the metalloporphyrins and allowed for proper separation I the mixtures. Several other solvent systems were tested in the HPLC, but 75% ethyl acetate and 25% toluene proved to be the most efficient. The chromatography analysis was performed using an Agilent 1100 system.

3.3.3 Mass Spectrometry

In order to verify the formation of the desired products (metalloporphyrins) it was performed MS over each experiment of competition and demetallation using the JEOL-DS equipment at chemistry building. The mixture of solvents was 75% ethyl acetate and 25% toluene. Reserpine, at 608.34, was used for the calibration of the instrument and determination of the m/z product signals. Electronspray ionization technique in positive mode was used for the characterization of the compounds.

3.4 RESULTS AND DISCUSSION

3.4.1 Chemical reactions

Detailed breakdowns of the reaction conditions as well as the specific yields of the reactions in column chromatography are found in the appendix A.

3.4.2 Ultraviolet-Visible characterization of TPP and MTPP

It was noted very early that the color intrinsic of porphyrins came about their conjugated 18 pi-electron system. Porphyrin spectra can be characterized into the Q-bands and the Soret bands coming from absorption in the visible and ultraviolet regions of the spectrum respectively. Thousands of variations coming from functionalization of the porphyrin molecule change the conjugation pathway of the aromatic system, which can affect the absorption pattern of the spectrum. (Gouterman, 1961; Whitten et al. 1968; Smith, 1976; Dolphin, 1978; Nappa & Valentine, 1978; Wang et al. 1984; Rubio et al. 1999).

Absorption spectra of porphyrin molecules has been explained using the Gouterman model, also named the four-orbital model that gives rise to the four absorption peaks in the UV-VIS spectrum. HOMO to LUMO transition come from the excitation of electrons from two p-orbitals to two anitibond thus the name. This was first applied in 1959 by Martin Gouterman tha enphisezed the importance of charge localization on properties of spectra. (Gouterman, 1959; Gouterman, 1961).

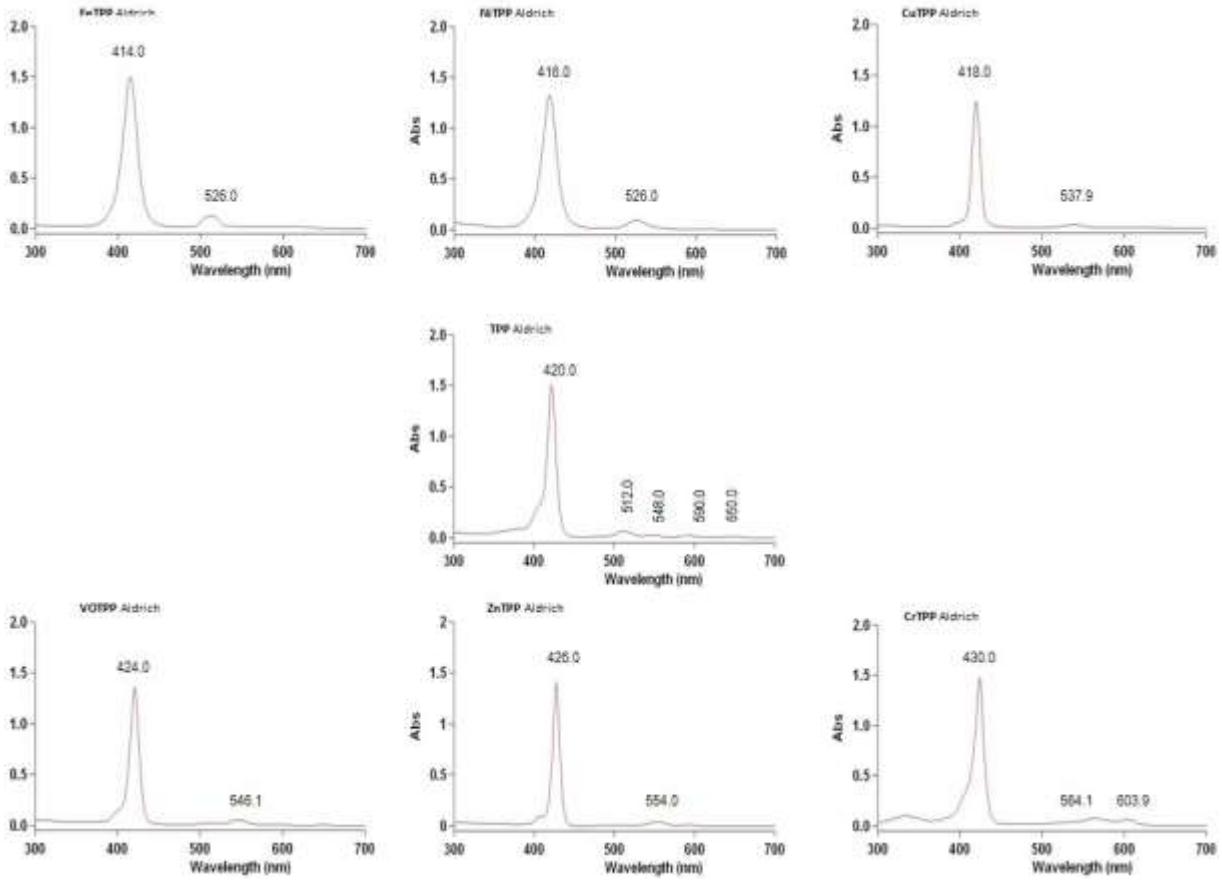

Figure 3.2 Ultraviolet-Visible spectra collected in 75% ethyl acetate and 25% toluene for TPP and MTPP derivatives.

According to this theory, as reported in Figure N, the four absorption peaks shown in the center spectrum of TPP arise from transitions between two HOMOs and two LUMOs. The formation of molecular orbitals results in the generation of higher energy antibonding orbitals and lower energy orbitals. The first electronic region in porphyrin spectra rises from electronic excitation from ground state to the second excited state (S0 S2), the resulting peak is named B or Soret band. The B and the Q bands both arise from $\pi - \pi^*$ transitions and can be explained by considering the four Gouterman orbitals (HOMO and LUMO orbitals) (the Gouterman four orbital model).

The wavelength absorption range is 380-500 nm depending on the type of functionalization in the ring. The second region of the spectra gives rise to a set of peak known

as the Q-bands, this rises from a weaker electronic transition (S0 S1) between 500-750 nm. UV-VIS is a good technique to observe guest binding changes in the electronic structure of the molecule. (Yang et al. 2002; Gulino et al., 2005; Di Natale et al. 2000; Paolesse & D'Amico, 2007) CD, (Scolaro et al. 2004; Balaz et al. , 2005) fluorescence, (Zhang et al., 2004; Zhou et al., 2006) and NMR spectroscopy (Shundo et al., 2009; Tong et al., 1999).

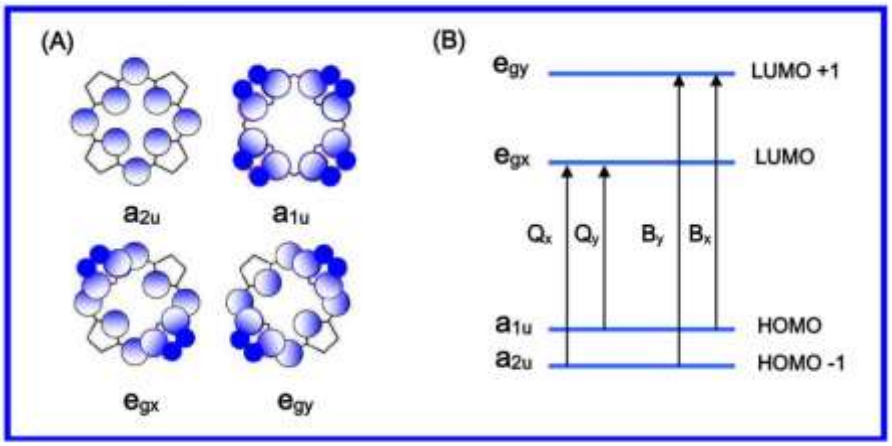

Figure 3.3 Left; Model of the four molecular orbitals from porphyrin rings, right; HOMO and LUMO electronic transitions that give rise to the characteristic and Soret Q bands in porphyrin UV-VIS spectra.

Intensity of the Q-bands depends on the type of functionalization of the porphyrin ring. In the case of tetraphenylporphyrin the substitution is done in the meso position of the ring, which gives rise to the *phyllo-type* spectrum that has a decreasing Q band intesntity of IV > II > III > I (Milgron 1997).

Porphyrin molecules are often associated with metals due to the chelate ability of the ring. In the laboratory usually the porphyrin molecules are synthesized first followed by metal chelation. In ordet to incorporate a metal ion M^{n+} into the porphyrin ring H_2P to form $MP^{(n-2)+}$, the two pyrrole amine with protons disassociate with them as shown in the reaction below

$$M^{n+} + H_2P \rightarrow MP^{(n-2)} + 2H^+$$

Ultraviolet-visible spectra for metalloporphyrins can be classiffien into two types based on metal d-orbital interaction with π orbitals in the ring. The first type comes from the coordination of metals with a closed shell including metals d0 or d10, which form relatively low energy spectra with little d- π interaction. When metals have partially filled subshells there is bigger backbonding to π orbitals in the system resulting in an increased Hypsoporphyrins are metalloporphyrins in π to π* energy separation causing the electronic absorptions to undergo hypsochromic or blue shifts.

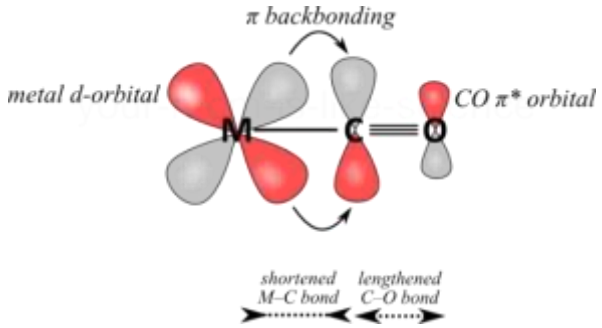

Figure 3.4 d- π backbonding interaction

The Figure 3.4 shows d- π backbonding interaction, which causes hypsochromic shifts by increased backbonding.

Figure 3.5 Representation of two type of metal coordination depending on ion size.

Left; Pyrrole amine metal coordination where the ion radius fits in the porphyrin pocket. Right; Pyrrole amine – metal coordination where the ion radius is too big and the porphyrin ring is distorted making these derivates more unstable (SAT porphyrins).

Metalloporphyrins are classified into two depending on the type of metal ion coordination to the center pyrrole rings. Factors like charge of the bound ion and charge have an effect on the

UV-VIS spectra and the stability of the complex overall. The bigger the size of the ions the more distortion is cause by its coordination to the porphyrin rings.

The majority of the metalloporphyrins are of the regular type and coordinate into the porphyrins without ring distortion. Once coordinated the meal ions fall within the plane of the ring due to their fitting size. Ions within 55 – 80 nm are allowed into the pocket formed by the pyrolle rings in the porphyrin center without causing molecular distortion. (Khan & Bruice, 2003).

If, however, the size of the metal ion is too big (80-90 pm or more) to fit into the porphyrin center, then the metal ions fall out of the porphyrin plane causing a distortion after orbital alignment. These type of complexes are much more stable than regular metallo-porphyrins due to the increase strain caused by the distortion of the structure. Metalloporphyrins of this type are known as *sitting on top or SAT,* (Sketch 1). (Fleischer & Wang 1960; Barkigia et al., 1980; Liao et al., 2006; Walker et al., 2010)

One can clearly observe consistency with the information presented just now and the spectra of tetraphenylporphyrin and its metalloporphyrin derivatives; Ni, Fe, Cu, Vo, Zn, and Cr. Tetraphenylporphyrin spectrum Q-band pattern appears at 512, 548, 590, and 650 nm. In addition the most energetic electronic transition comes from the electronic excitation giving rise to the Soret band at 420 nm. Simplification of the metalloporphyrins spectra resulting in a reduction in the number of Q-bands is confirmed on all metalloporphyrin measurements. (Bailey & Hambright, 2003; Hambright et al., 2001; Lavallee, 1987; Funahashi et al., 2001).

Through the analysis of the metalloporphyrin spectra one can observe that the complex that yield the most energetic transitions is the Nickel (II) tetraphenylporphyrin complex with a Soret band at 416 nm and a Q-band at 526 nm. Conversely the Chromium (II) tetraphenylporphyrin is the complex that displays the least energetic transitions with a Soret Band of 430nm, and a set of Q-band at 564 and 604nm. Iron (II) tetraphenylporphyrin soret band appears at 414 nm and its Q-band at 526 nm, Copper (II) tetraphenylporphyrin Soret Band appears at 418 nm while its Q-band at 538 nm, Zinc (II) tetraphenylporphyrin Soret band Soret

band shows at 426 nm and its Q-band at 554 nm, and finally vanadyl tetraphenylporphyrin has a Soret band at 424 nm and a Q-band at 546 nm.

One can observe that based on the theory the spectra recorded corresponds to a meso-tetraphenylporphyrin, and that metallo-tetraphenylporphyrins do in fact get simple Q-band pattern due to the increased symmetry of the molecule.

As to their electronic absorption, they display extreme intense bands, the so-called Soret or B-bands in the 380–500 nm range with molar extinction coefficients of 10^5 M^{-1} cm^{-1}. Moreover, at longer wavelengths, in the 500–750-nm range, their spectra contain a set of weaker, but still considerably intense Q bands with molar extinction coefficients of 10^4 M^{-1} cm^{-1}. Thus, their absorption bands significantly overlap with the emission spectrum of the solar radiation reaching the biosphere, resulting in efficient tools for conversion of radiation to chemical energy. In such a conversion, the favorable emission and energy transfer properties of porphyrin derivatives are indispensable as in the case of chlorophylls, which contain magnesium ion in the core of the macrocycle. Also, metalloporphyrins can be utilized in artificial photosynthetic systems, modelling the most important function of the green plants (Harriman et al., 1996).

The studies of the wavelength shift of their adsorption band and the absorbance changes as function of pH, temperature, solvent change, reaction with metal ions and other parameters permits to obtained accurate information about equilibrium, complexation, kinetic and aggregation of porphyrins.

This review, resumes the best successes in the use of spectrophotometer UV-Vis for explained the chemical characteristics of this extraordinary group of natural occurring molecules and clarifies the potential of these molecules in many fields of application.

3.4.3 Column chromatography characterization of competition and demetallation reactions

Reactions of metal demetallation as well as metal competitions for free base porphyrin were classified using column chromatography. Column was run in the conditions specified in the materials and methodology section. Products of reaction were isolated manually, rotovaporated to remove solvent, and weighted at the end of the experiment to determine yields.

3.4.3.1 Competitions reactions analyzed by silica column

Competition reactions are intended in this synthesis to determine the major product formed in order to determine the thermodynamically favored product of the reaction. Since both metal salts used in the competition carry sulfate ions then you can eliminate any kinetic factors that could arise.

GRAPH 3.1: COLUMNS COMPETITION Open System. $VOSO_4$ + MSO_4 +TPP

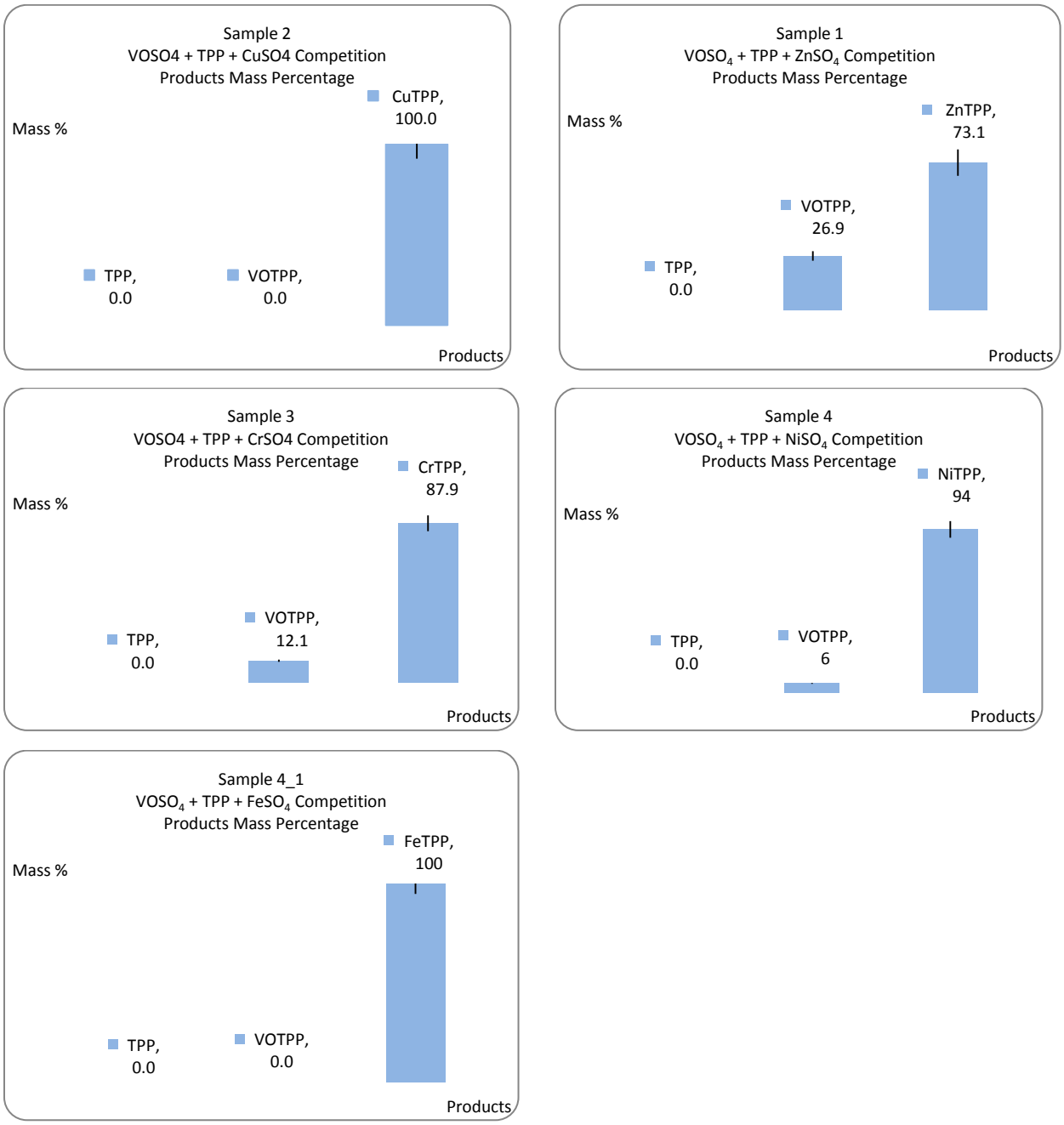

The first stage of competition reactions involves the competition of vanadyl with the rest of the metal candidates in the presence of oxygen. In this set of reactions one can see that the products formed in the greatest abundance are the iron and copper tetraphenylporphyrin molecules. From the rest of the competition you can see greater formation of Nickel, followed by chromium, followed by zinc. Each experiment was conducted at least three times and the yields

of the products are graphed with its error bar. This was due to the difficulty of dealing with small quantities and keeping compound loses at a minimum of the technique itself.

GRAPH 3.2: COLUMNS COMPETITION Open System. $NiSO_4 + MSO_4 + TPP$

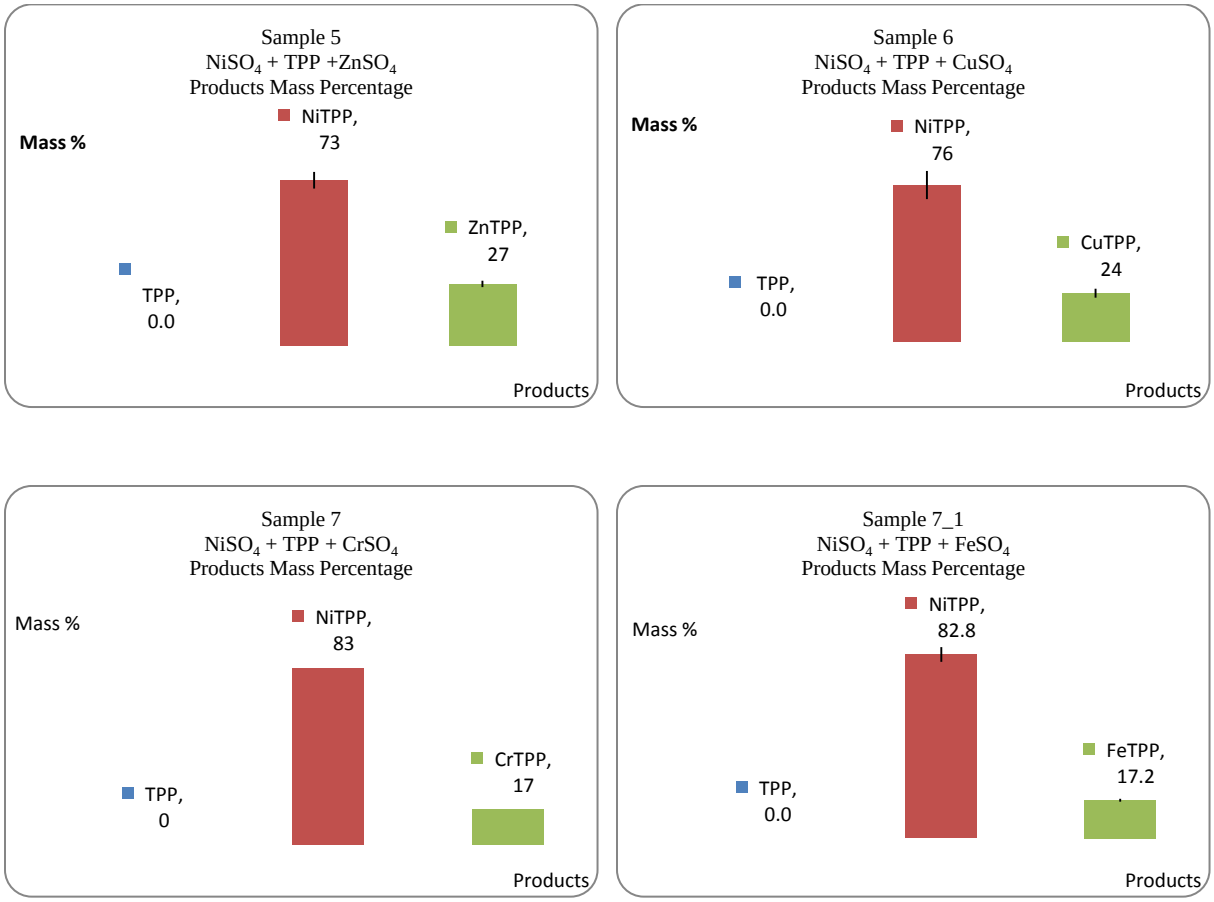

The second stages of the competition reactions involve nickel with the rest of the metal candidates in the presence of oxygen. In this set of reactions one can see that the product formed in greatest abundance is NiTPP molecules in all instances. One can see that chromium and zinc formed in larger quantities than iron and chromium under these conditions.

GRAPH 3.3: COLUMNS COMPETITION Nitrogen. $VOSO_4$ + MSO_4 +TPP

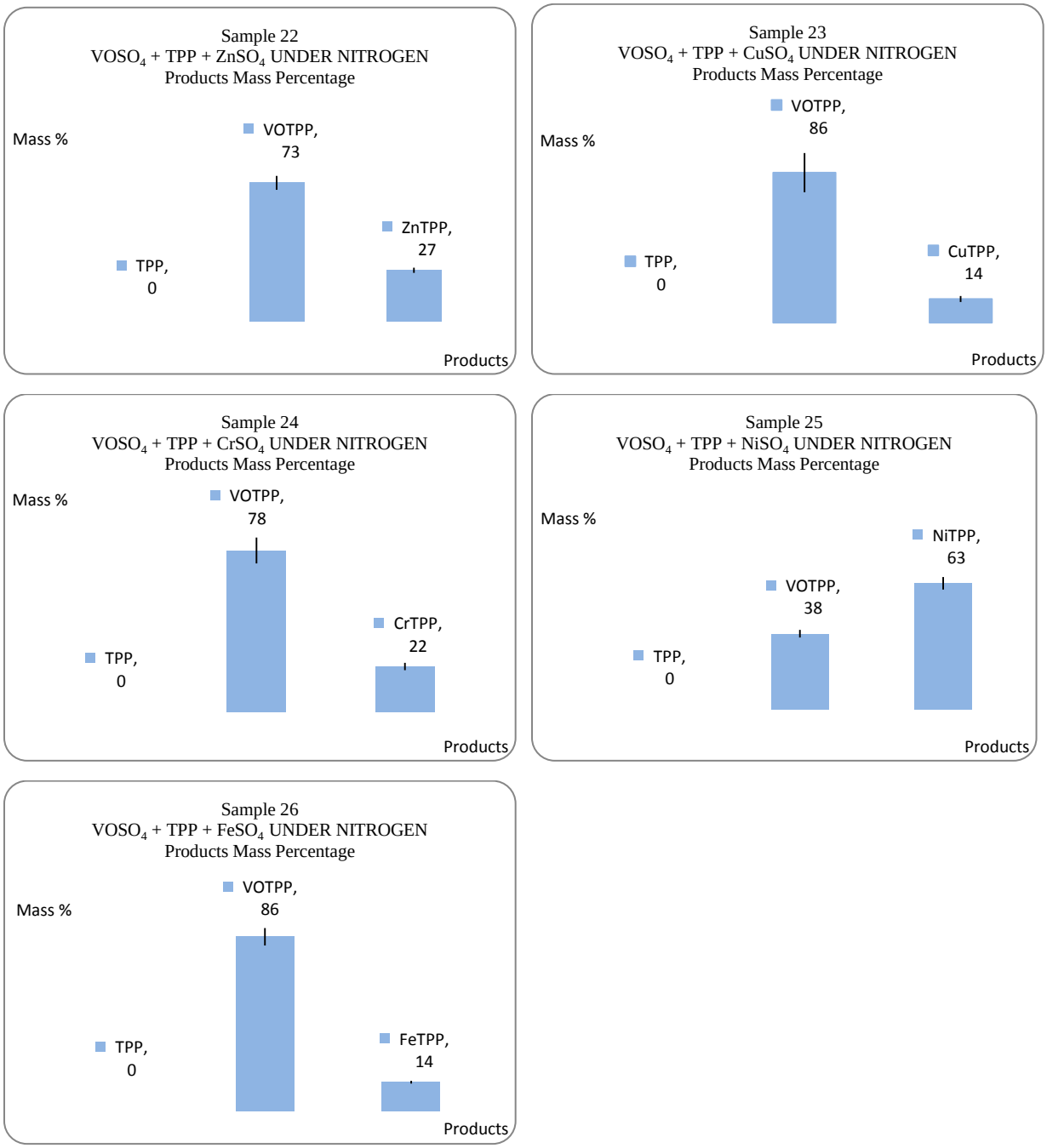

The third stage of competition reactions involves the competition of vanadyl and the rest of the metal candidates in the absence of oxygen. This stage compared to stage number 1 has the same reactants but exposed to nitrogen instead of oxygen, but reaction products display a very different pattern from those in stage 1. Vanadyl in the absence of oxygen favors the formation

VoTPP instead of other MTPP molecules except in the competition with NiTPP where this last product is generated in greater quanity. Competition with the other metals shows a greater formation of zinc followed by chromium followed by copper and iron.

GRAPH 3.4: COLUMNS COMPETITION Nitrogen. $NiSO_4$ + MSO_4 +TPP

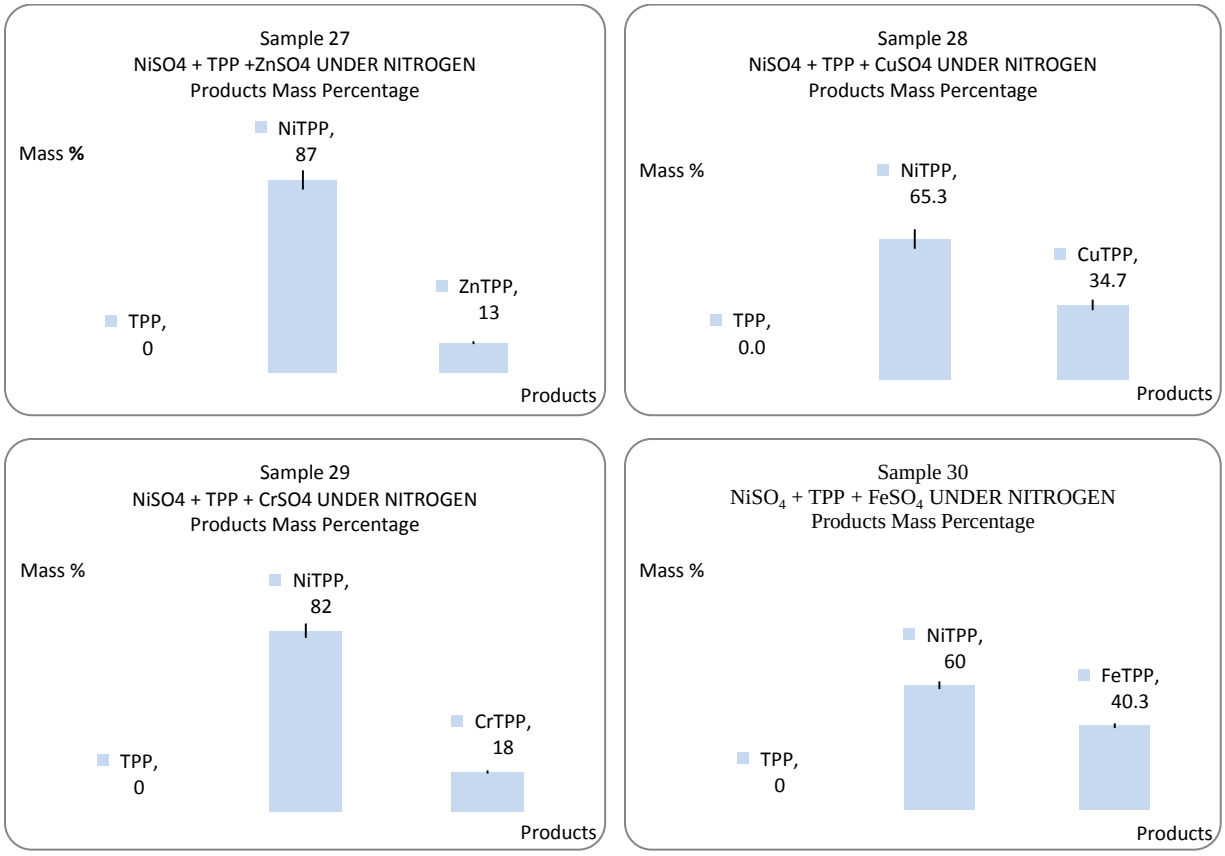

Stage number four results show the same pattern as stage 2, which uses the same reactants but in the absence of oxygen. The other MTPP formed showed a greater formation for FeTPP, CuTPP, CrTPP, and ZnTPP. In the first four stages there is no leftover TPP reactant left in solution.

GRAPH 3.5: COLUMNS COMPETITIONS Sodium Sulfide. $VOSO_4$ + MSO_4 + TPP

In order to emulate competition reactions occurring in nature in the presence of hydrogen sulfide, a sulfide salt in excess was used to determine the behavior of the competition under these anoxic conditions.

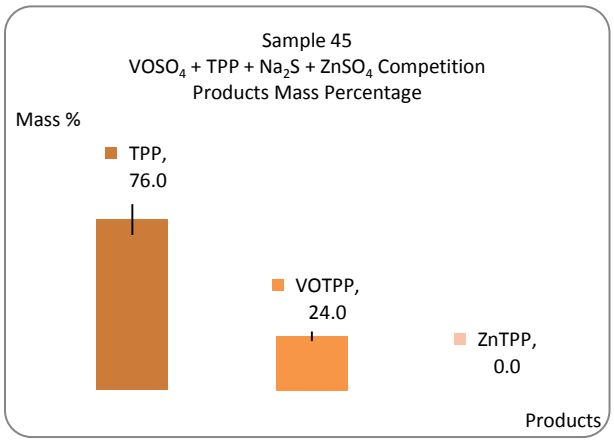

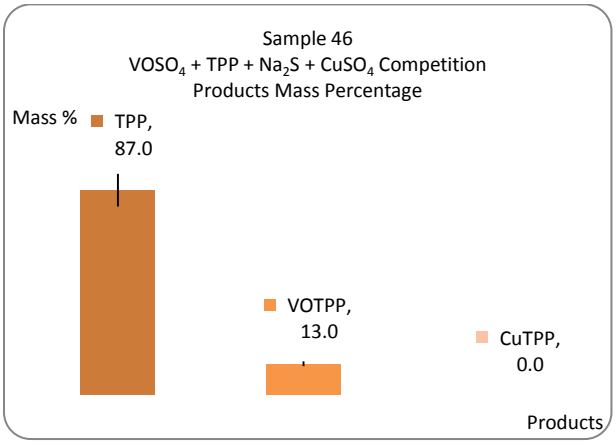

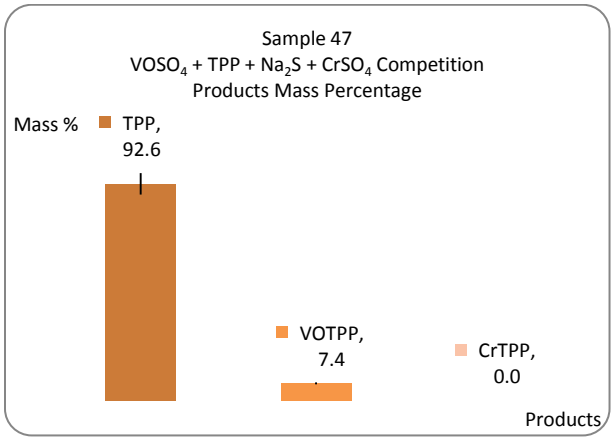

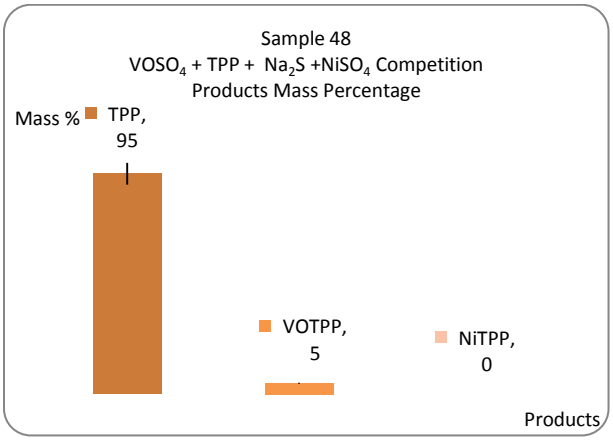

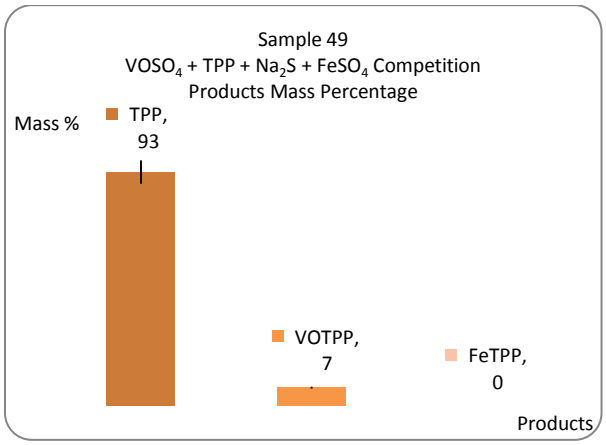

The fifth stage of competition reaction was performed in the presence of sulfide ions in excess. In these set of reactions vanadyl and metal salts competed for chelation with TPP. As one can see from the results vanadyl is the only metalloporphyrin formed from all of the reaction run. This shows less affinity of vanadyl for sulfide than other metals which upon reaction from insoluble salts and precipitate out of solution. Still aside from Na_2S all other reactants were introduced in the same molar quantities and since there is TPP available one can see that only part of the vanadyl. One can see from the relative abundance on all the different reactions that VoTPP formation ranges from 5-24% and through the experiment layout column chromatography seems to be a limited technique for such reactions setups.

GRAPH 3.6: COLUMNS COMPETITIONS Sodium Sulfide. $NiSO_4$ + MSO_4 + TPP

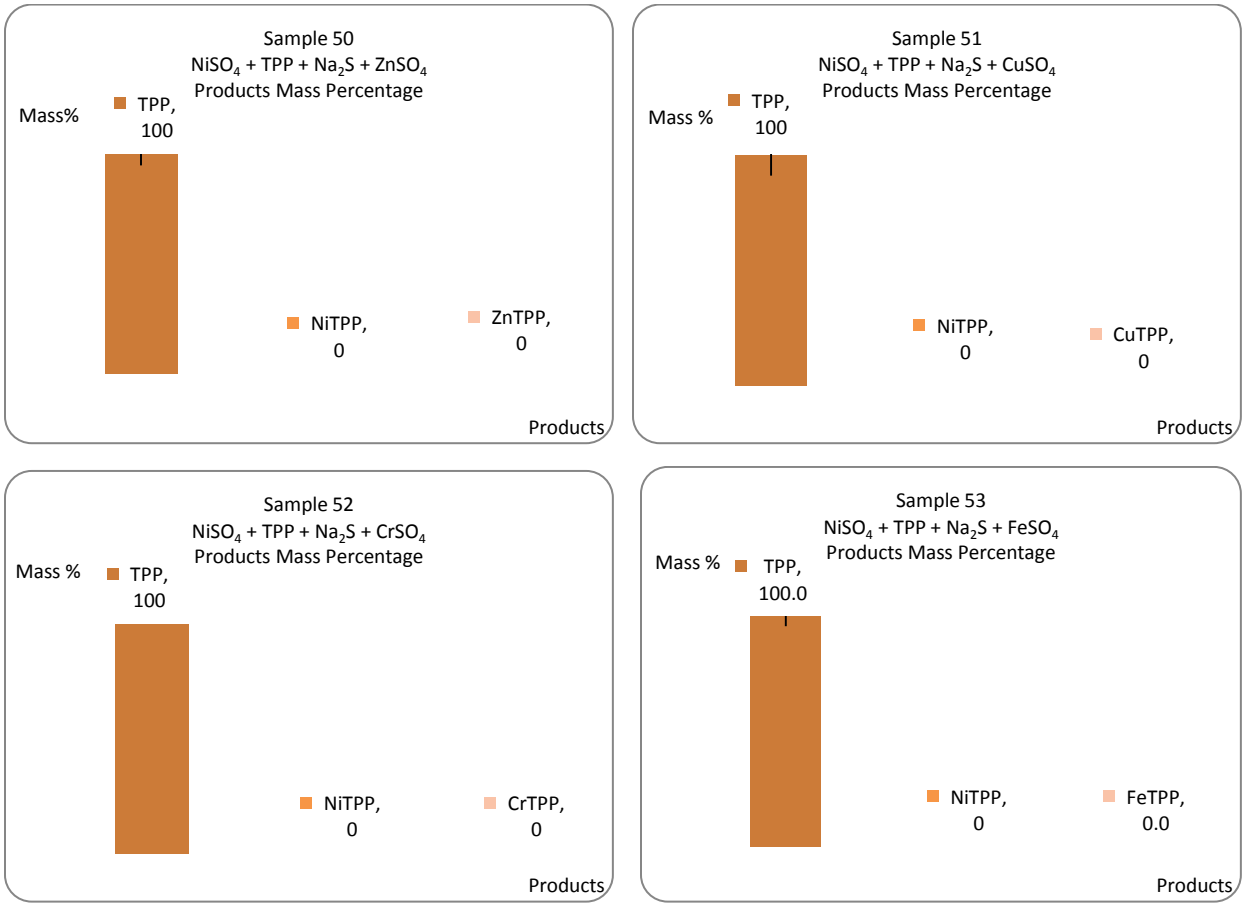

The sixth stage of competition reactions of Ni and other metal competition for chelation of TPP in the presence of excess Na_2S shows no formation of MTPP at all. These set of reactions shows that nickel does interact as observe in the literature to form insoluble minerals.

3.4.3.2 Transmetallation reactions analyzed by silica column

In order to test the possibility of transmetallation of vanadyl and nickel in the conditions already described for the reactions, experiments were conducted with all metal candidates MTPP.

GRAPH 3.7: COLUMNS TRANSMETALLATIONS. Open System. $VOSO_4$ + MTPP

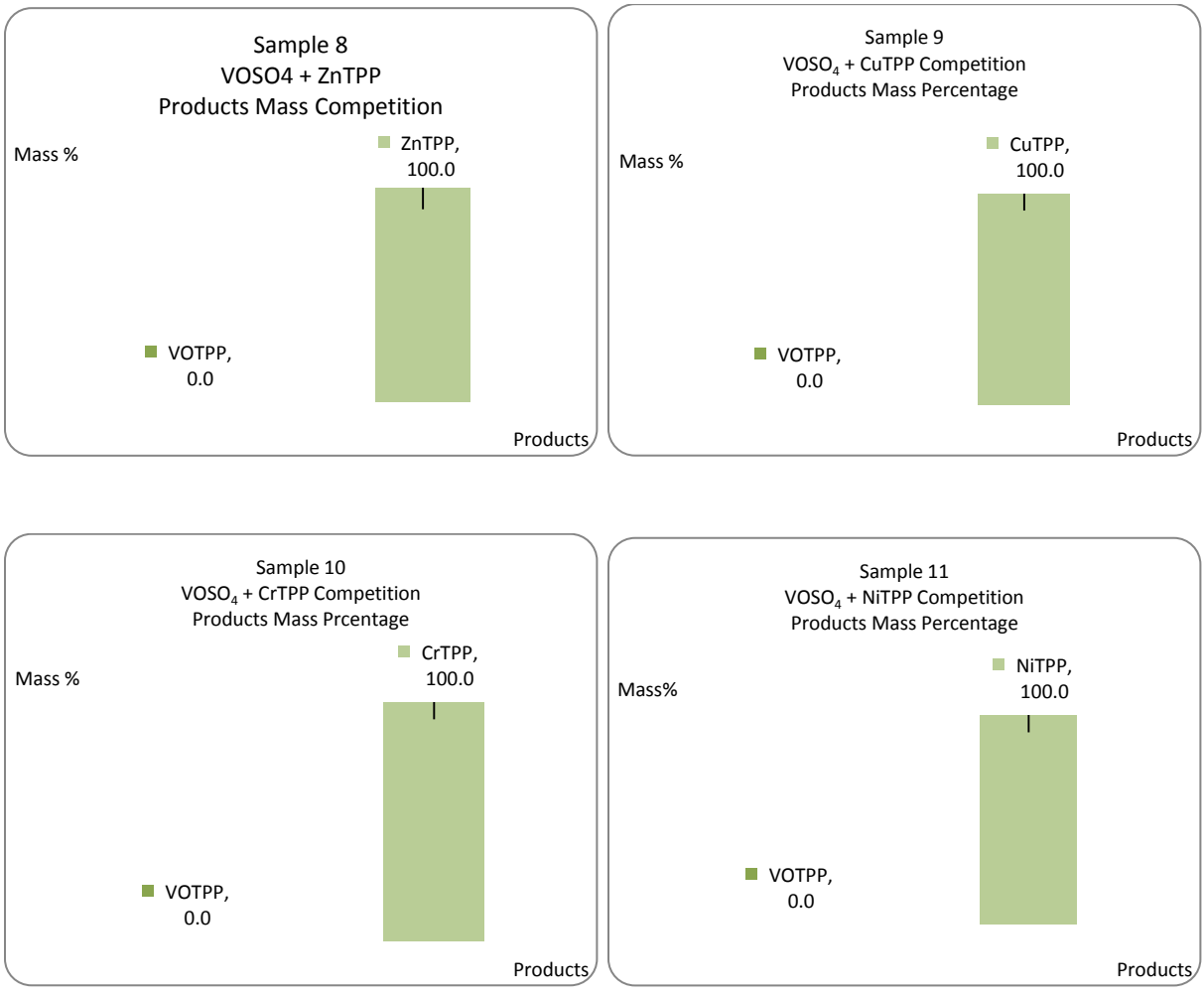

Transmetallation of MTPP by vanadyl behavior was tested by using equimolar ratios of each reactant in the presence of oxygen. The results of this transmetallation/demetallation stage

shows that the energy required for transmetallation is not met in the conditions at which the reactions took place. Due to the limited solubility of the porphyrin systems the ideal solvent system for this types of reaction remained DMF and the maximum temperature setting the reaction was taken to was 153 ^{o}C. This temperature setting completely covers the oil formation window temperature found in natural environments but not the pressure at which the samples are found.

GRAPH 3.8: COLUMNS TRANSMETALLATIONS. Open System. $NiSO_4$ + MTPP

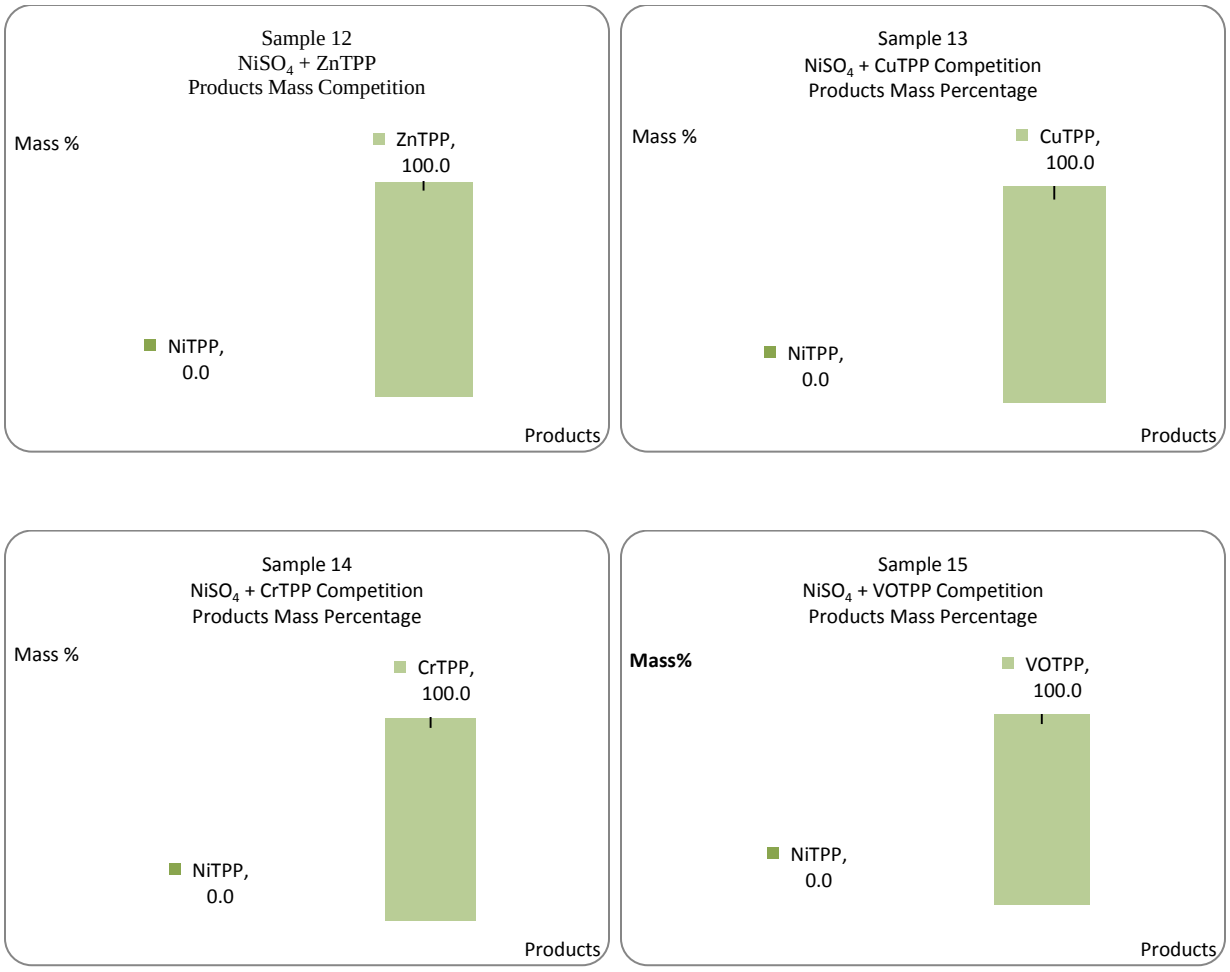

Transmetallation of MTPP by nickel behavior was tested by using equimolar ratios of each reactant in the presence of oxygen. The results of this transmetallation/demetallation stage shows that the energy required for transmetallation is not met in the conditions at which the reactions took place.

GRAPH 3.9: COLUMNS TRANSMETALLATIONS. Nitrogen. $VOSO_4$ + MTPP

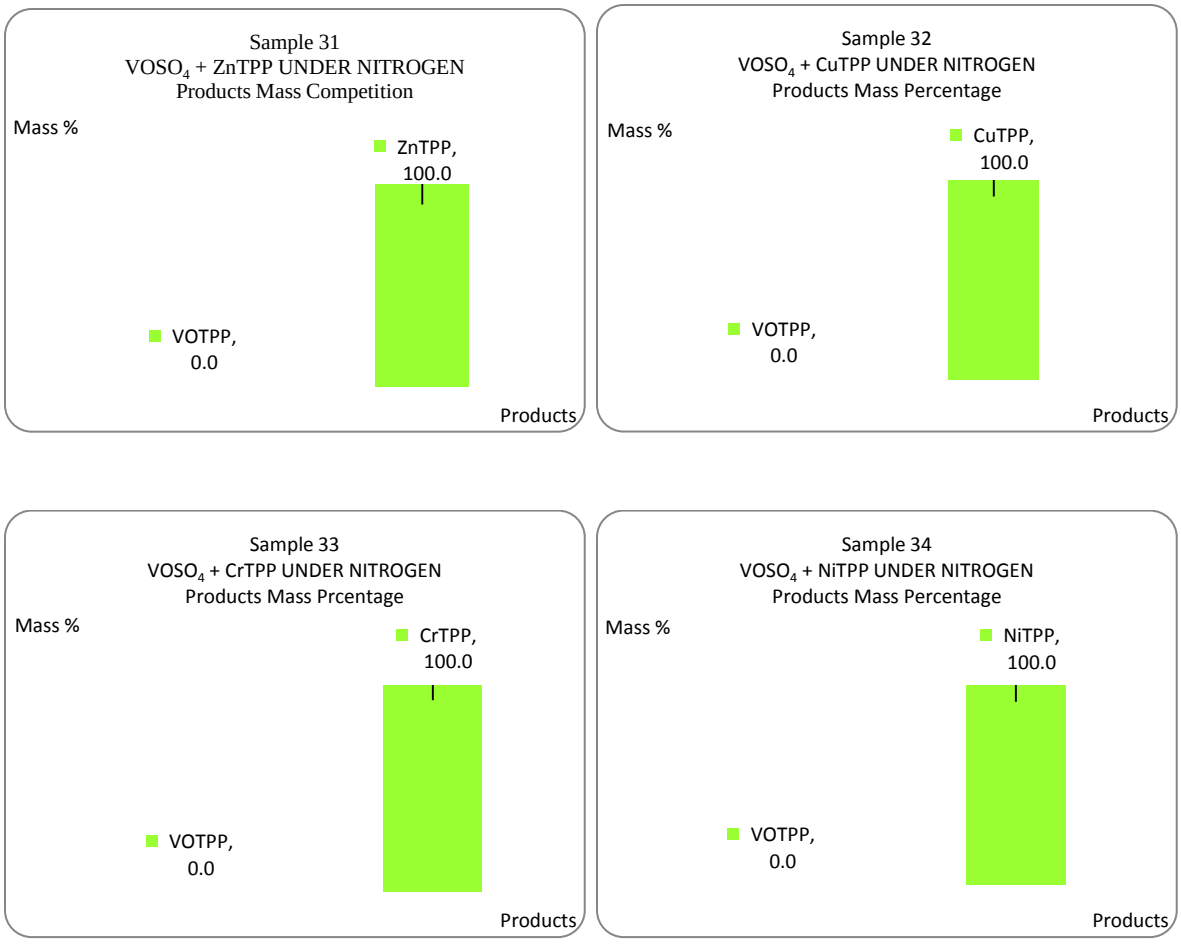

Transmetallation of MTPP by vanadyl behavior was tested by using equimolar ratios of each reactant in the absence of oxygen. The results of this transmetallation/demetallation stage shows that the energy required for transmetallation is not met in the conditions at which the reactions took place.

GRAPH 3.10: COLUMNS TRANSMETALLATIONS. Nitrogen. $NiSO_4$ + MTPP

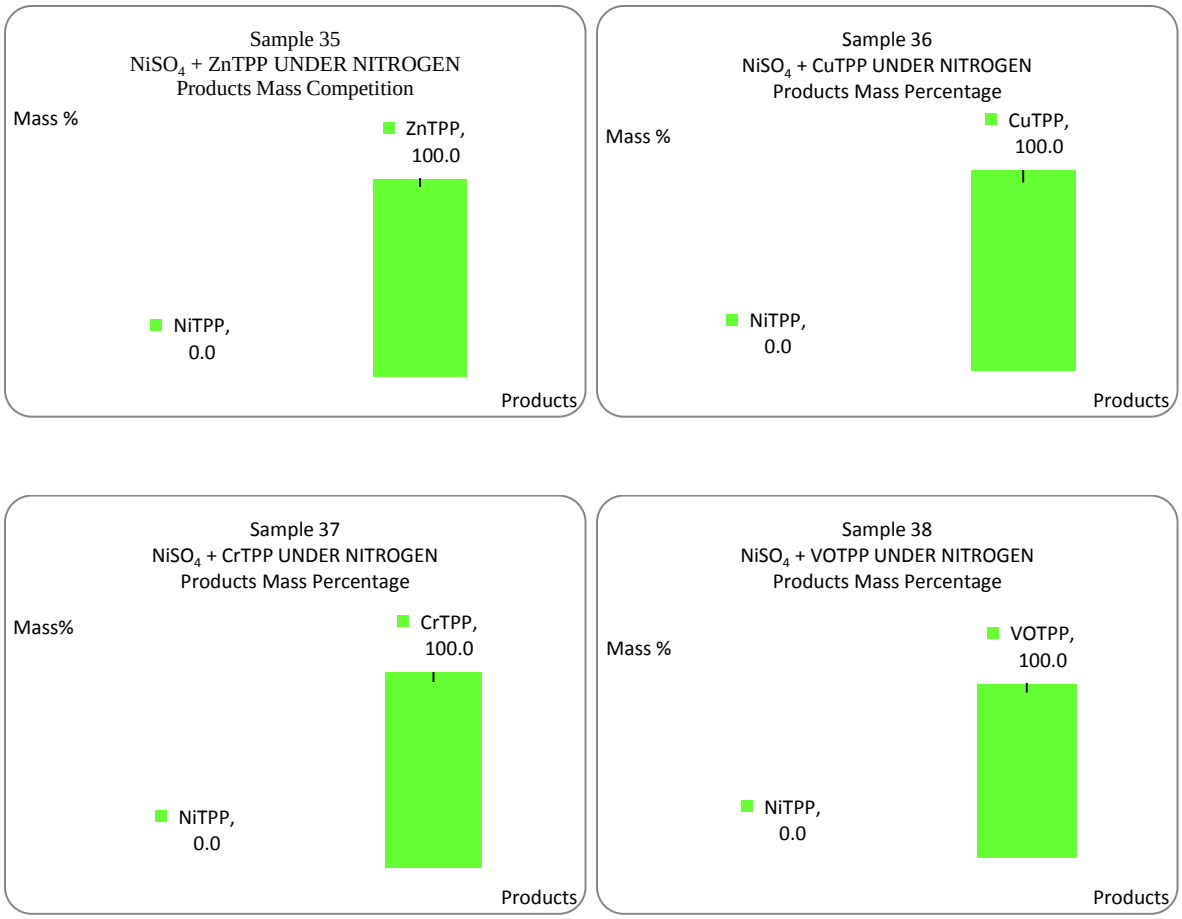

Transmetallation of MTPP by nickel behavior was tested by using equimolar ratios of each reactant in the absence of oxygen. The results of this transmetallation/demetallation stage shows that the energy required for transmetallation is not met in the conditions at which the reactions took place.

GRAPH 3.11: COLUMNS TRANSMETALLATIONS. Open System. VOTPP + MSO_4

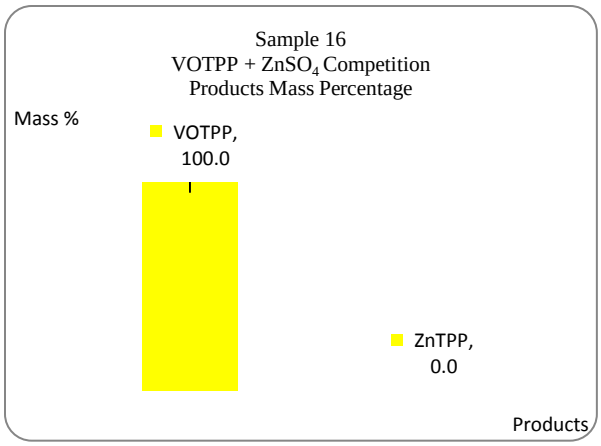

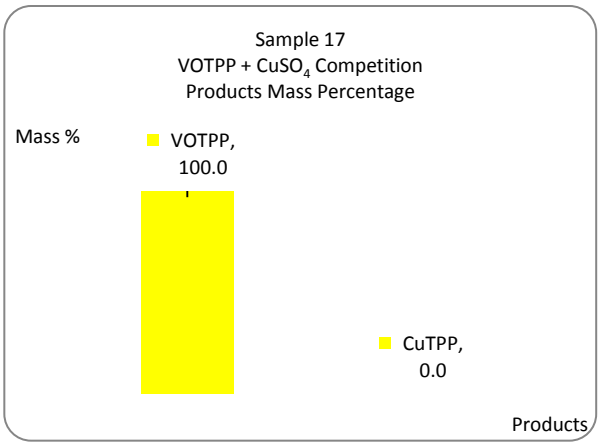

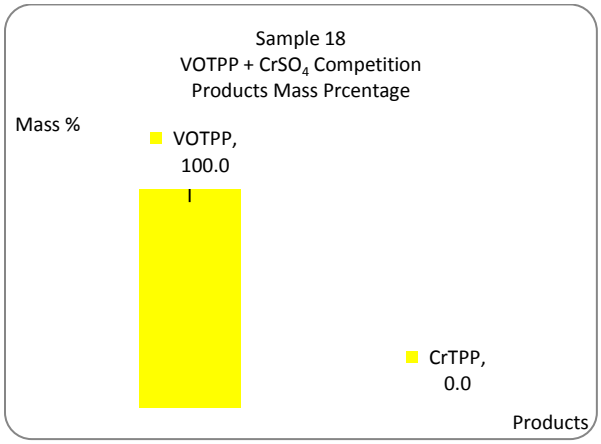

GRAPH 3.12: COLUMNS TRANSMETALLATIONS. Open System. NiTPP + MSO_4

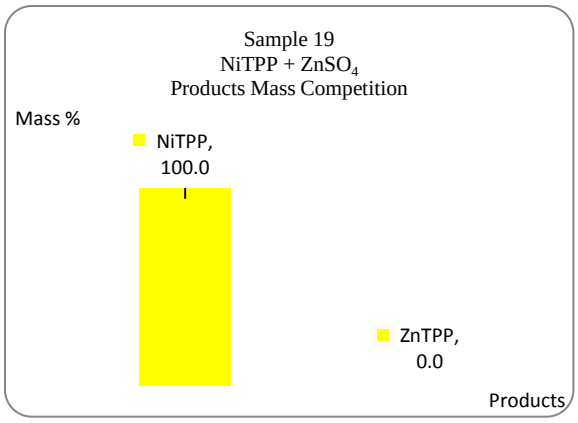

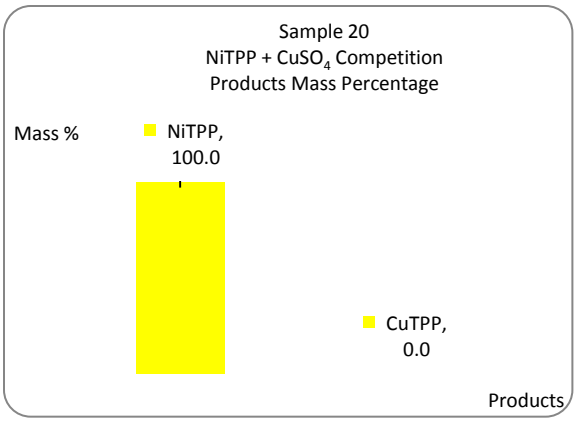

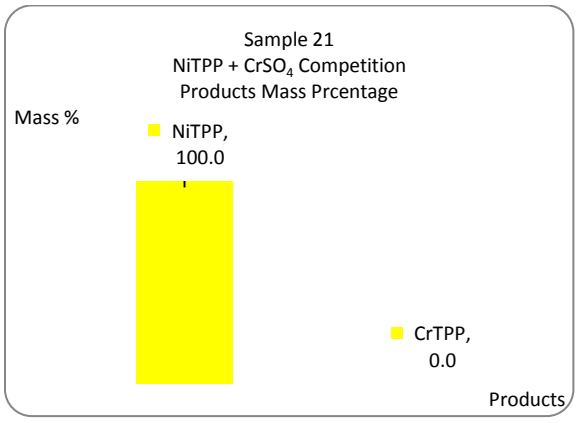

GRAPH 3.13: COLUMNS TRANSMETALLATIONS. Nitrogen. VOTPP + MSO_4

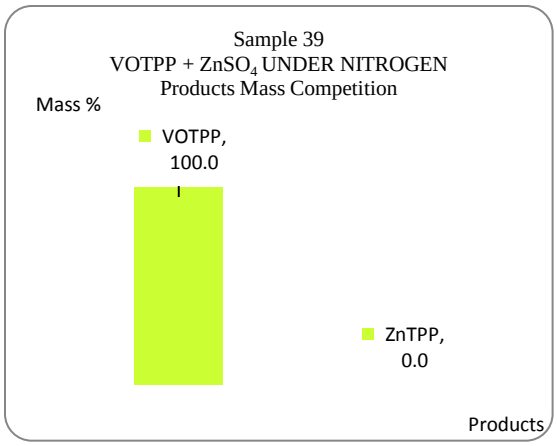

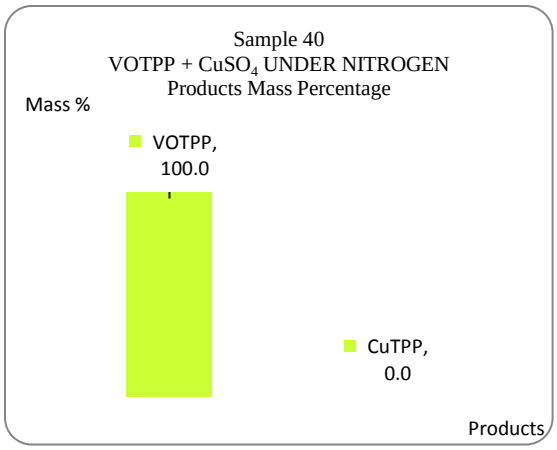

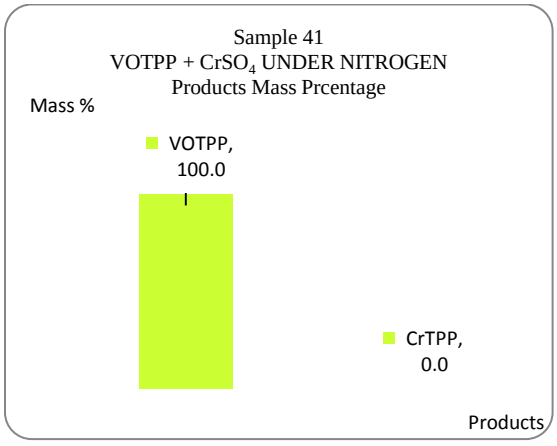

GRAPH 3.14: COLUMNS TRANSMETALLATIONS. Nitrogen. NiTPP + MSO_4

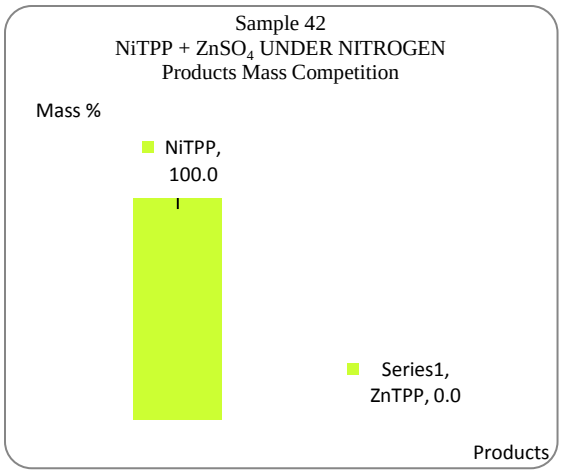

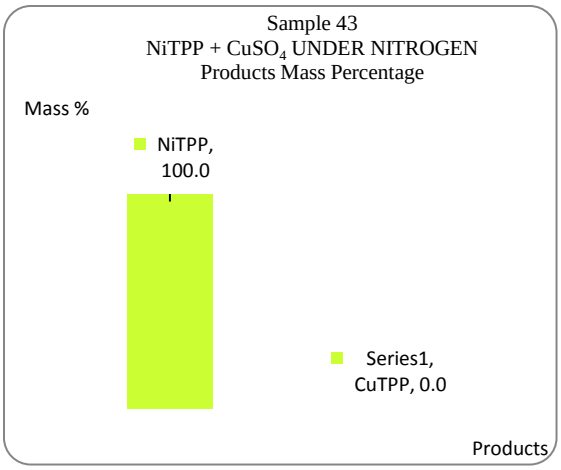

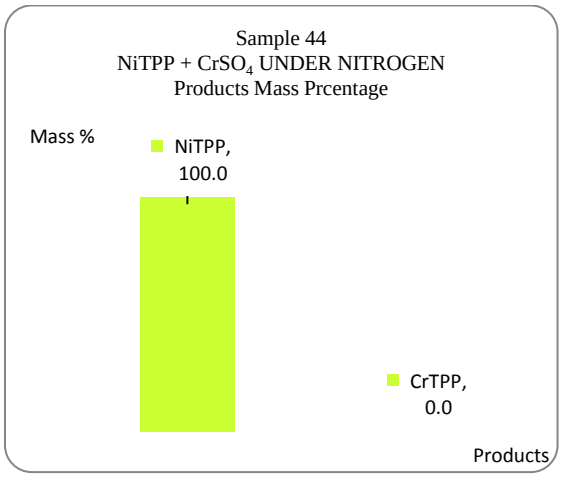

The final demetallation stage in the presence and absence of oxygen for the demetallation of VOTPP and NiTPP by MSO_4 showed no demetallation in any of the stages conducted.

3.4.4 High Performance Liquid Chromatography of Competition reactions

Column chromatography results showed interesting trends that were tested using a more refined technique in which products could be tracked by light absorption and a more accurate yield values can be found. In an attempt to determine, which metal forms the most thermodynamically stable product competition experiments were carried using similar metal salts. Since ion radii is a stability factor all salts with the exception of vanadyl were chosen to have an +2 oxidized metal, and also all salts shared the same counterion to eliminate affinity variations of suing different salt classes. Furthermore each reaction was run at least three times in order to give more validity to the results shown here.

Yields were taken from comparison of the peak areas in the different reaction chromatographs. In order to observe all the components in the reaction samples they were run at 420, 526, 546, 560, and 600 nm. Not all chromatographs shown in this work were run at the same wavelength, but the ones selected were those that showed all of the components in the reaction mixture. Exact detection times for peak appearance were used for the identification of each compound in the mixtures.

3.4.4.1 Vanadyl competition with Zn, Cu, Cr, Ni, and Fe in the presence of oxygen

Competition reaction of Vanadyl and Zinc in the presence of oxygen shows a product preference for the formation of ZnTPP with 76% yield and 24% yield of the VOTPP product. The competition with copper on the other hand shows a more dominant preference for the copper metal with a yield of 96% against 4% of VOTPP. The reaction with Chromium showed also showed a lesser preference for the vanadyl at 27% and 73% yield of the CrTPP. Nickel and vanadyl competition shows a preference for Nickel at 98% and vanadyl at 2%. Finally iron and vanadyl reaction shows a strong preference for iron at 95% yield against 5% of the vanadyl complex. In the presence of oxygen, copper and iron had the strongest preference for the porphyrin complexes, while vanadyl showed to be the least favorable product in every reaction. Since all of the salts used for competition contain the same counterion then one can rule out any kinetic factors for the formation of the metalloporphyrins. Therefore the competitions only

reflect the thermodynamic driven product. In the case for all competitions vanadyl lost in every single contest in the presence of oxygen as shown in the figure below. Metals available for the competition reaction completely exhausted the TPP in solution leaving only MTPP complexes.

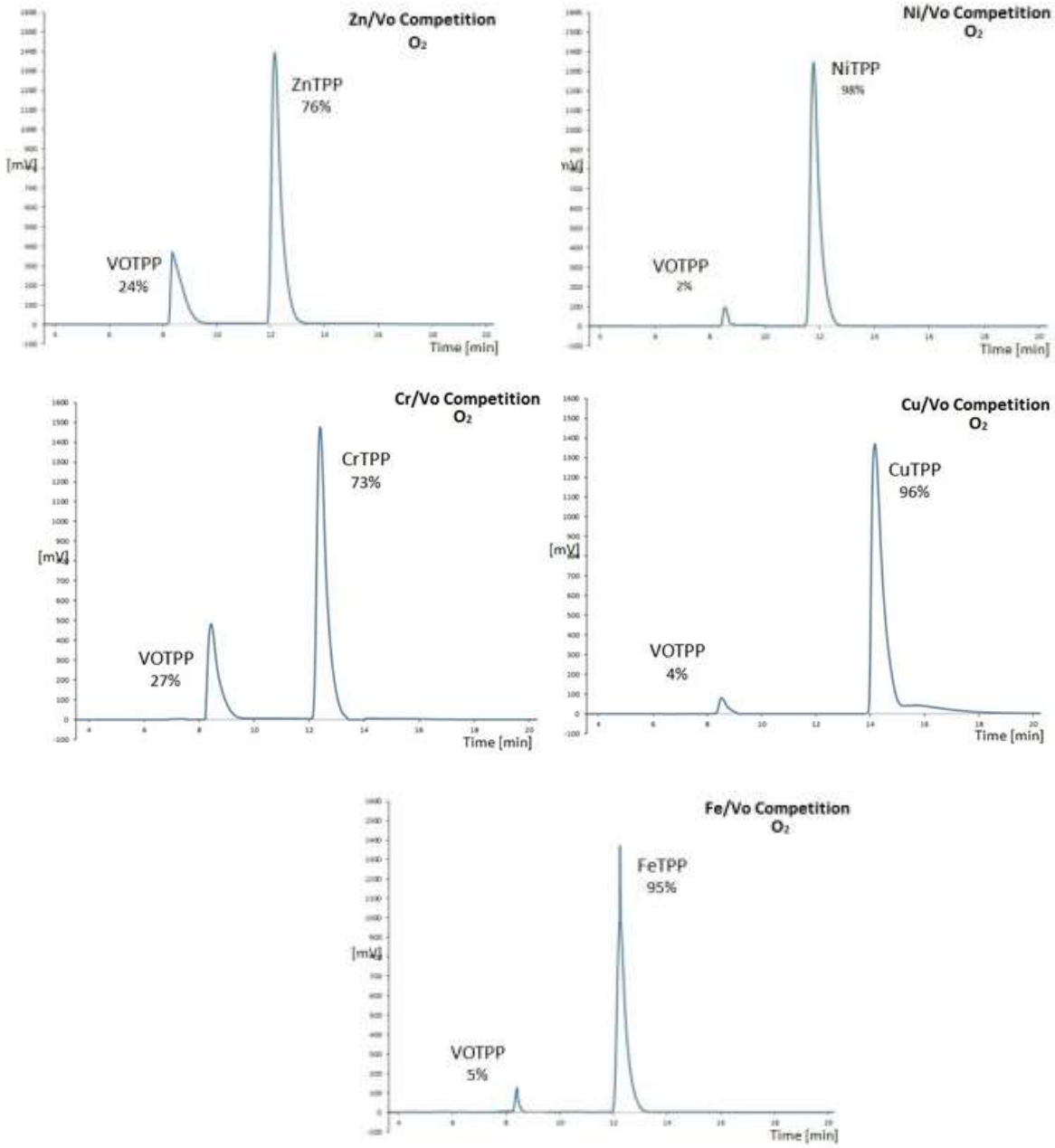

Figure 3.6: Vanadyl competition with Zn, Cu, Cr, Ni, and Fe in the presence of Oxygen

3.4.4.2 Nickel competition with Zn, Cu, Cr, Vo, and Fe in the presence of oxygen

Nickel reaction with zinc competition for TPP in the presence of oxygen favored the formation of the Nickel product with a yield of 56% and Zinc with a 44%. Contest reaction with copper showed selection of nickel at 52% yield and 48% of CuTPP. In the case of the reaction with Chromium metal it also showed a preference for NiTPP with a yield of 54% and CrTPP with 46%. Finally the competition reaction with Iron salt showed 46% yield of FeTPP and 54% of NiTPP. In this set of reactions Nickel was the thermodynamic product in all competitions in the presence of oxygen. Although the closest competition was between Nickel and Copper with only 4% yield difference. On the other hand the competition with vanadyl formed mostly nickel product. In this competition the yields of Iron and Chromium came out to be the same. Metals available for the competition reaction completely exhausted the TPP in solution leaving only MTPP complexes.

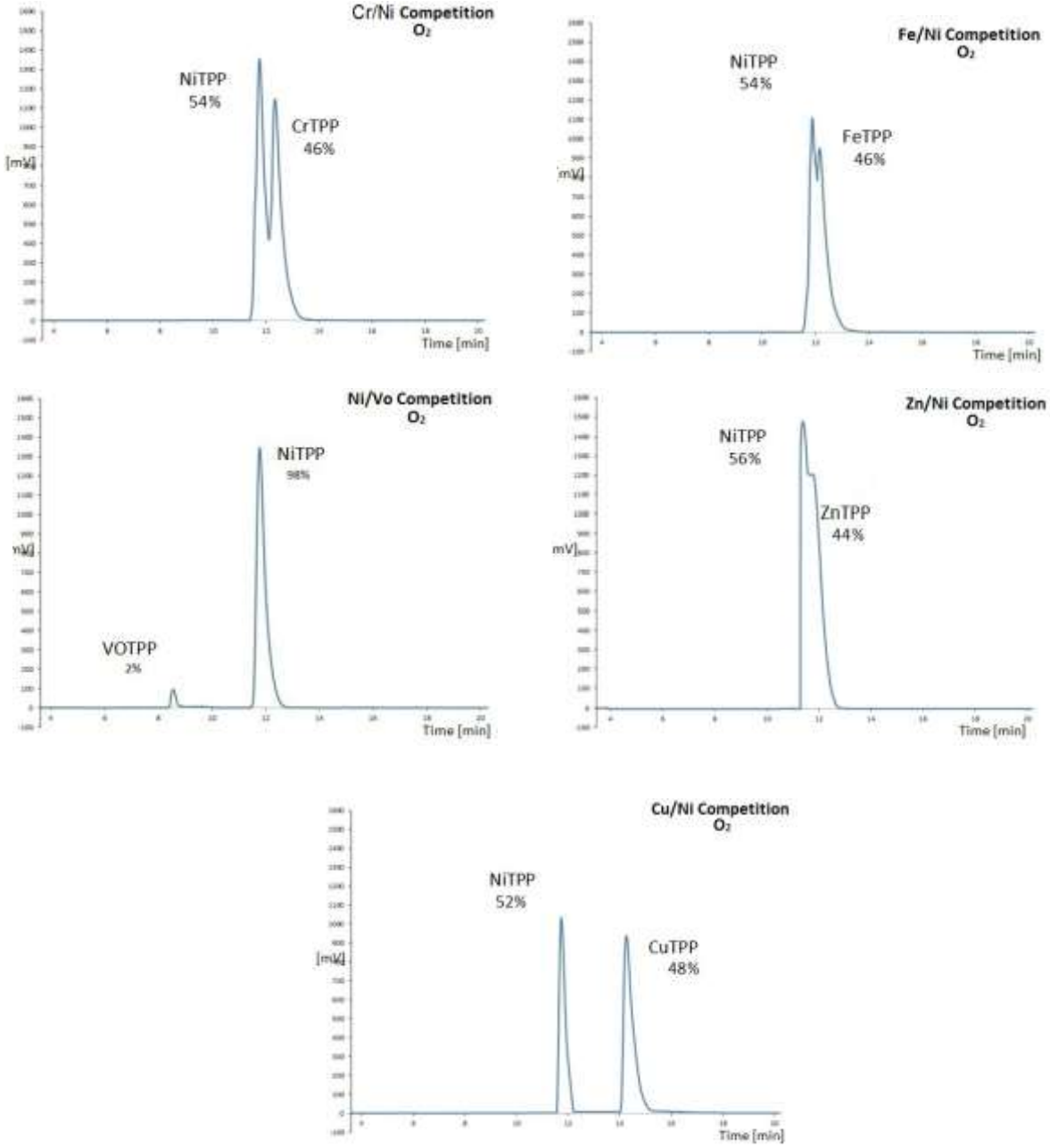

Figure 3.7: Nickel competition with Zn, Cu, Cr, VO and Fe in the presence of Oxygen

3.4.4.3 Vanadyl competition with Zn, Cu, Cr, Ni, and Fe in the absence of oxygen

Competition reaction of Vanadyl and Zinc in the absence presence of oxygen showed a different product distribution compared to the same reactions with oxygen. In the proper conditions for reaction the vanadyl salt actually forms the dominant VOTPP product at 85% yield against 15% of the ZnTPP product. In the case of the copper competition a less marked difference is seen with 34% yield and a 64% VOTPP dominant product. The reaction with Chromium showed a bigger preference for the vanadyl at 83% and 17% yield of the CrTPP. Iron and vanadyl reaction shows a strong preference for iron at 18% yield against 82% of the vanadyl complex. The competition reaction with the Nickel showed more a dominant NiTPP with a 52% abundance and a 48% VOTPP exhausting any free base porphyrin. In contrast with the reactions conducted in the presence of oxygen this set of reactions favored the formation of VOTPP mostly except for the competition with Nickel which showed a slightly bigger proportion of the NiTPP. One potential reason for this difference in reactivity could the poor stability of vanadyl ion in the presence of oxygen. Metals available for the competition reaction completely exhausted the TPP in solution leaving only MTPP complexes.

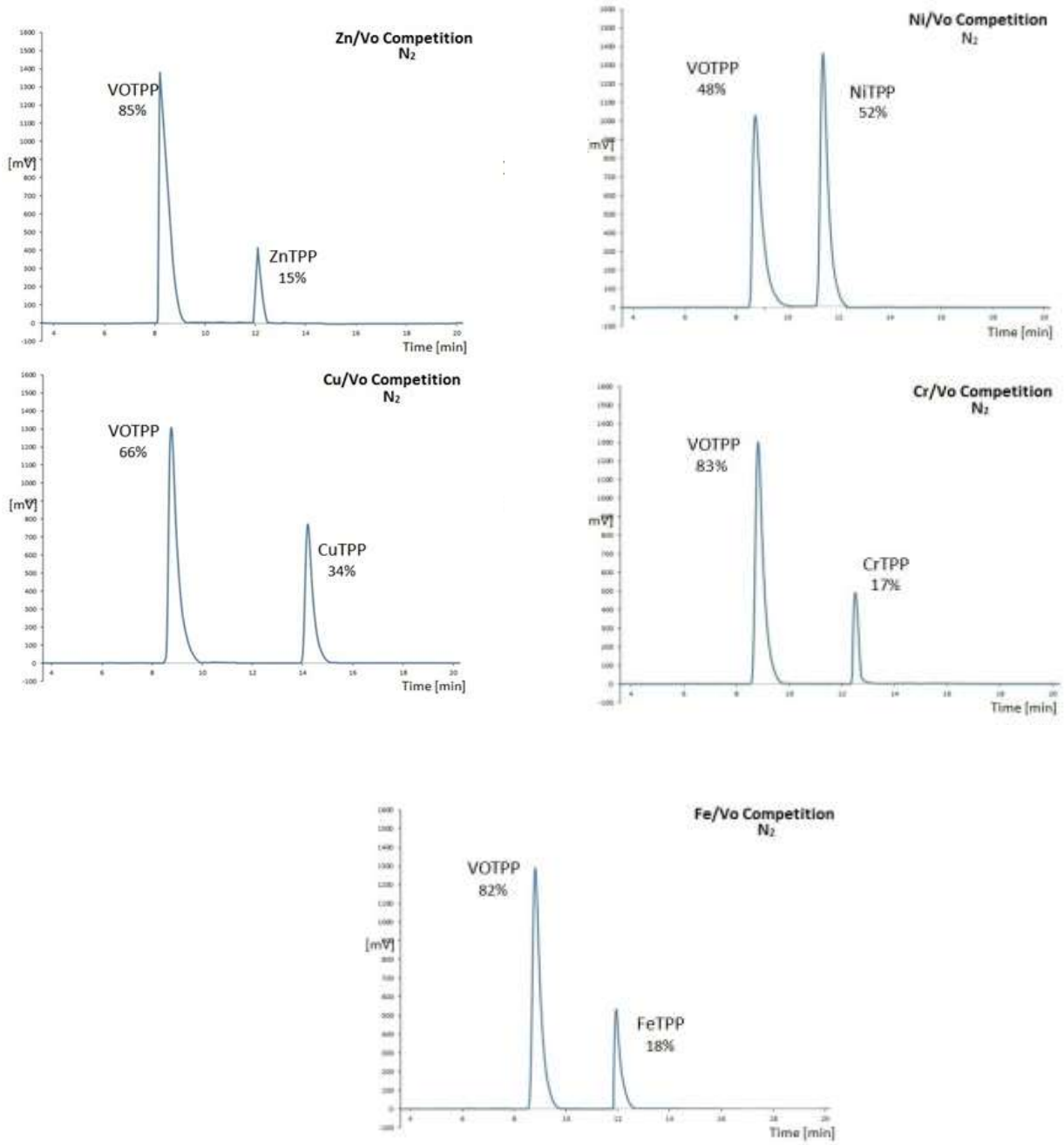

Figure 3.8: Vanadyl competition with Zn, Cu, Cr, Ni and Fe in the absence of Oxygen

3.4.4.4 Nickel competition with Zn, Cu, Cr, and Fe in the absence of oxygen

Contest reaction with Chromium metal gave a 42% yield of CrTPP while a dominant 58% NiTPP was spotted. Iron Nickel reaction on the other hand showed a 56% yield of NiTPP and 44% FeTPP product. In the case of the competition with Zinc one can observe that 46% of ZnTPP was formed and 54% of NiTPP product was recovered. Copper reaction yielded 44% of CuTPP while the major product was spotted in 56%. Finally, in the case of the competition reaction between Vanadyl and Nickel one saw a smaller difference of 48% VOTPP against a 52% NiTPP. This set of competitions behaved very similar to the same set of reactions exposed to air with the exception that in this reaction set VOTPP formation was much more prominent. Although the reaction has a slight difference exposed to air and under nitrogen, one can clearly observe that in both sets the major product is always Nickel. Metals available for the competition reaction completely exhausted the TPP in solution leaving only MTPP complexes.

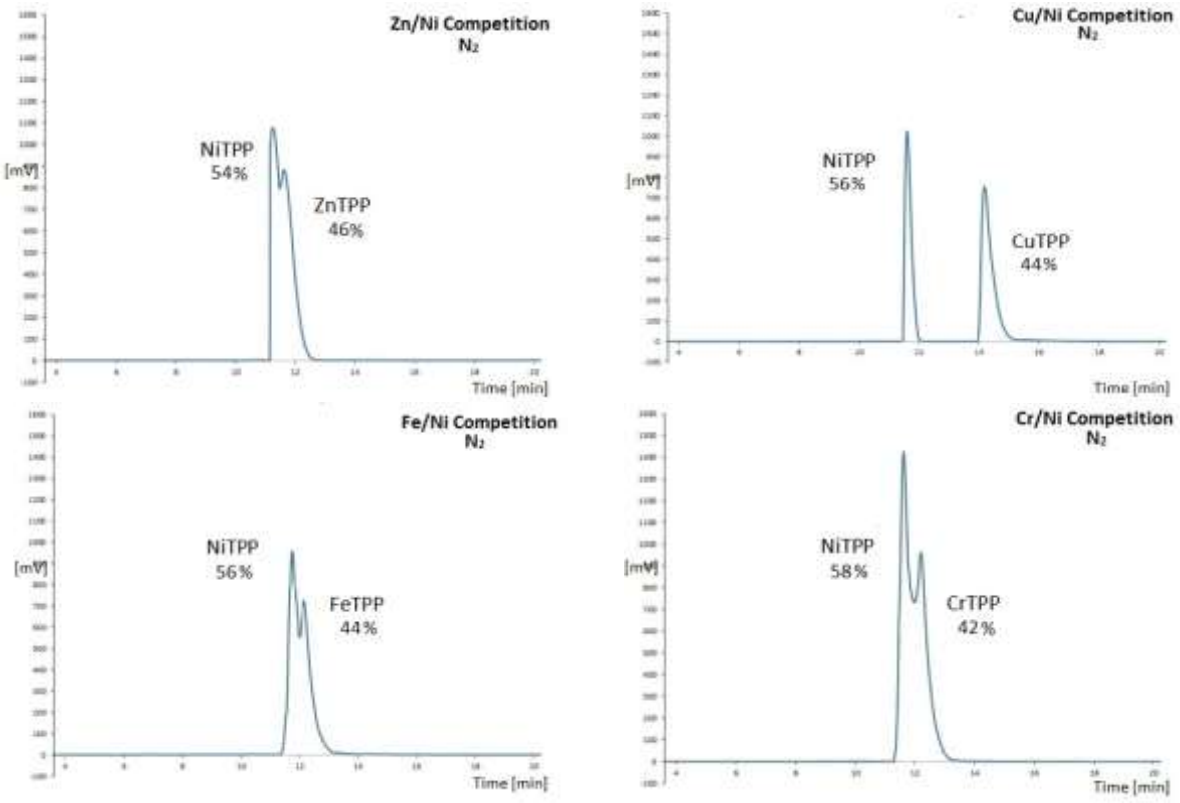

Figure 3.9: Nickel competition with Zn, Cu, Cr, VO and Fe in the absence of Oxygen

3.4.4.5 Vanadyl competition with Zn, Cu, Cr, Ni, and Fe in the presence of excess sulfide ion

Competition reaction with zinc in the presence of oxygen showed no ZnTPP product, 96% free TPP, and 4% formed VOTPP. In the case of copper reaction no CuTPP complex was seen either with 6% VOTPP formation with 94% free TPP. Chromium contest reaction showed 2% VOTPP formation while no formation of CrTPP and 98% free TPP. Finally, competition reaction with Nickel showed no formation of NiTPP while a 5% formation of VOTPP and 95% free base TPP. In the case of competition reactions with sulfide ion in solution, the behavior demonstrated reduced affinity for Vanadyl salts while precipitation of the other metals withdrawing their availability for reaction. Metals available for the competition reaction completely exhausted the TPP in solution leaving only MTPP complexes.

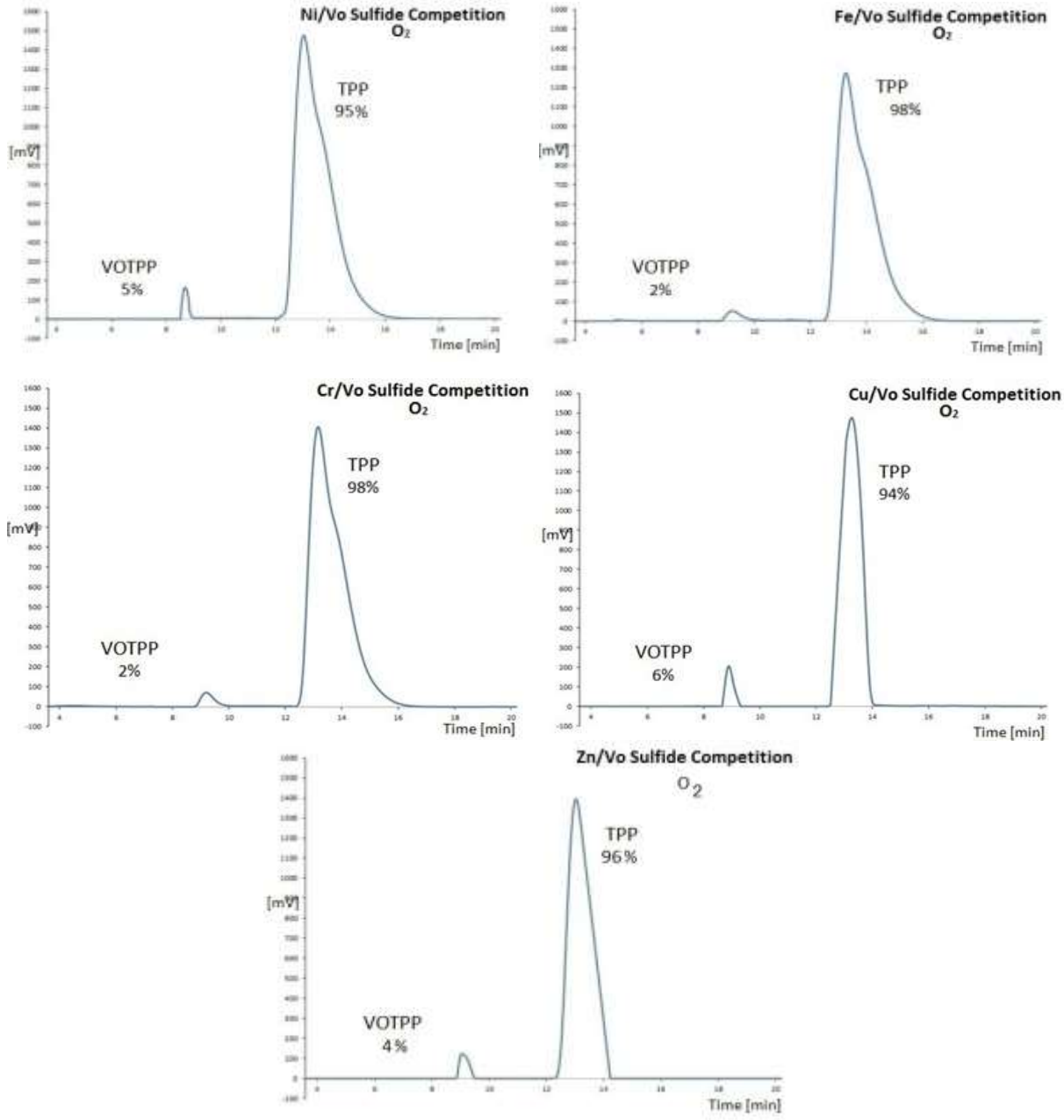

Figure 3.10: Vanadyl competition with Zn, Cu, Cr, Ni and Fe in the presence of excess sulfide ions

3.4.4.6 Nickel competition with Zn, Cu, Cr, Vo, and Fe in the presence of excess sulfide ion.

Competition reactions with Zinc, Copper, Chromium, Vanadyl and Iron showed the same behavior. All reactions did not generate any MTPP complexes while leaving TPP unreacted. This showed indiscriminating sulfide reaction with all ions in the competition reacting causing their sulfide metal salts precipitation and no MTPP formation. Metals available for the competition reaction completely exhausted the TPP in solution leaving only MTPP complexes.

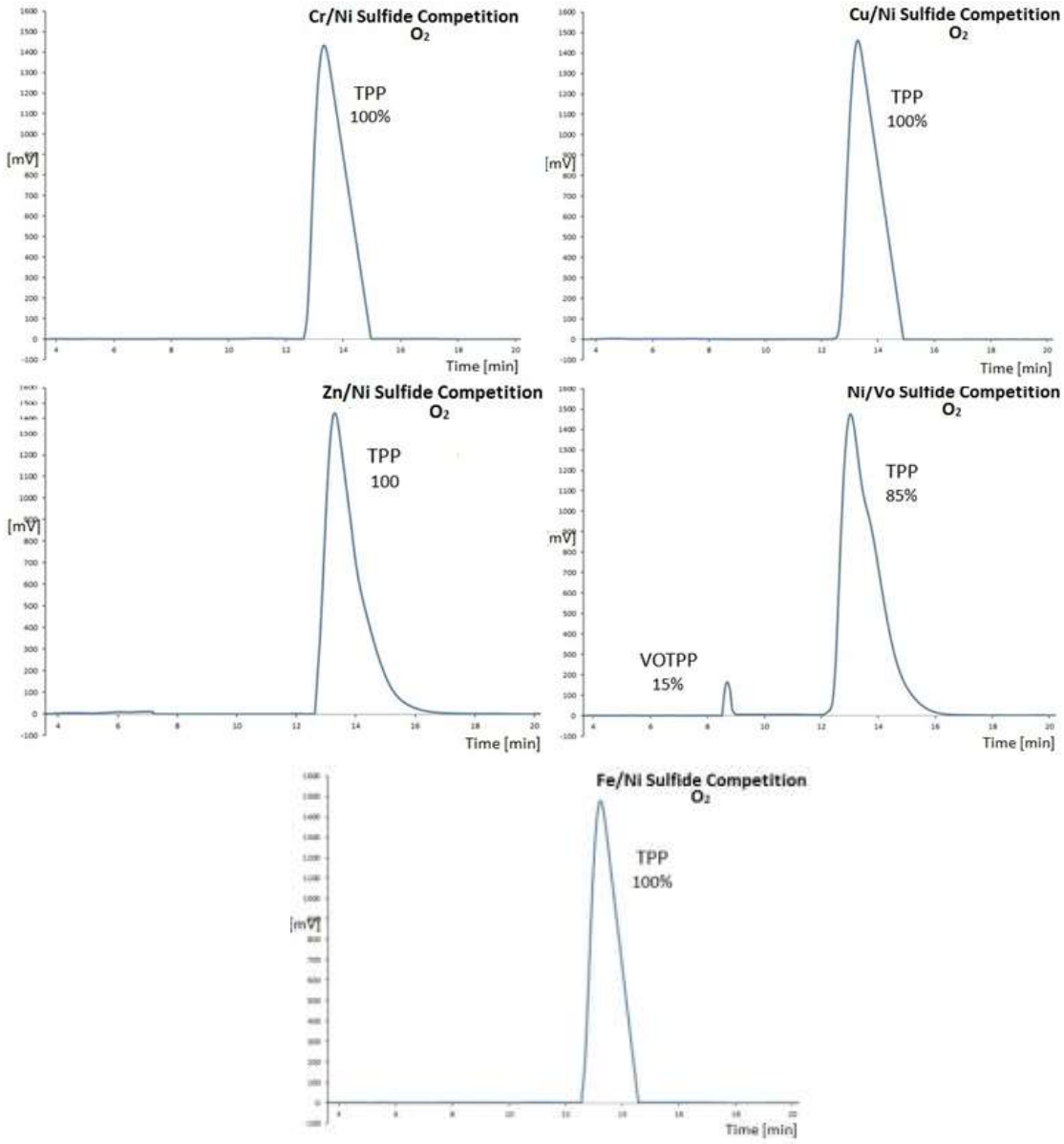

Figure 3.11: Ni competition with Zn, Cu, Cr, VO and Fe in the presence of excess sulfide ions

3.4.4.7 Transmetallation of MTPP by vanadyl ion experiments in the presence of oxygen

Porphyrin molecules are stabilizes due to their aromaticity nonetheless when coordinated with metal ions the d-π backbonding increases the stability of the complexes greatly. Demetallation of chelate ions would involve the disassociation of four metal – nitrogen bonds which require a lot of energy. In order to test the possibility of transmetallation by Nickel and Vanadyl ion, experiments were setup with the other metal studied in this thesis.

All the reactions were using equimolar quantities of VO Sulfate ($VOSO_4$) and Metallotetraphenylporphyrin (MTPP)

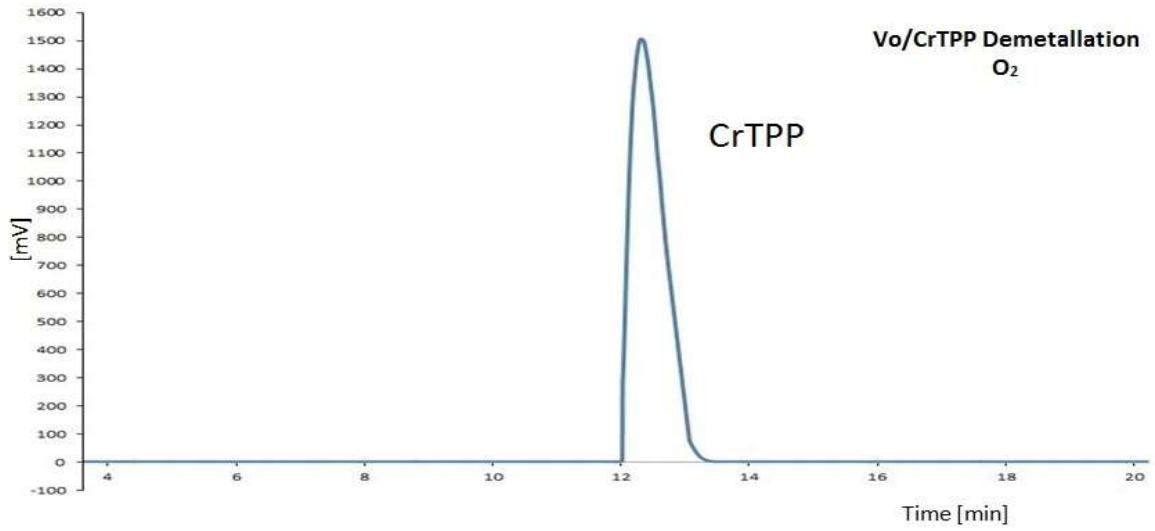

Figure 3.12: Transmetallation experiment. Vanadyl Sulfate and Chromium (II) tetraphenylporphyrin in the presence of oxygen

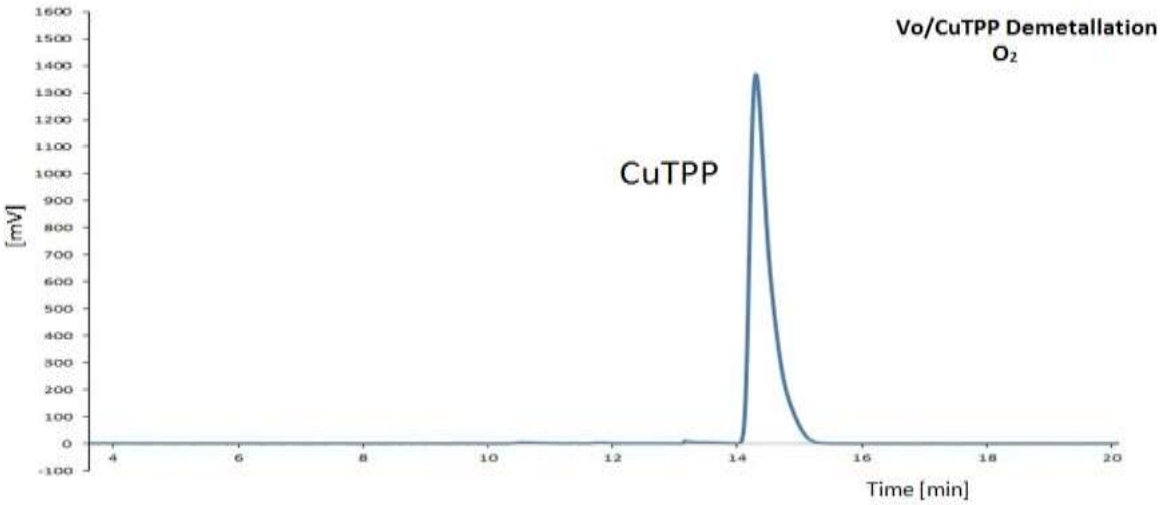

Figure 3.13: Transmetallation experiment. Vanadyl sulfate and Copper (II) tetraphenylporphyrin in the presence of oxygen.

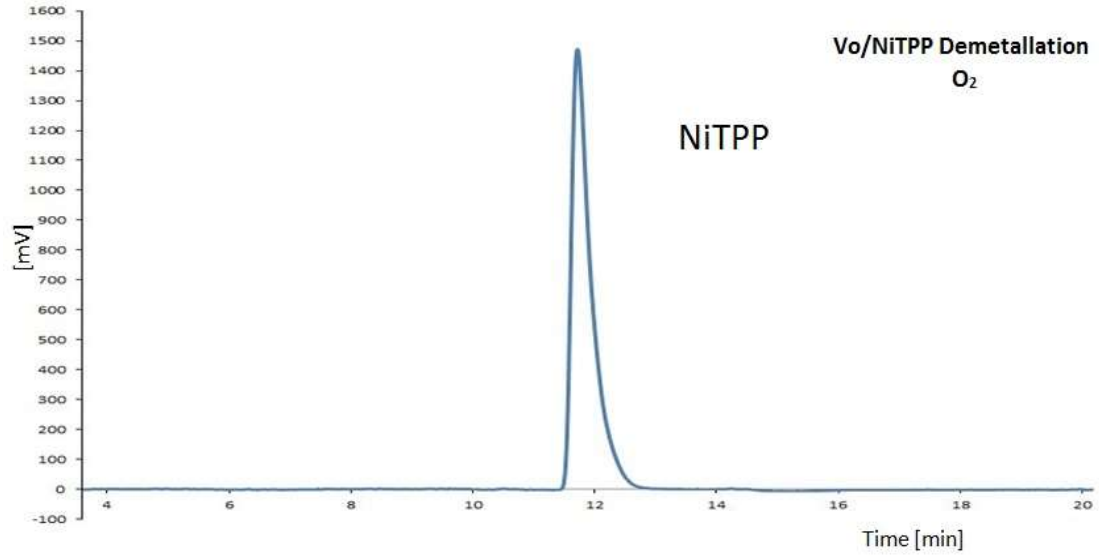

Figure 3.14: Transmetallation experiment. Vanadyl sulfate and Nickel (II) tetraphenylporphyrin in the presence of oxygen.

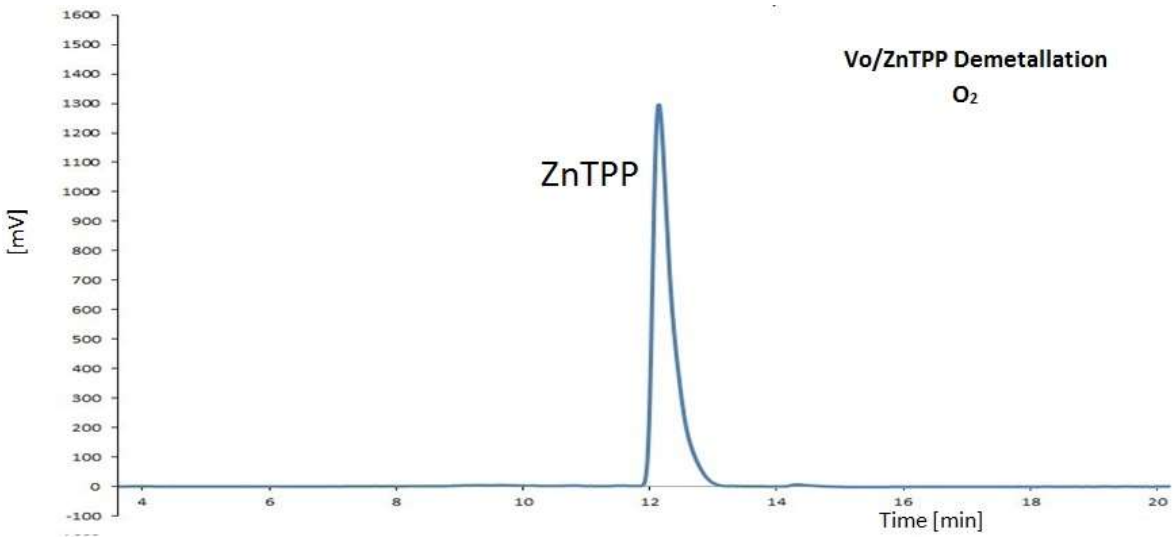

Figure 3.15: Transmetallation experiment. Vanadyl Sulfate and Zinc (II) tetraphenylporphyrin in the presence of oxygen.

Experiments were conducted to determine the potential demetallation of ZnTPP, CuTPP, CrTPP, and NiTPP and transmetallation by vanadyl ion. All the experiments were conducted exposed to air where all reactions showed no transmetallation whatsoever. The set of reactions were ran for twenty-four hours, so it's worth no note that petroleum cooks for thousands of year to achieve maturation stage where you find that vanadyl and nickel porphyrins are the only present in crude oil.

3.4.4.8 Transmetallation of MTPP by vanadyl ion experiments in the absence of oxygen

In order to test if it would be a difference due to the difference in reduction potential of metals and the molecule stability in nitrogen, these test were also performed in the absence of oxygen.

All the reactions were using equimolar quantities of VO Sulfate ($VOSO_4$) and Metallotetraphenylporphyrin (MTPP)

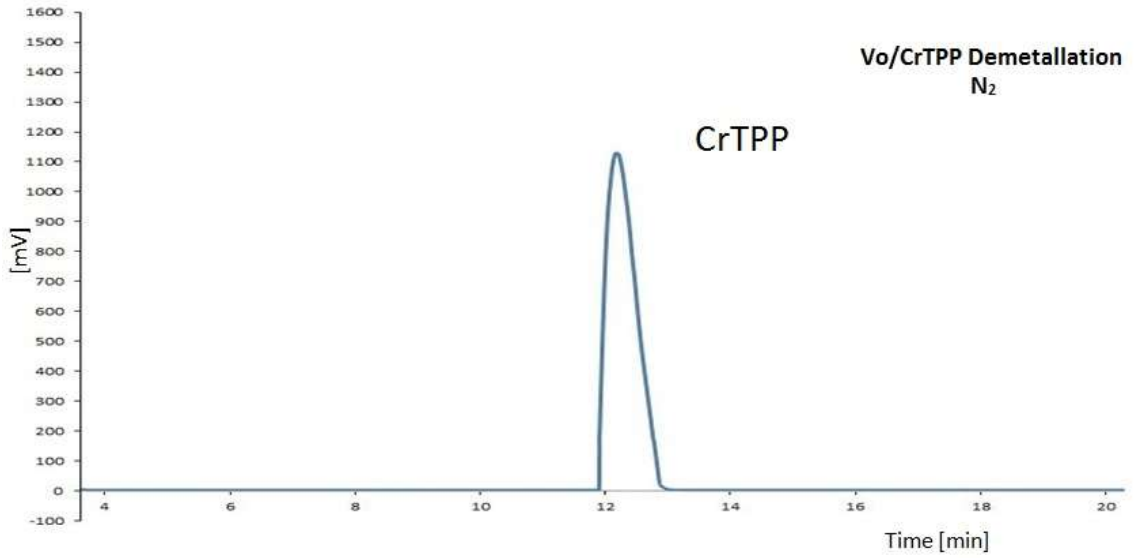

Figure 3.16: Transmetallation experiment. Vanadyl sulfate and Chromium (II) tetraphenylporphyrin in the absence of oxygen.

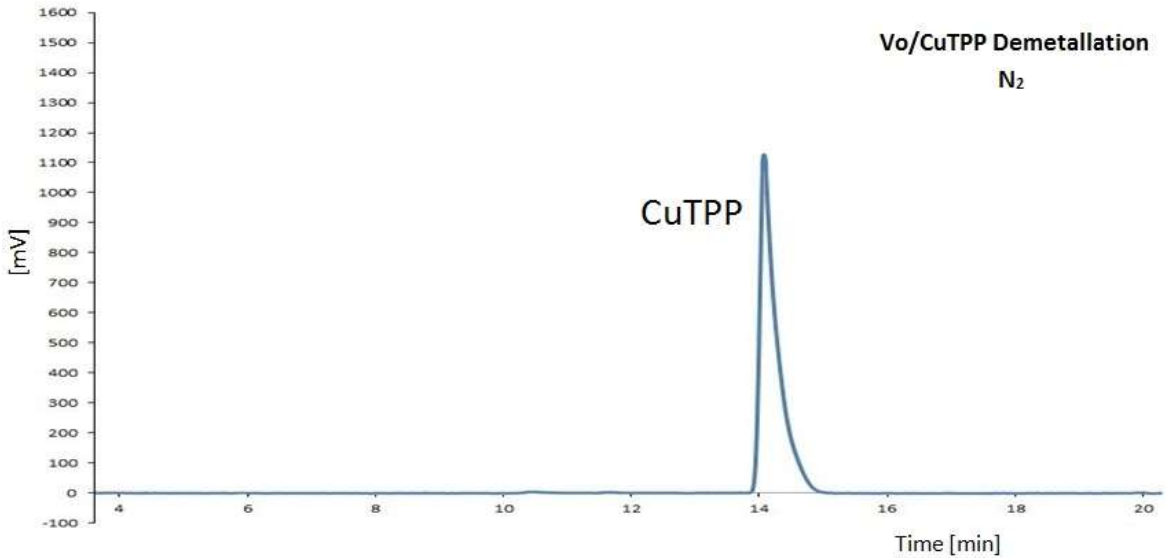

Figure 3.17: Transmetallation experiment. Vanadyl Sulfate and Copper (II) tetraphenylporphyrin in the absence of oxygen.

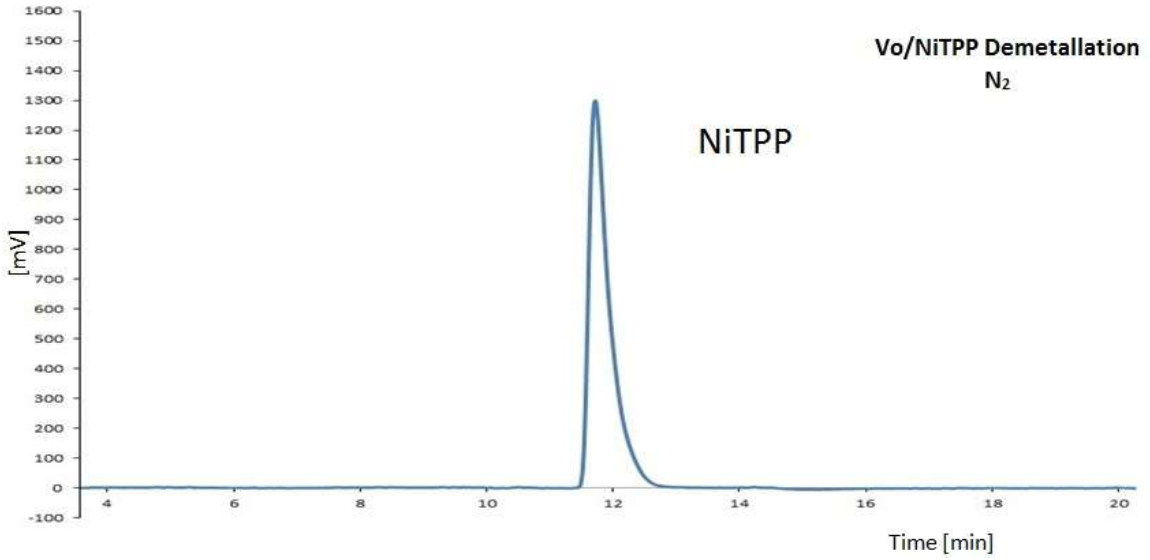

Figure 3.18: Transmetallation experiment. Vanadyl sulfate and nickel (II) tetraphenylporphyrin in the absence of oxygen.

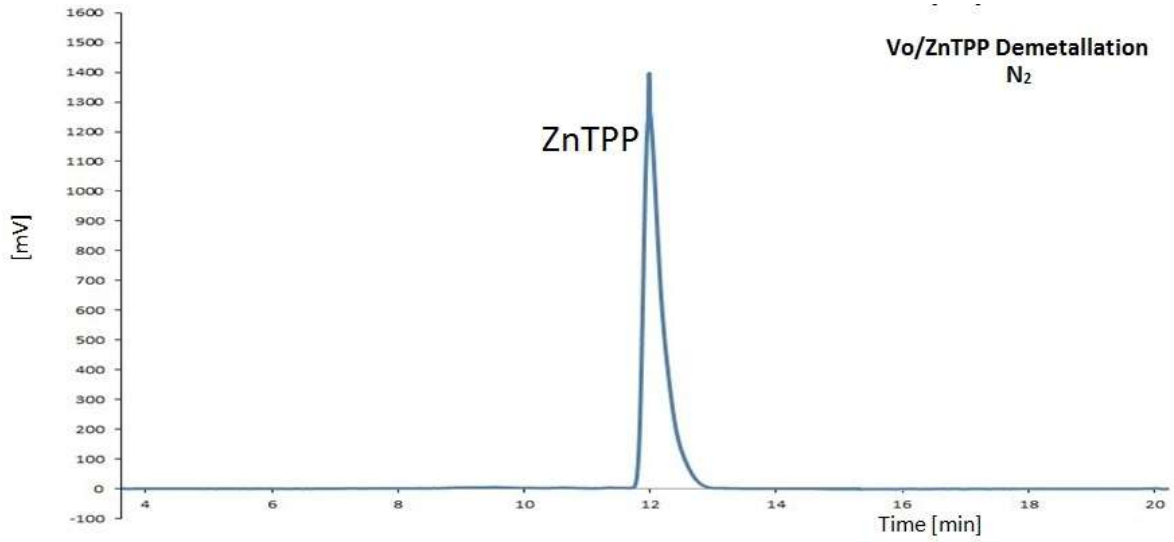

Figure 3.19: Transmetallation experiment. Vanadyl sulfate and zinc (II) tetraphenylporphyrin in the absence of oxygen.

The transmetallation experiments showed the same pattern as the reaction conducted in the presence of oxygen. In the competition reaction chromatograms involving vanadyl in the presence and absence of oxygen one could observe that vanadyl seems to be more stable in an

inert atmosphere. Nonetheless, the stability of the formed metalloporphyrin complexes shows to be too great for demetallation with vanadyl ion.

3.4.4.9 Transmetallation of MTPP by nickel ion experiments in the presence of oxygen

In order to complete the series of reactions the other metal found associated with porphyrins upon crude oil extraction was also tested for transmetallation with the other metal ions studied in this thesis.

All the reactions were using equimolar quantities of Ni Sulfate ($NiSO_4$) and Metallotetraphenylporphyrin (MTPP)

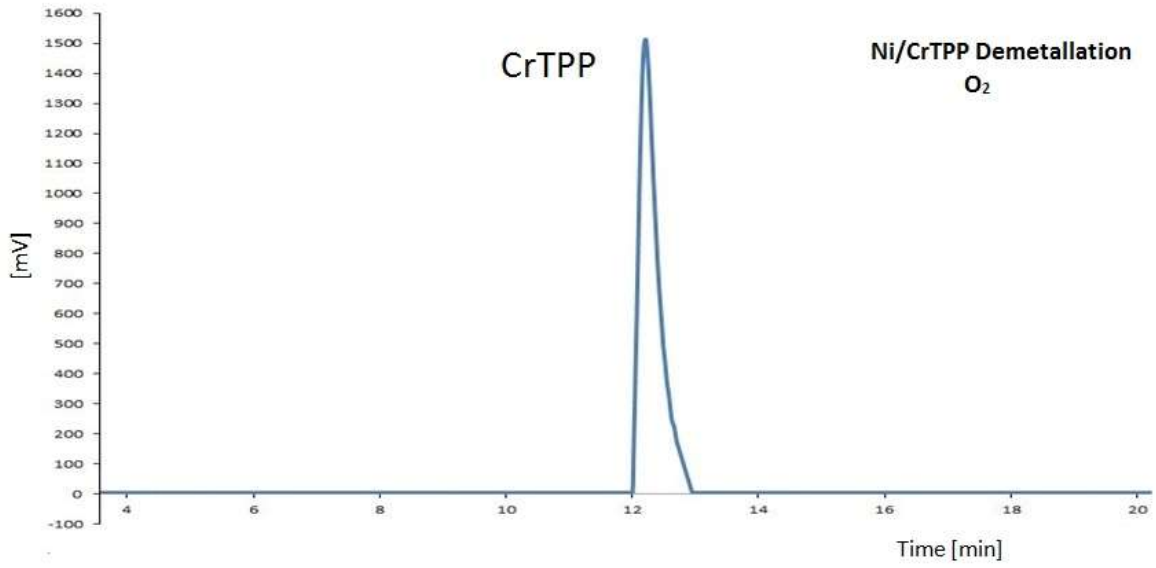

Figure 3.20: Transmetallation experiment. Nickel (II) sulfate and chromium (II) tetraphenylporphyrin in the presence of oxygen.

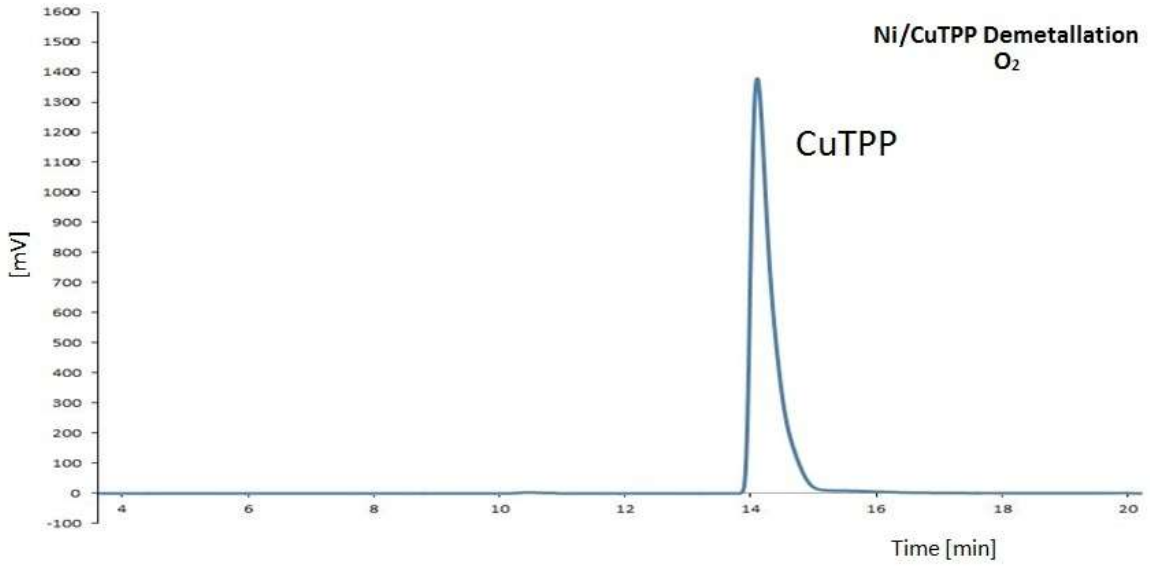

Figure 3.21: Transmetallation experiment. Nickel (II) sulfate and copper (II) tetraphenylporphyrin in the presence of oxygen.

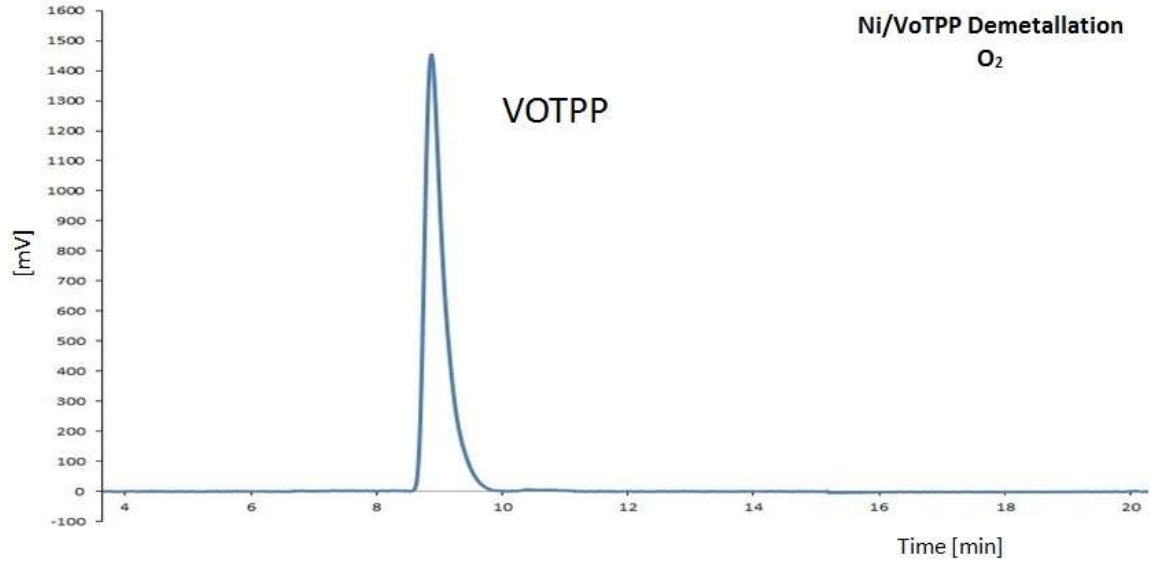

Figure 3.22: Transmetallation experiment. Nickel (II) sulfate and vanadyl tetraphenylporphyrin in the presence of oxygen.

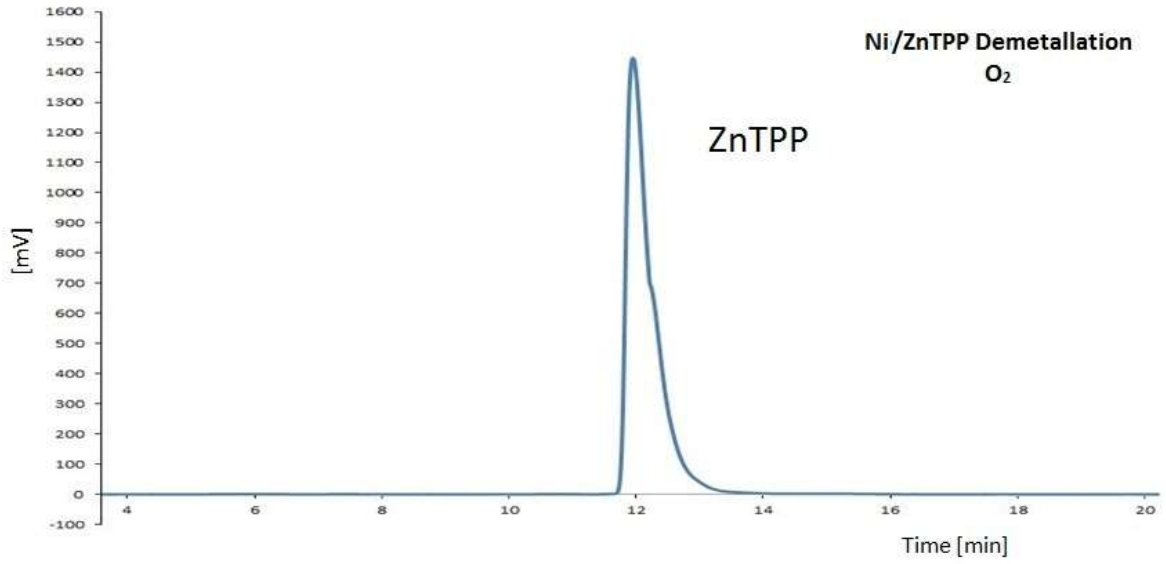

Figure 3.23: Transmetallation experiment. Nickel (II) sulfate and chromium (II) tetraphenylporphyrin in the presence of oxygen.

In the competition reactions chromatographs it was seen that nickel appears to be the most thermodynamically stable of all of the metalloporphyrins due to its greater formation of NiTPP. In here transmetallation experiments showed that regardless the energy for the disassociation of the metal is too great for the introduction of nickel into the ring system.

3.4.4.10 Transmetallation of MTPP by nickel ion experiments in the absence of oxygen

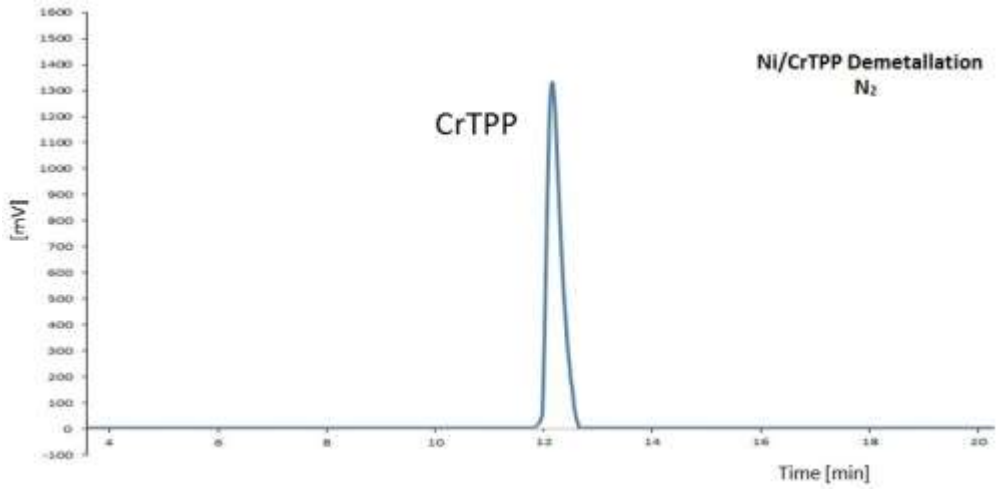

Figure 3.24: Transmetallation experiment. Nickel (II) sulfate and chromium (II) tetraphenylporphyrin in the absence of oxygen.

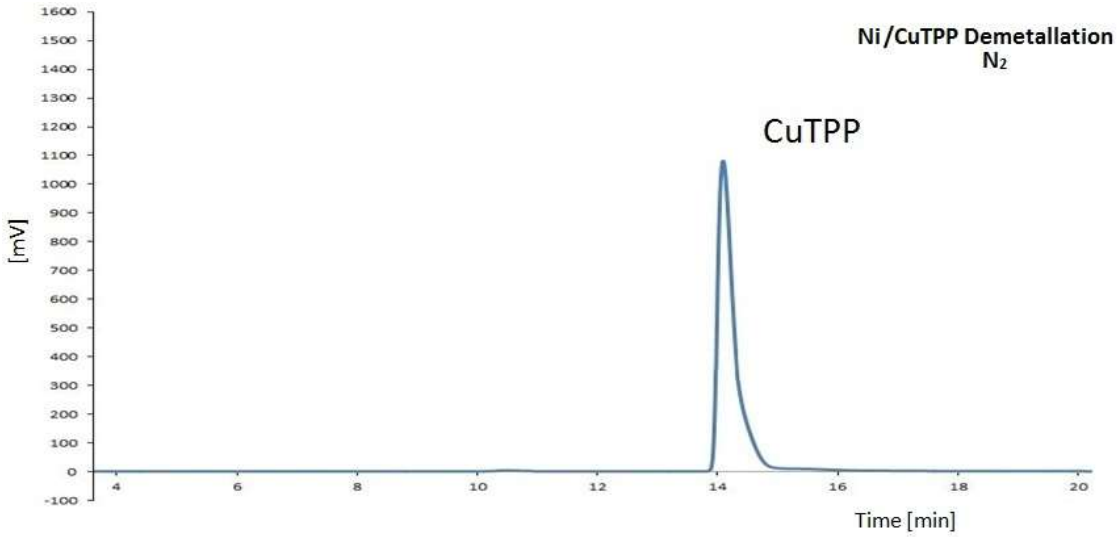

Figure 3.25: Transmetallation experiment. Nickel (II) sulfate and copper (II) tetraphenylporphyrin in the absence of oxygen.

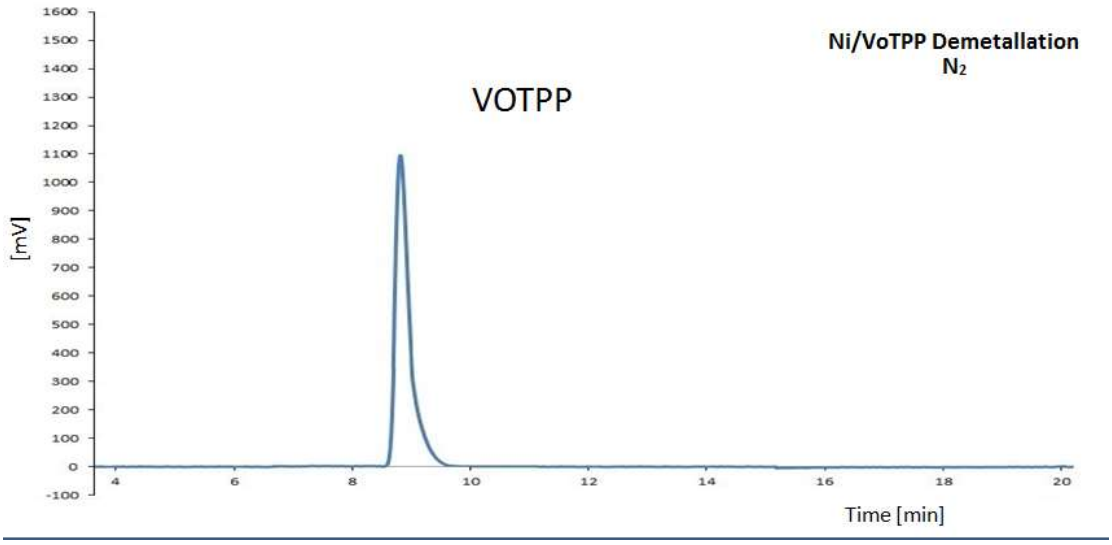

Figure 3.26: Transmetallation experiment. Nickel (II) sulfate and vanadyl tetraphenylporphyrin in the absence of oxygen.

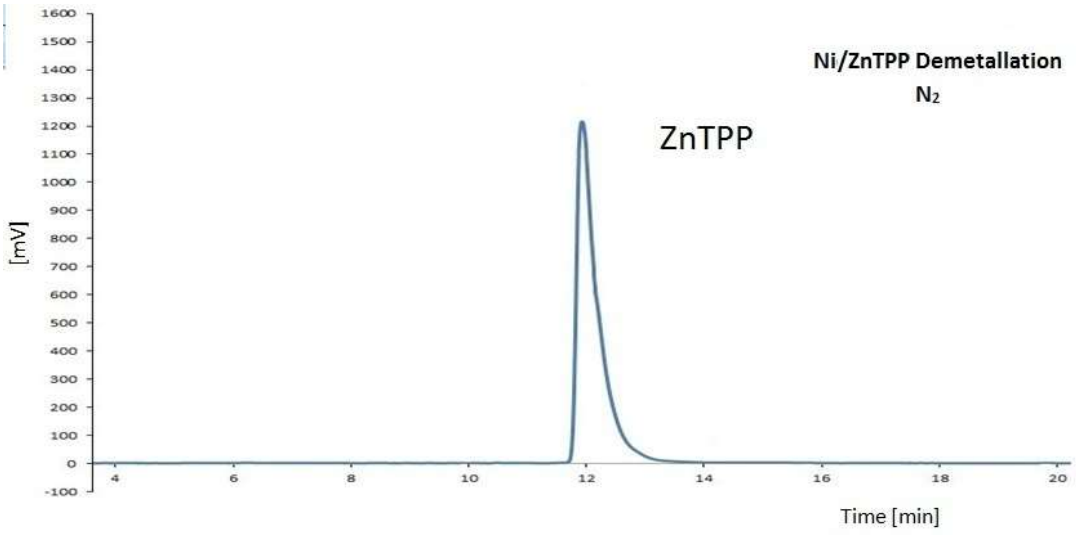

Figure 3.27: Transmetallation experiment. Nickel (II) sulfate and zinc (II) tetraphenylporphyrin in the absence of oxygen.

Demetallation experiments in the absence of oxygen showed the same pattern as in the presence of it. This is not a surprise as in the competition experiments nickel showed to behave the same in both conditions.

3.4.5 Mass Spectrometry

In order to confirm the presence of products in the reaction mass spectrometry was conducted on all competition and demetallation reactions. Monoisotopic masses of TPP and all MTPP were acquired from the program TSS pro v 3.0 and displayed in the table below.

Table 3.2: Monoisotopic masses of all TPP and MTPP

	Average Mass	Monoisotopic Mass	Monoisotopic Mass in Mass Specs
TPP	614.752	614.247	614.240
CrTPP	664.732	664.172	664.172
FeTPP	668.581	668.166	668.165
NiTPP	671.429	670.167	670.163
CuTPP	676.282	675.161	675.162
ZnTPP	678.126	676.161	676.153
VOTPP	679.677	679.170	679.178

The table shows the monoisotopic masses of all TPP and MTPP used in the competition and demetallation experiments.

Samples from each reaction were run in HPLC and signals searched in the time lapsed spectrum. In order to verify the identity of the products for each reaction not only signals by mass were searched, but also the isotopic pattern of the different metalloporphyrins was analyzed. Samples were calibrated with the reserpine signal at 608.34 m/z. Mass spectra proved to be a required technique to complement the identification of the HPLC due to the closeness of some signals in some chromatograms.

Furthermore, sensitivity of the MS is much more than that of HPLC, so this technique also served to verify that only the products seen in the HPLC were present. Reaction sample mass spectra are provided in the appendix of this dissertation to improve the flow of this work. The matched compound signals and the isotopic patterns were matched with peak times and areas in HPLC to determine the yields and identity of the products in this work.

Chapter 4: Conclusion

In order to answer why Nickel and Vanadium are naturally selected to form metalloporphyrins in asphaltene fraction of the crude oil, we have to take into consideration factors like metal abundance, oxidation state of available metals, bacterial derived changes in the water column, as well as the fact that porphyrins are not kept under the same conditions through the maturation of the crude. Due to the fact that porphyrins are subjected to so many variable in nature makes this a hard subject to study that's why it is essential to know as much of the maturation process of the crude.

Formation of crude oil rises from the maturation of organic matter of marine origin, therefore its rich in plant and microorganisms. The porphyrin sources of such organisms are the phorbide molecules chlorophyll and bacteriophyll, as such magnesium phorbides as aromatized into porphyrins. Due to the abundance of phytoplankton of this type of crude it's expected to encounter very high vanadium concentrations. As seen in the sea water and shale rock ion concentrations Vanadium is less abundant in sea water than Zinc, but in shale rock vanadium is much more abundant. In the case of water sample vanadyl is at least three times more abundant than the other candidate ions and nickel 1.3 times. Therefore, sea water and shale rock abundance is not standing argument of the natural selection of nickel and vanadyl metalloporphyrins. It's important to notice that microbial organisms intake water column ions to use as cofactors for their metabolic processes, and as such metal losses through maturation of crude cannot be accounted for. Abundant literature characterization of the process of crude maturation is found in the literature, but exact timing of metalloporphyrin formation is something that has not been explained with certainty.

Metal candidates selected for this work included Zn^{2+}, Cu^{2+} , Cr^{2+}, Ni^{2+}, Fe^{2+}, and Vanadyl ions. In the case of copper there is scientific evidence that supports that copper is used as one of the metals responsible for porphyrin formation, but the metal itself is demetallated quickly upon exposure with clays.

The rest of the metal candidates were subjected to competition and transmetallation reactions to try and determine their behaviors in solution. Competition reactions in the presence and absence of oxygen showed that Nickel is the preferred metalloporphyrin formed. Although in the reaction formation of the rest MTPP products was observed in less proportion. Demetallation reactions showed that once form metalloporphyrin tested are stable for transmetallation under the temperature and time selected for the study. It's important to note that there are other natural products that have high activation energies for their conversion, but still happen like the formation of diamond, and since crude maturation occurred during millions of years it's expected to find the most thermodynamically stable products.

Natural selection of Nickel can be reasoned using the results of this dissertation due to thermodynamics. As such formation of this metalloporphyrin would have to occur late diagenesis or in catagenesis where shale rocks are exposed to higher temperatures and product formation can be driven by the stability of the products. Either way formation of the rest of the metal candidate would be expected in less proportion.

In the anoxic layer in the stage where sulfate reducing bacteria produce copious amounts of hydrogen sulfide, metal abundance is greatly affected in the water column. Excess presence of sulfides in the water column at this point is reduced by hydrogen sulfide metal mineralization. Competition reactions with sulfides in this dissertation showed a reduced precipitation of vanadyl while all other candidates came out of solution leaving unreacted TPP. Most crude samples analyzed all over the world show a dominance of vanadyl porphyrins with common ratios 10:1 to 100:1. Therefore, I propose that metalloporphyrin formation, in particular Ni and VO porphyrins, occurs with a high hydrogen sulfide concentration in the water column. As a reduced concentration of ions would be available under such conditions it would make sense for Nickel to be the second favor metalloporphyrin in late diagenesis or early catagenesis.

The work of this dissertation shows that Nickel metalloporphyrin product would the thermodynamically selected product in nature and well as vanadyl, since these two ions are formed in the greatest proportion in all competition reactions. Furthermore, vanadyl ions are expected to be more abundant in anoxic environments with high hydrogen sulfide concentration. Finally, once formed metalloporphyrin molecules are very stable especially vanadyl, since other

MTPP are susceptible to chemical and biological attack from both side of the planar molecule, while vanadyl is protected on one side due to the oxygen atom.

In summary, nickel and vanadyl ion selection for metalloporphyrin formation is due to a combination of factors like oxidation state of metals in the anoxic water column, timing of the metalloporphyrin formation, thermodynamic stability of Vanadyl and nickel metalloporphyrins, and the increased abundance of vanadyl while in the presence of hydrogen sulfide when other metals are being mineralized.

Appendix A. Relation of Samples

STAGE I OPEN SYSTEM			Experiment #
A	VOSO4 + TPP +	ZnSO4	1
		CuSO4	2
		CrSO4	3
		NiSO4	4
		FeSO4	4_1
B	NiSO4 + TPP +	ZnSO4	5
		CuSO4	6
		CrSO4	7
		FeSO4	7_1

STAGE IV UNDER NITROGEN			Experiment #
A	VOSO4 + TPP +	ZnSO4	22
		CuSO4	23
		CrSO4	24
		NiSO4	25
		FeSO4	26
B	NiSO4 + TPP +	ZnSO4	27
		CuSO4	28
		CrSO4	29
		FeSO4	30

STAGE II OPEN SYSTEM			Experiment #
A	VOSO4 +	ZnTPPP	8
		CuTPP	9
		CrTPP	10
		NiTPP	11
B	NiSO4 +	ZnTPPP	12
		CuTPP	13
		CrTPP	14
		VOTPP	15

STAGE V UNDER NITROGEN			Experiment #
A	VOSO4 +	ZnTPPP	31
		CuTPP	32
		CrTPP	33
		NiTPP	34
B	NiSO4 +	ZnTPPP	35
		CuTPP	36
		CrTPP	37
		VOTPP	38

STAGE III OPEN SYSTEM			Experiment #
A	VOTPP +	ZnSO4	16
		CuSO4	17
		CrSO4	18
B	NiTPP +	ZnSO4	19
		CuSO4	20
		CrSO4	21

STAGE VI UNDER NITROGEN			Experiment #
A	VOTPP +	ZnSO4	39
		CuSO4	40
		CrSO4	41
B	NiTPP +	ZnSO4	42
		CuSO4	43
		CrSO4	44

STAGE VII with Sodium Sulfide							Experiment #
A	VOSO4	+	TPP	+	Na2S	+	ZnSO4	45
							CuSO4	46
							CrSO4	47
							NiSO4	48
							FeSO4	49
B	NiSO4	+	TPP	+	Na2S	+	ZnSO4	50
							CuSO4	51
							CrSO4	52
							FeSO4	53

Appendix B. Chemical Reactions Competition

STAGE 1 A. Open System. $VOSO_4$ + TPP + MSO_4

Table B1: Sample 1 $VOSO_4$ + $ZnSO_4$ + TPP.

	Compound	Molecular Weigth [g/moles]	Mass = moles x MW [g]	Ratio	Moles = Mass / MW	After Rx Solid obtained [g]
EX 1	TPP	614.752	1.00	1	1.63E-03	1.32
	VOSO4	163.005	0.27	1	1.63E-03	
	ZnSO4	161.454	0.26	1	1.63E-03	
EX 2	TPP	614.752	1.00	1	1.63E-03	1.34
	VOSO4	163.005	0.27	1	1.63E-03	
	ZnSO4	161.454	0.26	1	1.63E-03	
EX 3	TPP	614.752	1.00	1	1.63E-03	1.35
	VOSO4	163.005	0.27	1	1.63E-03	
	ZnSO4	161.454	0.26	1	1.63E-03	
EX 4	TPP	614.752	1.00	1	1.63E-03	1.35
	VOSO4	163.005	0.27	1	1.63E-03	
	ZnSO4	161.454	0.26	1	1.63E-03	
EX 5	TPP	614.752	1.00	1	1.63E-03	1.36
	VOSO4	163.005	0.27	1	1.63E-03	
	ZnSO4	161.454	0.26	1	1.63E-03	

Table B2: Sample 2 $VOSO_4$ + $CuSO_4$ + TPP

	Compound	Molecular Weigth [g/moles]	Mass = moles x MW [g]	Ratio	Moles = Mass / MW	After Rx Solid obtained [g]
EX 1	TPP	614.752	1.00	1	1.63E-03	1.22
	VOSO4	163.005	0.27	1	1.63E-03	
	CuSO4	159.610	0.26	1	1.63E-03	
EX 2	TPP	614.752	1.00	1	1.63E-03	1.3
	VOSO4	163.005	0.27	1	1.63E-03	
	CuSO4	159.610	0.26	1	1.63E-03	
EX 3	TPP	614.752	1.00	1	1.63E-03	1.25
	VOSO4	163.005	0.27	1	1.63E-03	
	CuSO4	159.610	0.26	1	1.63E-03	
EX 4	TPP	614.752	1.00	1	1.63E-03	1.29
	VOSO4	163.005	0.27	1	1.63E-03	
	CuSO4	159.610	0.26	1	1.63E-03	
EX 5	TPP	614.752	1.00	1	1.63E-03	1.32
	VOSO4	163.005	0.27	1	1.63E-03	
	CuSO4	159.610	0.26	1	1.63E-03	

Table B3: Sample 3 $VOSO_4$ + $CrSO_4$ + TPP

	Compound	Molecular Weigth [g/moles]	Mass = moles x MW [g]	Ratio	Moles = Mass / MW	After Rx Solid obtained [g]
EX 1	TPP	614.752	1.00	1	1.63E-03	1.2
	VOSO4	163.005	0.27	1	1.63E-03	
	CrSO4	148.06	0.24	1	1.63E-03	
EX 2	TPP	614.752	1.00	1	1.63E-03	1.24
	VOSO4	163.005	0.27	1	1.63E-03	
	CrSO4	148.06	0.24	1	1.63E-03	
EX 3	TPP	614.752	1.00	1	1.63E-03	1.25
	VOSO4	163.005	0.27	1	1.63E-03	
	CrSO4	148.06	0.24	1	1.63E-03	
EX 4	TPP	614.752	1.00	1	1.63E-03	1.27
	VOSO4	163.005	0.27	1	1.63E-03	
	CrSO4	148.06	0.24	1	1.63E-03	
EX 5	TPP	614.752	1.00	1	1.63E-03	1.30
	VOSO4	163.005	0.27	1	1.63E-03	
	CrSO4	148.06	0.24	1	1.63E-03	

Table B4: Sample 4 $VOSO_4$ + $NiSO_4$ + TPP

	Compound	Molecular Weigth [g/moles]	Mass = moles x MW [g]	Ratio	Moles = Mass / MW	After Rx Solid obtained [g]
EX 1	TPP	614.752	1.00	1	1.63E-03	1.34
	VOSO4	163.005	0.27	1	1.63E-03	
	NiSO4	154.757	0.25	1	1.63E-03	
EX 2	TPP	614.752	1.00	1	1.63E-03	1.25
	VOSO4	163.005	0.27	1	1.63E-03	
	NiSO4	154.757	0.25	1	1.63E-03	
EX 3	TPP	614.752	1.00	1	1.63E-03	1.21
	VOSO4	163.005	0.27	1	1.63E-03	
	NiSO4	154.757	0.25	1	1.63E-03	
EX 4	TPP	614.752	1.00	1	1.63E-03	1.3
	VOSO4	163.005	0.27	1	1.63E-03	
	NiSO4	154.757	0.25	1	1.63E-03	
EX 5	TPP	614.752	1.00	1	1.63E-03	1.2
	VOSO4	163.005	0.27	1	1.63E-03	
	NiSO4	154.757	0.25	1	1.63E-03	

Table B5: Sample 4_1 $VOSO_4$ + $FeSO_4$ + TPP.

	Compound	Molecular Weigth [g/moles]	Mass = moles x MW [g]	Ratio	Moles = Mass / MW	After Rx Solid obtained [g]
EX 1	TPP	614.752	1.00	1	1.63E-03	1.25
	VOSO4	163.005	0.27	1	1.63E-03	
	FeSO4	151.909	0.25	1	1.63E-03	
EX 2	TPP	614.752	1.00	1	1.63E-03	1.2
	VOSO4	163.005	0.27	1	1.63E-03	
	FeSO4	151.909	0.25	1	1.63E-03	
EX 3	TPP	614.752	1.00	1	1.63E-03	1.25
	VOSO4	163.005	0.27	1	1.63E-03	
	FeSO4	151.909	0.25	1	1.63E-03	
EX 4	TPP	614.752	1.00	1	1.63E-03	1.27
	VOSO4	163.005	0.27	1	1.63E-03	
	FeSO4	151.909	0.25	1	1.63E-03	
EX 5	TPP	614.752	1.00	1	1.63E-03	1.32
	VOSO4	163.005	0.27	1	1.63E-03	
	FeSO4	151.909	0.25	1	1.63E-03	

Table B6: Sample 5 $NiSO_4$ + $ZnSO_4$ + TPP.

	Compound	Molecular Weigth [g/moles]	Mass = moles x MW [g]	Ratio	Moles = Mass / MW	After Rx Solid obtained [g]
EX 1	TPP	614.752	1.00	1	1.63E-03	1.27
	NiSO4	154.757	0.25	1	1.63E-03	
	ZnSO4	161.454	0.26	1	1.63E-03	
EX 2	TPP	614.752	1.00	1	1.63E-03	1.16
	NiSO4	154.757	0.25	1	1.63E-03	
	ZnSO4	161.454	0.26	1	1.63E-03	
EX 3	TPP	614.752	1.00	1	1.63E-03	1.31
	NiSO4	154.757	0.25	1	1.63E-03	
	ZnSO4	161.454	0.26	1	1.63E-03	

Table B7: Sample 6 $NiSO_4$ + $CuSO_4$ + TPP.

	Compound	Molecular Weigth [g/moles]	Mass = moles x MW [g]	Ratio	Moles = Mass / MW	After Rx Solid obtained [g]
EX 1	TPP	614.752	1.00	1	1.63E-03	1.34
	NiSO4	154.757	0.25	1	1.63E-03	
	CuSO4	159.61	0.26	1	1.63E-03	
EX 2	TPP	614.752	1.00	1	1.63E-03	1.29
	NiSO4	154.757	0.25	1	1.63E-03	
	CuSO4	159.61	0.26	1	1.63E-03	
EX 3	TPP	614.752	1.00	1	1.63E-03	1.32
	NiSO4	154.757	0.25	1	1.63E-03	
	CuSO4	159.61	0.26	1	1.63E-03	

Table B8: Sample 7 $NiSO_4$ + $CrSO_4$ + TPP.

	Compound	Molecular Weigth [g/moles]	Mass = moles x MW [g]	Ratio	Moles = Mass / MW	After Rx Solid obtained [g]
EX 1	TPP	614.752	1.00	1	1.63E-03	1.19
	NiSO4	154.757	0.25	1	1.63E-03	
	CrSO4	148.06	0.24	1	1.63E-03	
EX 2	TPP	614.752	1.00	1	1.63E-03	1.21
	NiSO4	154.757	0.25	1	1.63E-03	
	CrSO4	148.06	0.24	1	1.63E-03	
EX 3	TPP	614.752	1.00	1	1.63E-03	1.27
	NiSO4	154.757	0.25	1	1.63E-03	
	CrSO4	148.06	0.24	1	1.63E-03	

Table B9: Sample 7_1 $NiSO_4$ + $FeSO_4$ + TPP.

	Compound	Molecular Weigth [g/moles]	Mass = moles x MW [g]	Ratio	Moles = Mass / MW	After Rx Solid obtained [g]
EX 1	TPP	614.752	1.00	1	1.63E-03	1.32
	NiSO4	154.757	0.25	1	1.63E-03	
	FeSO4	151.909	0.25	1	1.63E-03	
EX 2	TPP	614.752	1.00	1	1.63E-03	1.27
	NiSO4	154.757	0.25	1	1.63E-03	
	FeSO4	151.909	0.25	1	1.63E-03	
EX 3	TPP	614.752	1.00	1	1.63E-03	1.3
	NiSO4	154.757	0.25	1	1.63E-03	
	FeSO4	151.909	0.25	1	1.63E-03	

STAGE 4A. Under Nitrogen $VOSO_4$ + TPP + MSO_4

Table B10: Sample 22 $VOSO_4$ + $ZnSO_4$ + TPP.

	Compound	Molecular Weigth [g/moles]	Mass = moles x MW [g]	Ratio	Moles = Mass / MW	After Rx Solid obtained [g]
EX 1	TPP	614.752	1.00	1	1.63E-03	1.27
	VOSO4	163.005	0.27	1	1.63E-03	
	ZnSO4	161.454	0.26	1	1.63E-03	
EX 2	TPP	614.752	1.00	1	1.63E-03	1.24
	VOSO4	163.005	0.27	1	1.63E-03	
	ZnSO4	161.454	0.26	1	1.63E-03	
EX 3	TPP	614.752	1.00	1	1.63E-03	1.19
	VOSO4	163.005	0.27	1	1.63E-03	
	ZnSO4	161.454	0.26	1	1.63E-03	
EX 4	TPP	614.752	1.00	1	1.63E-03	1.21
	VOSO4	163.005	0.27	1	1.63E-03	
	ZnSO4	161.454	0.26	1	1.63E-03	
EX 5	TPP	614.752	1.00	1	1.63E-03	1.3
	VOSO4	163.005	0.27	1	1.63E-03	
	ZnSO4	161.454	0.26	1	1.63E-03	

Table B11: Sample 23 $VOSO_4$ + $CuSO_4$ + TPP.

	Compound	Molecular Weigth [g/moles]	Mass = moles x MW [g]	Ratio	Moles = Mass / MW	After Rx Solid obtained [g]
EX 1	TPP	614.752	1.00	1	1.63E-03	1.16
	VOSO4	163.005	0.27	1	1.63E-03	
	CuSO4	159.610	0.26	1	1.63E-03	
EX 2	TPP	614.752	1.00	1	1.63E-03	1.17
	VOSO4	163.005	0.27	1	1.63E-03	
	CuSO4	159.610	0.26	1	1.63E-03	
EX 3	TPP	614.752	1.00	1	1.63E-03	1.2
	VOSO4	163.005	0.27	1	1.63E-03	
	CuSO4	159.610	0.26	1	1.63E-03	
EX 4	TPP	614.752	1.00	1	1.63E-03	1.24
	VOSO4	163.005	0.27	1	1.63E-03	
	CuSO4	159.610	0.26	1	1.63E-03	
EX 5	TPP	614.752	1.00	1	1.63E-03	1.28
	VOSO4	163.005	0.27	1	1.63E-03	
	CuSO4	159.610	0.26	1	1.63E-03	

Table B12: Sample 24 $VOSO_4$ + $CrSO_4$ + TPP.

	Compound	Molecular Weigth [g/moles]	Mass = moles x MW [g]	Ratio	Moles = Mass / MW	After Rx Solid obtained [g]
EX 1	TPP	614.752	1.00	1	1.63E-03	1.16
	VOSO4	163.005	0.27	1	1.63E-03	
	CrSO4	148.06	0.24	1	1.63E-03	
EX 2	TPP	614.752	1.00	1	1.63E-03	1.13
	VOSO4	163.005	0.27	1	1.63E-03	
	CrSO4	148.06	0.24	1	1.63E-03	
EX 3	TPP	614.752	1.00	1	1.63E-03	1.2
	VOSO4	163.005	0.27	1	1.63E-03	
	CrSO4	148.06	0.24	1	1.63E-03	
EX 4	TPP	614.752	1.00	1	1.63E-03	1.18
	VOSO4	163.005	0.27	1	1.63E-03	
	CrSO4	148.06	0.24	1	1.63E-03	
EX 5	TPP	614.752	1.00	1	1.63E-03	1.15
	VOSO4	163.005	0.27	1	1.63E-03	
	CrSO4	148.06	0.24	1	1.63E-03	

Table B13: Sample 25 $VOSO_4$ + $NiSO_4$ + TPP.

	Compound	Molecular Weigth [g/moles]	Mass = moles x MW [g]	Ratio	Moles = Mass / MW	After Rx Solid obtained [g]
EX 1	TPP	614.752	1.00	1	1.63E-03	1.24
	VOSO4	163.005	0.27	1	1.63E-03	
	NiSO4	154.757	0.25	1	1.63E-03	
EX 2	TPP	614.752	1.00	1	1.63E-03	1.25
	VOSO4	163.005	0.27	1	1.63E-03	
	NiSO4	154.757	0.25	1	1.63E-03	
EX 3	TPP	614.752	1.00	1	1.63E-03	1.31
	VOSO4	163.005	0.27	1	1.63E-03	
	NiSO4	154.757	0.25	1	1.63E-03	
EX 4	TPP	614.752	1.00	1	1.63E-03	1.27
	VOSO4	163.005	0.27	1	1.63E-03	
	NiSO4	154.757	0.25	1	1.63E-03	
EX 5	TPP	614.752	1.00	1	1.63E-03	1.3
	VOSO4	163.005	0.27	1	1.63E-03	
	NiSO4	154.757	0.25	1	1.63E-03	

Table B14: Sample 26 $VOSO_4$ + $FeSO_4$ + TPP.

	Compound	Molecular Weigth [g/moles]	Mass = moles x MW [g]	Ratio	Moles = Mass / MW	After Rx Solid obtained [g]
EX 1	TPP	614.752	1.00	1	1.63E-03	1.27
	VOSO4	163.005	0.27	1	1.63E-03	
	FeSO4	151.909	0.25	1	1.63E-03	
EX 2	TPP	614.752	1.00	1	1.63E-03	1.19
	VOSO4	163.005	0.27	1	1.63E-03	
	FeSO4	151.909	0.25	1	1.63E-03	
EX 3	TPP	614.752	1.00	1	1.63E-03	1.24
	VOSO4	163.005	0.27	1	1.63E-03	
	FeSO4	151.909	0.25	1	1.63E-03	
EX 4	TPP	614.752	1.00	1	1.63E-03	1.29
	VOSO4	163.005	0.27	1	1.63E-03	
	FeSO4	151.909	0.25	1	1.63E-03	
EX 5	TPP	614.752	1.00	1	1.63E-03	1.21
	VOSO4	163.005	0.27	1	1.63E-03	
	FeSO4	151.909	0.25	1	1.63E-03	

STAGE 4B. Under Nitrogen $NiSO_4$ + TPP + MSO_4

Table B15: Sample 27 $NiSO_4$ + $ZnSO_4$ + TPP.

	Compound	Molecular Weigth [g/moles]	Mass = moles x MW [g]	Ratio	Moles = Mass / MW	After Rx Solid obtained [g]
EX 1	TPP	614.752	1.00	1	1.63E-03	1.29
	NiSO4	154.757	0.25	1	1.63E-03	
	ZnSO4	161.454	0.26	1	1.63E-03	
EX 2	TPP	614.752	1.00	1	1.63E-03	1.23
	NiSO4	154.757	0.25	1	1.63E-03	
	ZnSO4	161.454	0.26	1	1.63E-03	
EX 3	TPP	614.752	1.00	1	1.63E-03	1.33
	NiSO4	154.757	0.25	1	1.63E-03	
	ZnSO4	161.454	0.26	1	1.63E-03	

Table B16: Sample 28 $NiSO_4$ + $CuSO_4$ + TPP.

	Compound	Molecular Weigth [g/moles]	Mass = moles x MW [g]	Ratio	Moles = Mass / MW	After Rx Solid obtained [g]
EX 1	TPP	614.752	1.00	1	1.63E-03	1.31
	NiSO4	154.757	0.25	1	1.63E-03	
	CuSO4	159.61	0.26	1	1.63E-03	
EX 2	TPP	614.752	1.00	1	1.63E-03	0.28
	NiSO4	154.757	0.25	1	1.63E-03	
	CuSO4	159.61	0.26	1	1.63E-03	
EX 3	TPP	614.752	1.00	1	1.63E-03	1.33
	NiSO4	154.757	0.25	1	1.63E-03	
	CuSO4	159.61	0.26	1	1.63E-03	

Table B17: Sample 29 $NiSO_4$ + $CrSO_4$ + TPP.

	Compound	Molecular Weigth [g/moles]	Mass = moles x MW [g]	Ratio	Moles = Mass / MW	After Rx Solid obtained [g]
EX 1	TPP	614.752	1.00	1	1.63E-03	1.24
	NiSO4	154.757	0.25	1	1.63E-03	
	CrSO4	148.06	0.24	1	1.63E-03	
EX 2	TPP	614.752	1.00	1	1.63E-03	1.18
	NiSO4	154.757	0.25	1	1.63E-03	
	CrSO4	148.06	0.24	1	1.63E-03	
EX 3	TPP	614.752	1.00	1	1.63E-03	1.15
	NiSO4	154.757	0.25	1	1.63E-03	
	CrSO4	148.06	0.24	1	1.63E-03	

Table B18: Sample 30 $NiSO_4$ + $FeSO_4$ + TPP.

	Compound	Molecular Weigth [g/moles]	Mass = moles x MW [g]	Ratio	Moles = Mass / MW	After Rx Solid obtained [g]
EX 1	TPP	614.752	1.00	1	1.63E-03	1.23
	NiSO4	154.757	0.25	1	1.63E-03	
	FeSO4	151.909	0.25	1	1.63E-03	
EX 2	TPP	614.752	1.00	1	1.63E-03	1.21
	NiSO4	154.757	0.25	1	1.63E-03	
	FeSO4	151.909	0.25	1	1.63E-03	
EX 3	TPP	614.752	1.00	1	1.63E-03	1.29
	NiSO4	154.757	0.25	1	1.63E-03	
	FeSO4	151.909	0.25	1	1.63E-03	

STAGE 7 A. Open System with Na_2S. $VOSO_4$ + TPP + Na_2S + MSO_4

Table B19: Sample 45 $VOSO_4$ + $ZnSO_4$ + Na_2S + TPP.

	Compound	Molecular Weigth [g/moles]	Mass = moles x MW [g]	Ratio	Moles = Mass / MW	After Rx Solid obtained [g]
EX 1	TPP	614.752	1.00	1	1.63E-03	1.27
	VOSO4	163.005	0.27	1	1.63E-03	
	ZnSO4	161.454	0.26	1	1.63E-03	
EX 2	TPP	614.752	1.00	1	1.63E-03	1.2
	VOSO4	163.005	0.27	1	1.63E-03	
	ZnSO4	161.454	0.26	1	1.63E-03	
EX 3	TPP	614.752	1.00	1	1.63E-03	1.21
	VOSO4	163.005	0.27	1	1.63E-03	
	ZnSO4	161.454	0.26	1	1.63E-03	
EX 4	TPP	614.752	1.00	1	1.63E-03	1.3
	VOSO4	163.005	0.27	1	1.63E-03	
	ZnSO4	161.454	0.26	1	1.63E-03	
EX 5	TPP	614.752	1.00	1	1.63E-03	1.35
	VOSO4	163.005	0.27	1	1.63E-03	
	ZnSO4	161.454	0.26	1	1.63E-03	

Table B20: Sample 46 $VOSO_4$ + $CuSO_4$ + Na_2S + TPP.

	Compound	Molecular Weigth [g/moles]	Mass = moles x MW [g]	Ratio	Moles = Mass / MW	After Rx Solid obtained [g]
EX 1	TPP	614.752	1.00	1	1.63E-03	1.28
	VOSO4	163.005	0.27	1	1.63E-03	
	CuSO4	159.610	0.26	1	1.63E-03	
EX 2	TPP	614.752	1.00	1	1.63E-03	1.25
	VOSO4	163.005	0.27	1	1.63E-03	
	CuSO4	159.610	0.26	1	1.63E-03	
EX 3	TPP	614.752	1.00	1	1.63E-03	1.31
	VOSO4	163.005	0.27	1	1.63E-03	
	CuSO4	159.610	0.26	1	1.63E-03	
EX 4	TPP	614.752	1.00	1	1.63E-03	1.22
	VOSO4	163.005	0.27	1	1.63E-03	
	CuSO4	159.610	0.26	1	1.63E-03	
EX 5	TPP	614.752	1.00	1	1.63E-03	1.37
	VOSO4	163.005	0.27	1	1.63E-03	
	CuSO4	159.610	0.26	1	1.63E-03	

Table B21: Sample 47 $VOSO_4$ + $CrSO_4$ + Na_2S + TPP.

	Compound	Molecular Weigth [g/moles]	Mass = moles x MW [g]	Ratio	Moles = Mass / MW	After Rx Solid obtained [g]
EX 1	TPP	614.752	1.00	1	1.63E-03	1.33
	VOSO4	163.005	0.27	1	1.63E-03	
	CrSO4	148.06	0.24	1	1.63E-03	
EX 2	TPP	614.752	1.00	1	1.63E-03	1.21
	VOSO4	163.005	0.27	1	1.63E-03	
	CrSO4	148.06	0.24	1	1.63E-03	
EX 3	TPP	614.752	1.00	1	1.63E-03	1.35
	VOSO4	163.005	0.27	1	1.63E-03	
	CrSO4	148.06	0.24	1	1.63E-03	
EX 4	TPP	614.752	1.00	1	1.63E-03	1.34
	VOSO4	163.005	0.27	1	1.63E-03	
	CrSO4	148.06	0.24	1	1.63E-03	
EX 5	TPP	614.752	1.00	1	1.63E-03	1.24
	VOSO4	163.005	0.27	1	1.63E-03	
	CrSO4	148.06	0.24	1	1.63E-03	

Table B22: Sample 48 $VOSO_4$ + $NiSO_4$ + Na_2S + TPP.

	Compound	Molecular Weigth [g/moles]	Mass = moles x MW [g]	Ratio	Moles = Mass / MW	After Rx Solid obtained [g]
EX 1	TPP	614.752	1.00	1	1.63E-03	1.33
	VOSO4	163.005	0.27	1	1.63E-03	
	NiSO4	154.757	0.25	1	1.63E-03	
EX 2	TPP	614.752	1.00	1	1.63E-03	1.29
	VOSO4	163.005	0.27	1	1.63E-03	
	NiSO4	154.757	0.25	1	1.63E-03	
EX 3	TPP	614.752	1.00	1	1.63E-03	1.2
	VOSO4	163.005	0.27	1	1.63E-03	
	NiSO4	154.757	0.25	1	1.63E-03	
EX 4	TPP	614.752	1.00	1	1.63E-03	1.3
	VOSO4	163.005	0.27	1	1.63E-03	
	NiSO4	154.757	0.25	1	1.63E-03	
EX 5	TPP	614.752	1.00	1	1.63E-03	1.35
	VOSO4	163.005	0.27	1	1.63E-03	
	NiSO4	154.757	0.25	1	1.63E-03	

Table B23: Sample 49 $VOSO_4$ + $FeSO_4$ + Na_2S + TPP.

	Compound	Molecular Weigth [g/moles]	Mass = moles x MW [g]	Ratio	Moles = Mass / MW	After Rx Solid obtained [g]
EX 1	TPP	614.752	1.00	1	1.63E-03	1.27
	VOSO4	163.005	0.27	1	1.63E-03	
	FeSO4	151.909	0.25	1	1.63E-03	
EX 2	TPP	614.752	1.00	1	1.63E-03	1.35
	VOSO4	163.005	0.27	1	1.63E-03	
	FeSO4	151.909	0.25	1	1.63E-03	
EX 3	TPP	614.752	1.00	1	1.63E-03	1.33
	VOSO4	163.005	0.27	1	1.63E-03	
	FeSO4	151.909	0.25	1	1.63E-03	
EX 4	TPP	614.752	1.00	1	1.63E-03	1.26
	VOSO4	163.005	0.27	1	1.63E-03	
	FeSO4	151.909	0.25	1	1.63E-03	
EX 5	TPP	614.752	1.00	1	1.63E-03	1.30
	VOSO4	163.005	0.27	1	1.63E-03	
	FeSO4	151.909	0.25	1	1.63E-03	

STAGE 7 B. Open System with Na_2S. $NiSO_4$ + TPP + Na_2S + MSO_4

Table B24: Sample 50 $NiSO_4$ + $ZnSO_4$ + Na_2S + TPP.

	Compound	Molecular Weigth [g/moles]	Mass = moles x MW [g]	Ratio	Moles = Mass / MW	After Rx Solid obtained [g]
EX 1	TPP	614.752	1.00	1	1.63E-03	1.25
	NiSO4	154.757	0.25	1	1.63E-03	
	ZnSO4	161.454	0.26	1	1.63E-03	
EX 2	TPP	614.752	1.00	1	1.63E-03	1.22
	NiSO4	154.757	0.25	1	1.63E-03	
	ZnSO4	161.454	0.26	1	1.63E-03	
EX 3	TPP	614.752	1.00	1	1.63E-03	1.29
	NiSO4	154.757	0.25	1	1.63E-03	
	ZnSO4	161.454	0.26	1	1.63E-03	

Table B25: Sample 51 $NiSO_4$ + $CuSO_4$ + Na_2S + TPP.

	Compound	Molecular Weigth [g/moles]	Mass = moles x MW [g]	Ratio	Moles = Mass / MW	After Rx Solid obtained [g]
EX 1	TPP	614.752	1.00	1	1.63E-03	1.31
	NiSO4	154.757	0.25	1	1.63E-03	
	CuSO4	159.61	0.26	1	1.63E-03	
EX 2	TPP	614.752	1.00	1	1.63E-03	1.3
	NiSO4	154.757	0.25	1	1.63E-03	
	CuSO4	159.61	0.26	1	1.63E-03	
EX 3	TPP	614.752	1.00	1	1.63E-03	1.26
	NiSO4	154.757	0.25	1	1.63E-03	
	CuSO4	159.61	0.26	1	1.63E-03	

Table B26: Sample 52 $NiSO_4$ + $CrSO_4$ + Na_2S + TPP.

	Compound	Molecular Weigth [g/moles]	Mass = moles x MW [g]	Ratio	Moles = Mass / MW	After Rx Solid obtained [g]
EX 1	TPP	614.752	1.00	1	1.63E-03	1.3
	NiSO4	154.757	0.25	1	1.63E-03	
	CrSO4	148.06	0.24	1	1.63E-03	
EX 2	TPP	614.752	1.00	1	1.63E-03	1.19
	NiSO4	154.757	0.25	1	1.63E-03	
	CrSO4	148.06	0.24	1	1.63E-03	
EX 3	TPP	614.752	1.00	1	1.63E-03	1.24
	NiSO4	154.757	0.25	1	1.63E-03	
	CrSO4	148.06	0.24	1	1.63E-03	

Table B27: Sample 53 $NiSO_4$ + $FeSO_4$ + Na_2S + TPP.

	Compound	Molecular Weigth [g/moles]	Mass = moles x MW [g]	Ratio	Moles = Mass / MW	After Rx Solid obtained [g]
EX 1	TPP	614.752	1.00	1	1.63E-03	1.27
	NiSO4	154.757	0.25	1	1.63E-03	
	FeSO4	151.909	0.25	1	1.63E-03	
EX 2	TPP	614.752	1.00	1	1.63E-03	1.32
	NiSO4	154.757	0.25	1	1.63E-03	
	FeSO4	151.909	0.25	1	1.63E-03	
EX 3	TPP	614.752	1.00	1	1.63E-03	1.23
	NiSO4	154.757	0.25	1	1.63E-03	
	FeSO4	151.909	0.25	1	1.63E-03	

Appendix C. CHEMICAL REACTIONS DEMETALLATIONS

STAGE 2A. Open System. $VOSO_4$ + MTPP

Table C1: Sample 8 VOSO4 + ZnTPP

	Compound	Molecular Weigth [g/moles]	Mass = moles x MW [g]	Ratio	Moles = Mass / MW	After Rx Solid obtained [g]
EX 1	$VOSO_4$	163.005	0.27	1	1.63E-03	0.96
	ZnTPP	678.126	1.10	1	1.63E-03	
EX 2	$VOSO_4$	163.005	0.27	1	1.63E-03	1
	ZnTPP	678.126	1.10	1	1.63E-03	
EX 3	VOSO4	163.005	0.27	1	1.63E-03	1.02
	ZnTPP	678.126	1.10	1	1.63E-03	

Table C2: Sample 9 $VOSO_4$ + CuTPP

	Compound	Molecular Weigth [g/moles]	Mass = moles x MW [g]	Ratio	Moles = Mass / MW	After Rx Solid obtained [g]
EX 1	$VOSO_4$	163.005	0.27	1	1.63E-03	0.91
	CuTPP	676.282	1.10	1	1.63E-03	
EX 2	$VOSO_4$	163.005	0.27	1	1.63E-03	0.97
	CuTPP	676.282	1.10	1	1.63E-03	
EX 3	VOSO4	163.005	0.27	1	1.63E-03	0.86
	CuTPP	676.282	1.10	1	1.63E-03	

Table C3: Sample 10 $VOSO_4$ + CrTPP

	Compound	Molecular Weigth [g/moles]	Mass = moles x MW [g]	Ratio	Moles = Mass / MW	After Rx Solid obtained [g]
EX 1	$VOSO_4$	163.005	0.27	1	1.63E-03	1.2
	CrTPP	664.732	1.08	1	1.63E-03	
EX 2	$VOSO_4$	163.005	0.27	1	1.63E-03	1.17
	CrTPP	664.732	1.08	1	1.63E-03	
EX 3	VOSO4	163.005	0.27	1	1.63E-03	1.15
	CrTPP	664.732	1.08	1	1.63E-03	

Table C4: Sample 11 $VOSO_4$ + NiTPP

	Compound	Molecular Weigth [g/moles]	Mass = moles x MW [g]	Ratio	Moles = Mass / MW	After Rx Solid obtained [g]
EX 1	$VOSO_4$	163.005	0.27	1	1.63E-03	1.17
	NiTPP	671.429	1.09	1	1.63E-03	
EX 2	$VOSO_4$	163.005	0.27	1	1.63E-03	1.15
	NiTPP	671.429	1.09	1	1.63E-03	
EX 3	VOSO4	163.005	0.27	1	1.63E-03	1.12
	NiTPP	671.429	1.09	1	1.63E-03	

STAGE 2B. Open System. $NiSO_4$ + MTPP

Table C5: Sample 12 $NiSO_4$ + ZnTPP

	Compound	Molecular Weigth [g/moles]	Mass = moles x MW [g]	Ratio	Moles = Mass / MW	After Rx Solid obtained [g]
EX 1	$NiSO_4$	154.757	0.25	1	1.63E-03	1.12
	ZnTPP	678.126	1.10	1	1.63E-03	
EX 2	$NiSO_4$	154.757	0.25	1	1.63E-03	1.2
	ZnTPP	678.126	1.10	1	1.63E-03	
EX 3	$NiSO_4$	154.757	0.25	1	1.63E-03	1.09
	ZnTPP	678.126	1.10	1	1.63E-03	

Table C6: Sample 13 $NiSO_4$ + CuTPP

	Compound	Molecular Weigth [g/moles]	Mass = moles x MW [g]	Ratio	Moles = Mass / MW	After Rx Solid obtained [g]
EX 1	$NiSO_4$	154.757	0.25	1	1.63E-03	1.09
	CuTPP	676.282	1.10	1	1.63E-03	
EX 2	$NiSO_4$	154.757	0.25	1	1.63E-03	1.16
	CuTPP	676.282	1.10	1	1.63E-03	
EX 3	$NiSO_4$	154.757	0.25	1	1.63E-03	1.14
	CuTPP	676.282	1.10	1	1.63E-03	

Table C7: Sample 14 $NiSO_4$ + CrTPP

	Compound	Molecular Weigth [g/moles]	Mass = moles x MW [g]	Ratio	Moles = Mass / MW	After Rx Solid obtained [g]
EX 1	$NiSO_4$	154.757	0.25	1	1.63E-03	1.13
	CrTPP	664.732	1.08	1	1.63E-03	
EX 2	$NiSO_4$	154.757	0.25	1	1.63E-03	1.18
	CrTPP	664.732	1.08	1	1.63E-03	
EX 3	$NiSO_4$	154.757	0.25	1	1.63E-03	1.08
	CrTPP	664.732	1.08	1	1.63E-03	

Table C8: Sample 15 $NiSO_4$ + VOTPP

	Compound	Molecular Weigth [g/moles]	Mass = moles x MW [g]	Ratio	Moles = Mass / MW	After Rx Solid obtained [g]
EX 1	$NiSO_4$	154.757	0.25	1	1.63E-03	1.18
	VOTPP	679.677	1.11	1	1.63E-03	
EX 2	$NiSO_4$	154.757	0.25	1	1.63E-03	1.14
	VOTPP	679.677	1.11	1	1.63E-03	
EX 3	$NiSO_4$	154.757	0.25	1	1.63E-03	1.12
	VOTPP	679.677	1.11	1	1.63E-03	

STAGE 3A. Open System. VOTPP + MSO_4

Table C9: Sample 16 VOTPP + $ZnSO_4$

	Compound	Molecular Weigth [g/moles]	Mass = moles x MW [g]	Ratio	Moles = Mass / MW	After Rx Solid obtained [g]
EX 1	$ZnSO_4$	161.454	0.26	1	1.63E-03	1.15
	VOTPP	679.677	1.11	1	1.63E-03	
EX 2	$ZnSO_4$	161.454	0.26	1	1.63E-03	1.08
	VOTPP	679.677	1.11	1	1.63E-03	
EX 3	ZnSO4	161.454	0.26	1	1.63E-03	1.17
	VOTPP	679.677	1.11	1	1.63E-03	

Table C10: Sample 17 VOTPP + $CuSO_4$

	Compound	Molecular Weigth [g/moles]	Mass = moles x MW [g]	Ratio	Moles = Mass / MW	After Rx Solid obtained [g]
EX 1	VOTPP	679.677	1.11	1	1.63E-03	1.12
	$CuSO_4$	159.61	0.26	1	1.63E-03	
EX 2	VOTPP	679.677	1.11	1	1.63E-03	0.98
	$CuSO_4$	159.61	0.26	1	1.63E-03	
EX 3	VOTPP	679.677	1.11	1	1.63E-03	1.06
	$CuSO_4$	159.61	0.26	1	1.63E-03	

Table C11: Sample 18 VOTPP + $CrSO_4$

	Compound	Molecular Weigth [g/moles]	Mass = moles x MW [g]	Ratio	Moles = Mass / MW	After Rx Solid obtained [g]
EX 1	VOTPP	679.677	1.11	1	1.63E-03	1.14
	$CrSO_4$	148.06	0.24	1	1.63E-03	
EX 2	VOTPP	679.677	1.11	1	1.63E-03	1.07
	$CrSO_4$	148.06	0.24	1	1.63E-03	
EX 3	VOTPP	679.677	1.11	1	1.63E-03	1.11
	$CrSO_4$	148.06	0.24	1	1.63E-03	

STAGE 3B. Open System. NiTPP + MSO_4

Table C12: Sample 19 NiTPP + $ZnSO_4$

	Compound	Molecular Weigth [g/moles]	Mass = moles x MW [g]	Ratio	Moles = Mass / MW	After Rx Solid obtained [g]
EX 1	$ZnSO_4$	161.454	0.26	1	1.63E-03	1.12
	NiTPP	671.429	1.09	1	1.63E-03	
EX 2	$ZnSO_4$	161.454	0.26	1	1.63E-03	1.07
	NiTPP	671.429	1.09	1	1.63E-03	
EX 3	VOSO4	161.454	0.26	1	1.63E-03	1.16
	NiTPP	671.429	1.09	1	1.63E-03	

Table C13: Sample 20 NiTPP + $CuSO_4$

	Compound	Molecular Weigth [g/moles]	Mass = moles x MW [g]	Ratio	Moles = Mass / MW	After Rx Solid obtained [g]
EX 1	NiTPP	671.429	1.09	1	1.63E-03	1.06
	$CuSO_4$	159.61	0.26	1	1.63E-03	
EX 2	NiTPP	671.429	1.09	1	1.63E-03	1.04
	$CuSO_4$	159.61	0.26	1	1.63E-03	
EX 3	NiTPP	671.429	1.09	1	1.63E-03	1.06
	$CuSO_4$	159.61	0.26	1	1.63E-03	

Table C14: Sample 21 NiTPP + $CrSO_4$

	Compound	Molecular Weigth [g/moles]	Mass = moles x MW [g]	Ratio	Moles = Mass / MW	After Rx Solid obtained [g]
EX 1	NiTPP	671.429	1.09	1	1.63E-03	1.18
	$CrSO_4$	148.06	0.24	1	1.63E-03	
EX 2	NiTPP	671.429	1.09	1	1.63E-03	1.12
	$CrSO_4$	148.06	0.24	1	1.63E-03	
EX 3	NiTPP	671.429	1.09	1	1.63E-03	1.00
	$CrSO_4$	148.06	0.24	1	1.63E-03	

STAGE 5A. Under Nitrogen. $VOSO_4$ + MTPP

Table C15: Sample 31 $VOSO_4$ + ZnTPP

	Compound	Molecular Weigth [g/moles]	Mass = moles x MW [g]	Ratio	Moles = Mass / MW	After Rx Solid obtained [g]
EX 1	$VOSO_4$	163.005	0.27	1	1.63E-03	1.15
	ZnTPP	678.126	1.10	1	1.63E-03	
EX 2	$VOSO_4$	163.005	0.27	1	1.63E-03	1.08
	ZnTPP	678.126	1.10	1	1.63E-03	
EX 3	VOSO4	163.005	0.27	1	1.63E-03	1.12
	ZnTPP	678.126	1.10	1	1.63E-03	

Table C16: Sample 32 $VOSO_4$ + CuTPP

	Compound	Molecular Weigth [g/moles]	Mass = moles x MW [g]	Ratio	Moles = Mass / MW	After Rx Solid obtained [g]
EX 1	$VOSO_4$	163.005	0.27	1	1.63E-03	1.12
	CuTPP	676.282	1.10	1	1.63E-03	
EX 2	$VOSO_4$	163.005	0.27	1	1.63E-03	1.08
	CuTPP	676.282	1.10	1	1.63E-03	
EX 3	VOSO4	163.005	0.27	1	1.63E-03	1.05
	CuTPP	676.282	1.10	1	1.63E-03	

Table C17: Sample 33 $VOSO_4$ + CrTPP

	Compound	Molecular Weigth [g/moles]	Mass = moles x MW [g]	Ratio	Moles = Mass / MW	After Rx Solid obtained [g]
EX 1	$VOSO_4$	163.005	0.27	1	1.63E-03	1.12
	CrTPP	664.732	1.08	1	1.63E-03	
EX 2	$VOSO_4$	163.005	0.27	1	1.63E-03	1.1
	CrTPP	664.732	1.08	1	1.63E-03	
EX 3	VOSO4	163.005	0.27	1	1.63E-03	1.07
	CrTPP	664.732	1.08	1	1.63E-03	

Table C18: Sample 34 $VOSO_4$ + NiTPP

	Compound	Molecular Weigth [g/moles]	Mass = moles x MW [g]	Ratio	Moles = Mass / MW	After Rx Solid obtained [g]
EX 1	$VOSO_4$	163.005	0.27	1	1.63E-03	1.21
	NiTPP	671.429	1.09	1	1.63E-03	
EX 2	$VOSO_4$	163.005	0.27	1	1.63E-03	1.16
	NiTPP	671.429	1.09	1	1.63E-03	
EX 3	VOSO4	163.005	0.27	1	1.63E-03	1.13
	NiTPP	671.429	1.09	1	1.63E-03	

STAGE 5B. Under Nitrogen. $NiSO_4$ + MTPP

Table C19: Sample 35 $NiSO_4$ + ZnTPP

	Compound	Molecular Weigth [g/moles]	Mass = moles x MW [g]	Ratio	Moles = Mass / MW	After Rx Solid obtained [g]
EX 1	$NiSO_4$	154.757	0.25	1	1.63E-03	1.13
	ZnTPP	678.126	1.10	1	1.63E-03	
EX 2	$NiSO_4$	154.757	0.25	1	1.63E-03	1.08
	ZnTPP	678.126	1.10	1	1.63E-03	
EX 3	$NiSO_4$	154.757	0.25	1	1.63E-03	1.04
	ZnTPP	678.126	1.10	1	1.63E-03	

Table C20: Sample 36 $NiSO_4$ + CuTPP

	Compound	Molecular Weigth [g/moles]	Mass = moles x MW [g]	Ratio	Moles = Mass / MW	After Rx Solid obtained [g]
EX 1	$NiSO_4$	154.757	0.25	1	1.63E-03	1.01
	CuTPP	676.282	1.10	1	1.63E-03	
EX 2	$NiSO_4$	154.757	0.25	1	1.63E-03	1.07
	CuTPP	676.282	1.10	1	1.63E-03	
EX 3	$NiSO_4$	154.757	0.25	1	1.63E-03	0.99
	CuTPP	676.282	1.10	1	1.63E-03	

Table C21: Sample 37 $NiSO_4$ + CrTPP

	Compound	Molecular Weigth [g/moles]	Mass = moles x MW [g]	Ratio	Moles = Mass / MW	After Rx Solid obtained [g]
EX 1	$NiSO_4$	154.757	0.25	1	1.63E-03	1.2
	CrTPP	664.732	1.08	1	1.63E-03	
EX 2	$NiSO_4$	154.757	0.25	1	1.63E-03	1.16
	CrTPP	664.732	1.08	1	1.63E-03	
EX 3	$NiSO_4$	154.757	0.25	1	1.63E-03	1.11
	CrTPP	664.732	1.08	1	1.63E-03	

Table C22: Sample 38 $NiSO_4$ + VOTPP

	Compound	Molecular Weigth [g/moles]	Mass = moles x MW [g]	Ratio	Moles = Mass / MW	After Rx Solid obtained [g]
EX 1	$NiSO_4$	154.757	0.25	1	1.63E-03	1.06
	VOTPP	679.677	1.11	1	1.63E-03	
EX 2	$NiSO_4$	154.757	0.25	1	1.63E-03	1.08
	VOTPP	679.677	1.11	1	1.63E-03	
EX 3	$NiSO_4$	154.757	0.25	1	1.63E-03	1.14
	VOTPP	679.677	1.11	1	1.63E-03	

STAGE 6A. Under Nitrogen. VOTPP + MSO_4

Table C23: Sample 39 VOTPP + $ZnSO_4$

	Compound	Molecular Weigth [g/moles]	Mass = moles x MW [g]	Ratio	Moles = Mass / MW	After Rx Solid obtained [g]
EX 1	$ZnSO_4$	161.454	0.26	1	1.63E-03	1.06
	VOTPP	679.677	1.11	1	1.63E-03	
EX 2	$ZnSO_4$	161.454	0.26	1	1.63E-03	0.98
	VOTPP	679.677	1.11	1	1.63E-03	
EX 3	ZnSO4	161.454	0.26	1	1.63E-03	0.94
	VOTPP	679.677	1.11	1	1.63E-03	

Table C24: Sample 40 VOTPP + $CuSO_4$

	Compound	Molecular Weigth [g/moles]	Mass = moles x MW [g]	Ratio	Moles = Mass / MW	After Rx Solid obtained [g]
EX 1	VOTPP	679.677	1.11	1	1.63E-03	1.05
	$CuSO_4$	159.61	0.26	1	1.63E-03	
EX 2	VOTPP	679.677	1.11	1	1.63E-03	1.11
	$CuSO_4$	159.61	0.26	1	1.63E-03	
EX 3	VOTPP	679.677	1.11	1	1.63E-03	0.94
	$CuSO_4$	159.61	0.26	1	1.63E-03	

Table C25: Sample 41 VOTPP + $CrSO_4$

	Compound	Molecular Weigth [g/moles]	Mass = moles x MW [g]	Ratio	Moles = Mass / MW	After Rx Solid obtained [g]
EX 1	VOTPP	679.677	1.11	1	1.63E-03	1.12
	$CrSO_4$	148.06	0.24	1	1.63E-03	
EX 2	VOTPP	679.677	1.11	1	1.63E-03	1.05
	$CrSO_4$	148.06	0.24	1	1.63E-03	
EX 3	VOTPP	679.677	1.11	1	1.63E-03	1.01
	$CrSO_4$	148.06	0.24	1	1.63E-03	

STAGE 6B. Under Nitrogen. NiTPP + MSO_4

Table C26: Sample 42 NiTPP + $ZnSO_4$

	Compound	Molecular Weigth [g/moles]	Mass = moles x MW [g]	Ratio	Moles = Mass / MW	After Rx Solid obtained [g]
EX 1	$ZnSO_4$	161.454	0.26	1	1.63E-03	0.97
	NiTPP	671.429	1.09	1	1.63E-03	
EX 2	$ZnSO_4$	161.454	0.26	1	1.63E-03	0.92
	NiTPP	671.429	1.09	1	1.63E-03	
EX 3	VOSO4	161.454	0.26	1	1.63E-03	0.96
	NiTPP	671.429	1.09	1	1.63E-03	

Table C27: Sample 43 NiTPP + $CuSO_4$

	Compound	Molecular Weigth [g/moles]	Mass = moles x MW [g]	Ratio	Moles = Mass / MW	After Rx Solid obtained [g]
EX 1	NiTPP	671.429	1.09	1	1.63E-03	1.02
	$CuSO_4$	159.61	0.26	1	1.63E-03	
EX 2	NiTPP	671.429	1.09	1	1.63E-03	0.91
	$CuSO_4$	159.61	0.26	1	1.63E-03	
EX 3	NiTPP	671.429	1.09	1	1.63E-03	0.95
	$CuSO_4$	159.61	0.26	1	1.63E-03	

Table C28: Sample 44 NiTPP + $CrSO_4$

	Compound	Molecular Weigth [g/moles]	Mass = moles x MW [g]	Ratio	Moles = Mass / MW	After Rx Solid obtained [g]
EX 1	NiTPP	671.429	1.09	1	1.63E-03	1.2
	$CrSO_4$	148.06	0.24	1	1.63E-03	
EX 2	NiTPP	671.429	1.09	1	1.63E-03	0.93
	$CrSO_4$	148.06	0.24	1	1.63E-03	
EX 3	NiTPP	671.429	1.09	1	1.63E-03	1.00
	$CrSO_4$	148.06	0.24	1	1.63E-03	

Appendix D. COLUMNS CHROMATOGRAPHY - COMPETITIONS

Table D1: Sample 1 $VOSO_4$+$ZnSO_4$+TPP.

	After Rx Purification Si Column Chromatophraphy	
	Compound	[g]
EX 1	TPP	0
	VOTPP	0.35
	ZnTPP	0.89
EX 2	TPP	0
	VOTPP	0.41
	ZnTPP	0.87
EX 3	TPP	0
	VOTPP	0.31
	ZnTPP	0.87
EX 4	TPP	0
	VOTPP	0.27
	ZnTPP	0.81
EX 5	TPP	0
	VOTPP	0.21
	ZnTPP	0.78

Average Products		Error	Mass
Compound	[g]		%
TPP	0.00	0	0
VOTPP	0.31	± 0.1	26.9
ZnTPP	0.84	± 0.08	73.1

Table D2: Sample 2 $VOSO_4$+$CuSO_4$+TPP

	After Rx Purification Si Column Chromatophraphy	
	Compound	[g]
EX 1	TPP	0
	VOTPP	0
	CuTPP	0.94
EX 2	TPP	0
	VOTPP	0
	CuTPP	0.83
EX 3	TPP	0
	VOTPP	0
	CuTPP	0.76
EX 4	TPP	0
	VOTPP	0
	CuTPP	0.67
EX 5	TPP	0
	VOTPP	0
	CuTPP	0.81

Average Products		Error %	Mass %
Compound	[g]		
TPP	0.00	± 0.00	0
VOTPP	0.00	± 0.00	0
CuTPP	0.80	± 0.20	100

Table D3: Sample 3 $VOSO_4$+$CrSO_4$+TPP

	After Rx Purification Si Column Chromatophraphy	
	Compound	[g]
EX 1	TPP	0
	VOTPP	0.18
	CrTPP	0.87
EX 2	TPP	0
	VOTPP	0.1
	CrTPP	0.71
EX 3	TPP	0
	VOTPP	0.07
	CrTPP	0.81
EX 4	TPP	0
	VOTPP	0.13
	CrTPP	0.78
EX 5	TPP	0
	VOTPP	0.07
	CrTPP	0.83

Average Products		Error	Mass
Compound	[g]	%	%
TPP	0.00	± 0.00	0.0
VOTPP	0.11	± 0.09	12.1
CrTPP	0.80	± 0.12	87.9

Table D4: Sample 4 $VOSO_4$+$NiSO_4$+TPP

	After Rx Purification Si Column Chromatophraphy	
	Compound	[g]
EX 1	TPP	0
	VOTPP	0.05
	NiTPP	0.89
EX 2	TPP	0
	VOTPP	0.07
	NiTPP	0.74
EX 3	TPP	0
	VOTPP	0.04
	NiTPP	0.91
EX 4	TPP	0
	VOTPP	0.04
	NiTPP	0.71
EX 5	TPP	0
	VOTPP	0.04
	NiTPP	0.68

Average Products		Error	Mass
Compound	[g]	%	%
TPP	0.00	± 0.00	0
VOTPP	0.05	± 0.03	6
NiTPP	0.79	± 0.21	94

Table D5: Sample 4_1 $VOSO_4$+$FeSO_4$+TPP.

	After Rx Purification Si Column Chromatophraphy	
	Compound	[g]
EX 1	TPP	0
	VOTPP	0
	FeTPP	0.83
EX 2	TPP	0
	VOTPP	0
	FeTPP	0.91
EX 3	TPP	0
	VOTPP	0
	FeTPP	0.8
EX 4	TPP	0
	VOTPP	0
	FeTPP	0.75
EX 5	TPP	0
	VOTPP	0
	FeTPP	1.02

Average Products		Error	Mass %
Compound	[g]	%	
TPP	0.00	± 0.00	0
VOTPP	0.00	± 0.00	0
FeTPP	0.86	± 0.21	100

Table D6: Sample 5 $NiSO_4$ + $ZnSO_4$ + TPP.

	After Rx Purification Si Column Chromatophraphy	
	Compound	[g]
EX 1	TPP	0
	NiTPP	0.63
	ZnTPP	0.09
EX 2	TPP	0
	NiTPP	0.51
	ZnTPP	0.22
EX 3	TPP	0
	NiTPP	0.52
	ZnTPP	0.31

Average Products		Error	Mass
Compound	[g]		%
TPP	0.00	± 0.00	0
NiTPP	0.55	± 0.05	73
ZnTPP	0.21	± 0.09	27

Table D7: Sample 6 $NiSO_4$ + $CuSO_4$ + TPP.

	After Rx Purification Si Column Chromatophraphy	
	Compound	[g]
EX 1	TPP	0
	NiTPP	0.54
	CuTPP	0.12
EX 2	TPP	0
	NiTPP	0.47
	CuTPP	0.33
EX 3	TPP	0
	NiTPP	0.67
	CuTPP	0.07

Average Products		Error	Mass
Compound	[g]		%
TPP	0.00	± 0.00	0
NiTPP	0.56	± 0.083	76
CuTPP	0.17	± 0.113	24

Table D8: Sample 7 $NiSO_4$ + $CrSO_4$ + TPP.

	After Rx Purification Si Column Chromatophraphy	
	Compound	[g]
EX 1	TPP	0
	NiTPP	0.77
	CrTPP	0.12
EX 2	TPP	0
	NiTPP	0.8
	CrTPP	0.14
EX 3	TPP	0
	NiTPP	0.75
	CrTPP	0.2

Average Products		Error	Mass
Compound	[g]		%
TPP	0.00	± 0.00	0
NiTPP	0.77	± 0.02	83
CrTPP	0.15	± 0.03	17

Table D9: Sample 7_1 $NiSO_4$+$FeSO_4$+TPP

	After Rx Purification Si Column Chromatophraphy	
	Compound	[g]
EX 1	TPP	0
	NiTPP	0.66
	FeTPP	0.15
EX 2	TPP	0
	NiTPP	0.84
	FeTPP	0.11
EX 3	TPP	0
	NiTPP	0.67
	FeTPP	0.19

Average Products		Error	Mass
Compound	[g]		%
TPP	0.00	± 0.00	0.0
NiTPP	0.72	± 0.08	82.8
FeTPP	0.150	± 0.03	17.2

STAGE 4 A. Under Nitrogen

Table D10: Sample 22 $VOSO_4$+$ZnSO_4$+TPP.

	After Rx Purification Si Column Chromatophraphy	
	Compound	[g]
EX 1	TPP	0
	VOTPP	0.58
	ZnTPP	0.24
EX 2	TPP	0
	VOTPP	0.57
	ZnTPP	0.33
EX 3	TPP	0
	VOTPP	0.66
	ZnTPP	0.21
EX 4	TPP	0
	VOTPP	0.65
	ZnTPP	0.16
EX 5	TPP	0
	VOTPP	0.72
	ZnTPP	0.24

Average Products		Error	Mass
Compound	[g]		%
TPP	0.00	± 0	0
VOTPP	0.64	± 0.06	73
ZnTPP	0.24	± 0.06	27

Table D11: Sample 23 $VOSO_4$+$CuSO_4$+TPP.

	After Rx Purification Si Column Chromatophraphy	
	Compound	[g]
EX 1	TPP	0
	VOTPP	0.75
	CuTPP	0.14
EX 2	TPP	0
	VOTPP	0.71
	CuTPP	0.18
EX 3	TPP	0
	VOTPP	0.81
	CuTPP	0.09
EX 4	TPP	0
	VOTPP	0.69
	CuTPP	0.1
EX 5	TPP	0
	VOTPP	0.77
	CuTPP	0.08

Average Products		Error %	Mass %
Compound	[g]		
TPP	0.00	± 0.00	0
VOTPP	0.75	± 0.10	86
CuTPP	0.12	± 0.08	14

Table D12: Sample 24 $VOSO_4$+$CrSO_4$+TPP.

	After Rx Purification Si Column Chromatophraphy	
	Compound	[g]
EX 1	TPP	0
	VOTPP	0.51
	CrTPP	0.19
EX 2	TPP	0
	VOTPP	0.58
	CrTPP	0.21
EX 3	TPP	0
	VOTPP	0.67
	CrTPP	0.11
EX 4	TPP	0
	VOTPP	0.76
	CrTPP	0.17
EX 5	TPP	0
	VOTPP	0.69
	CrTPP	0.23

Average Products		Error	Mass
Compound	[g]	%	%
TPP	0.00	± 0.00	0
VOTPP	0.64	± 0.20	78
CrTPP	0.18	± 0.09209	22

Table D13: Sample 25 $VOSO_4$+$NiSO_4$+TPP.

	After Rx Purification Si Column Chromatophraphy	
	Compound	[g]
EX 1	TPP	0
	VOTPP	0.33
	NiTPP	0.51
EX 2	TPP	0
	VOTPP	0.28
	NiTPP	0.67
EX 3	TPP	0
	VOTPP	0.42
	NiTPP	0.71
EX 4	TPP	0
	VOTPP	0.4
	NiTPP	0.53
EX 5	TPP	0
	VOTPP	0.37
	NiTPP	0.58

Products		Error	Mass
Compound	[g]	%	%
TPP	0.00	± 0.00	0
VOTPP	0.36	± 0.11	38
NiTPP	0.60	± 0.17	63

Table D14: Sample 26 $VOSO_4$ + $FeSO_4$ + TPP.

	After Rx Purification Si Column Chromatophraphy	
	Compound	[g]
EX 1	TPP	0
	VOTPP	0.76
	FeTPP	0.19
EX 2	TPP	0
	VOTPP	0.71
	FeTPP	0.12
EX 3	TPP	0
	VOTPP	0.64
	FeTPP	0.13
EX 4	TPP	0.00
	VOTPP	0.79
	FeTPP	0.09
EX 5	TPP	0
	VOTPP	0.87
	FeTPP	0.1

Products		Error	Mass %
Compound	[g]	%	
TPP	0.00	± 0.00	0
VOTPP	0.75	± 0.17	86
FeTPP	0.13	± 0.08	14

Table D15: Sample 27 $NiSO_4$+$ZnSO_4$+TPP.

	After Rx Purification Si Column Chromatophraphy	
	Compound	[g]
EX 1	TPP	0
	NiTPP	0.78
	ZnTPP	0.08
EX 2	TPP	0
	NiTPP	0.72
	ZnTPP	0.16
EX 3	TPP	0
	NiTPP	0.65
	ZnTPP	0.09

Products		Error	Mass
Compound	[g]		%
TPP	0.00	± 0.00	0
NiTPP	0.72	± 0.05	87
ZnTPP	0.11	± 0.04	13

Table D16: Sample 28 $NiSO_4$+$CuSO_4$+TPP.

	After Rx Purification Si Column Chromatophraphy	
	Compound	[g]
EX 1	TPP	0
	NiTPP	0.72
	CuTPP	0.12
EX 2	TPP	0
	NiTPP	0.67
	CuTPP	0.42
EX 3	TPP	0
	NiTPP	0.53
	CuTPP	0.48

Products		Error	Mass
Compound	[g]		%
TPP	0.00	± 0.00	0.0
NiTPP	0.64	± 0.08	65.3
CuTPP	0.34	± 0.16	34.7

Table D17: Sample 29 $NiSO_4$+$CrSO_4$+TPP.

	After Rx Purification Si Column Chromatophraphy	
	Compound	[g]
EX 1	TPP	0
	NiTPP	0.64
	CrTPP	0.12
EX 2	TPP	0
	NiTPP	0.71
	CrTPP	0.08
EX 3	TPP	0
	NiTPP	0.52
	CrTPP	0.21

Products		Error	Mass
Compound	[g]		%
TPP	0.00	± 0.00	0
NiTPP	0.62	± 0.08	82
CrTPP	0.14	± 0.05	18

Table D18: Sample 30 $NiSO_4$+$FeSO_4$+TPP.

	After Rx Purification Si Column Chromatophraphy	
	Compound	[g]
EX 1	TPP	0
	NiTPP	0.48
	FeTPP	0.31
EX 2	TPP	0
	NiTPP	0.52
	FeTPP	0.45
EX 3	TPP	0
	NiTPP	0.69
	FeTPP	0.38

Products		Error	Mass
Compound	[g]		%
TPP	0.00	± 0.00	0.0
NiTPP	0.56	± 0.09	60
FeTPP	0.38	± 0.06	40.3

STAGE 7 A. With Na_2S

Table D19: Sample 45
$VOSO_4+ZnSO_4+Na_2S+TPP$.

	After Rx Purification Si Column Chromatophraphy	
	Compound	[g]
EX 1	TPP	0.79
	VOTPP	0.3
	ZnTPP	0
EX 2	TPP	0.73
	VOTPP	0.25
	ZnTPP	0
EX 3	TPP	0.71
	VOTPP	0.22
	ZnTPP	0
EX 4	TPP	0.7
	VOTPP	0.19
	ZnTPP	0
EX 5	TPP	0.68
	VOTPP	0.18
	ZnTPP	0

Products		Error	Mass
Compound	[g]		%
TPP	0.72	± 0.08	76.0
VOTPP	0.23	± 0.1	24.0
ZnTPP	0.00	0	0.0

Table D20: Sample 46
$VOSO_4+CuSO_4+Na_2S+TPP$.

	After Rx Purification Si Column Chromatophraphy	
	Compound	[g]
EX 1	TPP	0.75
	VOTPP	0.11
	CuTPP	0
EX 2	TPP	0.8
	VOTPP	0.09
	CuTPP	0
EX 3	TPP	0.86
	VOTPP	0.15
	CuTPP	0
EX 4	TPP	0.71
	VOTPP	0.19
	CuTPP	0
EX 5	TPP	0.83
	VOTPP	0.05
	CuTPP	0

Products		Error %	Mass %
Compound	[g]		
TPP	0.79	± 0.12	87
VOTPP	0.12	± 0.11	13
CuTPP	0.00	± 0.00	0

Table D21: Sample 47
$VOSO_4$+$CrSO_4$+Na_2S+TPP.

	After Rx Purification Si Column Chromatophraphy	
	Compound	[g]
EX 1	TPP	0.87
	VOTPP	0.11
	CrTPP	0
EX 2	TPP	0.8
	VOTPP	0.08
	CrTPP	0
EX 3	TPP	0.93
	VOTPP	0.07
	CrTPP	0
EX 4	TPP	0.95
	VOTPP	0.05
	CrTPP	0
EX 5	TPP	0.83
	VOTPP	0.04
	CrTPP	0

Products		Error	Mass
Compound	[g]	%	%
TPP	0.88	± 0.13	92.6
VOTPP	0.07	± 0.05	7.4
CrTPP	0.00	± 0	0.0

Table D22: Sample 48
$VOSO_4$+$NiSO_4$+Na_2S+TPP.

	After Rx Purification Si Column Chromatophraphy	
	Compound	[g]
EX 1	TPP	0.93
	VOTPP	0.06
	NiTPP	0
EX 2	TPP	0.81
	VOTPP	0.05
	NiTPP	0
EX 3	TPP	0.93
	VOTPP	0.04
	NiTPP	0
EX 4	TPP	0.88
	VOTPP	0.03
	NiTPP	0
EX 5	TPP	1.01
	VOTPP	0.05
	NiTPP	0

Products		Error	Mass
Compound	[g]	%	%
TPP	0.91	± 0.15	95
VOTPP	0.05	± 0.02	5
NiTPP	0.00	± 0.00	0

Table D23: Sample 49 $VOSO_4$+$FeSO_4$+Na_2S+TPP.

	After Rx Purification Si Column Chromatophraphy	
	Compound	[g]
EX 1	TPP	0.84
	VOTPP	0.07
	FeTPP	0
EX 2	TPP	0.92
	VOTPP	0.02
	FeTPP	0
EX 3	TPP	0.79
	VOTPP	0.08
	FeTPP	0
EX 4	TPP	0.96
	VOTPP	0.10
	FeTPP	0
EX 5	TPP	0.81
	VOTPP	0.07
	FeTPP	0

Products		Error		Mass %
Compound	[g]		%	
TPP	0.86	±	0.15	93
VOTPP	0.07	±	0.06	7
FeTPP	0.00	±	0.00	0

Table D24: Sample 50
$NiSO_4+ZnSO_4+Na_2S+TPP$.

	After Rx Purification Si Column Chromatophraphy	
	Compound	[g]
EX 1	TPP	0.93
	NiTPP	0
	ZnTPP	0
EX 2	TPP	0.89
	NiTPP	0
	ZnTPP	0
EX 3	TPP	0.81
	NiTPP	0
	ZnTPP	0

Products		Error	Mass
Compound	[g]		%
TPP	0.88	± 0.05	100
NiTPP	0.00	± 0.00	0
ZnTPP	0.00	± 0.00	0

Table D25: Sample 51
$NiSO_4+CuSO_4+Na_2S+TPP$.

	After Rx Purification Si Column Chromatophraphy	
	Compound	[g]
EX 1	TPP	0.98
	NiTPP	0
	CuTPP	0
EX 2	TPP	0.8
	NiTPP	0
	CuTPP	0
EX 3	TPP	0.84
	NiTPP	0
	CuTPP	0

Products		Error	Mass
Compound	[g]		%
TPP	0.87	± 0.08	100
NiTPP	0.00	± 0.000	0
CuTPP	0.00	± 0.000	0

Table D26: Sample 52
$NiSO_4$+$CrSO_4$+Na_2S+TPP.

	After Rx Purification Si Column Chromatophraphy	
	Compound	[g]
EX 1	TPP	0.87
	NiTPP	0
	CrTPP	0
EX 2	TPP	0.91
	NiTPP	0
	CrTPP	0
EX 3	TPP	0.82
	NiTPP	0
	CrTPP	0

Products		Error	Mass
Compound	[g]		%
TPP	0.87	± 0.04	100
NiTPP	0.00	± 0.00	0
CrTPP	0.00	± 0.00	0

Table D27: Sample 53
$NiSO_4$+$FeSO_4$+Na_2S+TPP.

	After Rx Purification Si Column Chromatophraphy	
	Compound	[g]
EX 1	TPP	1.12
	NiTPP	0
	FeTPP	0
EX 2	TPP	1.08
	NiTPP	0
	FeTPP	0
EX 3	TPP	1.02
	NiTPP	0
	FeTPP	0

Products		Error	Mass
Compound	[g]		%
TPP	1.07	± 0.04	100.0
NiTPP	0.00	± 0.00	0
FeTPP	0.000	± 0.00	0.0

APENDIX E. SILICA COLUMN CHROMATOGRAPHY DEMETALLATIONS

Table E1: Sample 8 $VOSO_4$ + ZnTPP

	Products	
	Compound	[g]
EX 1	VOTPP	0.00
	ZnTPP	0.63
EX 2	VOTPP	0.00
	ZnTPP	0.75
EX 3	VOTPP	0.00
	ZnTPP	0.87

Products		Error	Mass
Compound	[g]		%
VOTPP	0.00	± 0.00	0.0
ZnTPP	0.75	± 0.10	100.0

Table E2: Sample 9 $VOSO_4$ + CuTPP

	Products	
	Compound	[g]
EX 1	VOTPP	0.00
	CuTPP	0.54
EX 2	VOTPP	0.00
	CuTPP	0.61
EX 3	VOTPP	0.00
	CuTPP	0.63

Products		Error	Mass
Compound	[g]		%
VOTPP	0.00	± 0.00	0.0
CuTPP	0.59	± 0.04	100.0

Table E3: Sample 10 $VOSO_4$ + CrTPP

	Products	
	Compound	[g]
EX 1	VOTPP	0.00
	CrTPP	0.77
EX 2	VOTPP	0.00
	CrTPP	0.84
EX 3	VOTPP	0.00
	CrTPP	0.95

Products		Error	Mass
Compound	[g]		%
VOTPP	0.00	± 0.00	0.0
CrTPP	0.85	± 0.07	100.0

Table E4: Sample 11 $VOSO_4$ + NiTPP

	Products	
	Compound	[g]
EX 1	VOTPP	0.00
	NiTPP	0.86
EX 2	VOTPP	0.00
	NiTPP	0.94
EX 3	VOTPP	0.00
	NiTPP	0.75

Products		Error	Mass
Compound	[g]		%
VOTPP	0.00	± 0.00	0.0
NiTPP	0.85	± 0.08	100.0

Table E5: Sample 12 $NiSO_4$ + ZnTPP

	Products	
	Compound	[g]
EX 1	NiTPP	0.00
	ZnTPP	0.75
EX 2	NiTPP	0.00
	ZnTPP	0.85
EX 3	NiTPP	0.00
	ZnTPP	0.76

Products		Error	Mass
Compound	[g]		%
NiTPP	0.00	± 0.00	0.0
ZnTPP	0.79	± 0.04	100.0

Table E6: Sample 13 $NiSO_4$ + CuTPP

	Products	
	Compound	[g]
EX 1	NiTPP	0.00
	CuTPP	0.62
EX 2	NiTPP	0.00
	CuTPP	0.74
EX 3	NiTPP	0.00
	CuTPP	0.76

Products		Error	Mass
Compound	[g]		%
NiTPP	0.00	± 0.00	0.0
CuTPP	0.71	± 0.06	100.0

Table E7: Sample 14 $NiSO_4$ + CrTPP

	Products	
	Compound	[g]
EX 1	NiTPP	0.00
	CrTPP	0.98
EX 2	NiTPP	0.00
	CrTPP	0.94
EX 3	NiTPP	0.00
	CrTPP	0.86

Products		Error	Mass
Compound	[g]		%
NiTPP	0.00	± 0.00	0.0
CrTPP	0.93	± 0.05	100.0

Table E8: Sample 15 $NiSO_4$ + VOTPP

	Products	
	Compound	[g]
EX 1	NiTPP	0.00
	VOTPP	0.86
EX 2	NiTPP	0.00
	VOTPP	0.82
EX 3	NiTPP	0.00
	VOTPP	0.73

Products		Error	Mass
Compound	[g]		%
NiTPP	0.00	± 0.00	0.0
VOTPP	0.80	± 0.05	100.0

Table E9: Sample 16 VOTPP + $ZnSO_4$

	Products	
	Compound	[g]
EX 1	VOTPP	0.62
	ZnTPP	0
EX 2	VOTPP	0.74
	ZnTPP	0
EX 3	VOTPP	0.69
	ZnTPP	0

Products		Error	Mass
Compound	[g]		%
VOTPP	0.68	± 0.05	100.0
ZnTPP	0.00	± 0.00	0.0

Table E10: Sample 17 VOTPP + $CuSO_4$

	Products	
	Compound	[g]
EX 1	VOTPP	0.74
	CuTPP	0
EX 2	VOTPP	0.80
	CuTPP	0
EX 3	VOTPP	0.72
	CuTPP	0

Products		Error	Mass
Compound	[g]		%
VOTPP	0.75	± 0.03	100.0
CuTPP	0.00	± 0.00	0.0

Table E11: Sample 18 VOTPP + $CrSO_4$

	Products	
	Compound	[g]
EX 1	VOTPP	0.84
	CrTPP	0
EX 2	VOTPP	0.93
	CrTPP	0
EX 3	VOTPP	0.79
	CrTPP	0

Products		Error	Mass
Compound	[g]		%
VOTPP	0.85	± 0.06	100.0
CrTPP	0.00	± 0.00	0.0

Table E12: Sample 19 NiTPP + $ZnSO_4$

	Products	
	Compound	[g]
EX 1	NiTPP	0.97
	ZnTPP	0
EX 2	NiTPP	0.86
	ZnTPP	0
EX 3	NiTPP	0.78
	ZnTPP	0

Products		Error	Mass
Compound	[g]		%
NiTPP	0.87	± 0.08	100.0
ZnTPP	0.00	± 0.00	0.0

Table E13: Sample 20 NiTPP + $CuSO_4$

	Products	
	Compound	[g]
EX 1	NiTPP	0.86
	CuTPP	0
EX 2	NiTPP	0.74
	CuTPP	0
EX 3	NiTPP	0.71
	CuTPP	0

Products		Error	Mass
Compound	[g]		%
NiTPP	0.77	± 0.06	100.0
CuTPP	0.00	± 0.00	0.0

Table E14: Sample 21 NiTPP + $CrSO_4$

	Products	
	Compound	[g]
EX 1	NiTPP	0.83
	CrTPP	0
EX 2	NiTPP	0.91
	CrTPP	0
EX 3	NiTPP	0.87
	CrTPP	0

Products		Error	Mass
Compound	[g]		%
NiTPP	0.87	± 0.03	100.0
CrTPP	0.00	± 0.00	0.0

Table E15: Sample 31 $VOSO_4$ + ZnTPP

	Products	
	Compound	[g]
EX 1	VOTPP	0.00
	ZnTPP	0.98
EX 2	VOTPP	0.00
	ZnTPP	0.85
EX 3	VOTPP	0.00
	ZnTPP	0.88

Products		Error	Mass
Compound	[g]		%
VOTPP	0.00	± 0.00	0.0
ZnTPP	0.90	± 0.06	100.0

Table E16: Sample 32 $VOSO_4$ + CuTPP

	Products	
	Compound	[g]
EX 1	VOTPP	0.00
	CuTPP	0.73
EX 2	VOTPP	0.00
	CuTPP	0.69
EX 3	VOTPP	0.00
	CuTPP	0.75

Products		Error	Mass
Compound	[g]		%
VOTPP	0.00	± 0.00	0.0
CuTPP	0.72	± 0.02	100.0

Table E17: Sample 33 $VOSO_4$ + CrTPP

	Products	
	Compound	[g]
EX 1	VOTPP	0.00
	CrTPP	0.57
EX 2	VOTPP	0.00
	CrTPP	0.68
EX 3	VOTPP	0.00
	CrTPP	0.73

Products		Error	Mass
Compound	[g]		%
VOTPP	0.00	± 0.00	0.0
CrTPP	0.66	± 0.07	100.0

Table E18: Sample 34 $VOSO_4$ + NiTPP

	Products	
	Compound	[g]
EX 1	VOTPP	0.00
	NiTPP	0.76
EX 2	VOTPP	0.00
	NiTPP	0.83
EX 3	VOTPP	0.00
	NiTPP	0.73

Products		Error	Mass
Compound	[g]		%
VOTPP	0.00	± 0.00	0.0
NiTPP	0.77	± 0.04	100.0

Table E19: Sample 35 $NiSO_4$ + ZnTPP

	Products	
	Compound	[g]
EX 1	NiTPP	0.00
	ZnTPP	0.81
EX 2	NiTPP	0.00
	ZnTPP	0.75
EX 3	NiTPP	0.00
	ZnTPP	0.83

Products		Error	Mass
Compound	[g]		%
NiTPP	0.00	± 0.00	0.0
ZnTPP	0.80	± 0.03	100.0

Table E20: Sample 36 $NiSO_4$ + CuTPP

	Products	
	Compound	[g]
EX 1	NiTPP	0.00
	CuTPP	0.87
EX 2	NiTPP	0.00
	CuTPP	0.74
EX 3	NiTPP	0.00
	CuTPP	0.73

Products		Error	Mass
Compound	[g]		%
NiTPP	0.00	± 0.00	0.0
CuTPP	0.78	± 0.06	100.0

Table E21: Sample 37 $NiSO_4$ + CrTPP

	Products	
	Compound	[g]
EX 1	NiTPP	0.00
	CrTPP	0.83
EX 2	NiTPP	0.00
	CrTPP	0.77
EX 3	NiTPP	0.00
	CrTPP	0.71

Products		Error	Mass
Compound	[g]		%
NiTPP	0.00	± 0.00	0.0
CrTPP	0.77	± 0.05	100.0

Table E22: Sample 38 $NiSO_4$ + VOTPP

	Products	
	Compound	[g]
EX 1	NiTPP	0.00
	VOTPP	0.74
EX 2	NiTPP	0.00
	VOTPP	0.83
EX 3	NiTPP	0.00
	VOTPP	0.86

Products		Error	Mass
Compound	[g]		%
NiTPP	0.00	± 0.00	0.0
VOTPP	0.81	± 0.05	100.0

Table E23: Sample 39 VOTPP + $ZnSO_4$

	Products	
	Compound	[g]
EX 1	VOTPP	0.84
	ZnTPP	0
EX 2	VOTPP	0.89
	ZnTPP	0
EX 3	VOTPP	0.79
	ZnTPP	0

Products		Error	Mass
Compound	[g]		%
VOTPP	0.84	± 0.04	100.0
ZnTPP	0.00	± 0.00	0.0

Table E24: Sample 40 VOTPP + $CuSO_4$

	Products	
	Compound	[g]
EX 1	VOTPP	0.82
	CuTPP	0
EX 2	VOTPP	0.84
	CuTPP	0
EX 3	VOTPP	0.72
	CuTPP	0

Products		Error	Mass
Compound	[g]		%
VOTPP	0.79	± 0.05	100.0
CuTPP	0.00	± 0.00	0.0

Table E25: Sample 41 VOTPP + $CrSO_4$

	Products	
	Compound	[g]
EX 1	VOTPP	0.94
	CrTPP	0
EX 2	VOTPP	0.96
	CrTPP	0
EX 3	VOTPP	0.86
	CrTPP	0

Products		Error	Mass
Compound	[g]		%
VOTPP	0.92	± 0.04	100.0
CrTPP	0.00	± 0.00	0.0

Table E26: Sample 42 NiTPP + $ZnSO_4$

	Products	
	Compound	[g]
EX 1	NiTPP	0.83
	ZnTPP	0
EX 2	NiTPP	0.76
	ZnTPP	0
EX 3	NiTPP	0.77
	ZnTPP	0

Products		Error	Mass
Compound	[g]		%
NiTPP	0.79	± 0.03	100.0
ZnTPP	0.00	± 0.00	0.0

Table E27: Sample 43 NiTPP + $CuSO_4$

	Products	
	Compound	[g]
EX 1	NiTPP	0.71
	CuTPP	0
EX 2	NiTPP	0.75
	CuTPP	0
EX 3	NiTPP	0.64
	CuTPP	0

Products		Error	Mass
Compound	[g]		%
NiTPP	0.70	± 0.05	100.0
CuTPP	0.00	± 0.00	0.0

Table E28: Sample 44 NiTPP + $CrSO_4$

	Products	
	Compound	[g]
EX 1	NiTPP	0.74
	CrTPP	0
EX 2	NiTPP	0.65
	CrTPP	0
EX 3	NiTPP	0.79
	CrTPP	0

Products		Error	Mass
Compound	[g]		%
NiTPP	0.73	± 0.06	100.0
CrTPP	0.00	± 0.00	0.0

APENDIX F. MASS SPECTROMETRY

Monoisotopic Masses

	Average Mass	Monoisotopic Mass	Monoisotopic Mass in Mass Specs
TPP	614.752	614.247	614.240
CrTPP	664.732	664.172	664.172
FeTPP	668.581	668.166	668.165
NiTPP	671.429	670.167	670.163
CuTPP	676.282	675.161	675.162
ZnTPP	678.126	676.161	676.153
VOTPP	679.677	679.170	679.178

APENDIX G. MASS SPECS COMPETITION

COMPETITION $VOSO_4$ + $ZnSO_4$ +TPP OPEN SYSTEM

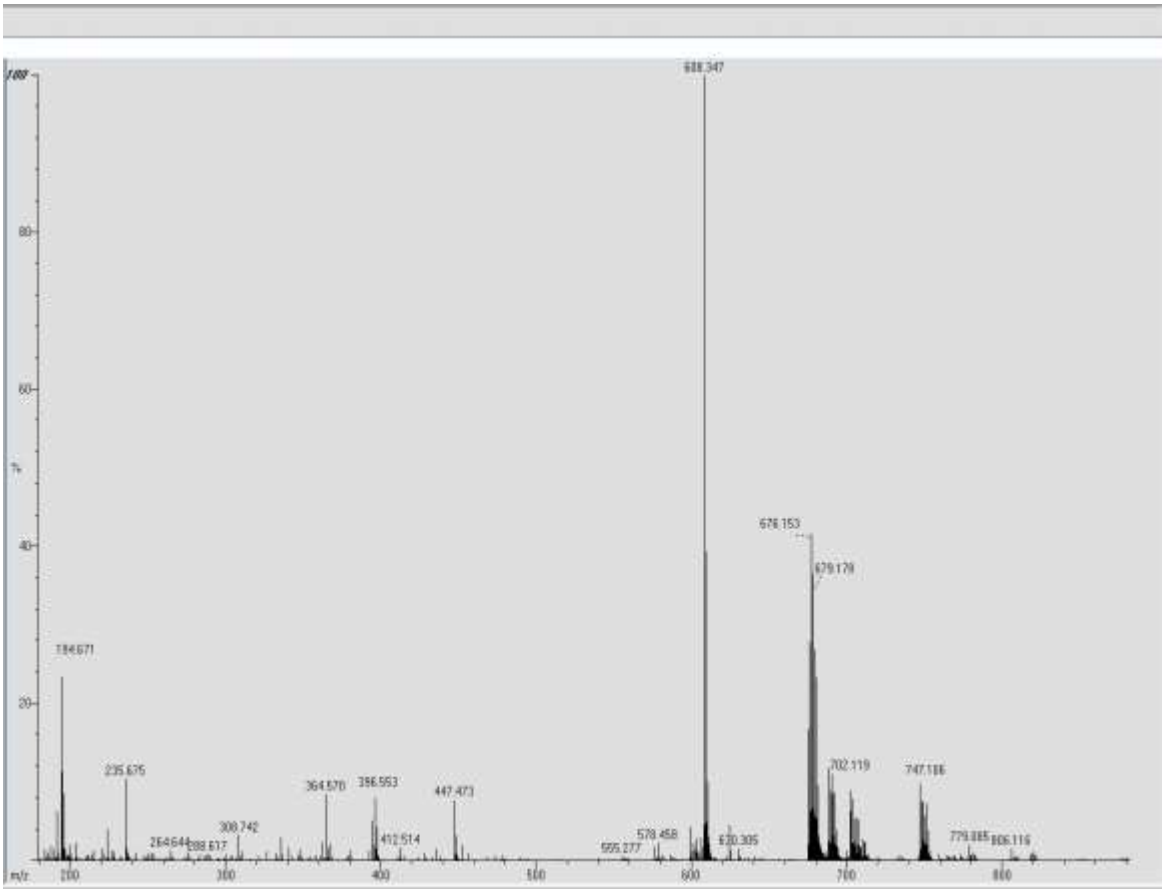

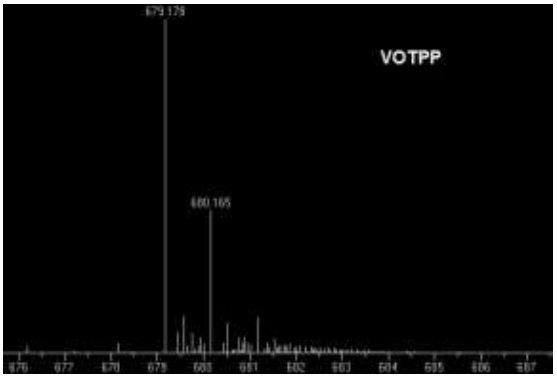

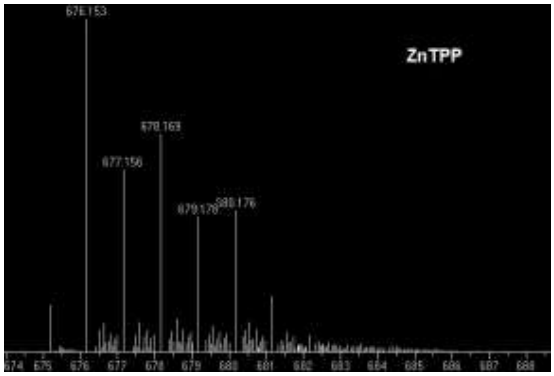

COMPETITION $VOSO_4$ + $CuSO_4$ +TPP OPEN SYSTEM

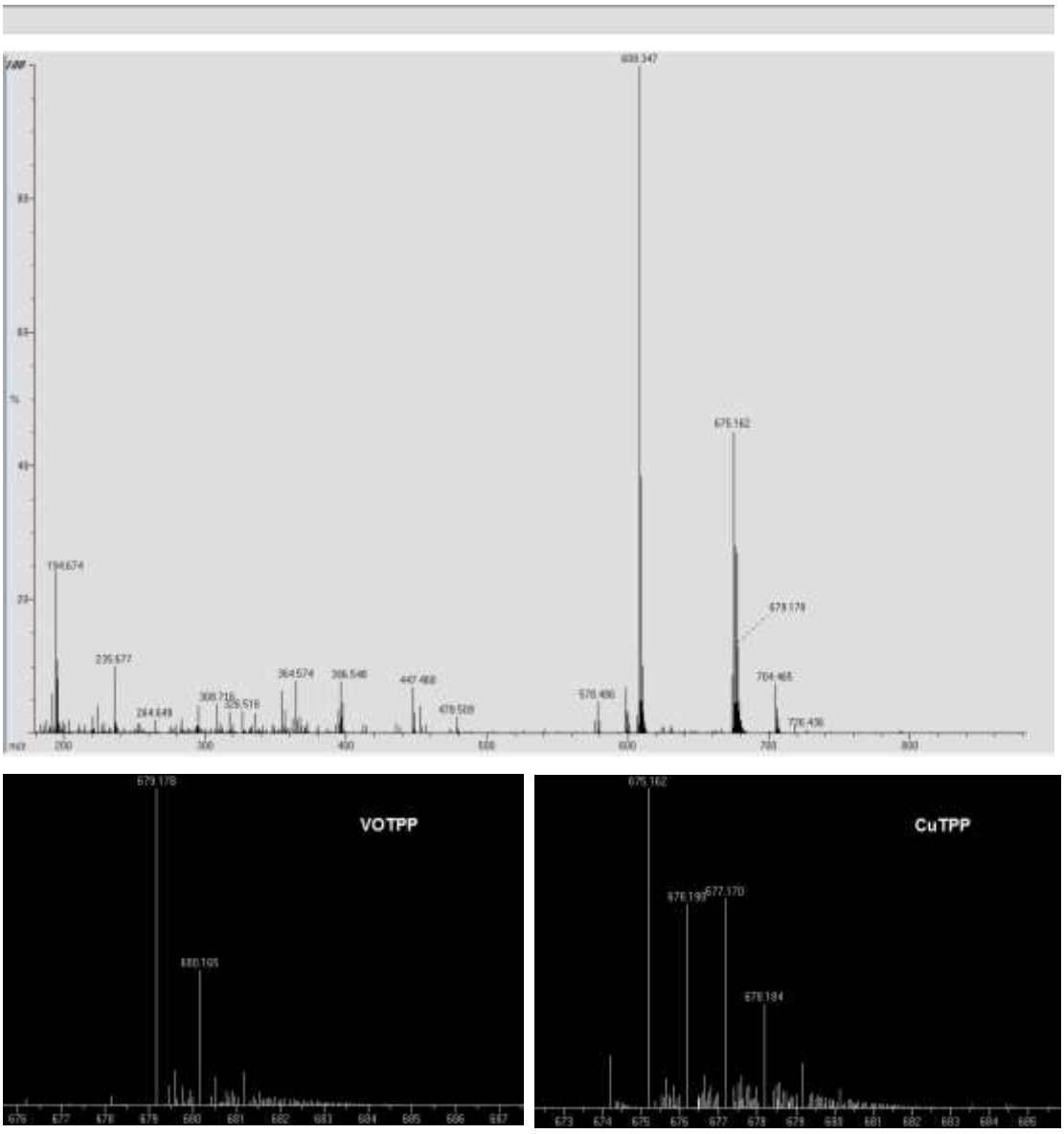

COMPETITION $VOSO_4$ + $CrSO_4$ +TPP OPEN SYSTEM

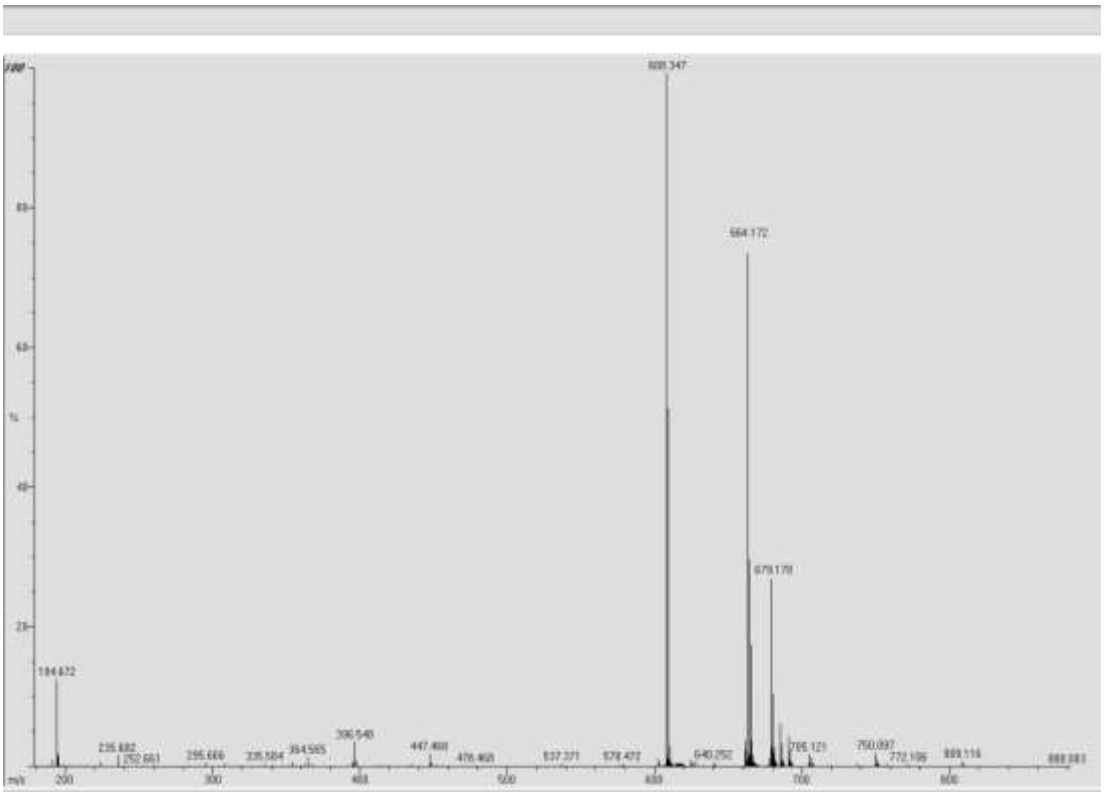

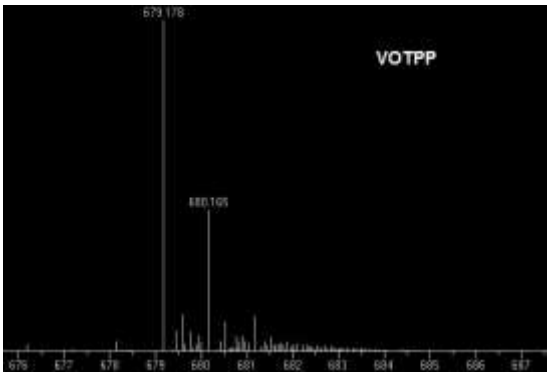

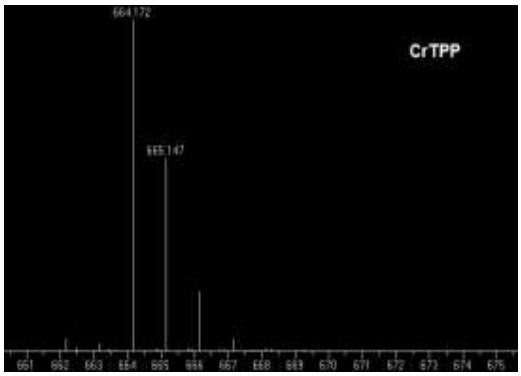

COMPETITION $VOSO_4$ + $NiSO_4$ +TPP OPEN SYSTEM

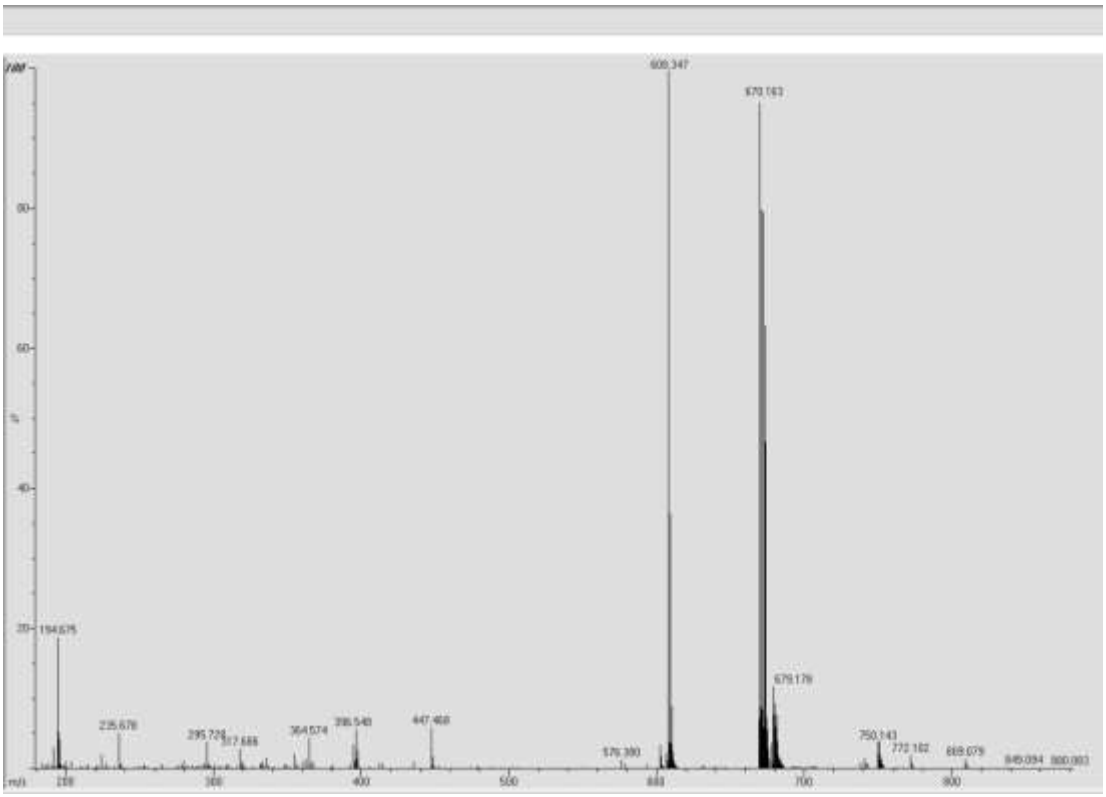

COMPETITION $VOSO_4$ + $FeSO_4$ +TPP OPEN SYSTEM

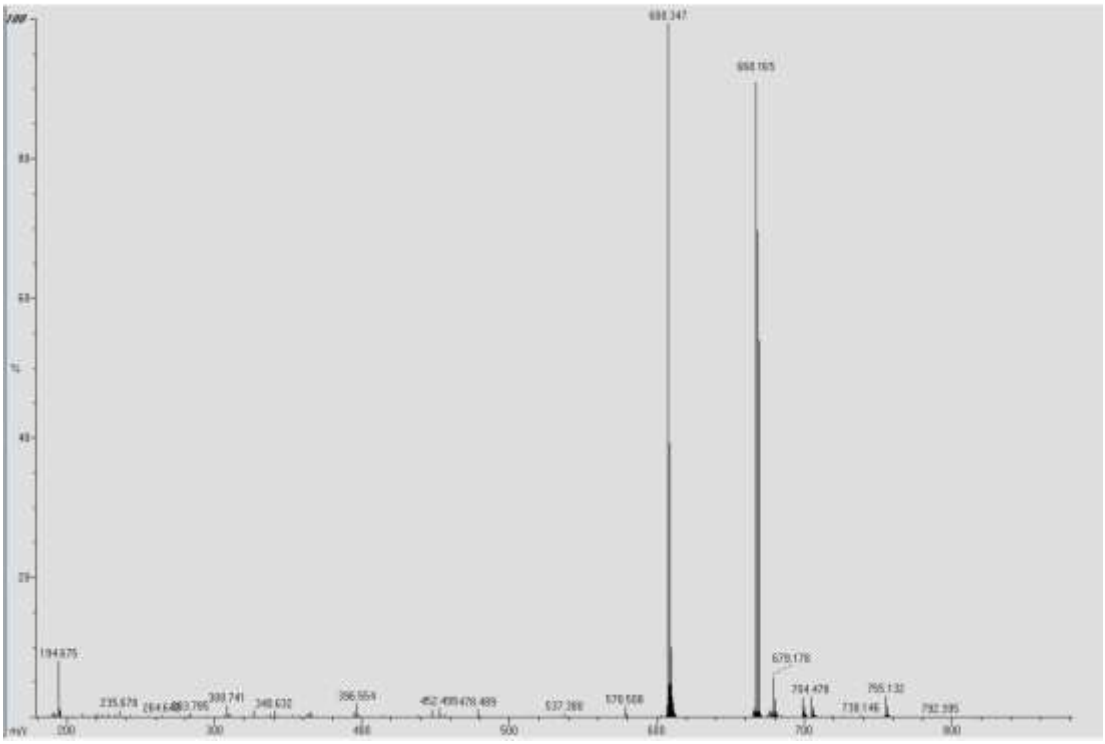

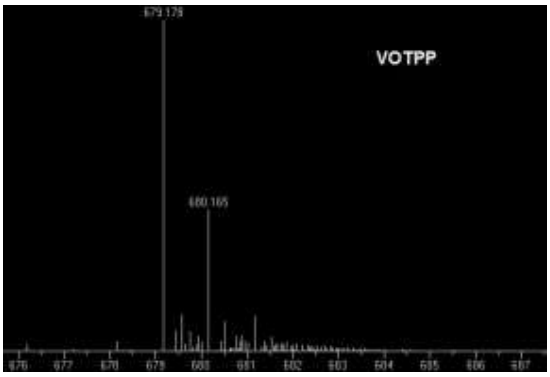

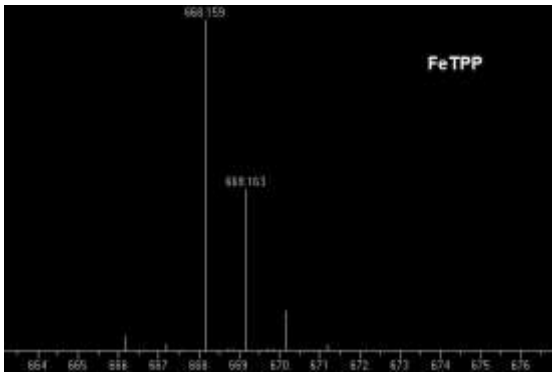

COMPETITION $NiSO_4$ + $ZnSO_4$ + TPP OPEN SYSTEM

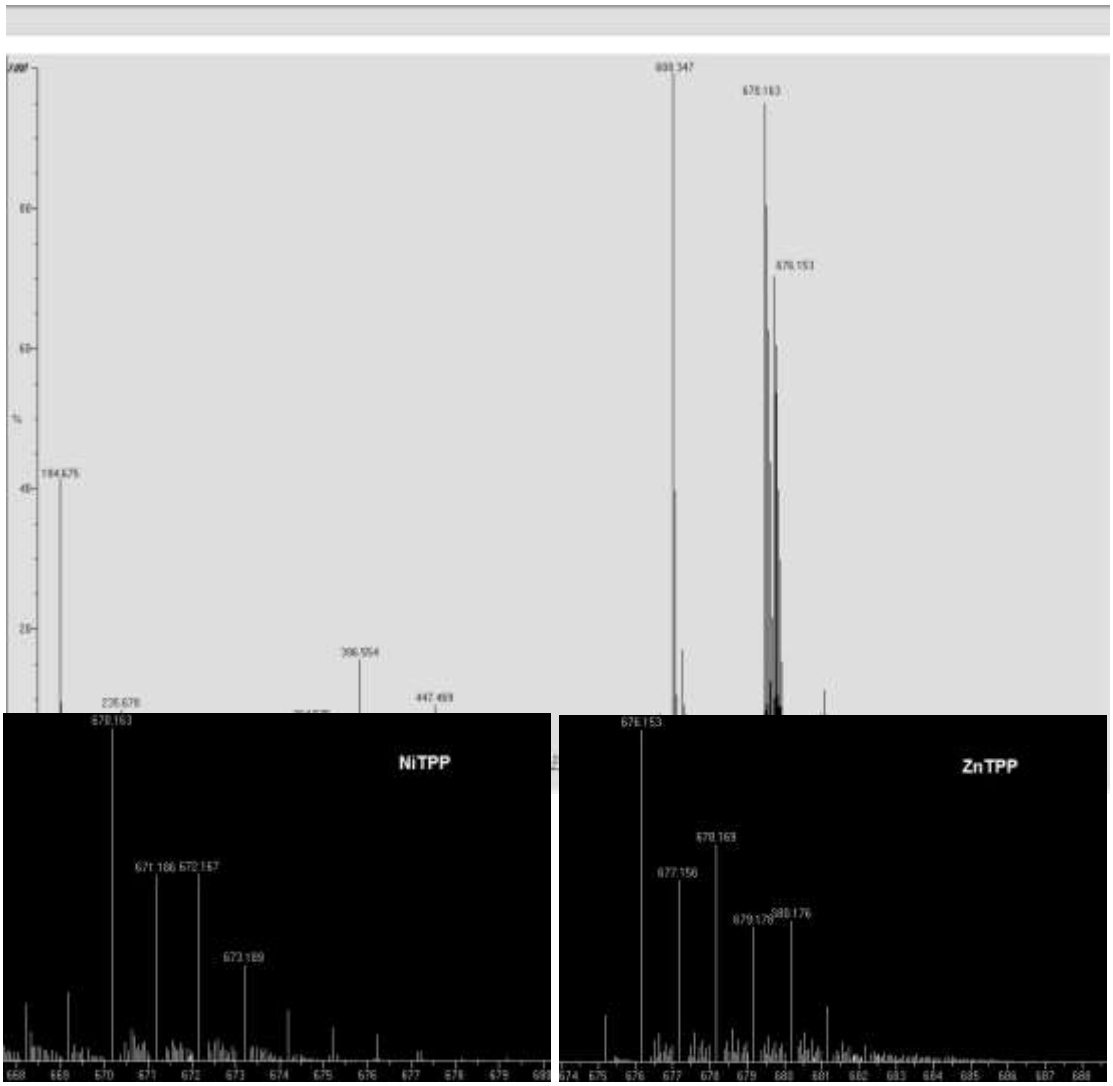

COMPETITION $NiSO_4$ + $CuSO_4$ + TPP OPEN SYSTEM

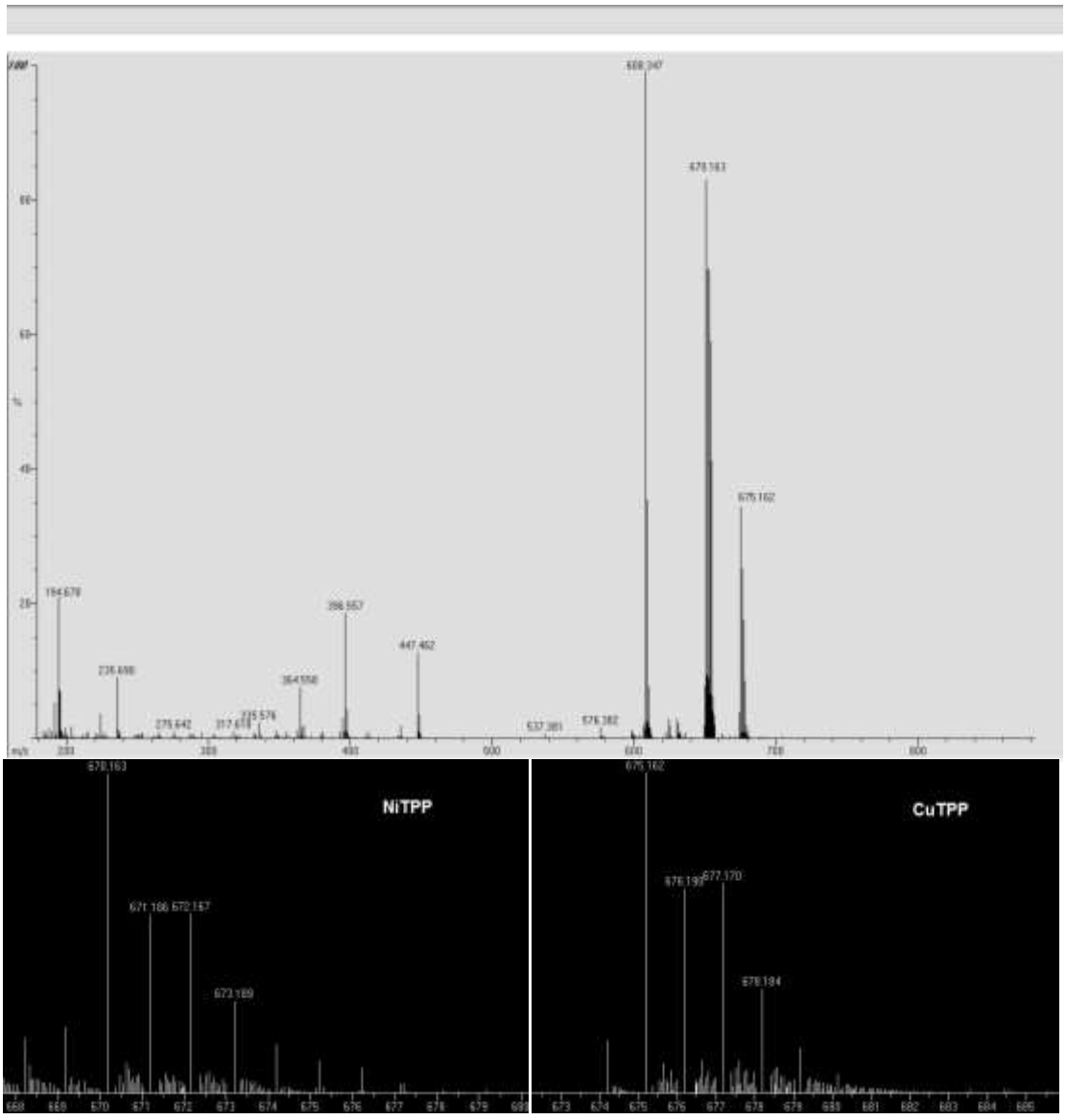

COMPETITION $NiSO_4$ + $CrSO_4$ + TPP OPEN SYSTEM

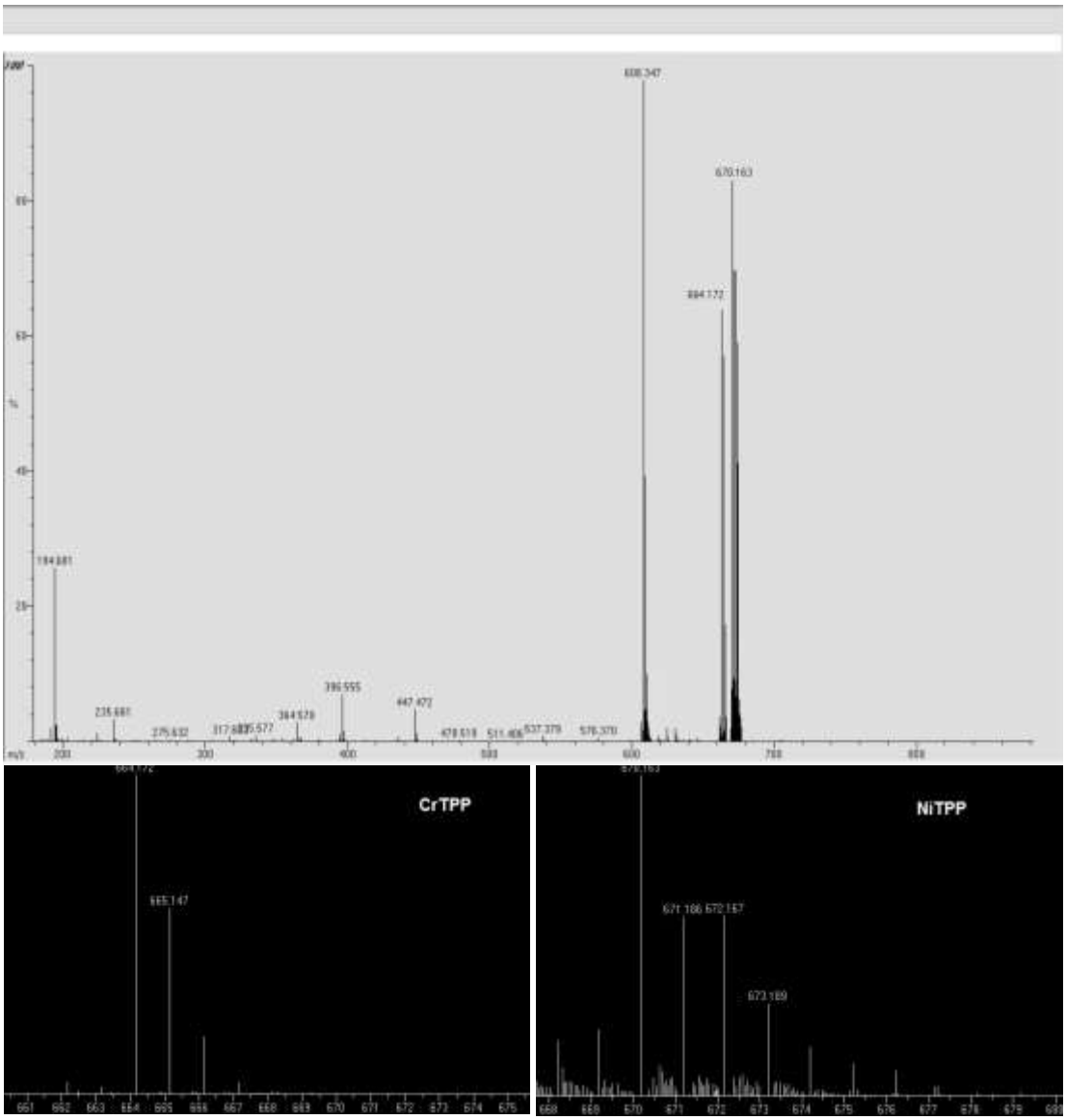

COMPETITION $NiSO_4$ + $FeSO_4$ + TPP OPEN SYSTEM

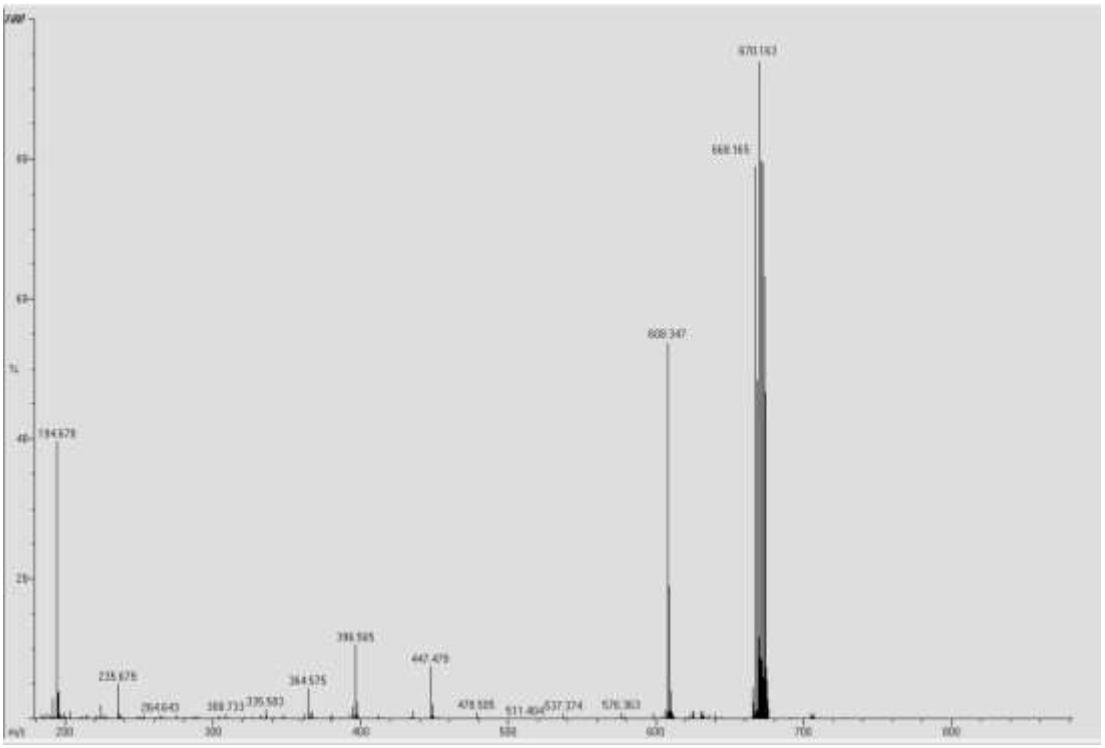

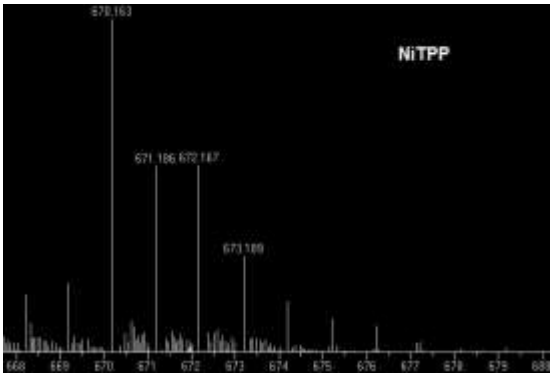

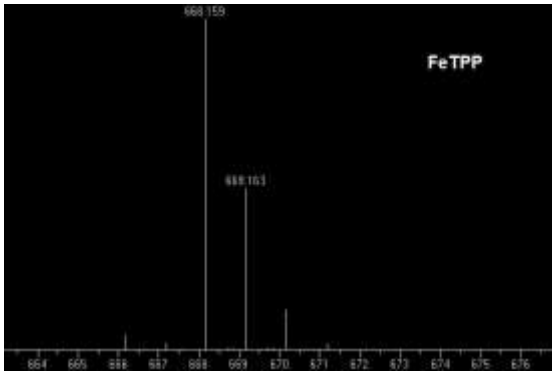

COMPETITION $VOSO_4$ + $ZnSO_4$ + TPP NITROGEN

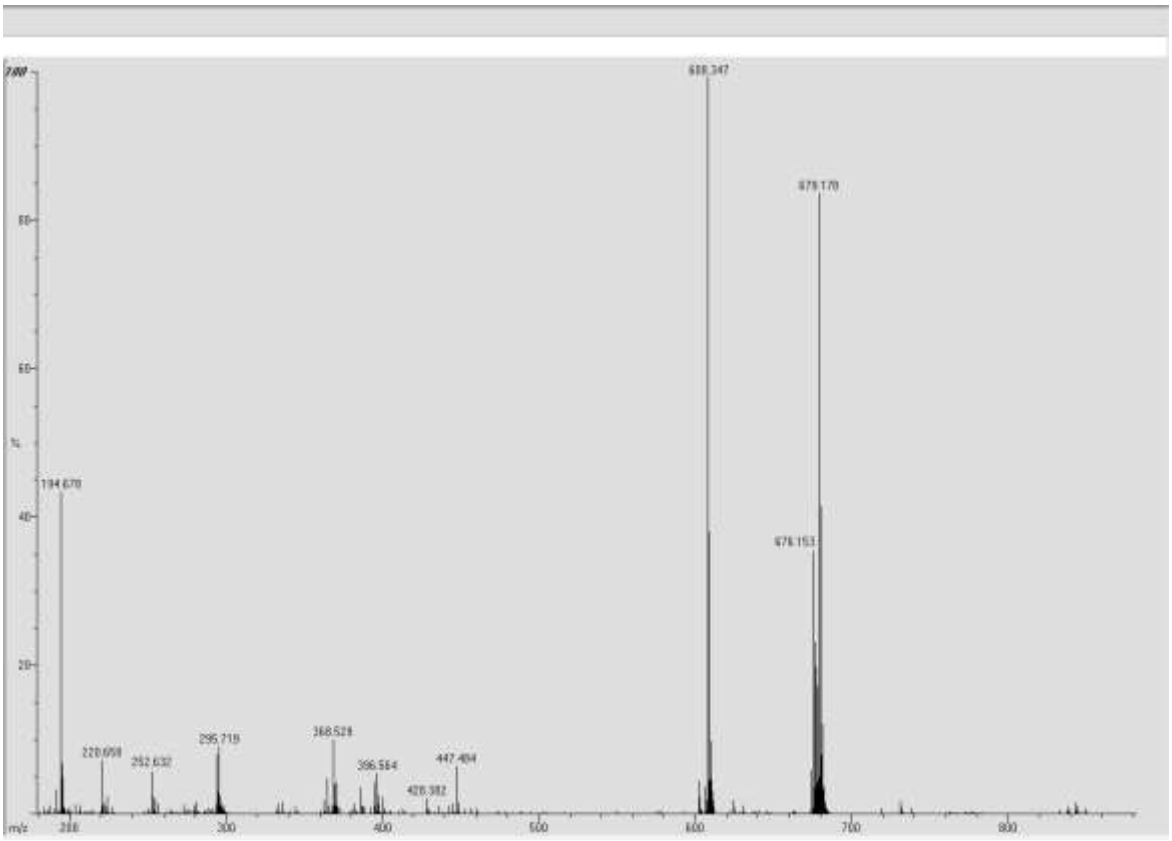

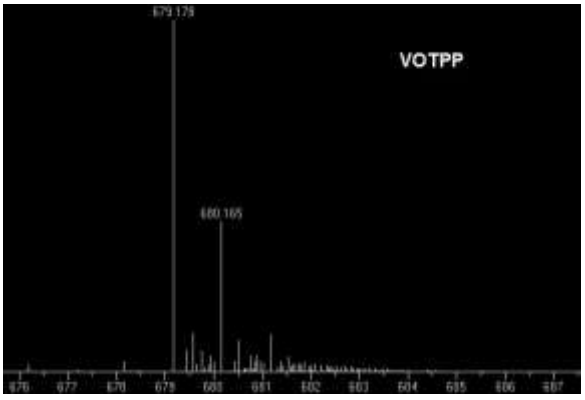

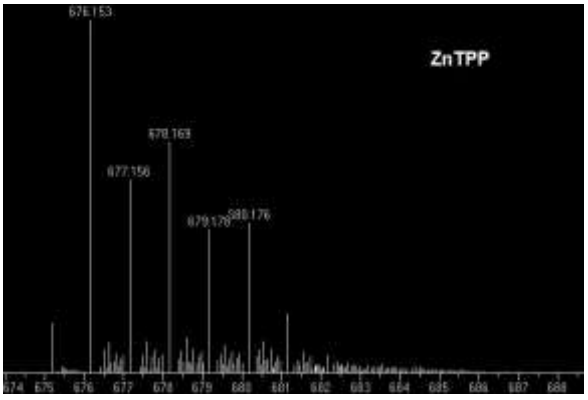

COMPETITION $VOSO_4$ + $CuSO_4$ + TPP NITROGEN

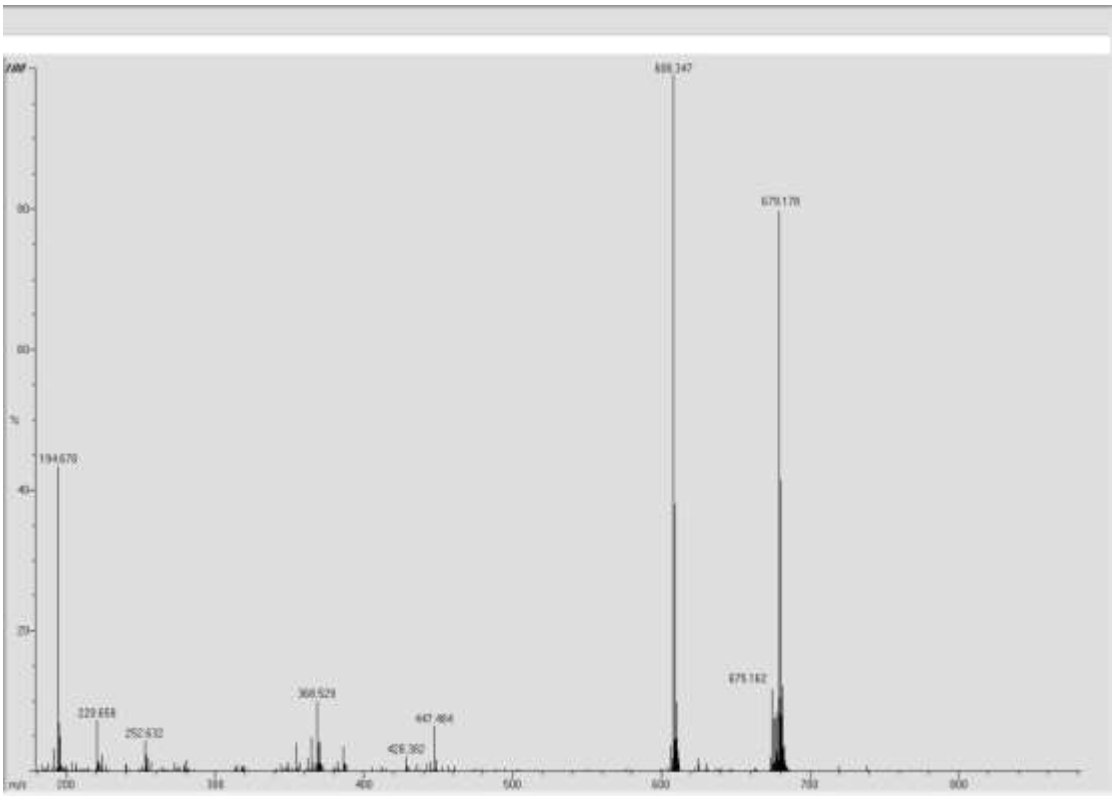

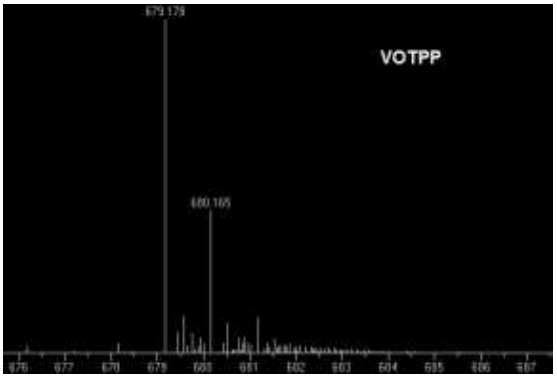

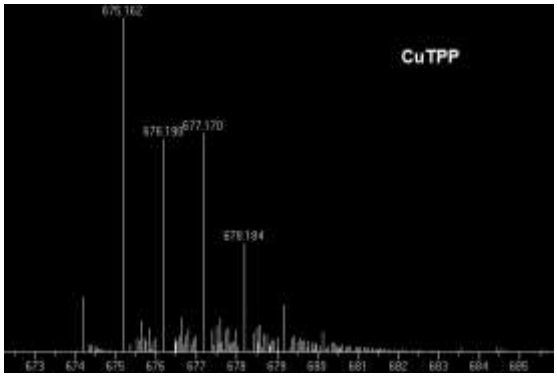

COMPETITION $VOSO_4$ + $CrSO_4$ + TPP NITROGEN

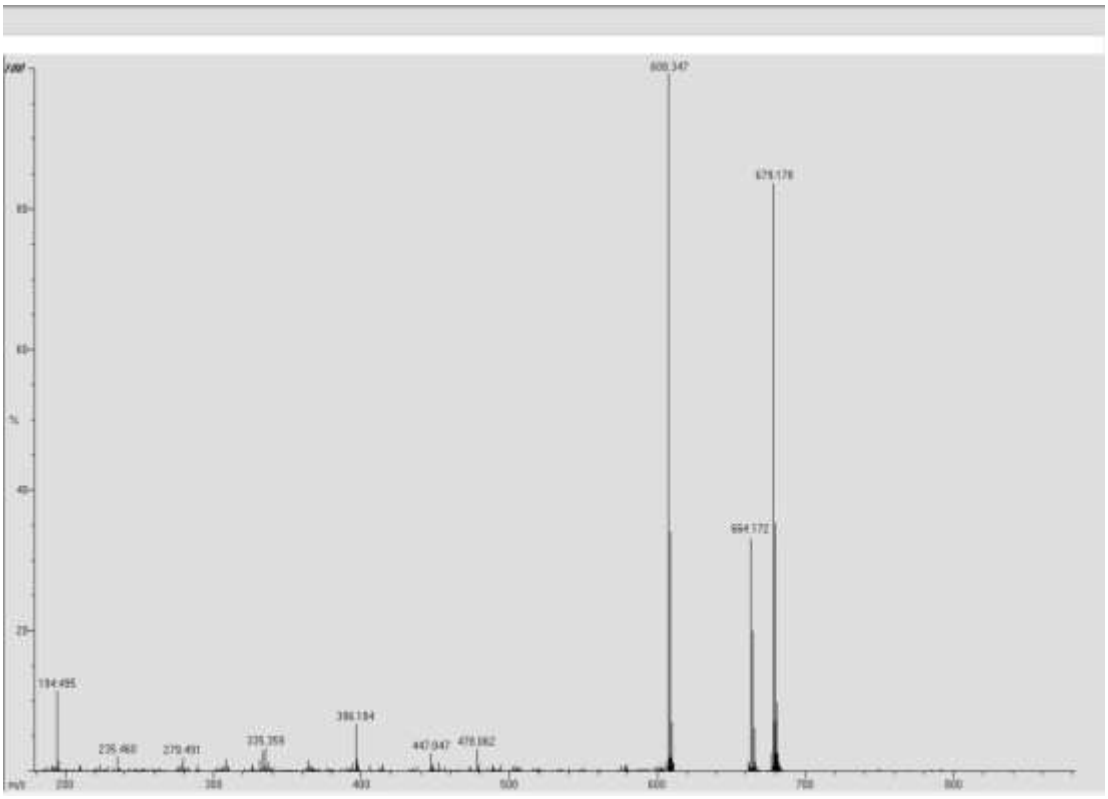

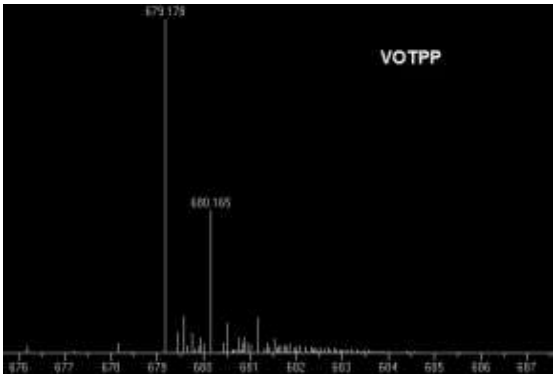

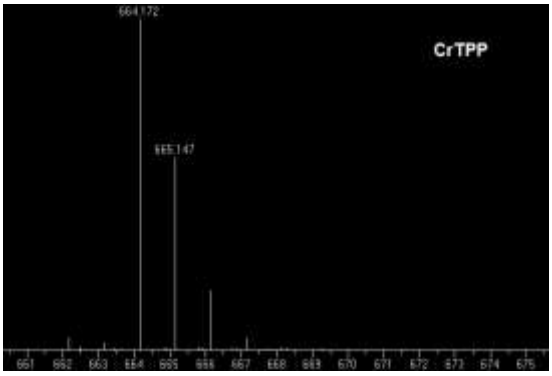

COMPETITION $VOSO_4$ + $NiSO_4$ + TPP NITROGEN

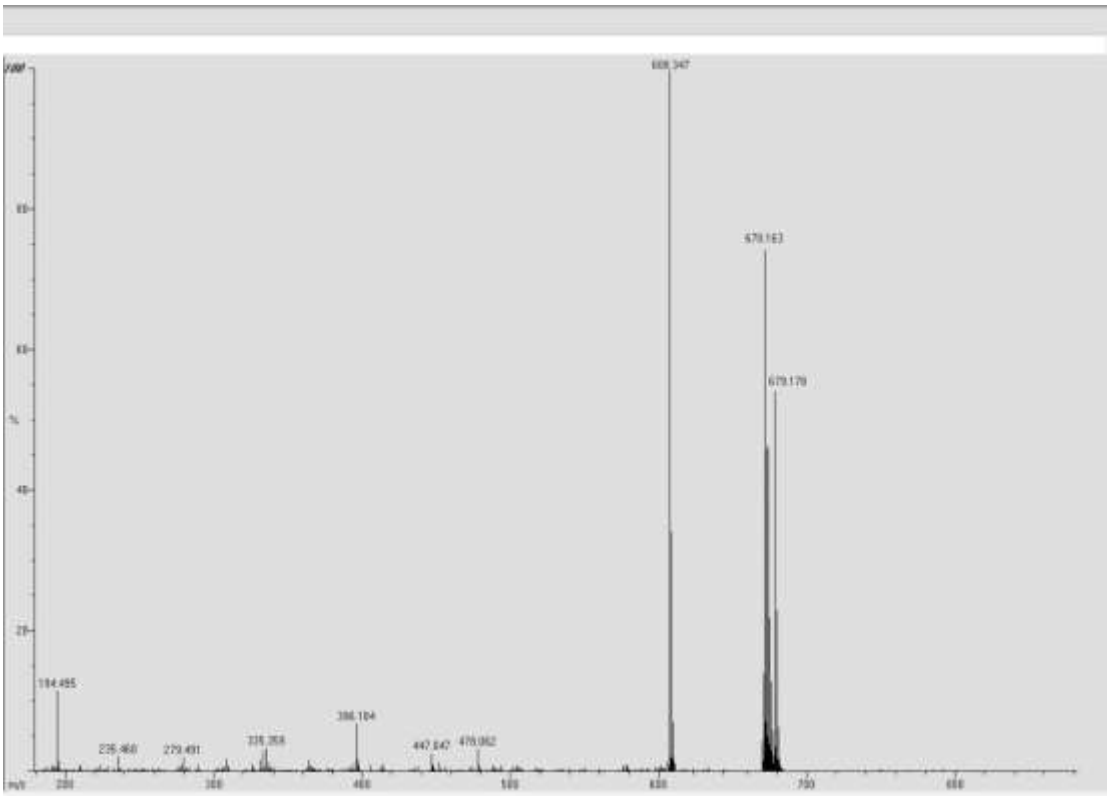

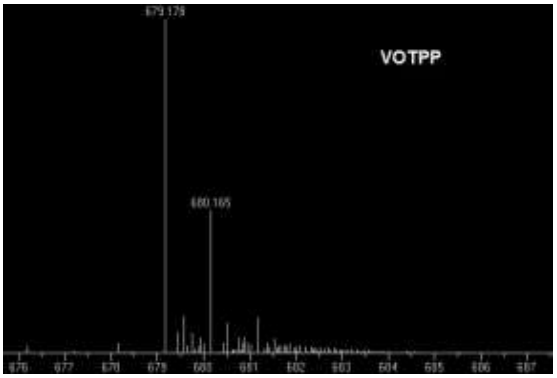

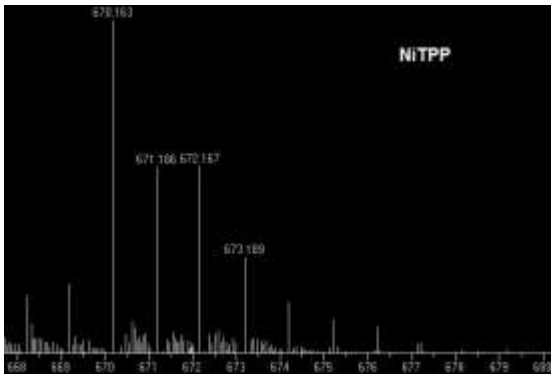

COMPETITION $VOSO_4$ + $FeSO_4$ + TPP NITROGEN

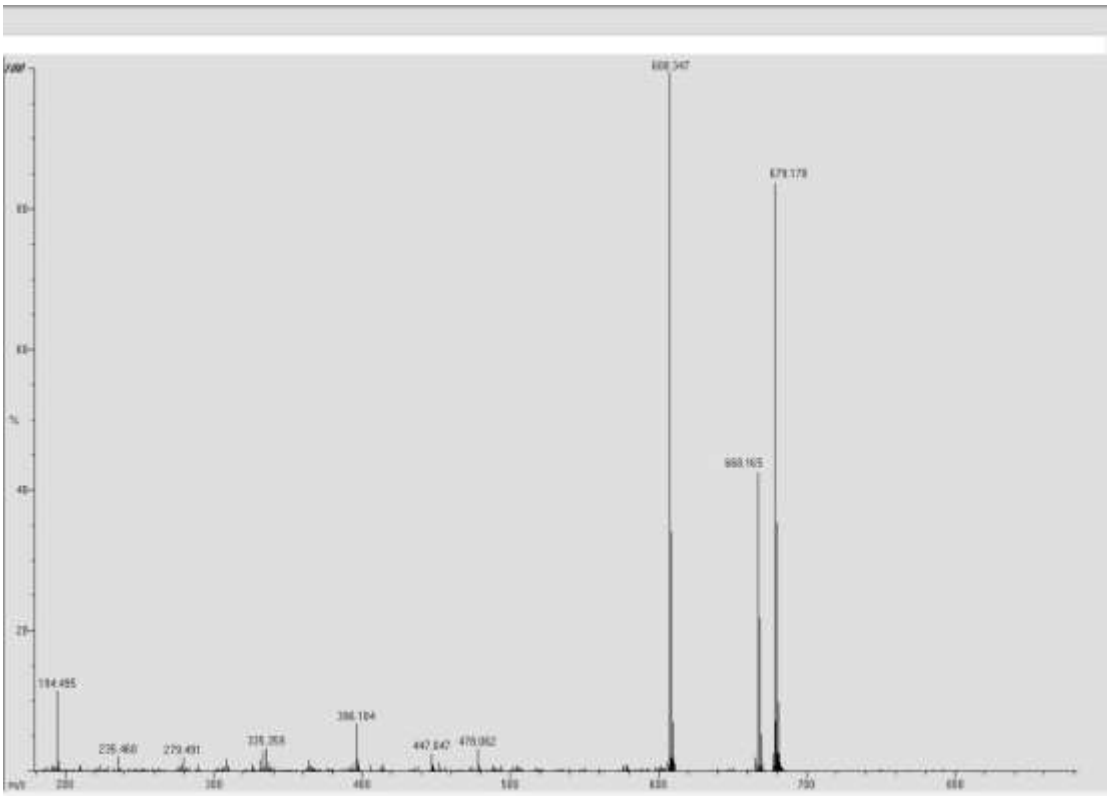

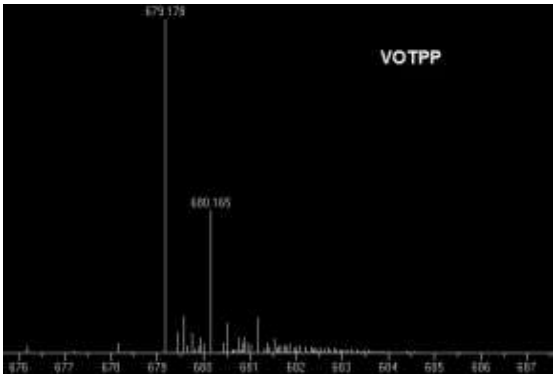

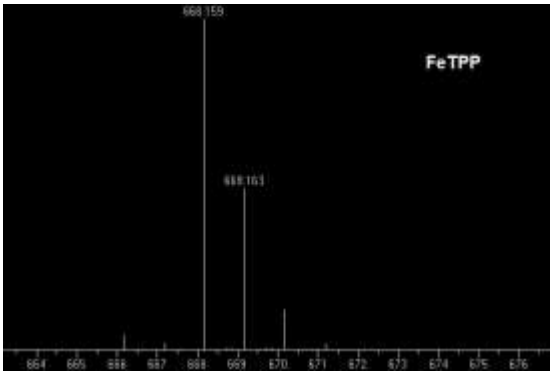

COMPETITION $NiSO_4$ + $ZnSO_4$ +TPP NITROGEN

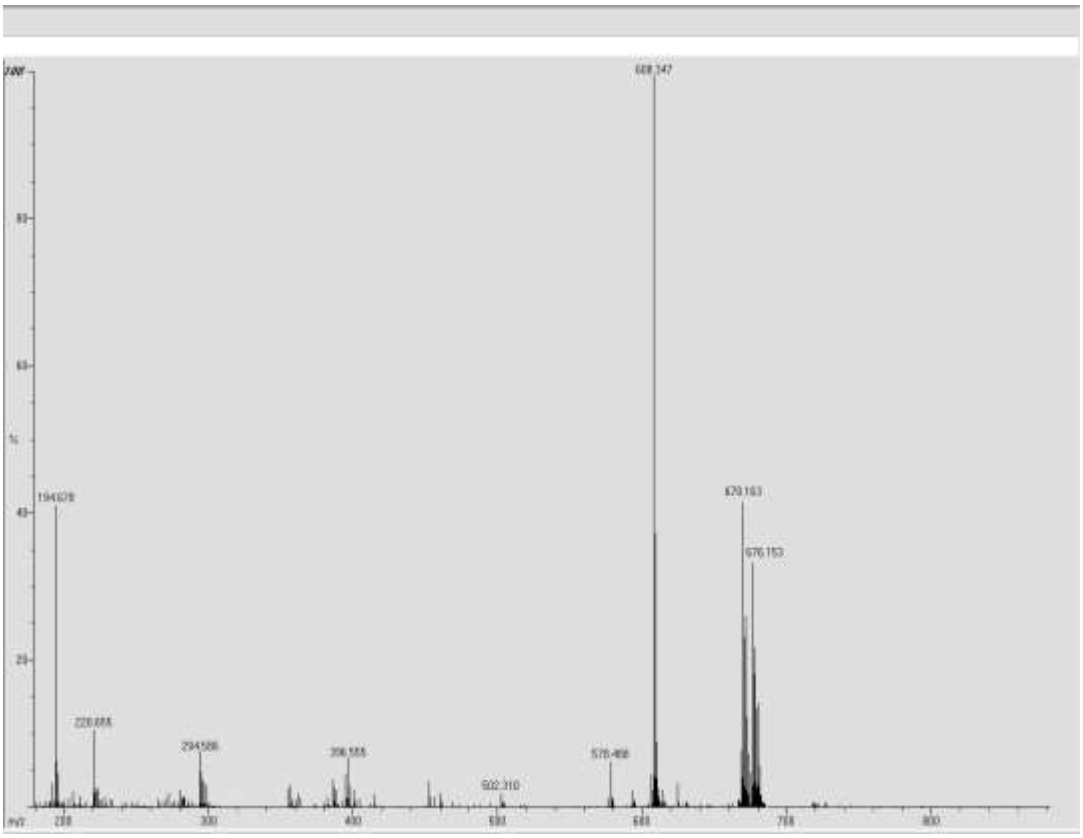

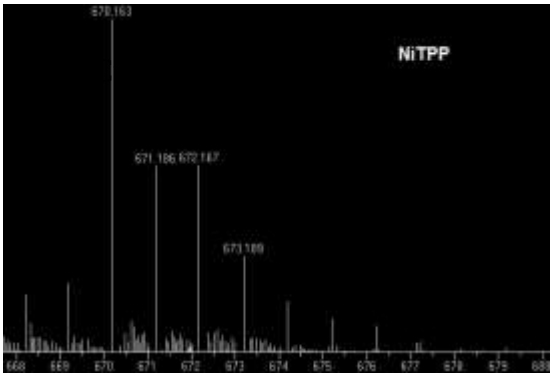

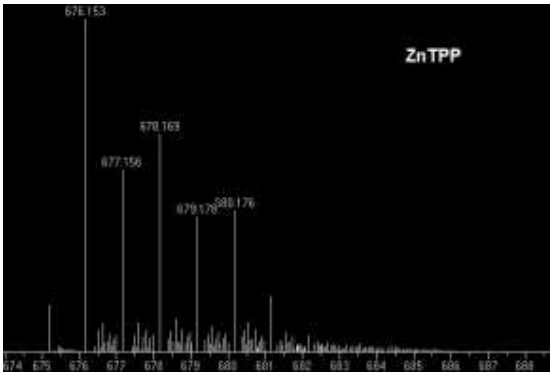

COMPETITION $NiSO_4$ + $CuSO_4$ +TPP NITROGEN

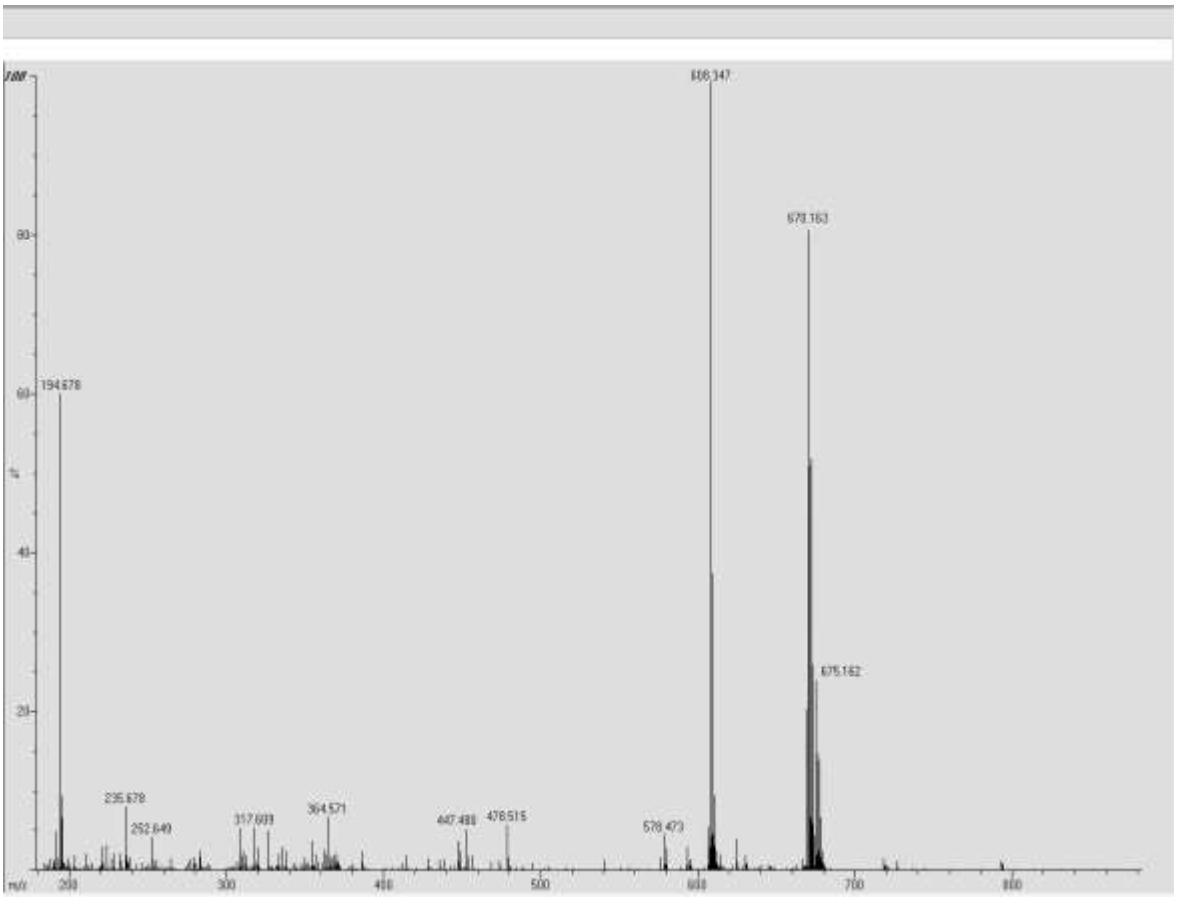

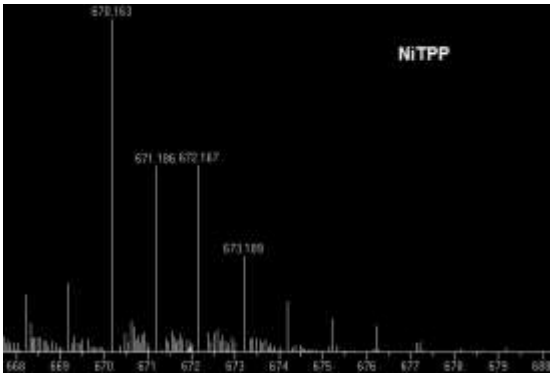

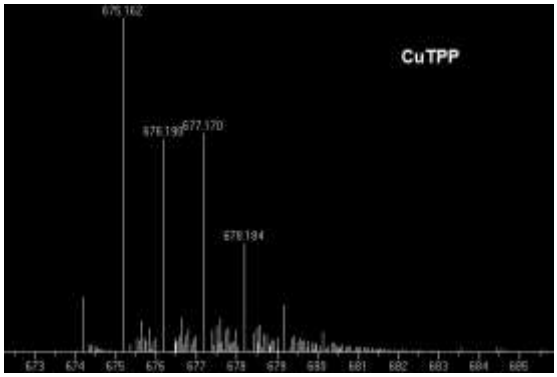

COMPETITION $NiSO_4$ + $CrSO_4$ +TPP NITROGEN

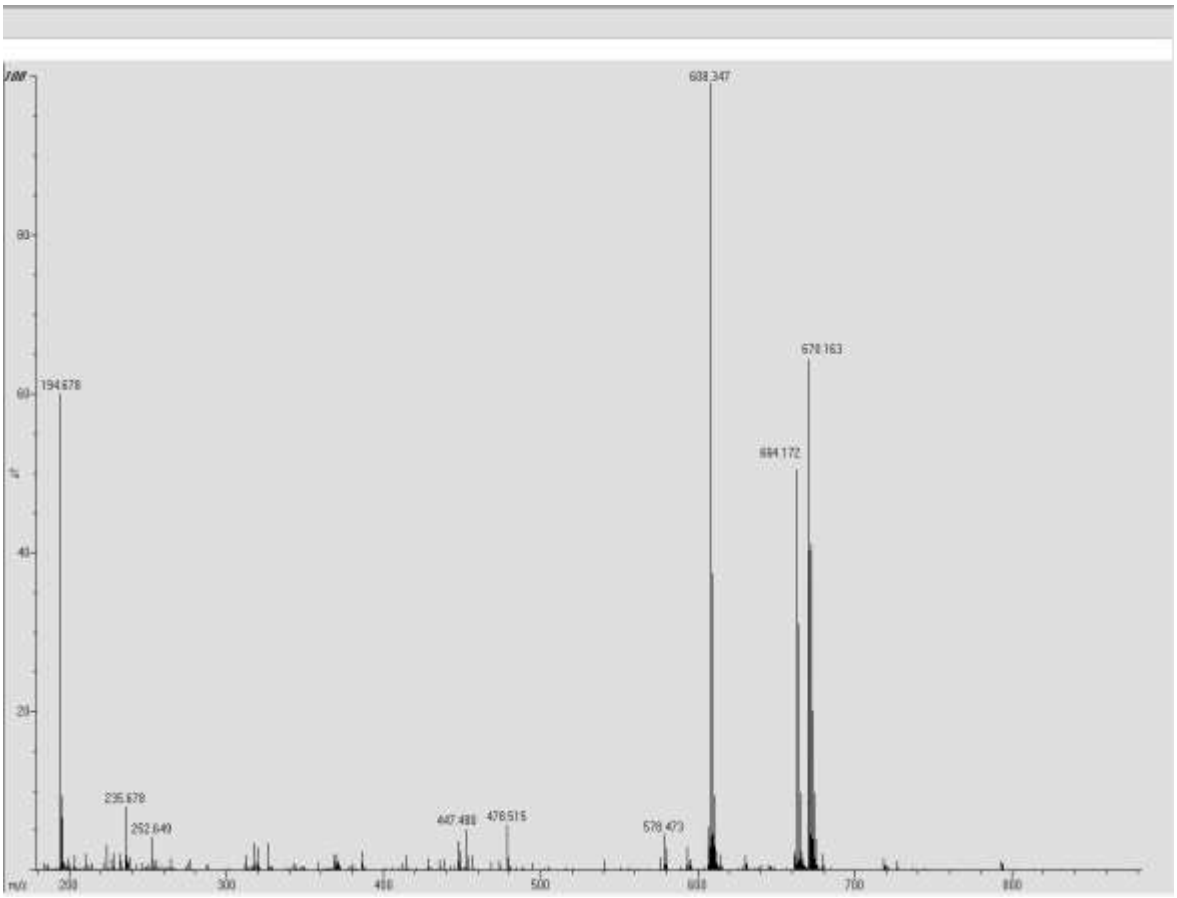

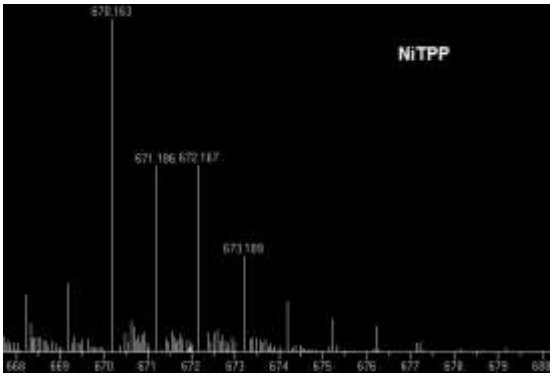

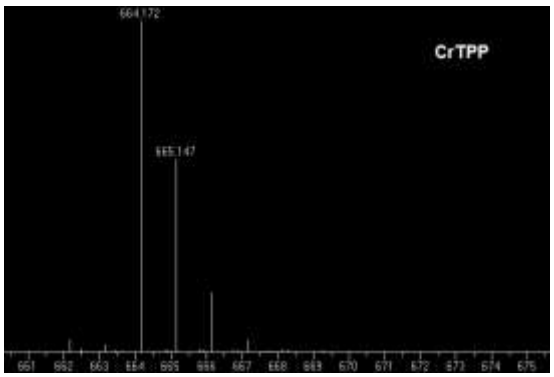

COMPETITION $NiSO_4$ + $FeSO_4$ +TPP NITROGEN

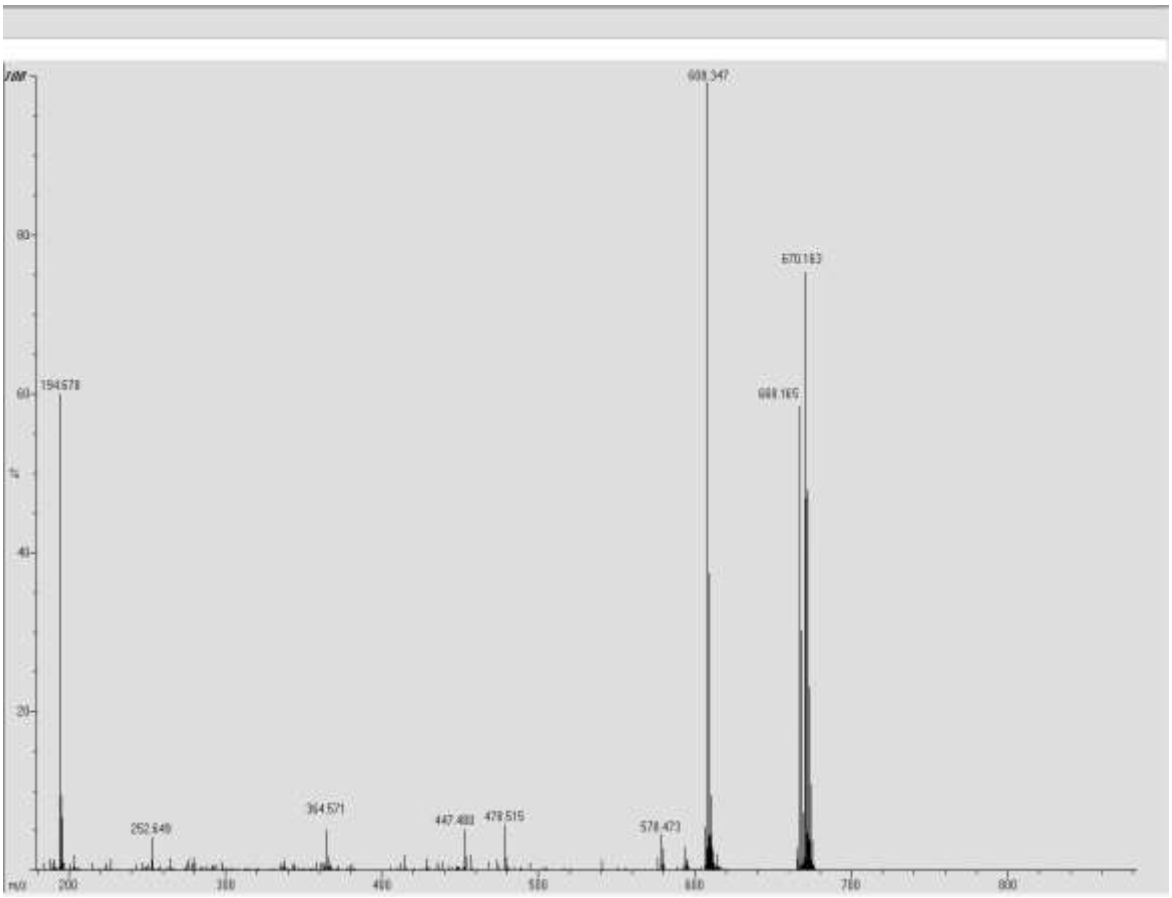

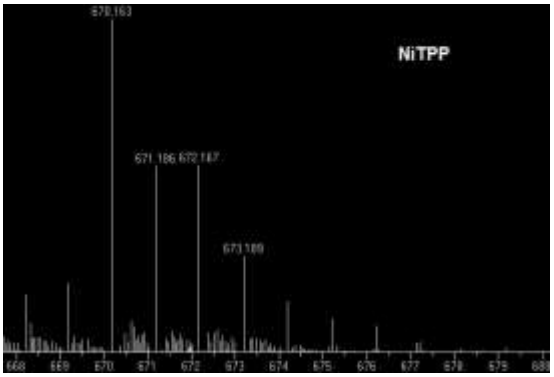

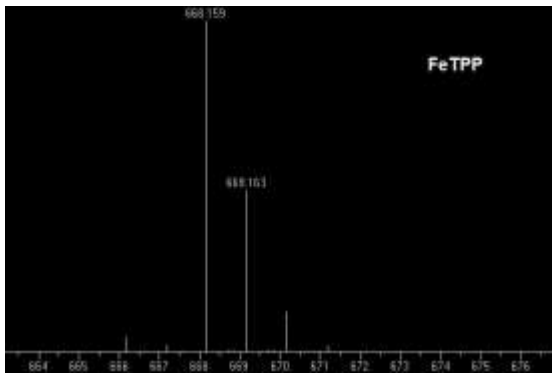

COMPETITIONS SODIUM SULFIDE $VOSO_4$ + $ZnSO_4$ + TPP

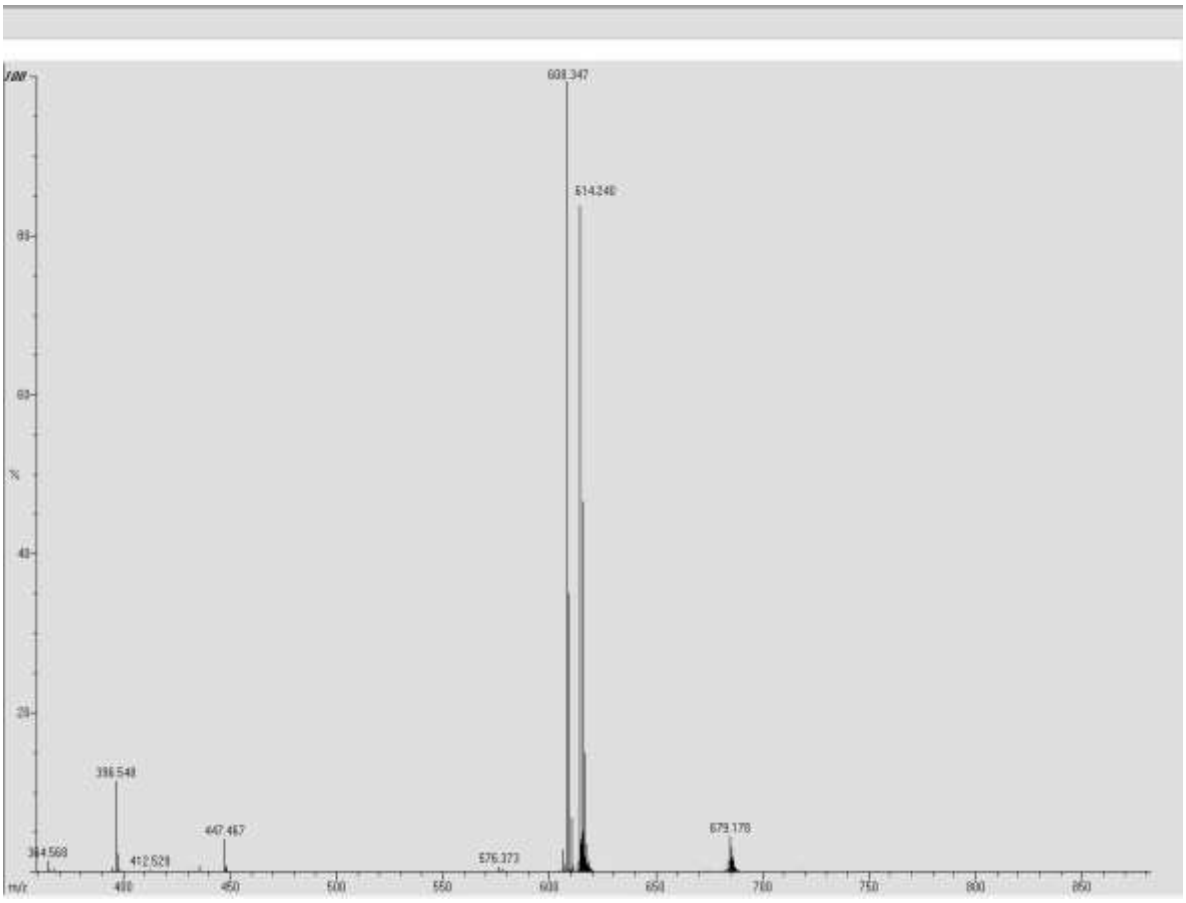

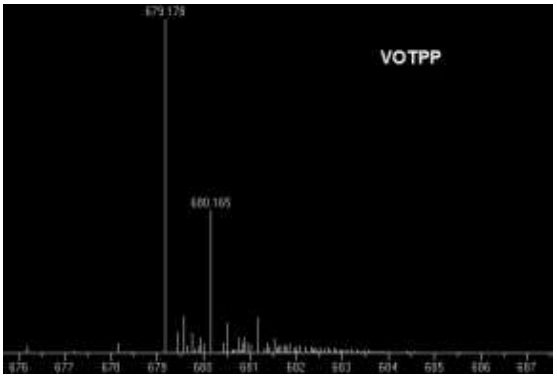

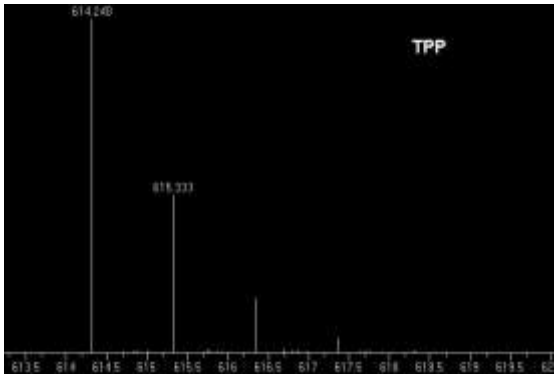

COMPETITIONS SODIUM SULFIDE $VOSO_4$ + $CuSO_4$ + TPP

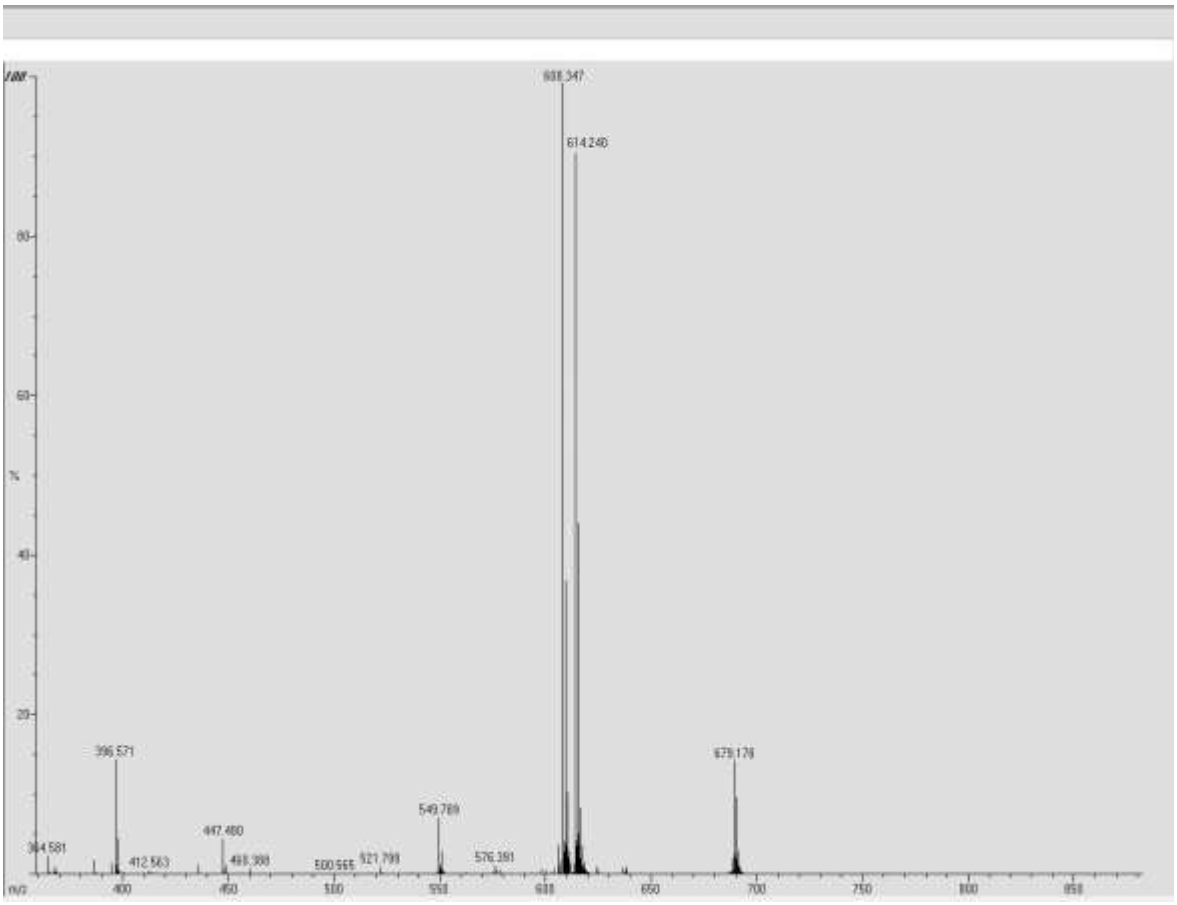

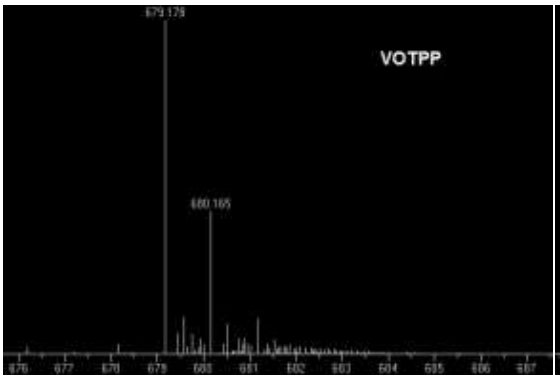

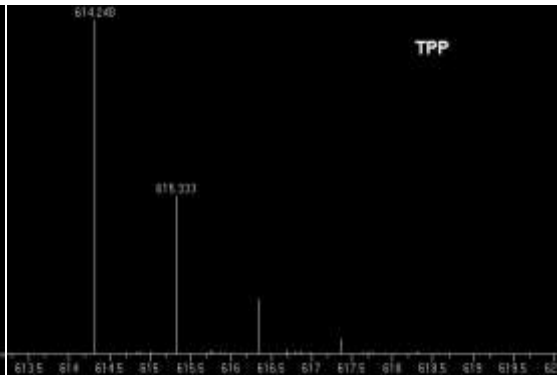

COMPETITIONS SODIUM SULFIDE $VOSO_4$ + $CrSO_4$ + TPP

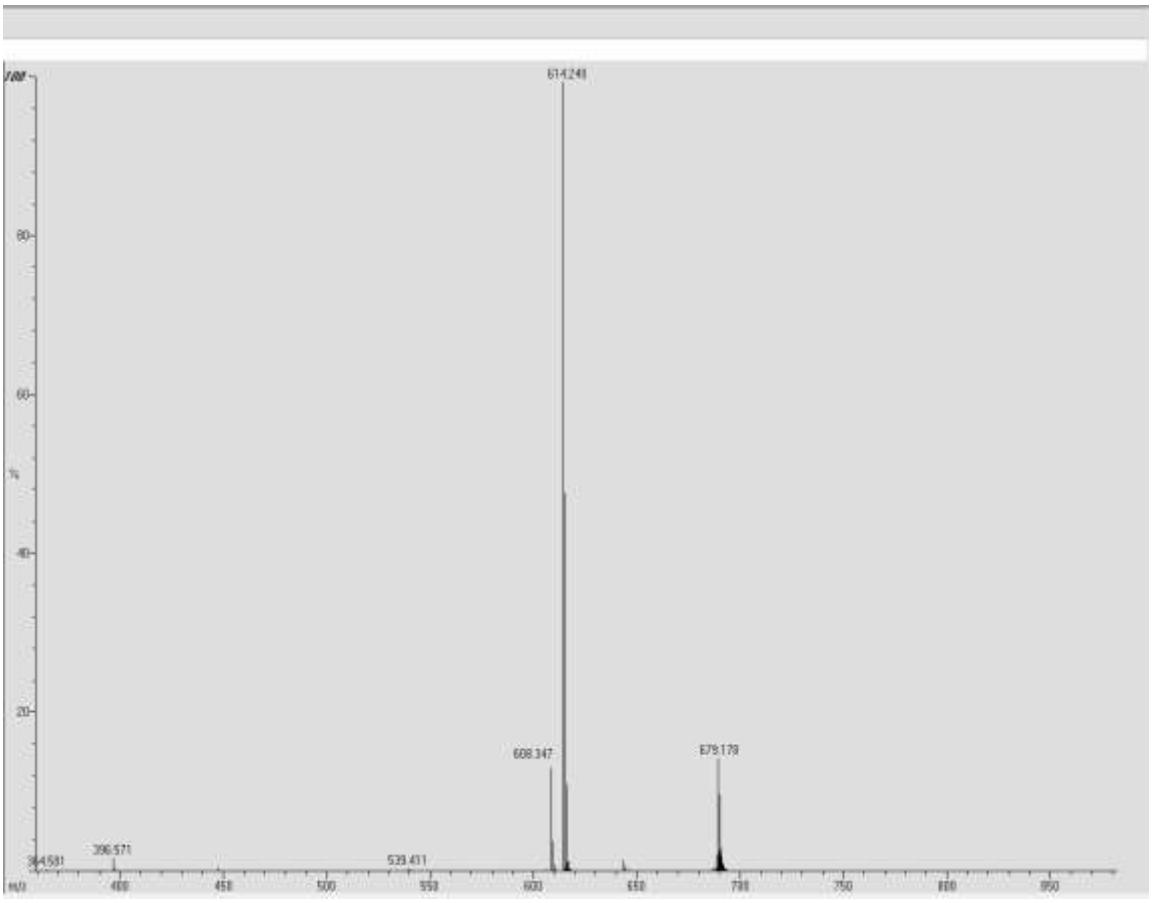

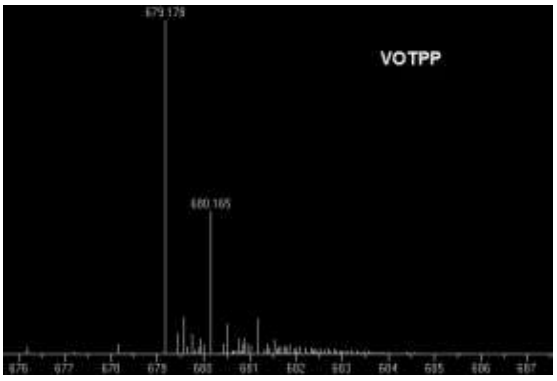

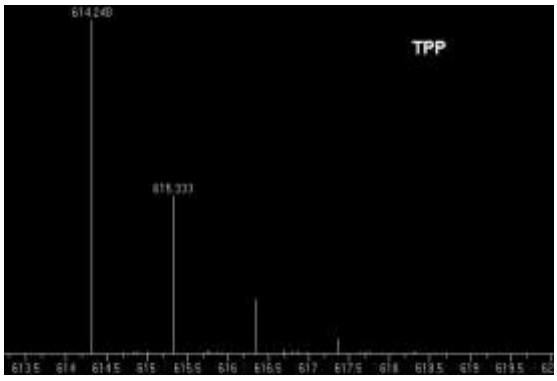

COMPETITIONS SODIUM SULFIDE $VOSO_4$ + $NiSO_4$ + TPP

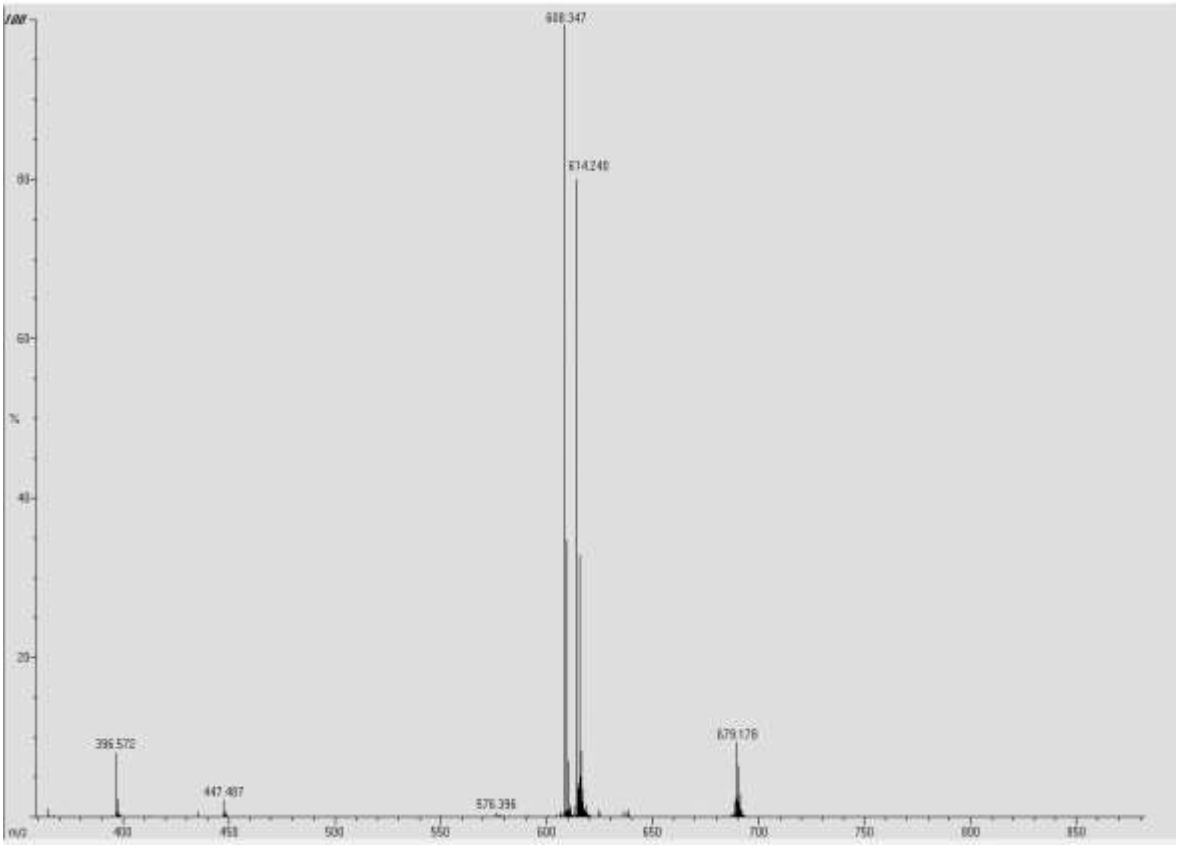

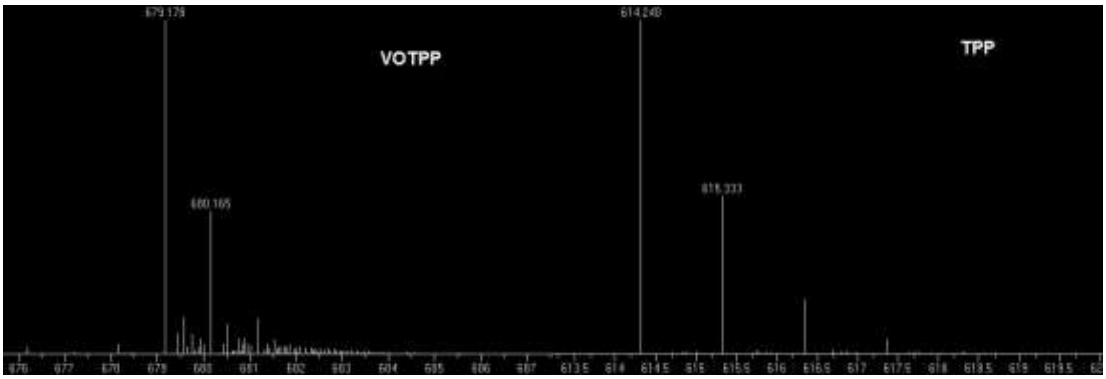

COMPETITIONS SODIUM SULFIDE $VOSO_4$ + $FeSO_4$ + TPP

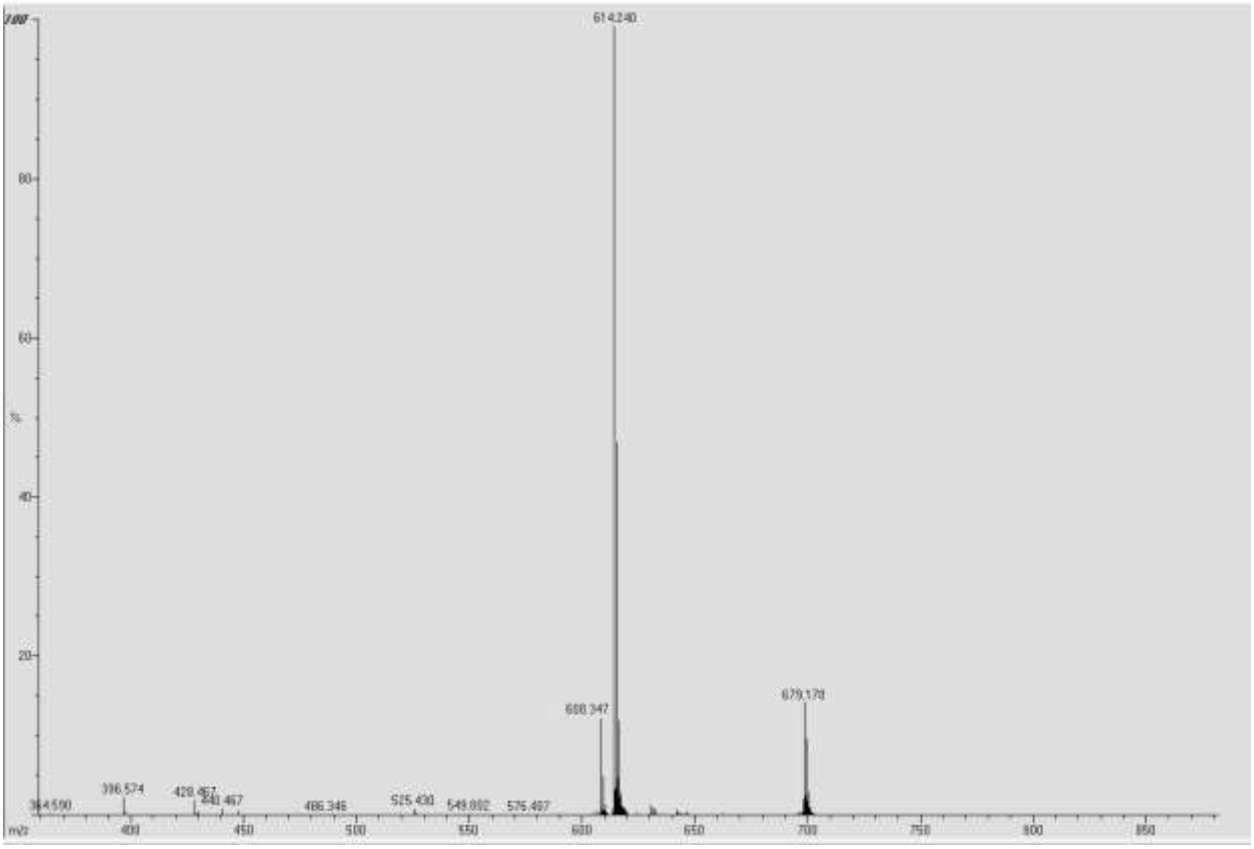

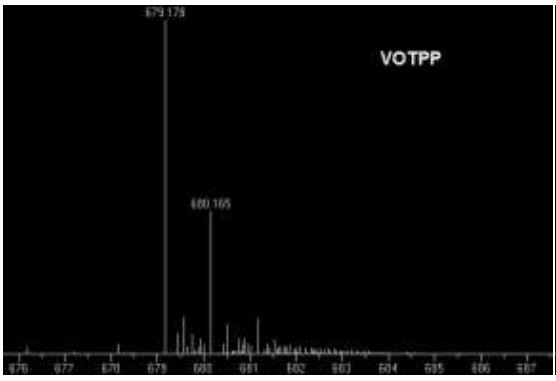

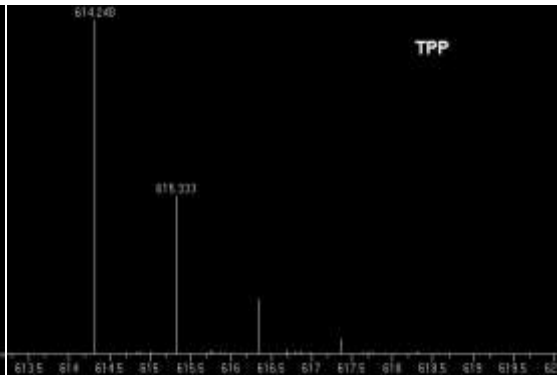

COMPETITIONS SODIUM SULFIDE $NiSO_4$ + $ZnSO_4$ + TPP

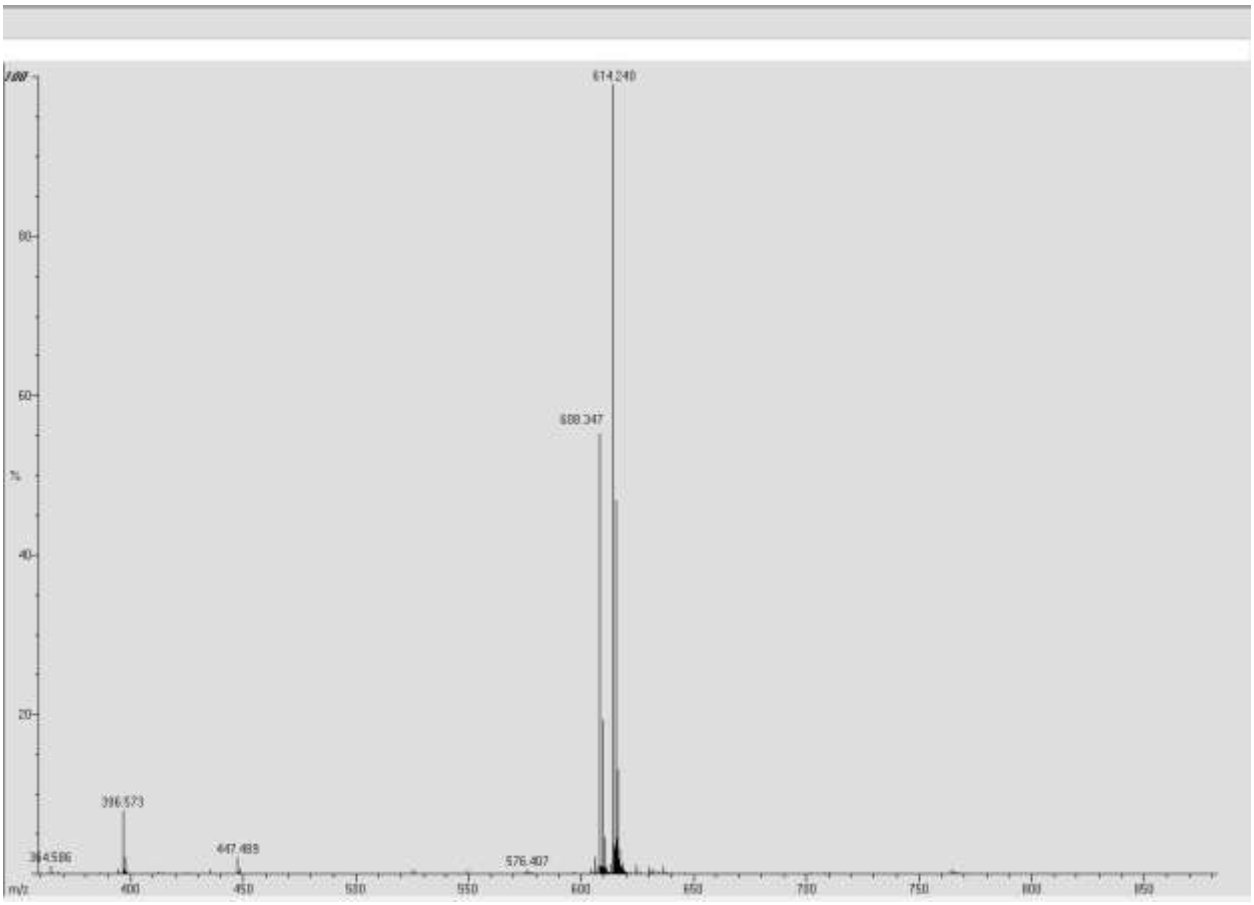

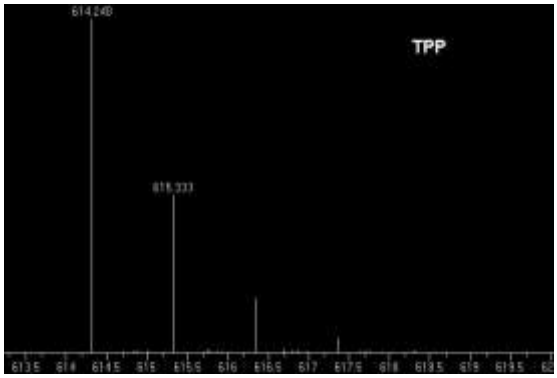

COMPETITIONS SODIUM SULFIDE $NiSO_4$ + $CuSO_4$ + TPP

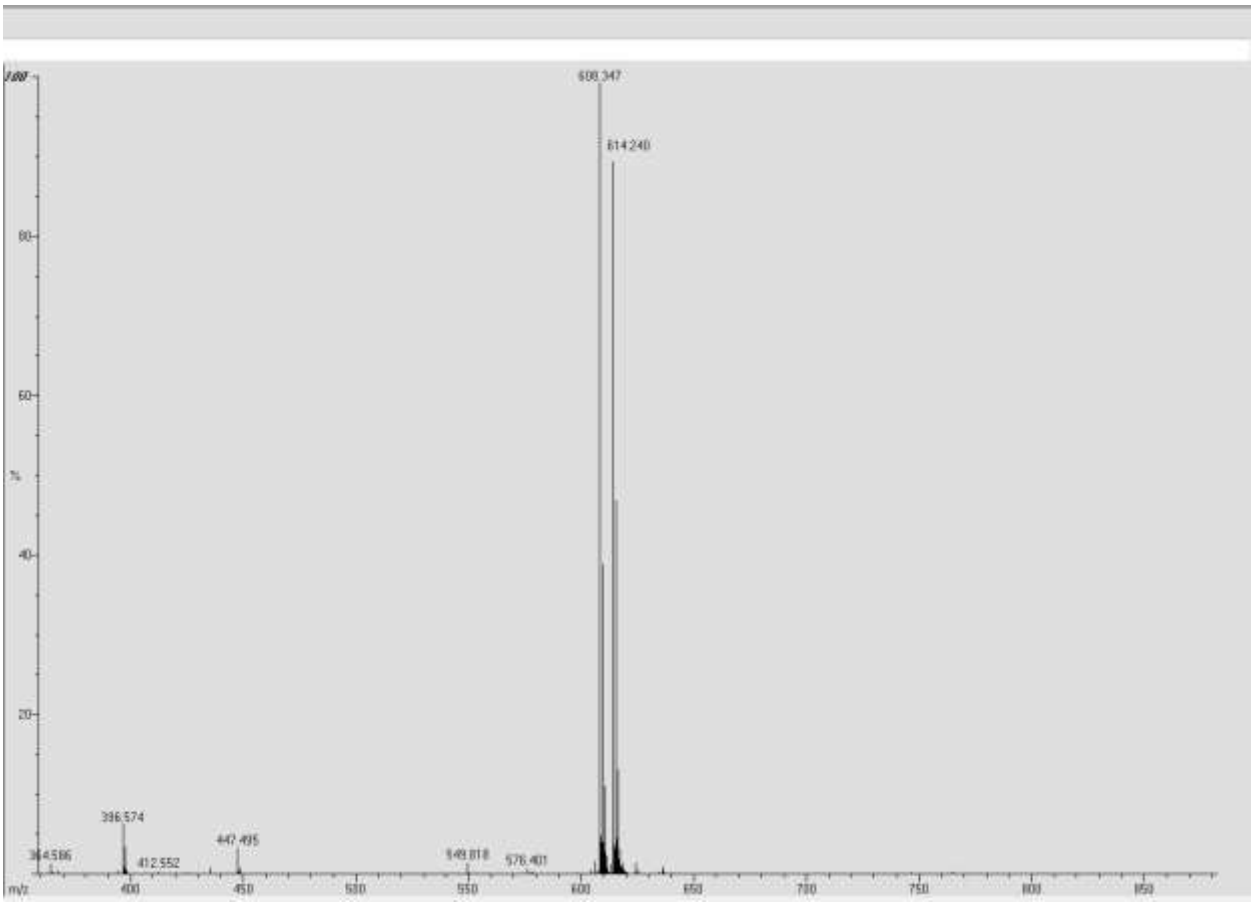

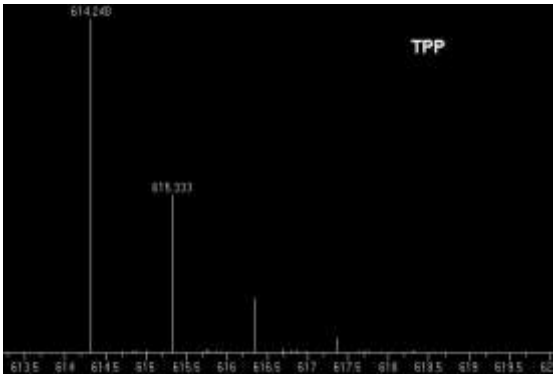

COMPETITIONS SODIUM SULFIDE $NiSO_4$ + $CrSO_4$ + TPP

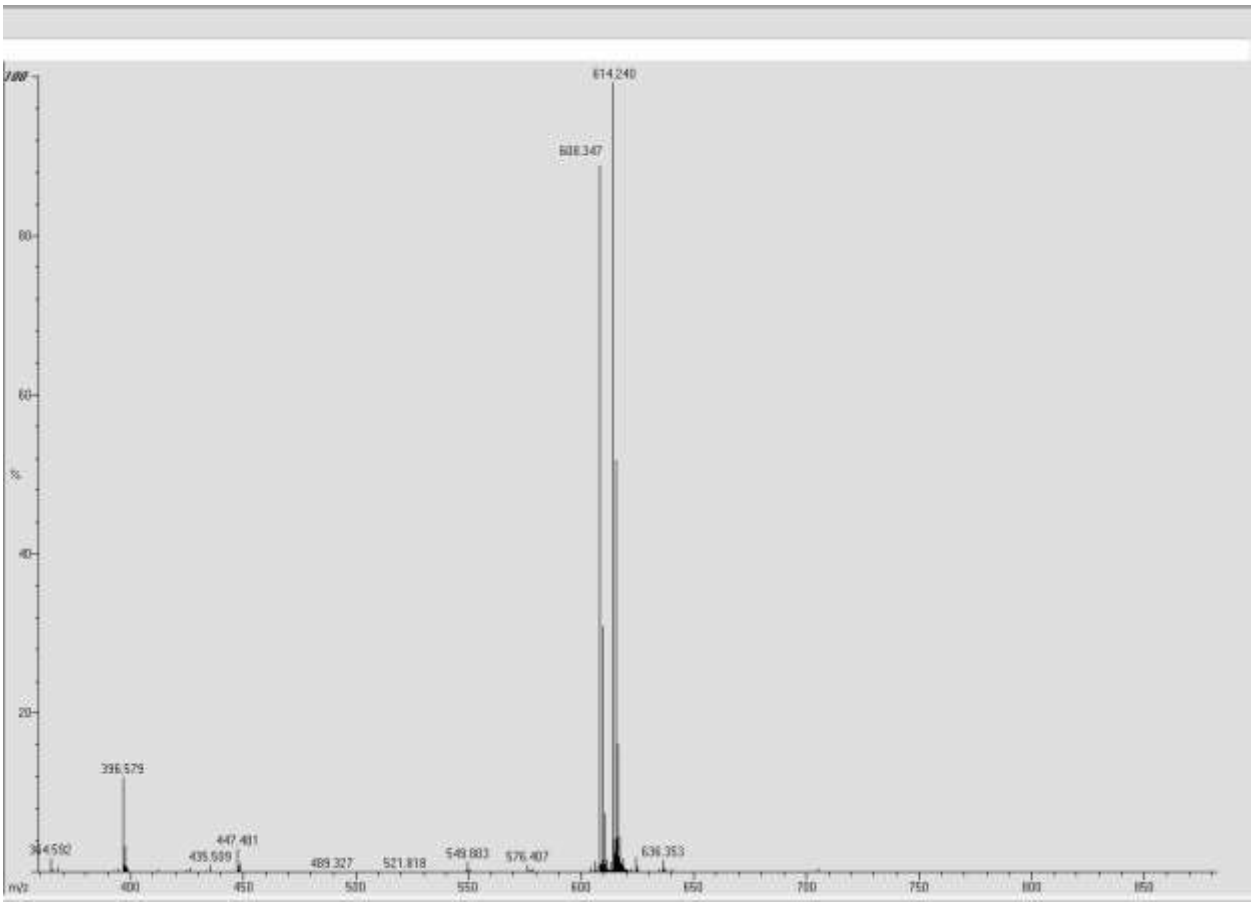

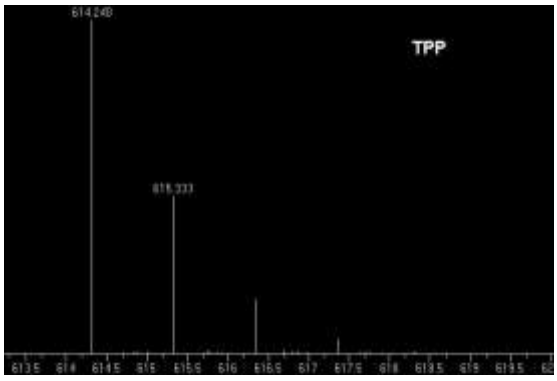

COMPETITIONS SODIUM SULFIDE $NiSO_4$ + $FeSO_4$ + TPP

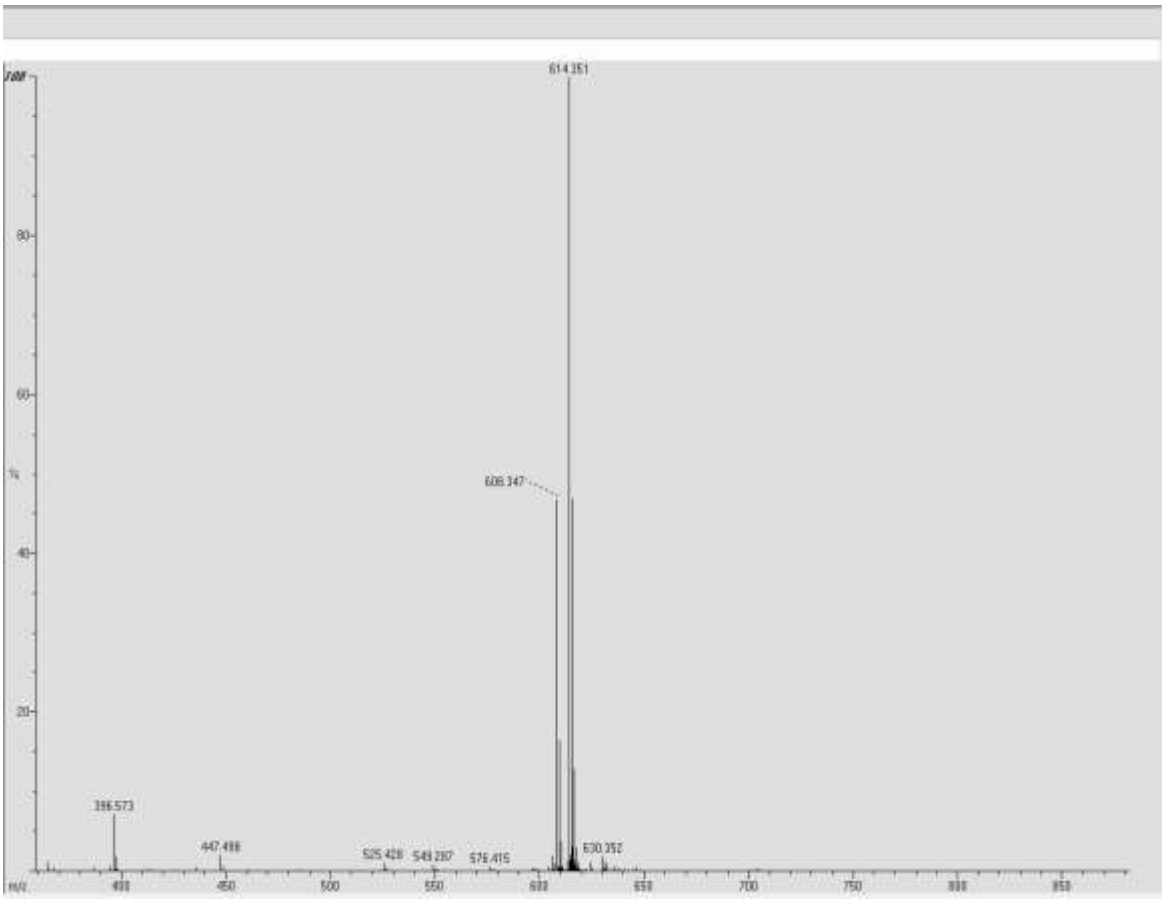

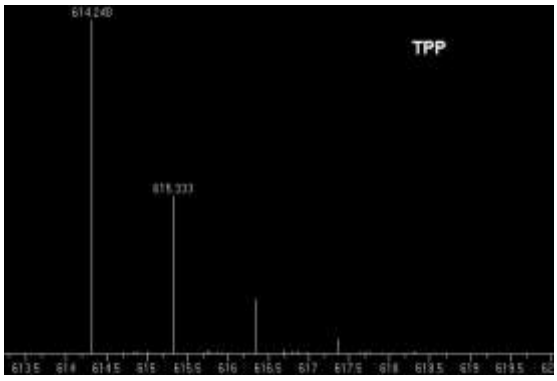

APENDIX H. MASS SPECS – DEMETALLATIONS

DEMETALLATION $VOSO_4$ + ZnTPP OPEN SYSTEM

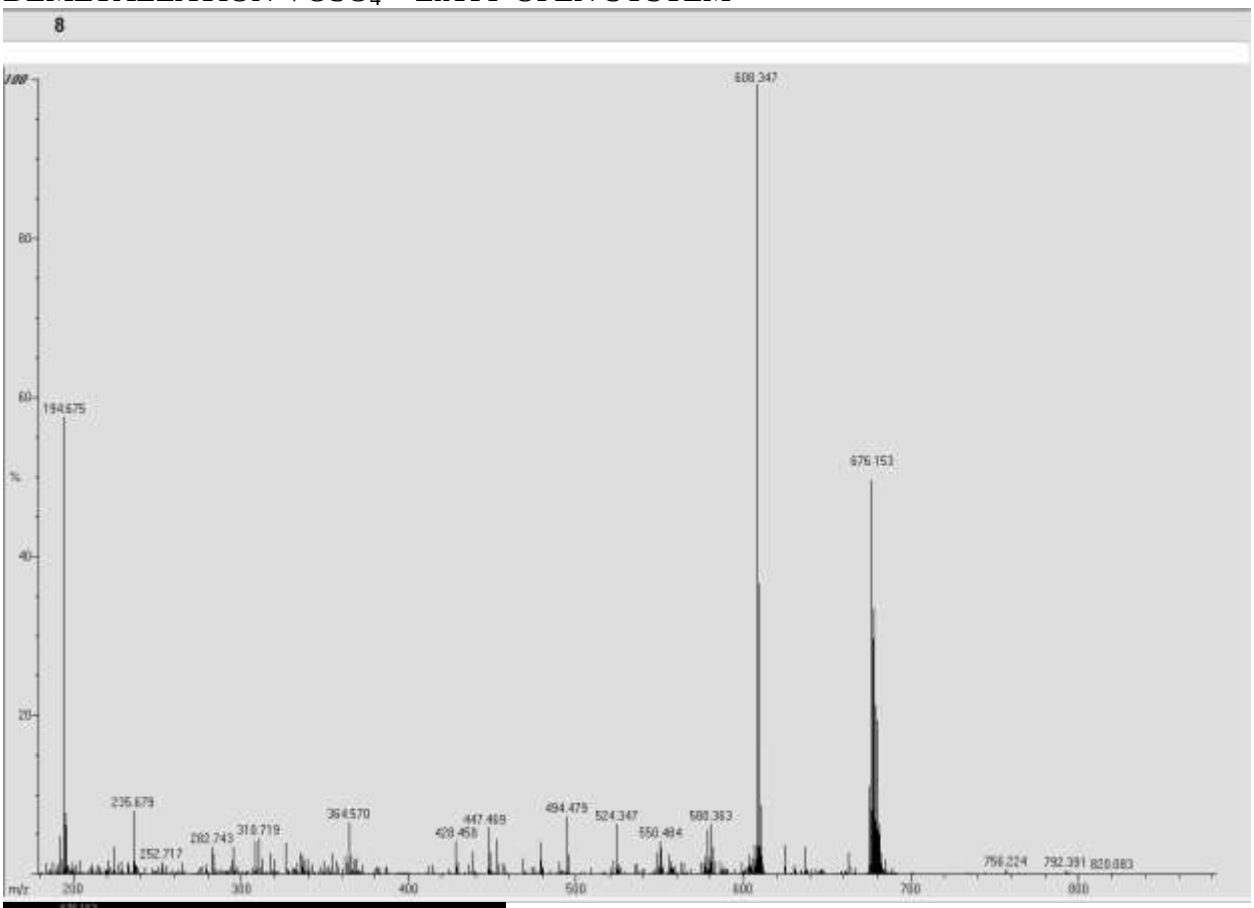

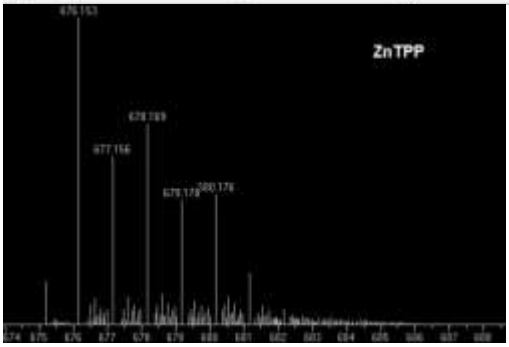

DEMETALLATION $VOSO_4$ + CuTPP OPEN SYSTEM

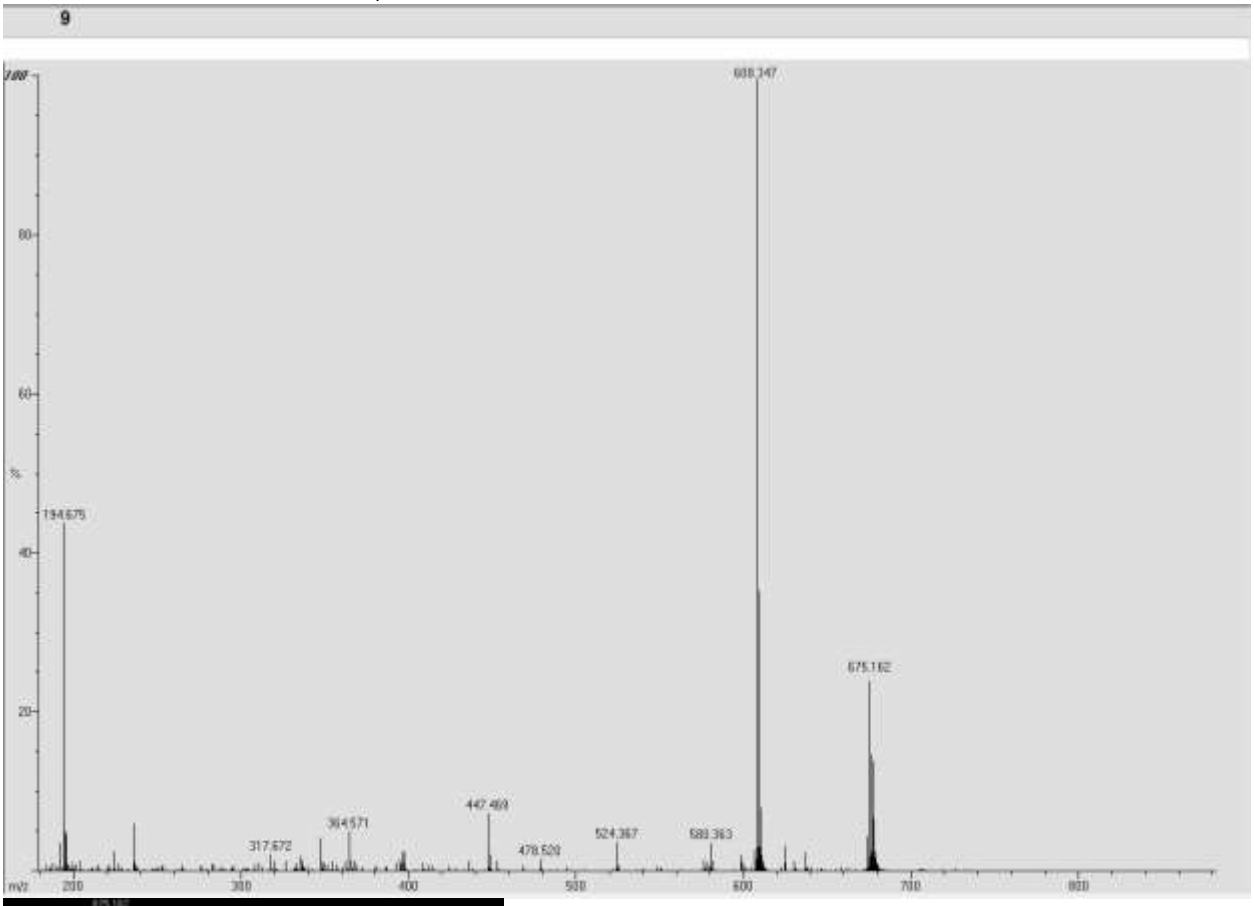

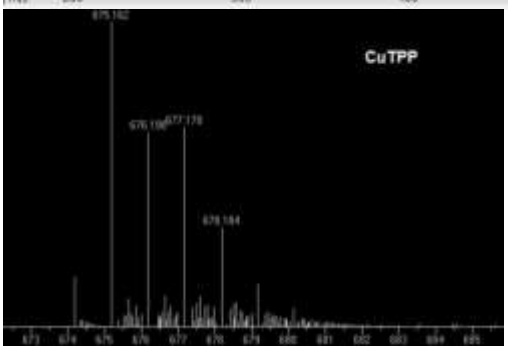

DEMETALLATION $VOSO_4$ + CrTPP OPEN SYSTEM

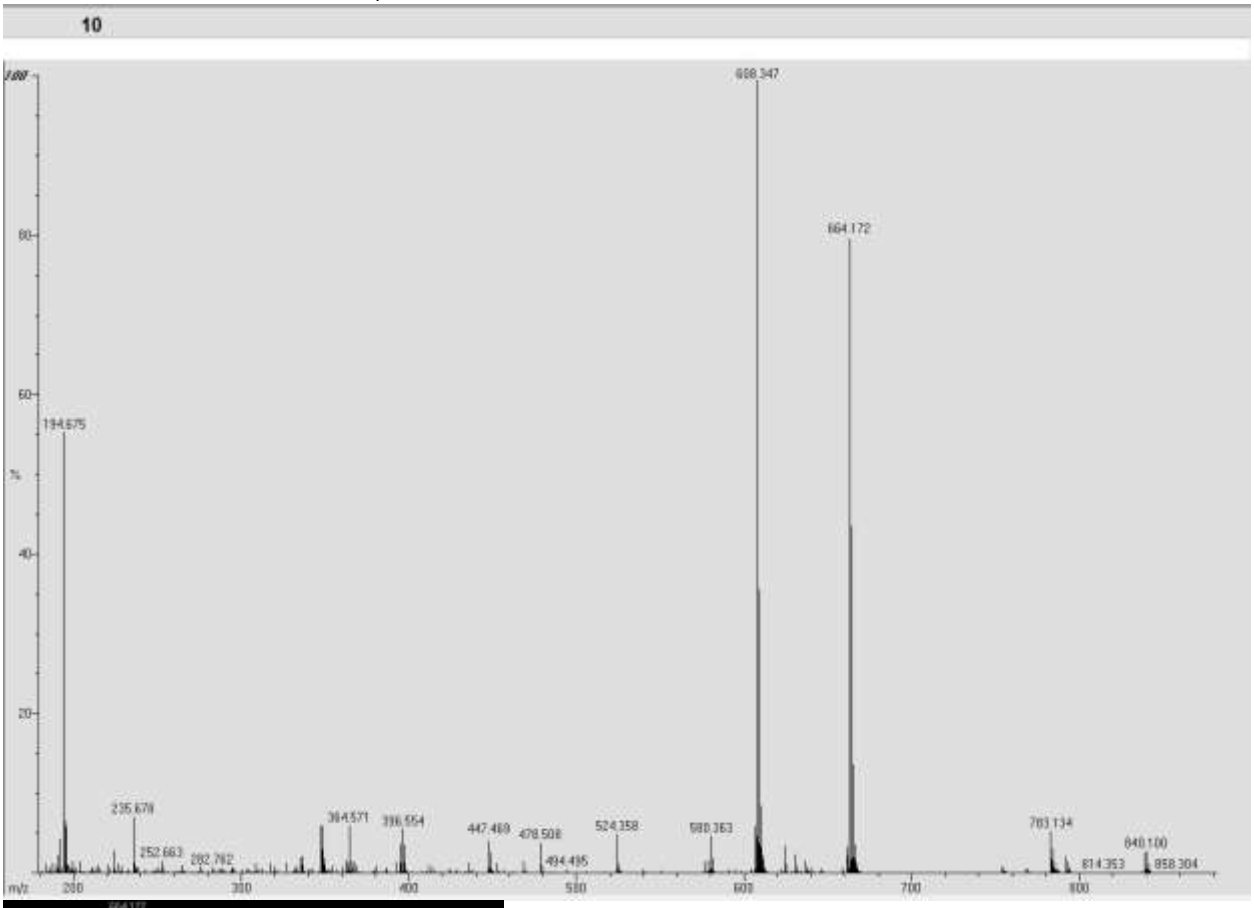

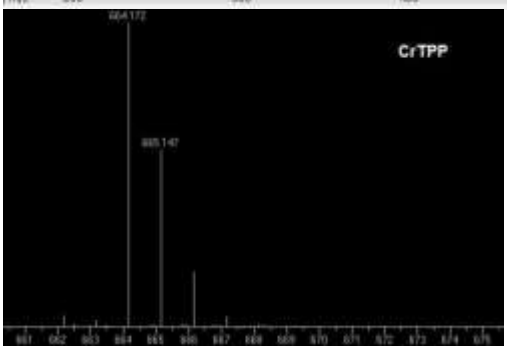

DEMETALLATION $VOSO_4$ + NiTPP OPEN SYSTEM

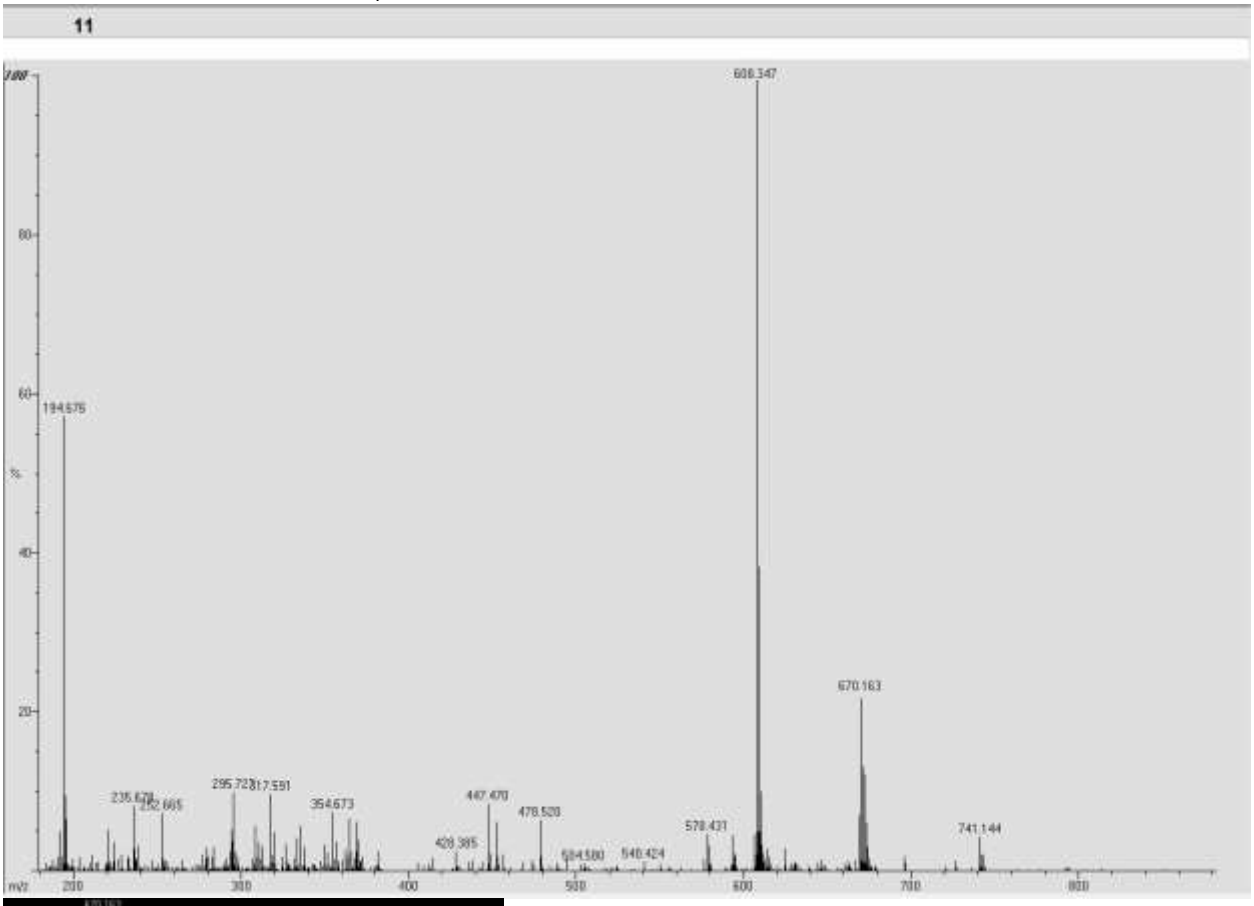

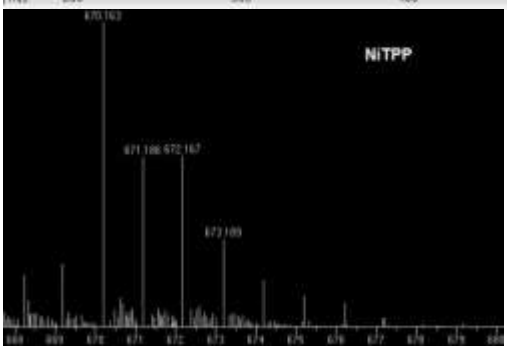

DEMETALLATION $NiSO_4$ + ZnTPP OPEN SYSTEM

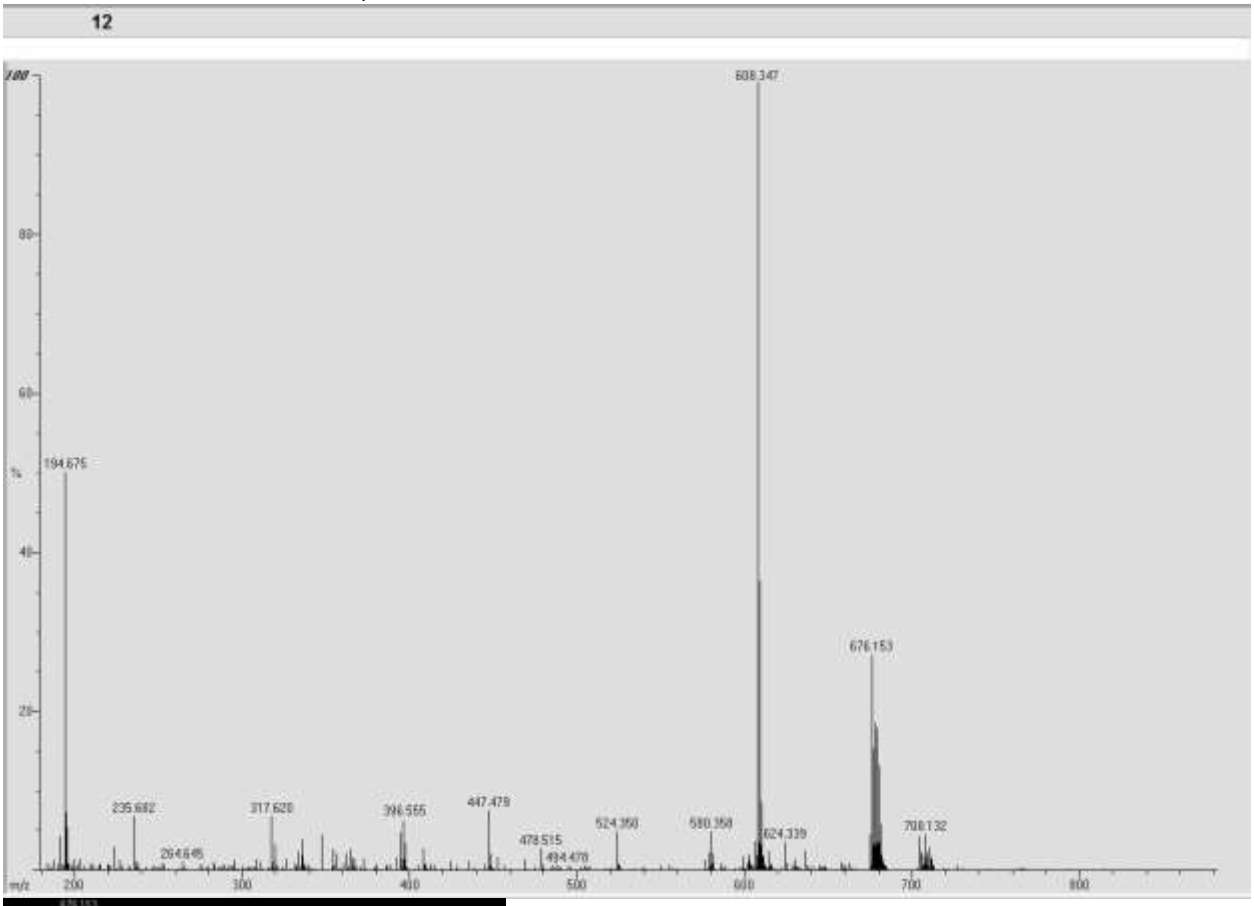

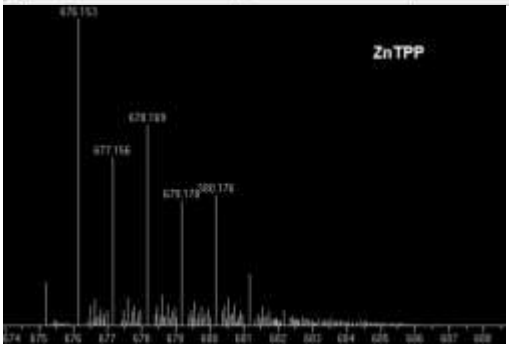

DEMETALLATION $NiSO_4$ + CuTPP OPEN SYSTEM

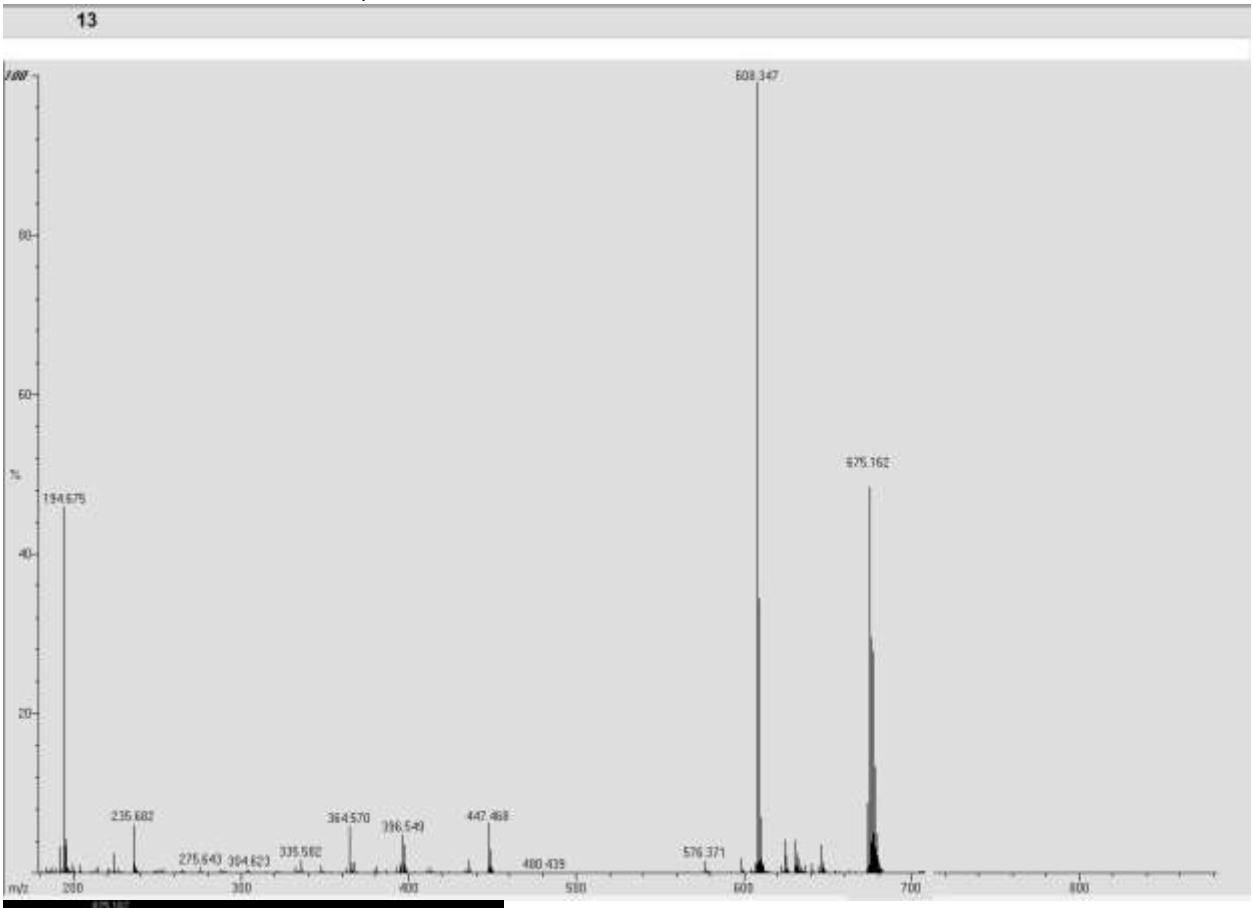

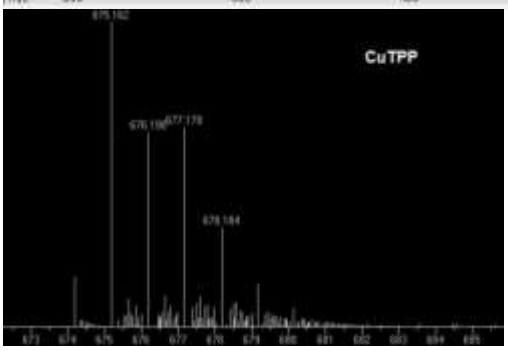

DEMETALLATION $NiSO_4$ + CrTPP OPEN SYSTEM

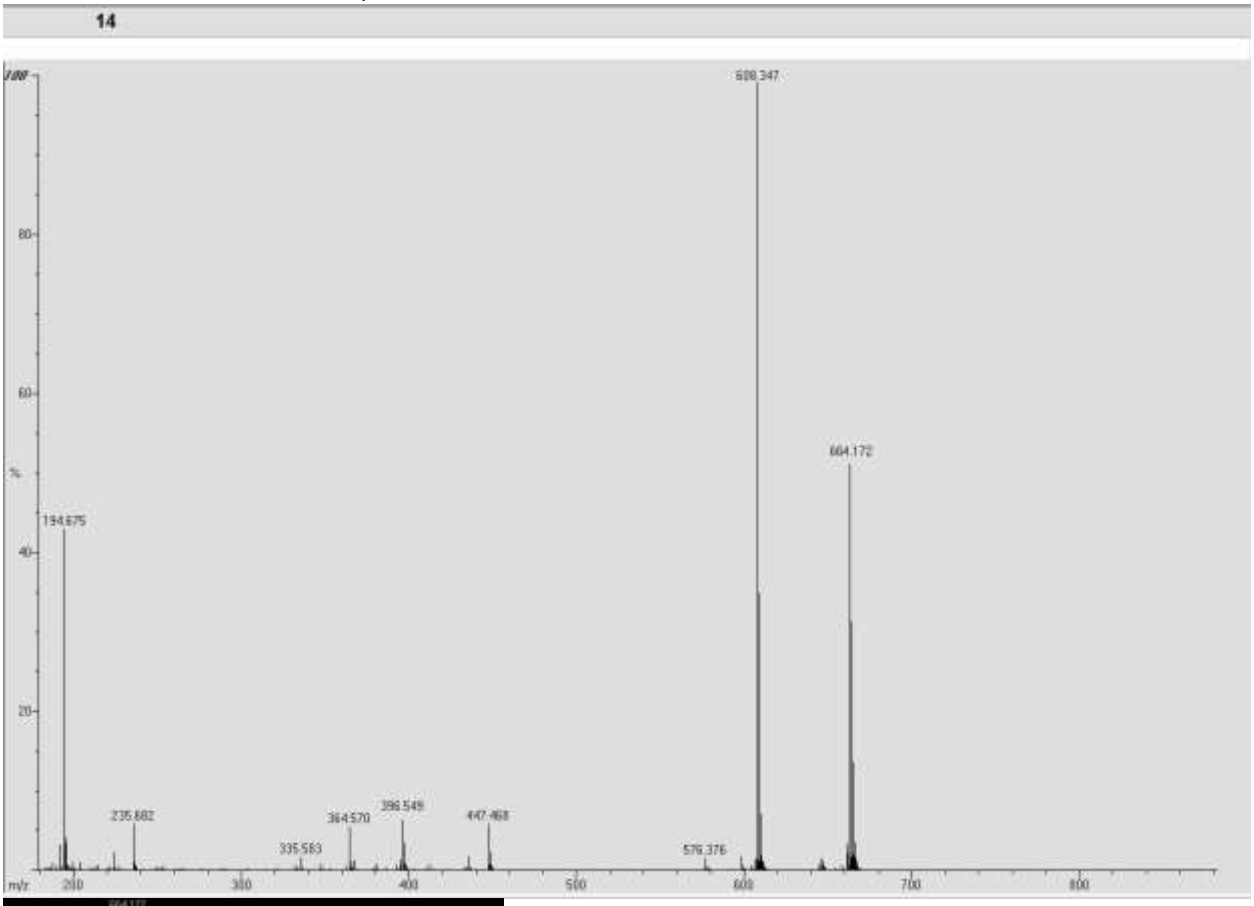

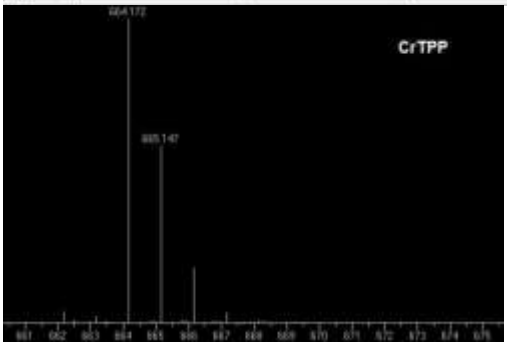

DEMETALLATION $NiSO_4$ + VoTPP OPEN SYSTEM

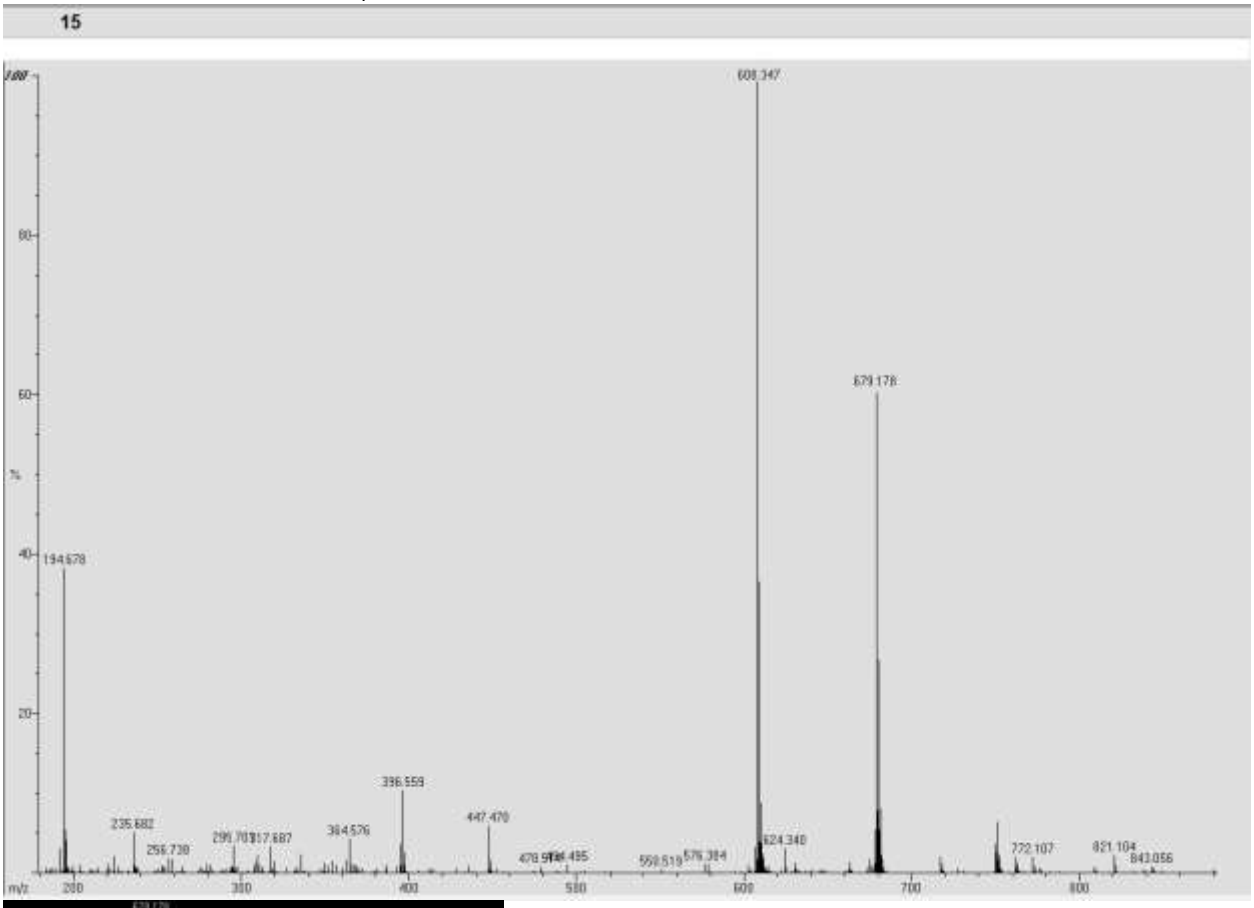

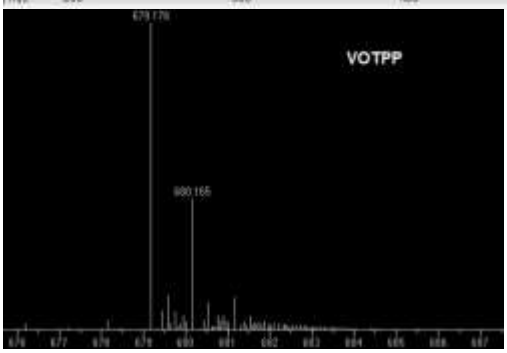

DEMETALLATION $VOSO_4$ + ZnTPP NITROGEN

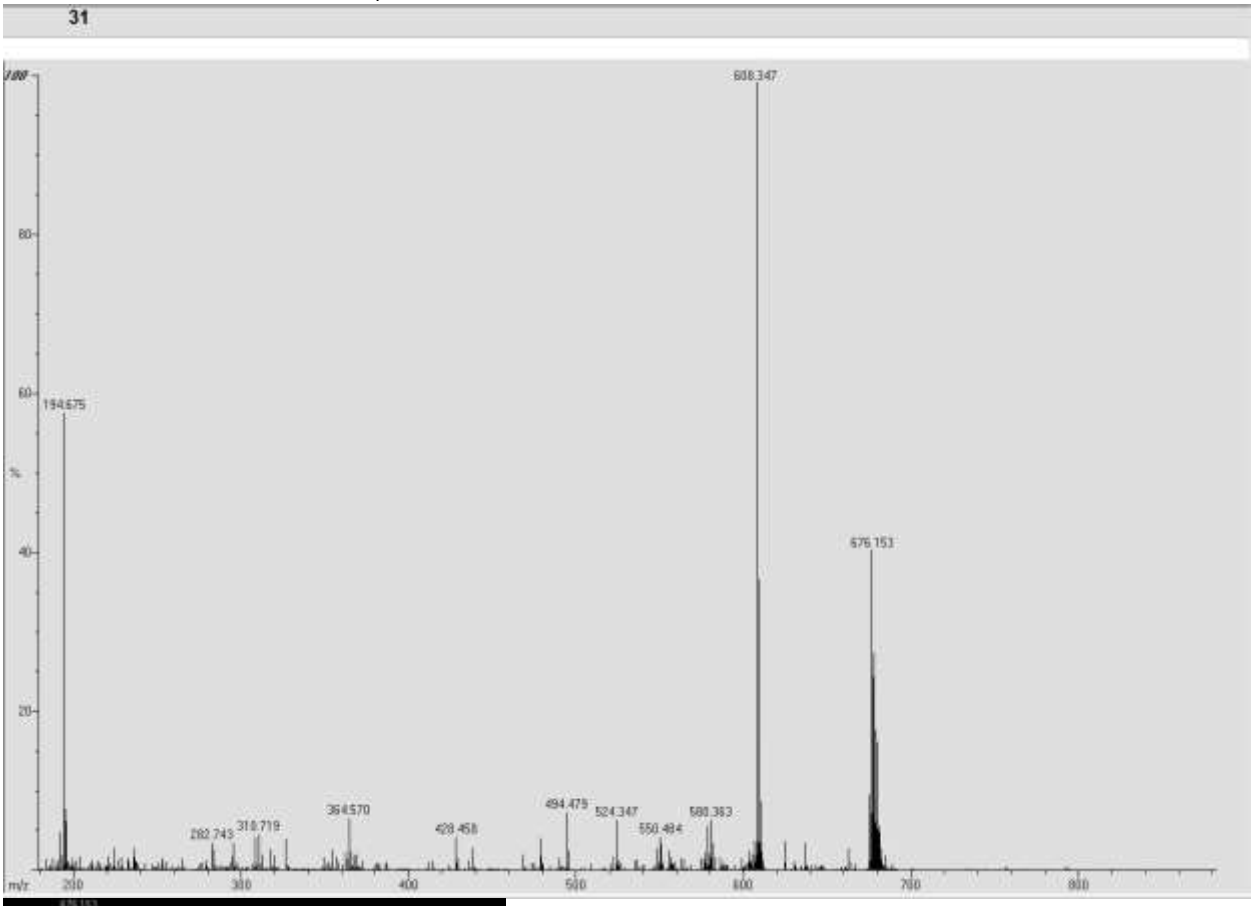

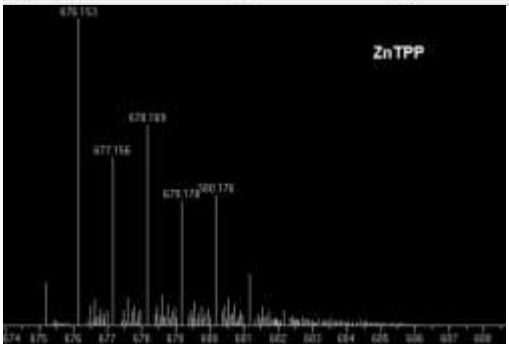

DEMETALLATION $VOSO_4$ + CuTPP NITROGEN

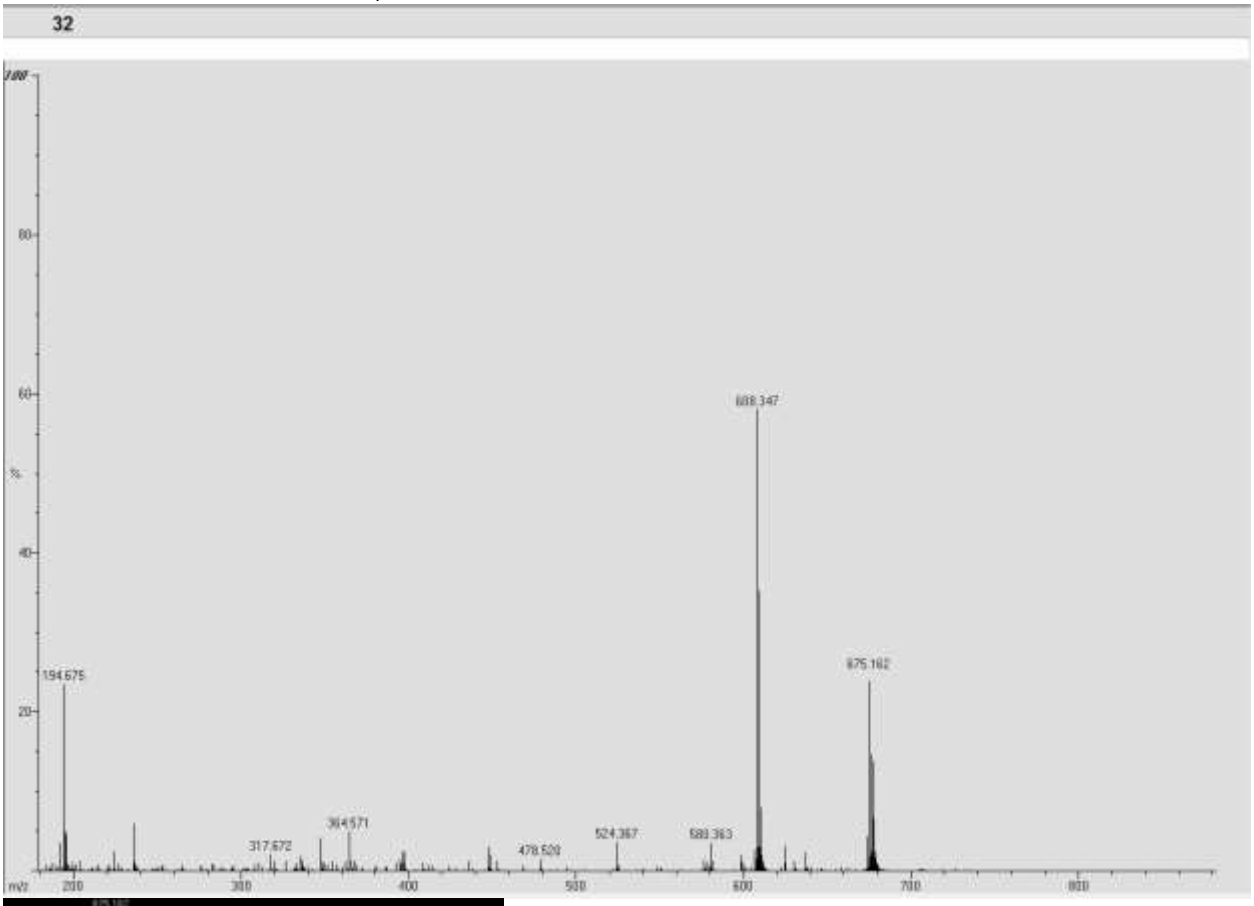

DEMETALLATION $VOSO_4$ + CrTPP NITROGEN

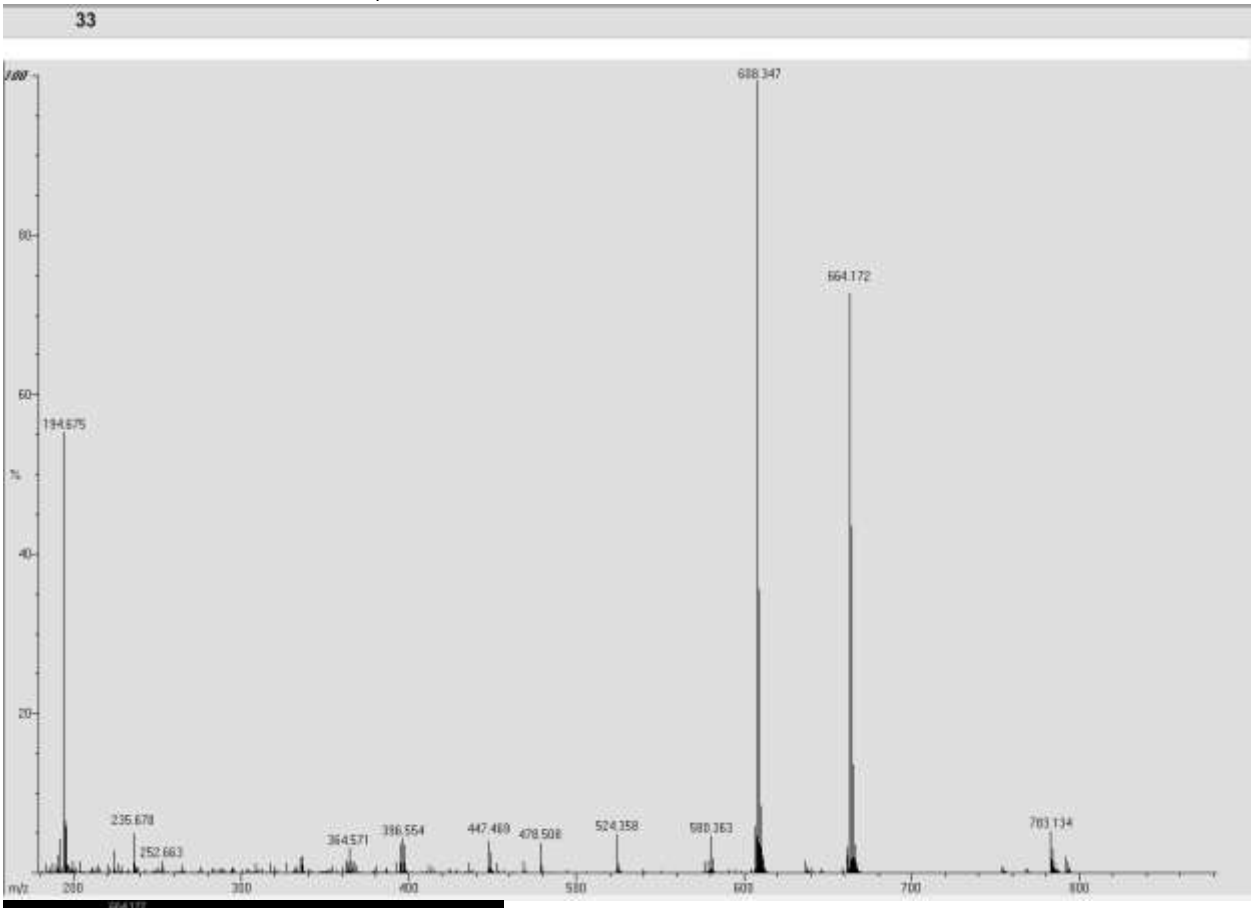

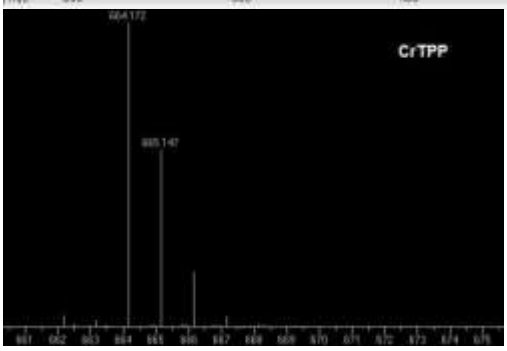

DEMETALLATION $VOSO_4$ + NiTPP NITROGEN

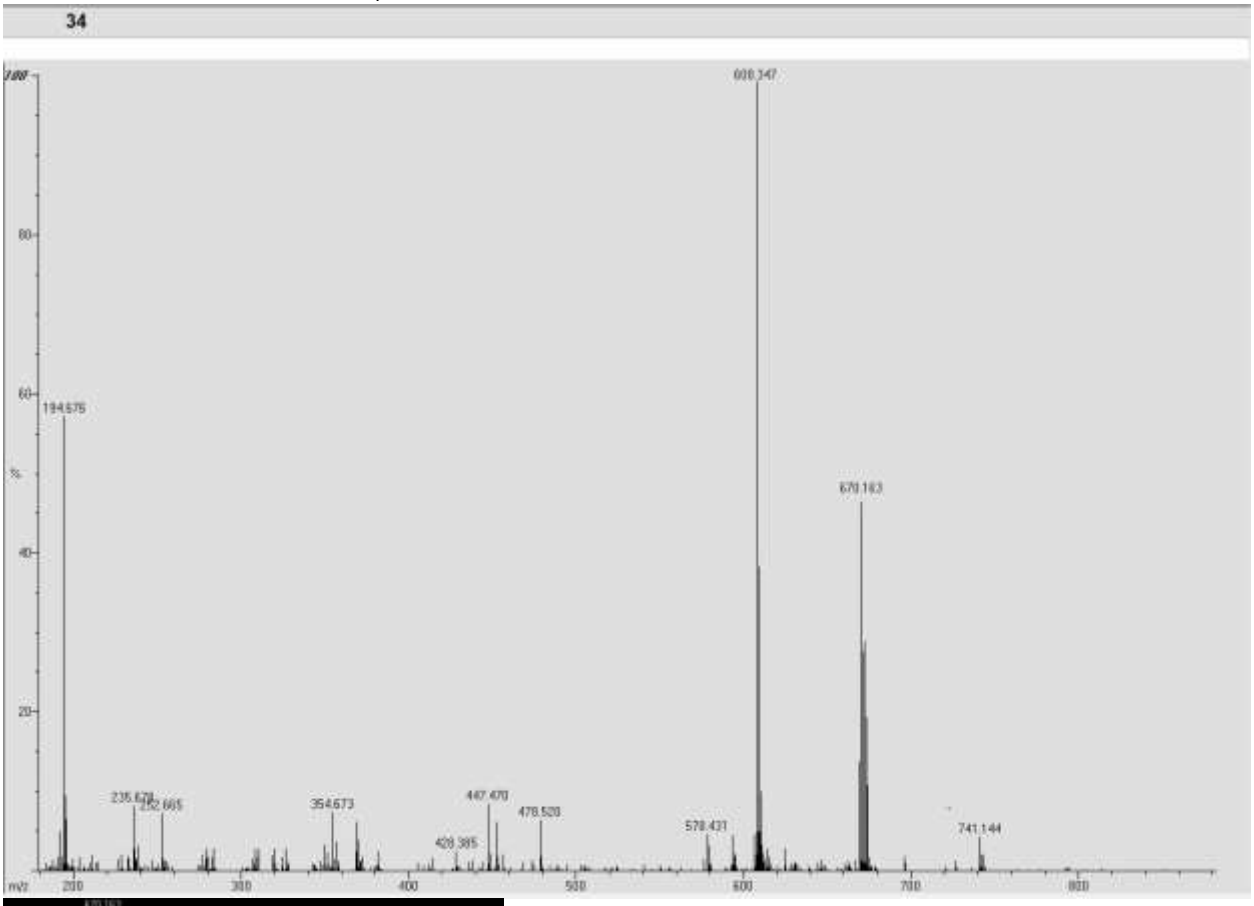

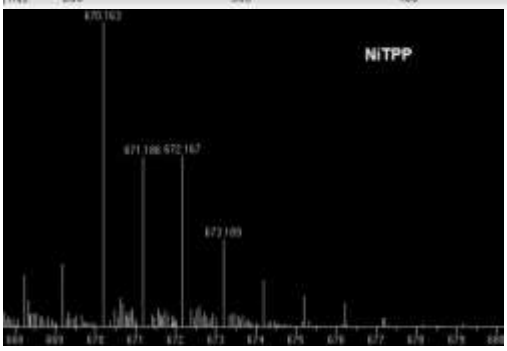

DEMETALLATION $NiSO_4$ + ZnTPP NITROGEN

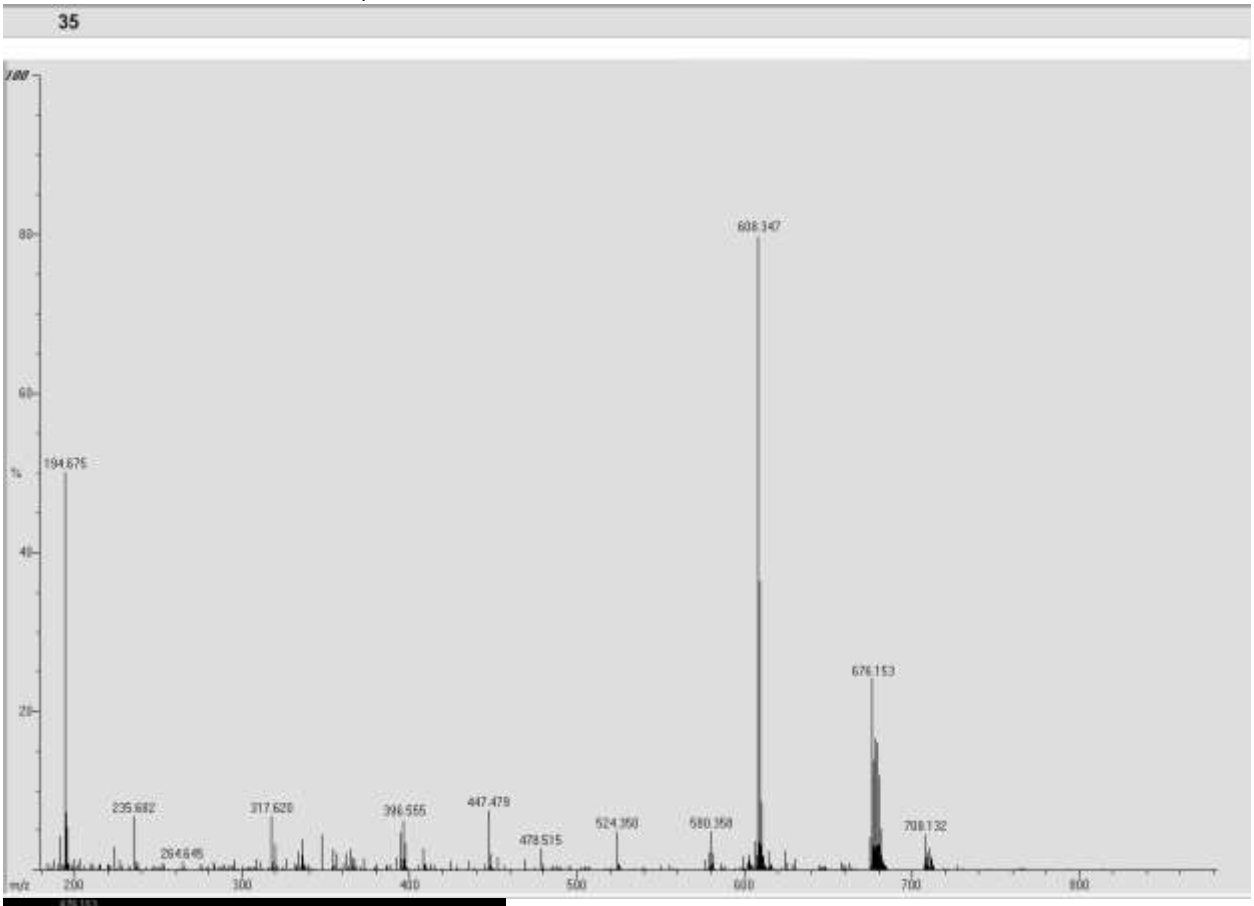

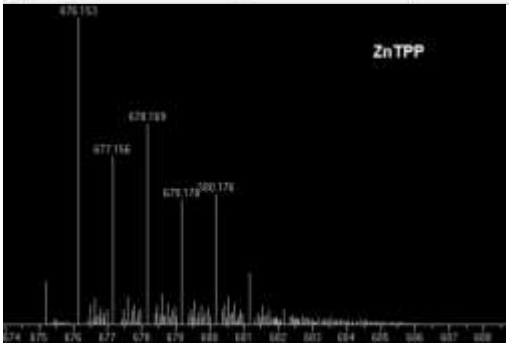

DEMETALLATION $NiSO_4$ + CuTPP NITROGEN

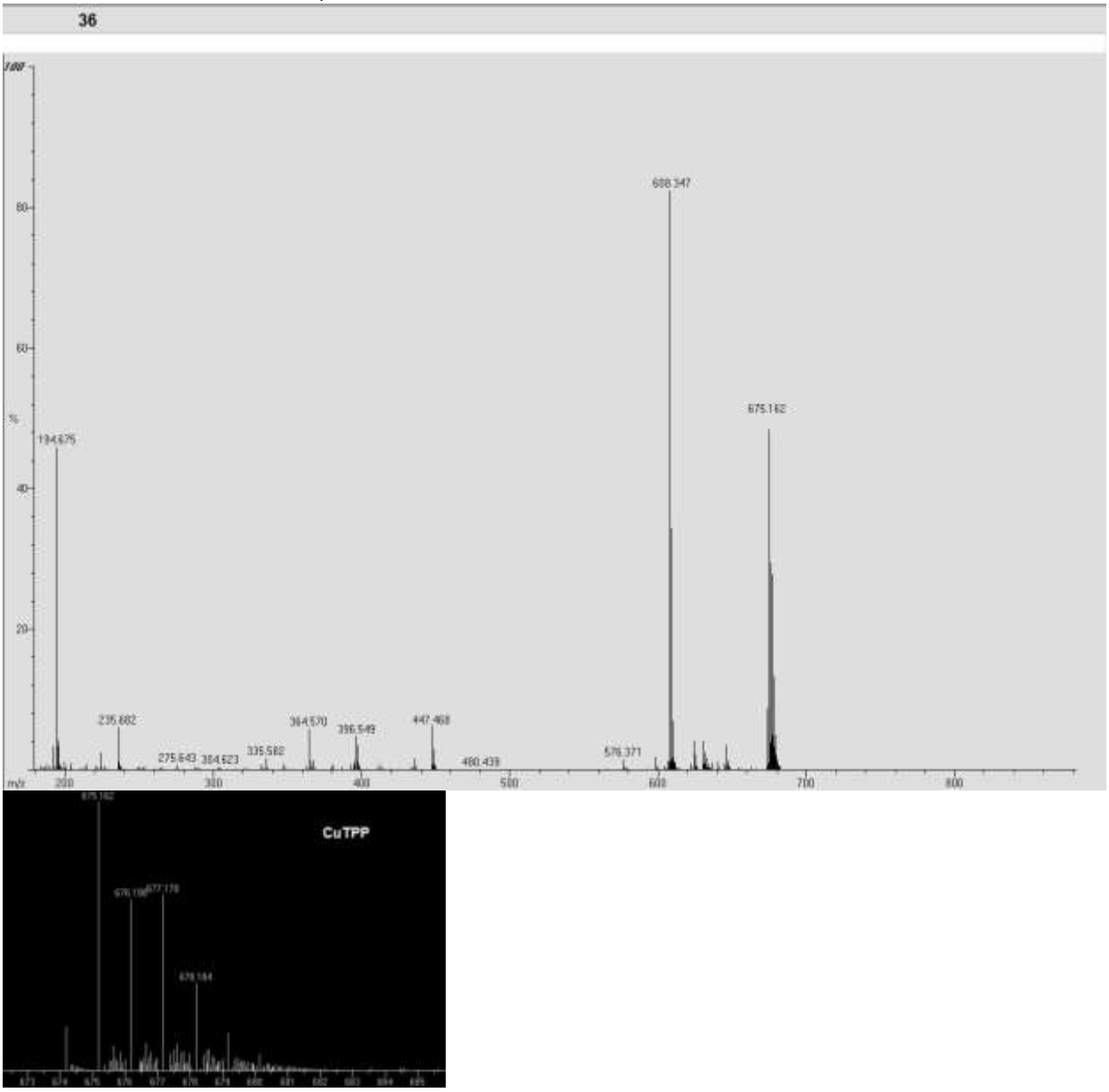

DEMETALLATION $NiSO_4$ + CrTPP NITROGEN

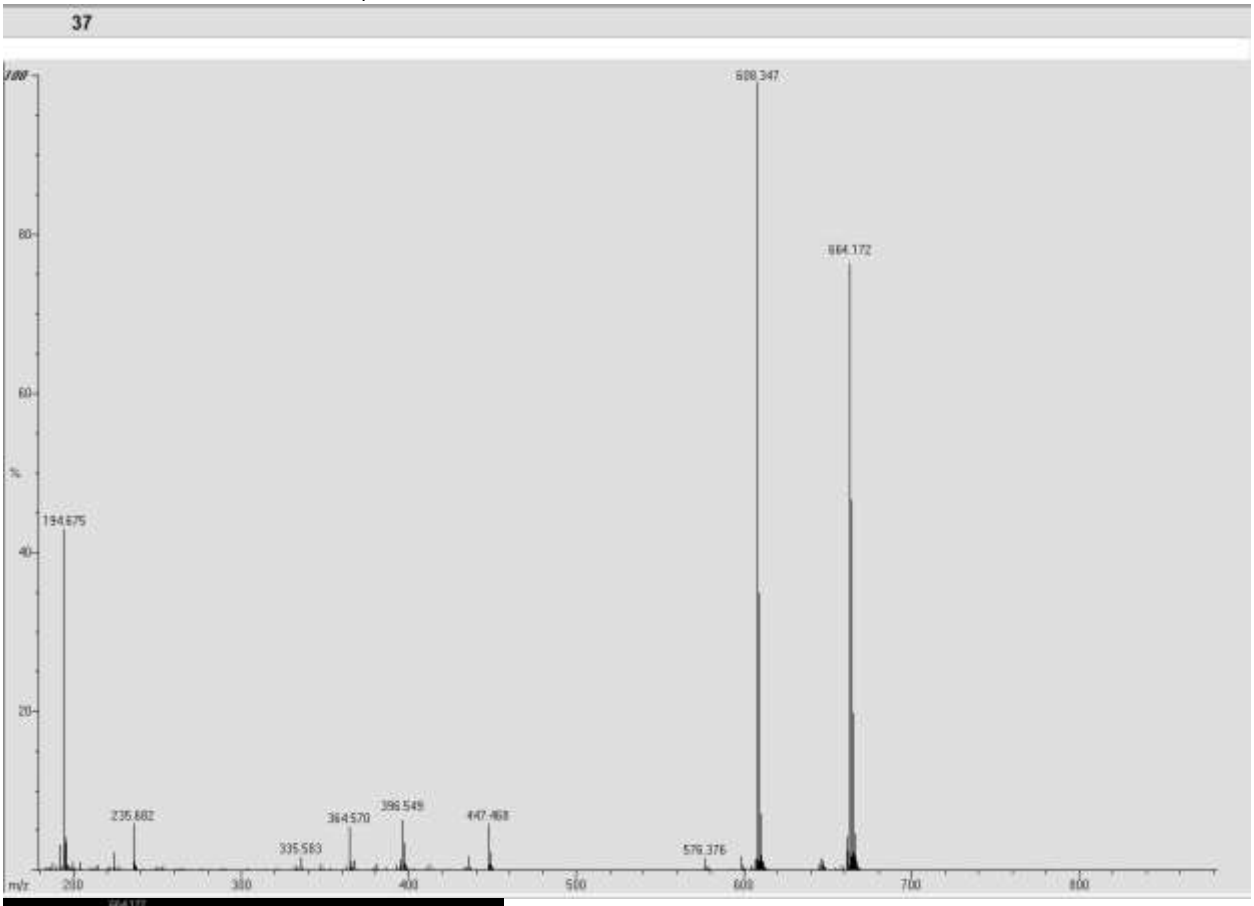

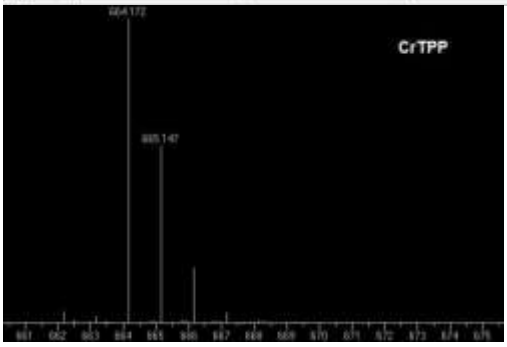

DEMETALLATION $NiSO_4$ + VoTPP NITROGEN

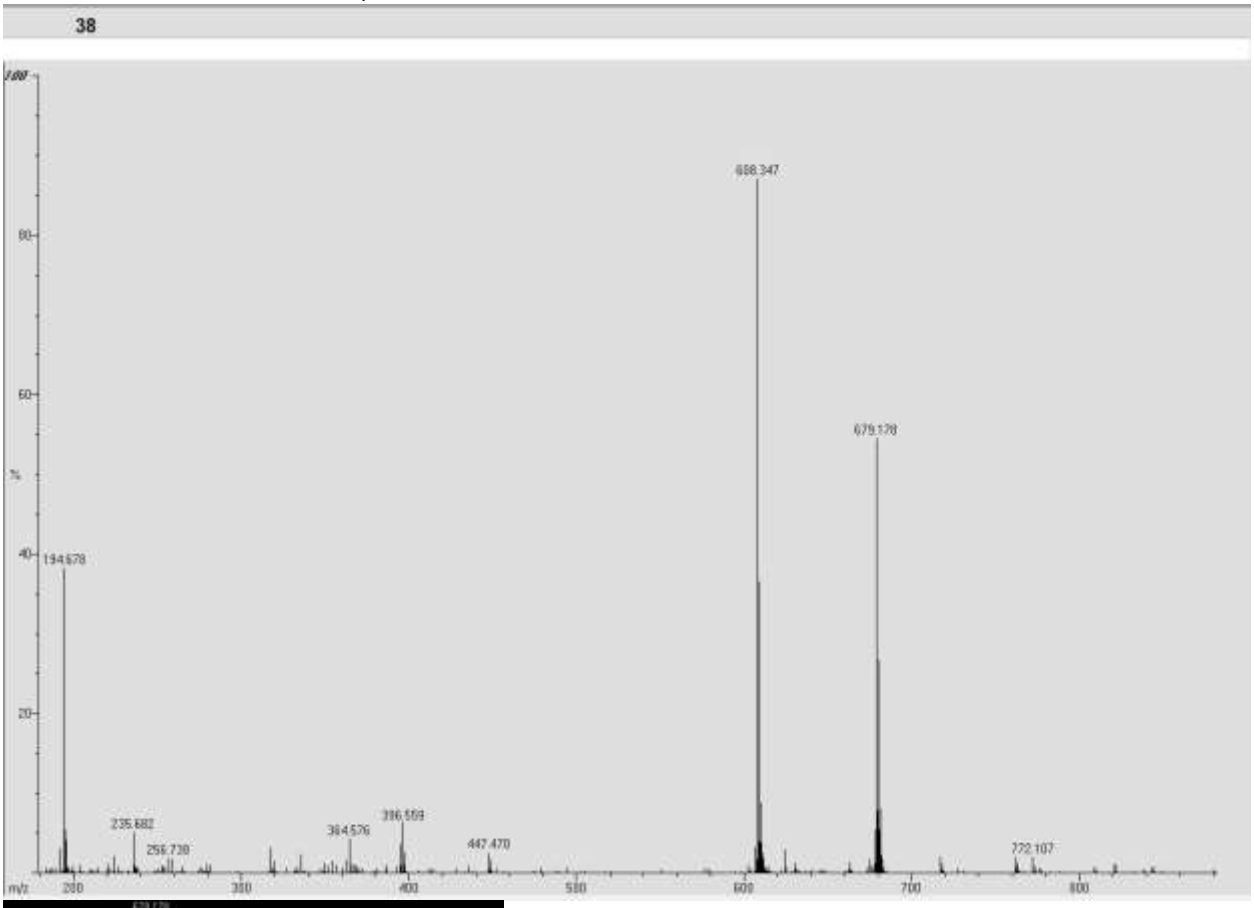

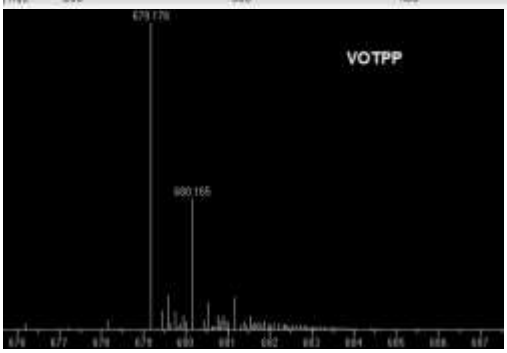

DEMETALLATION VOTPP + $ZnSO_4$ OPEN SYSTEM

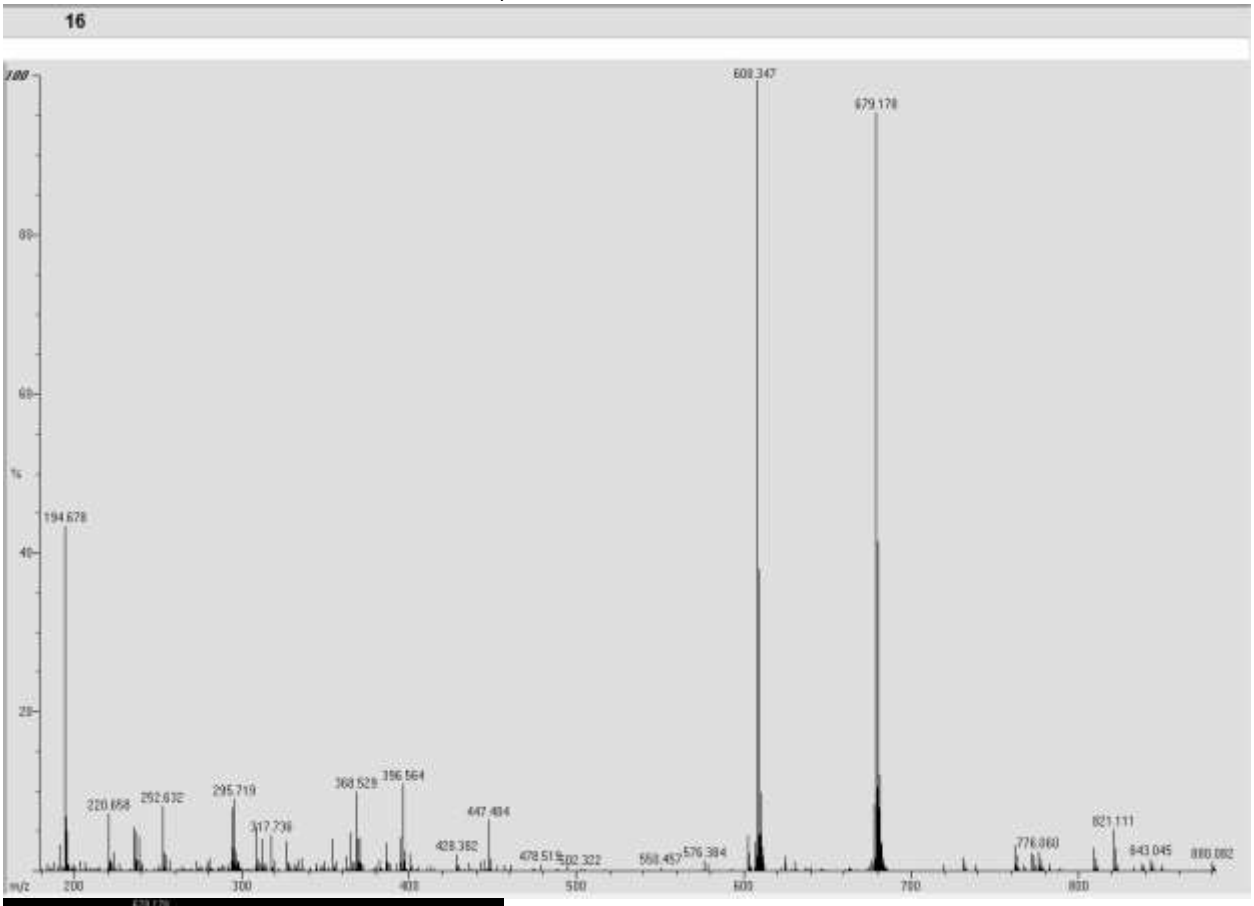

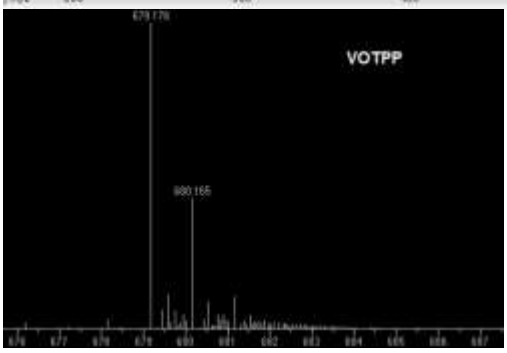

DEMETALLATION VOTPP + $CuSO_4$ OPEN SYSTEM

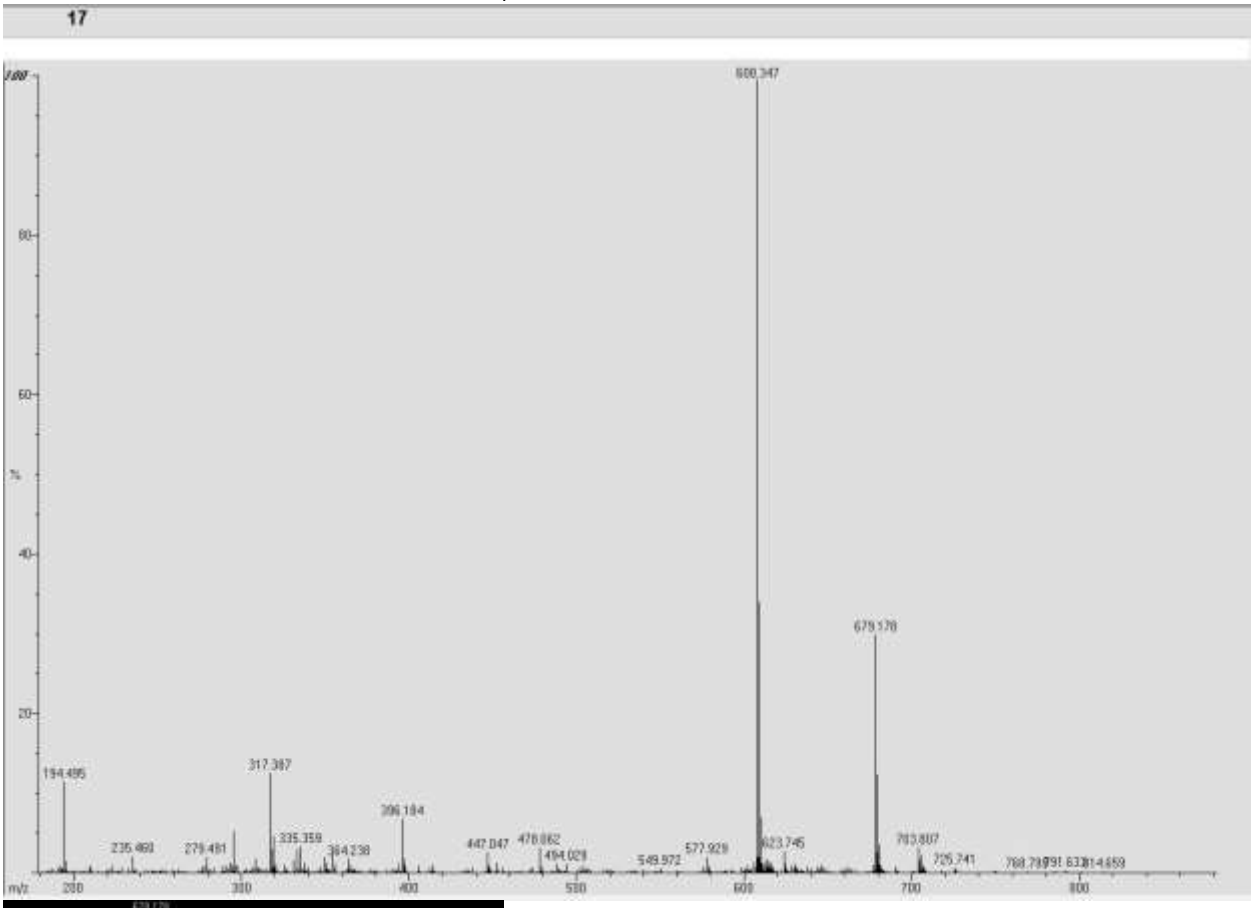

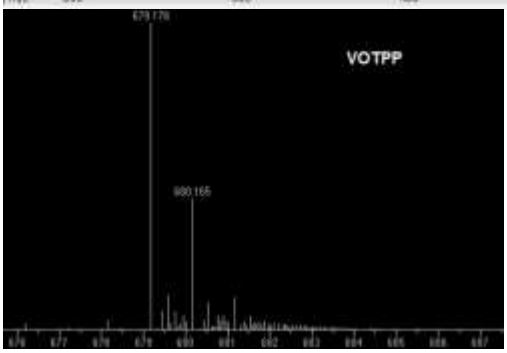

DEMETALLATION VOTPP + $CrSO_4$ OPEN SYSTEM

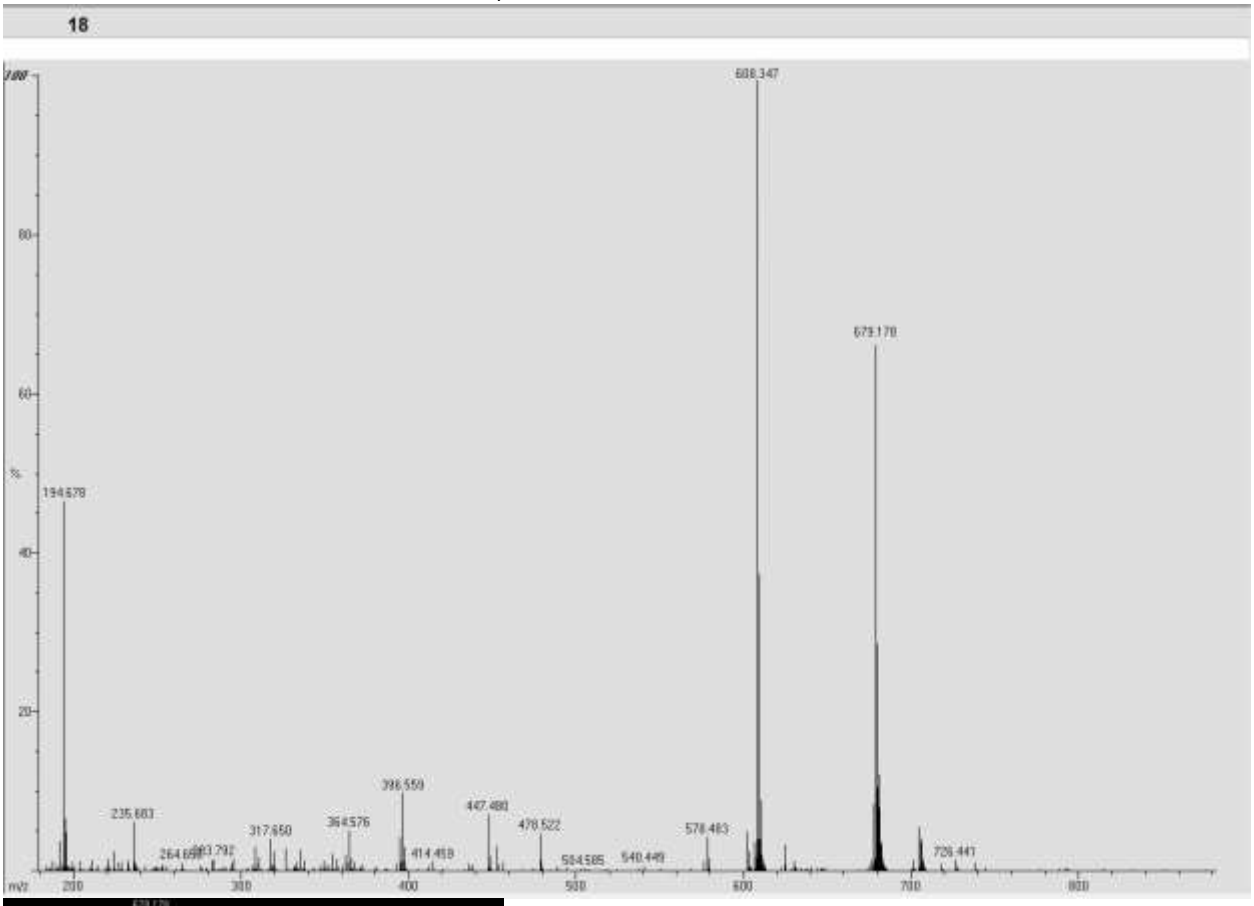

DEMETALLATION NiTPP + $ZnSO_4$ OPEN SYSTEM

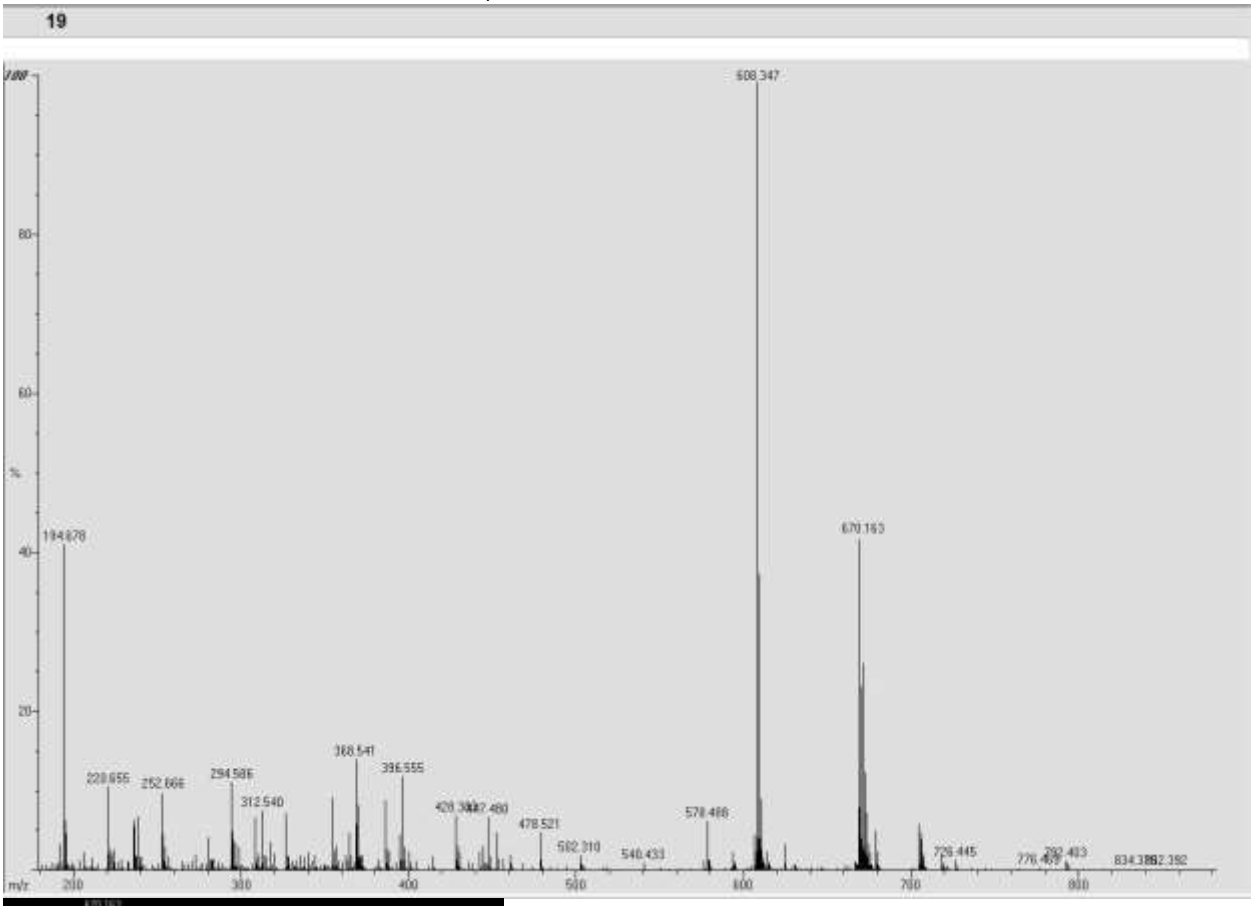

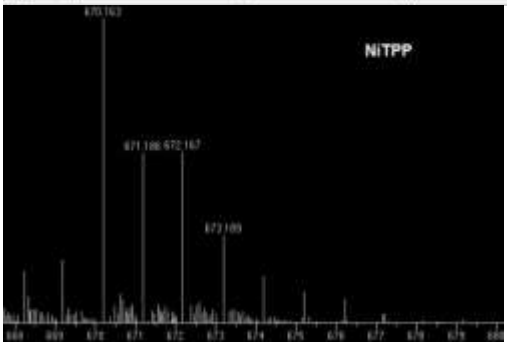

DEMETALLATION NiTPP + $CuSO_4$ OPEN SYSTEM

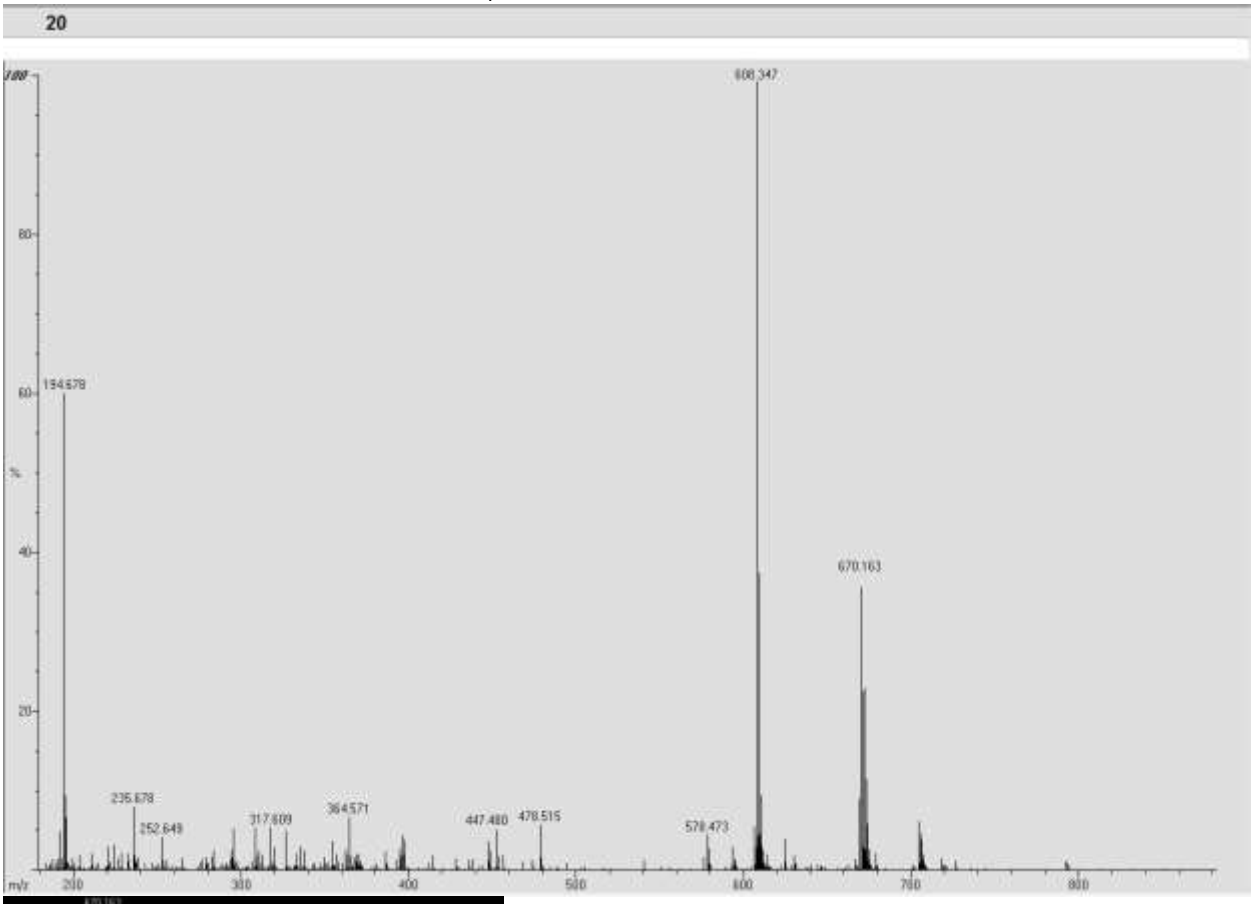

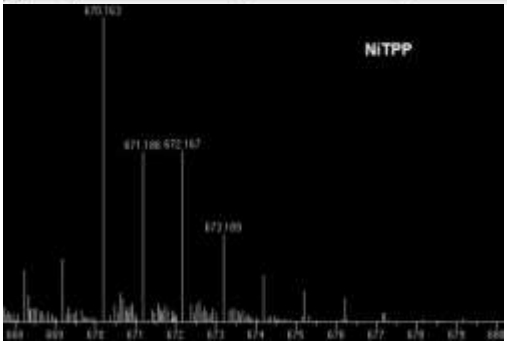

DEMETALLATION NiTPP + $CrSO_4$ OPEN SYSTEM

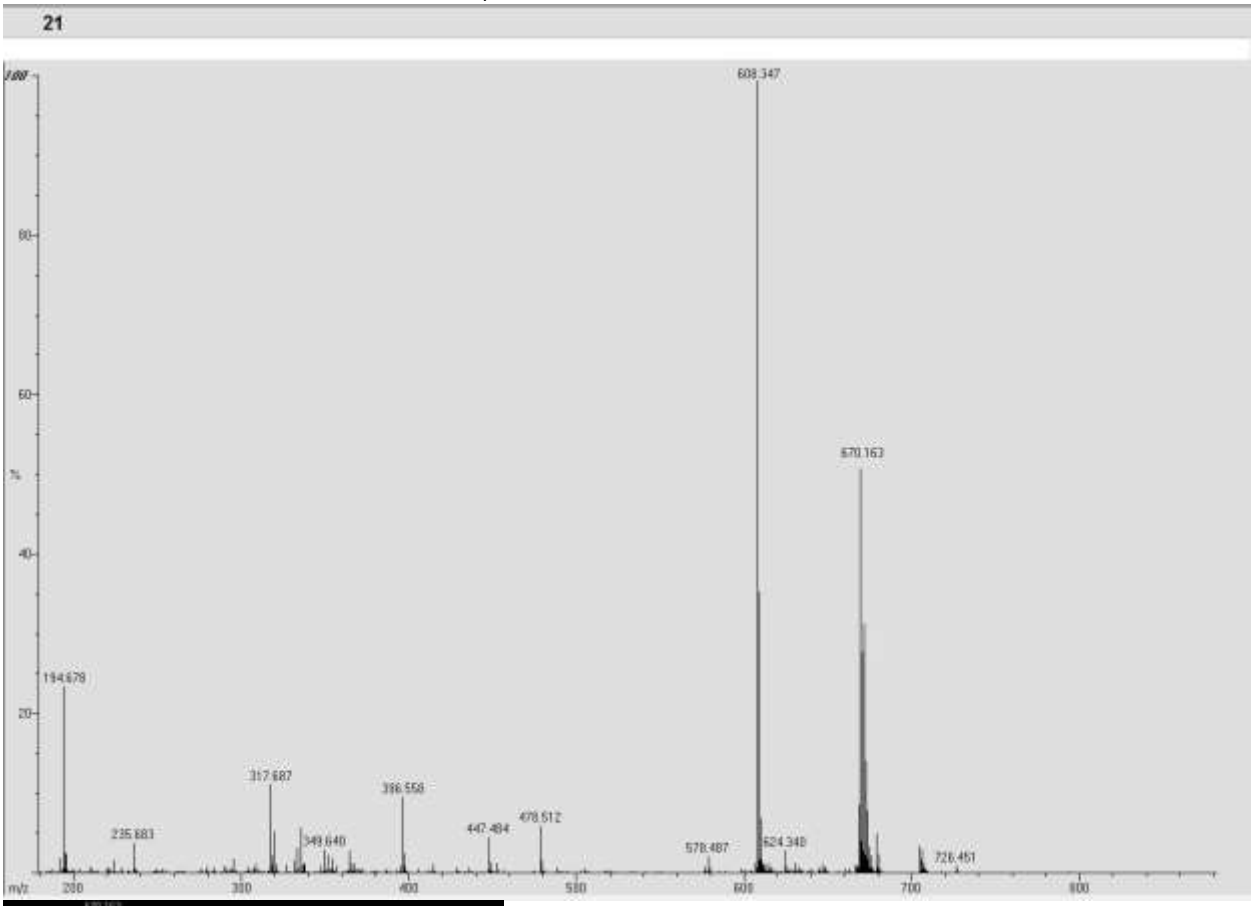

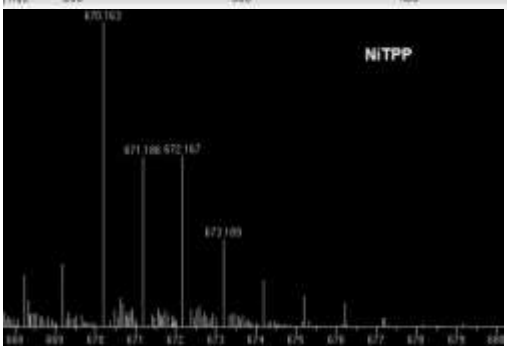

DEMETALLATION VOTPP + $ZnSO_4$ NITROGEN

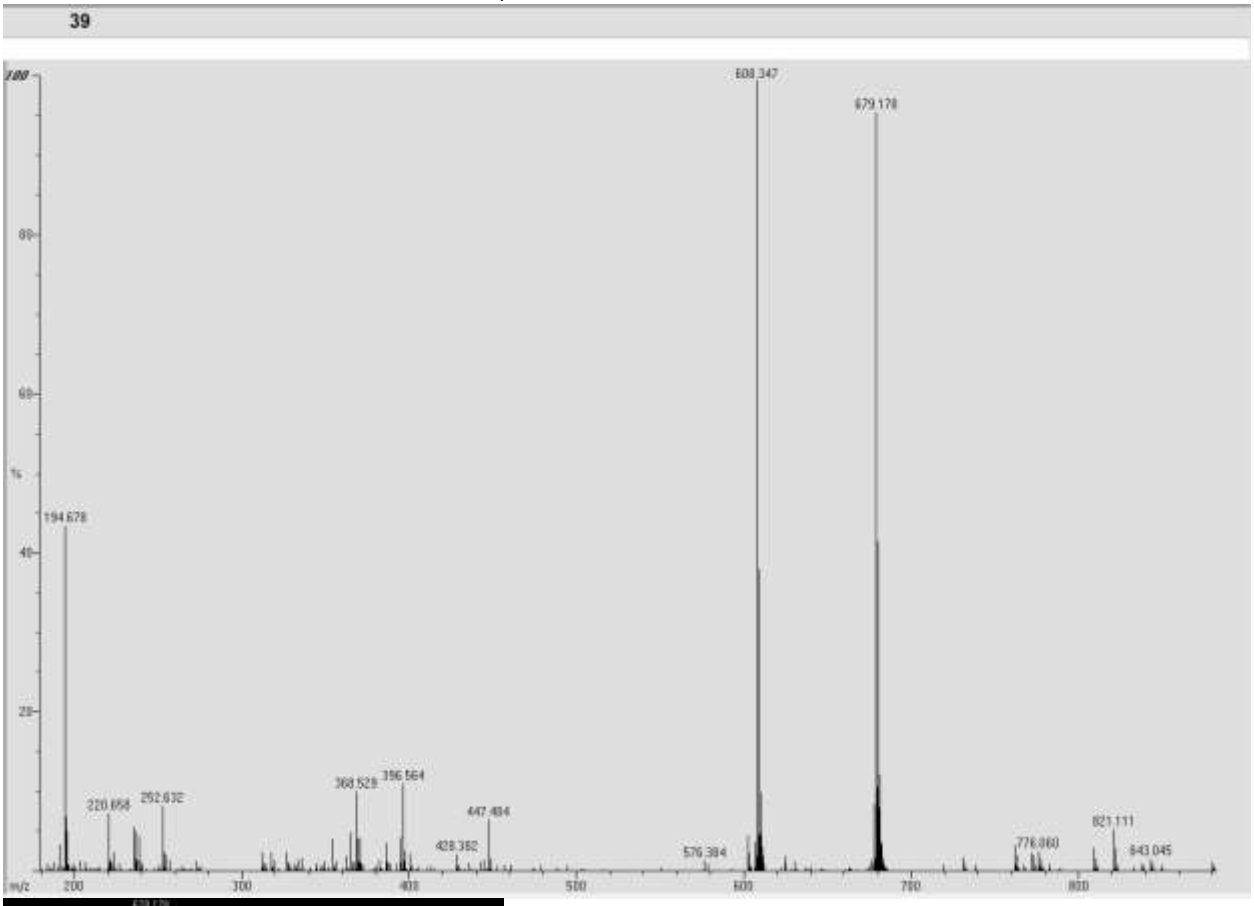

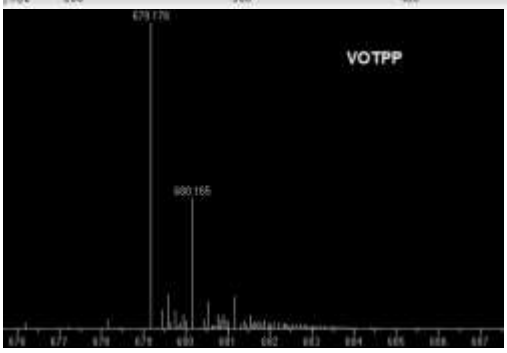

DEMETALLATION VOTPP + $CuSO_4$ NITROGEN

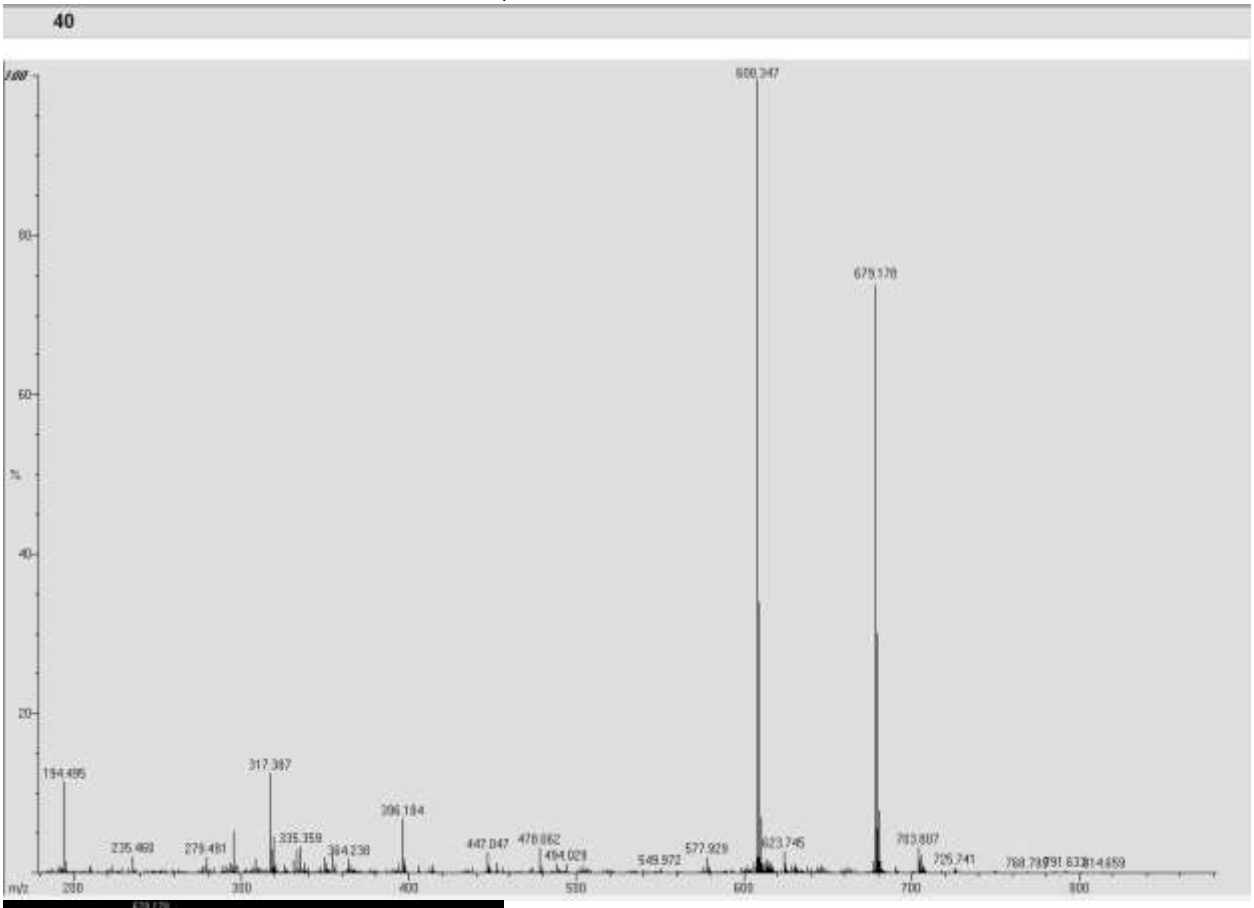

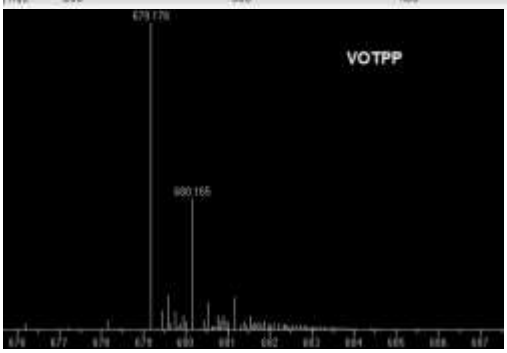

DEMETALLATION VOTPP + $CrSO_4$ NITROGEN

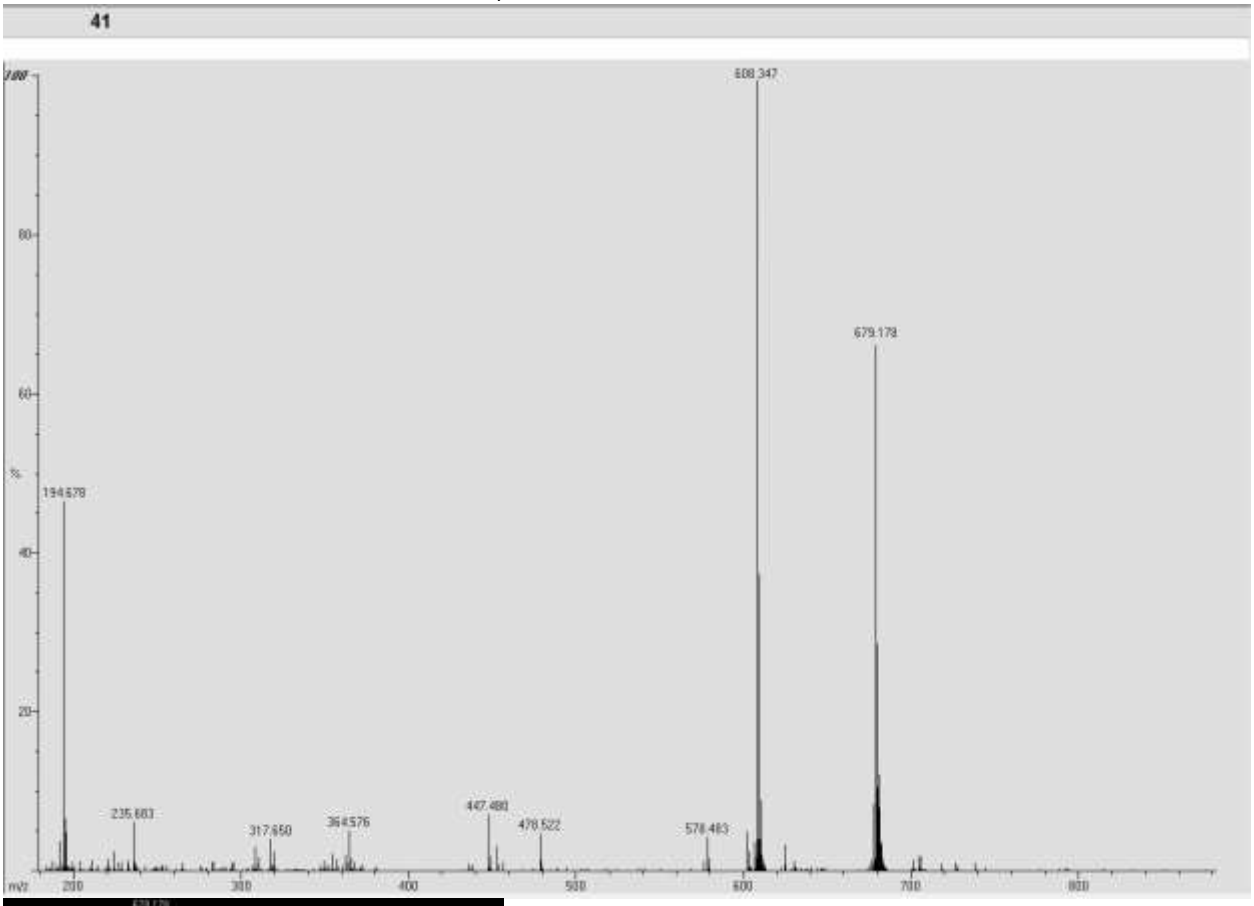

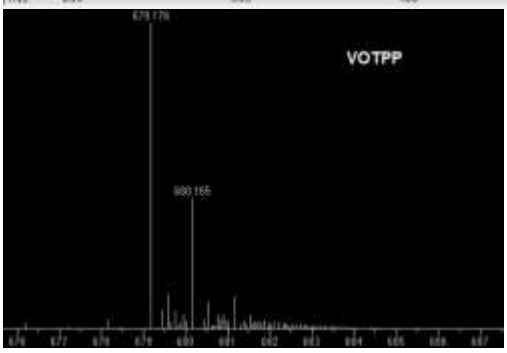

DEMETALLATION NiTPP + $ZnSO_4$ NITROGEN

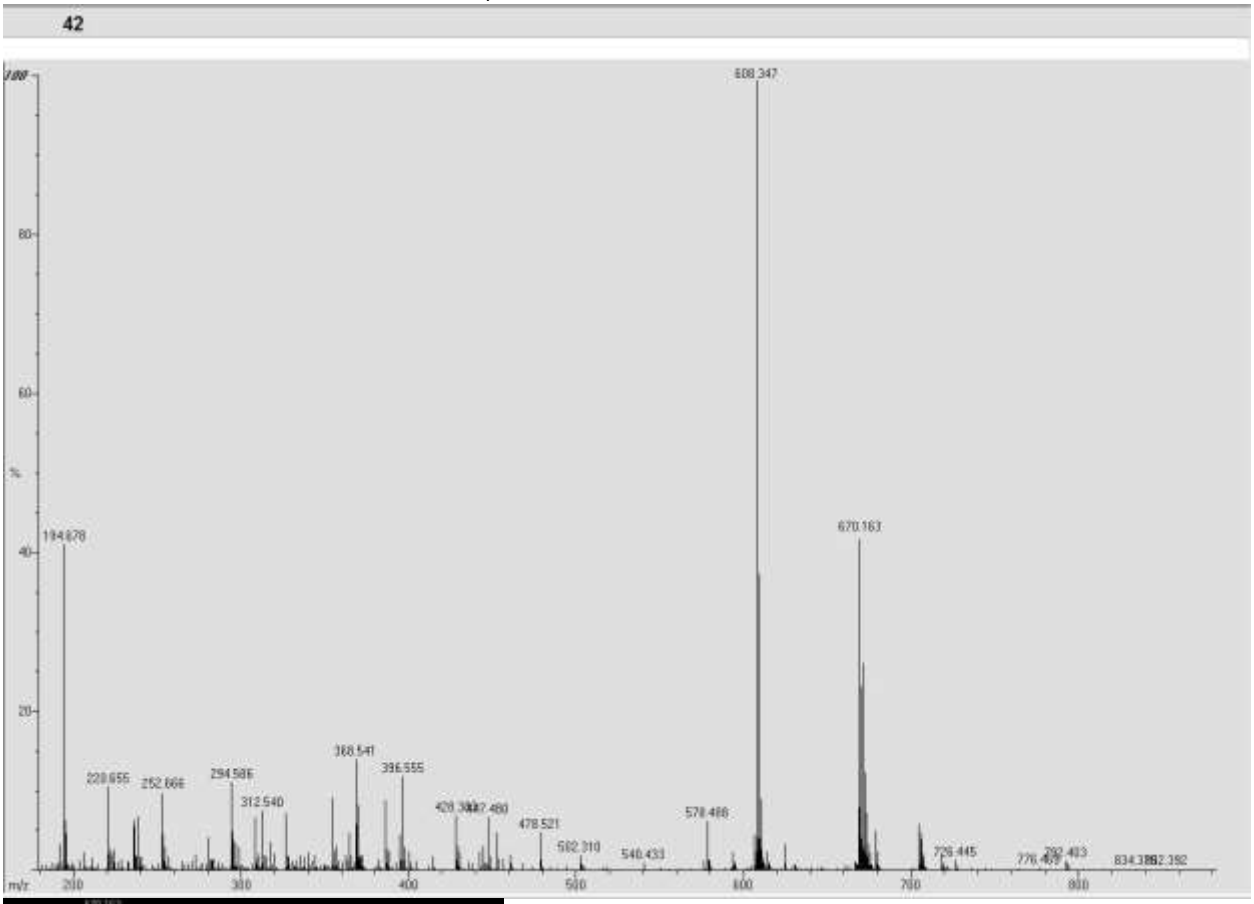

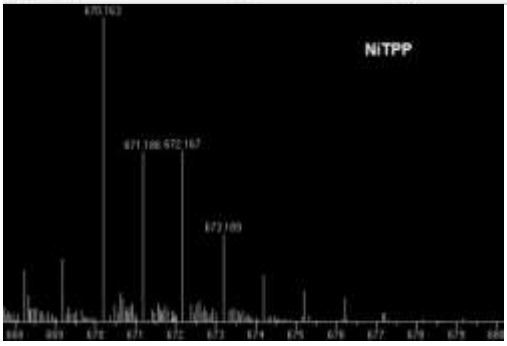

DEMETALLATION VOTPP + $CuSO_4$ NITROGEN

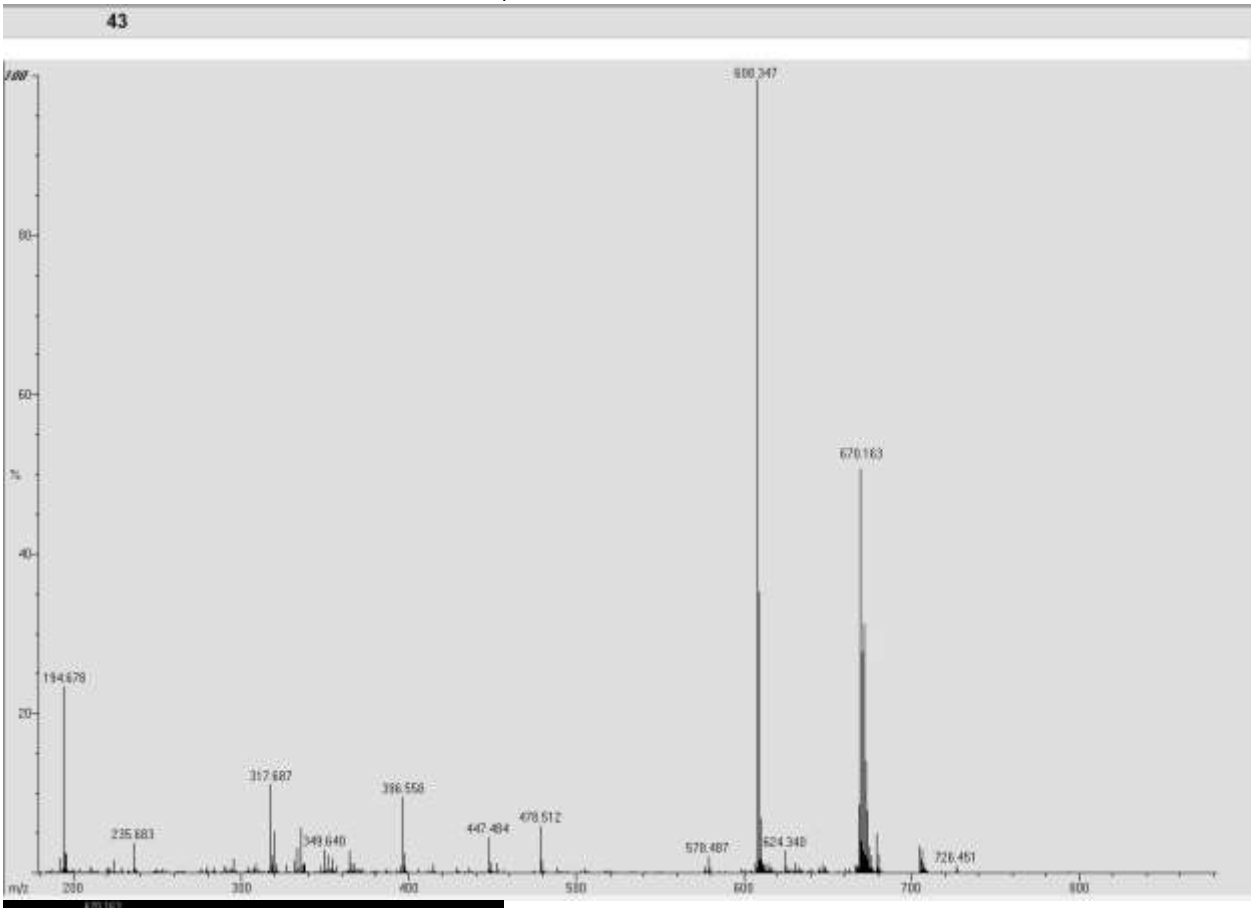

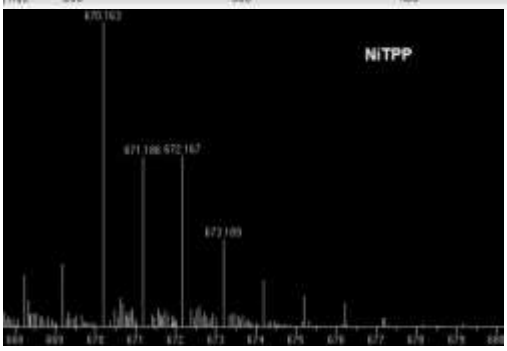

DEMETALLATION VOTPP + $CrSO_4$ NITROGEN

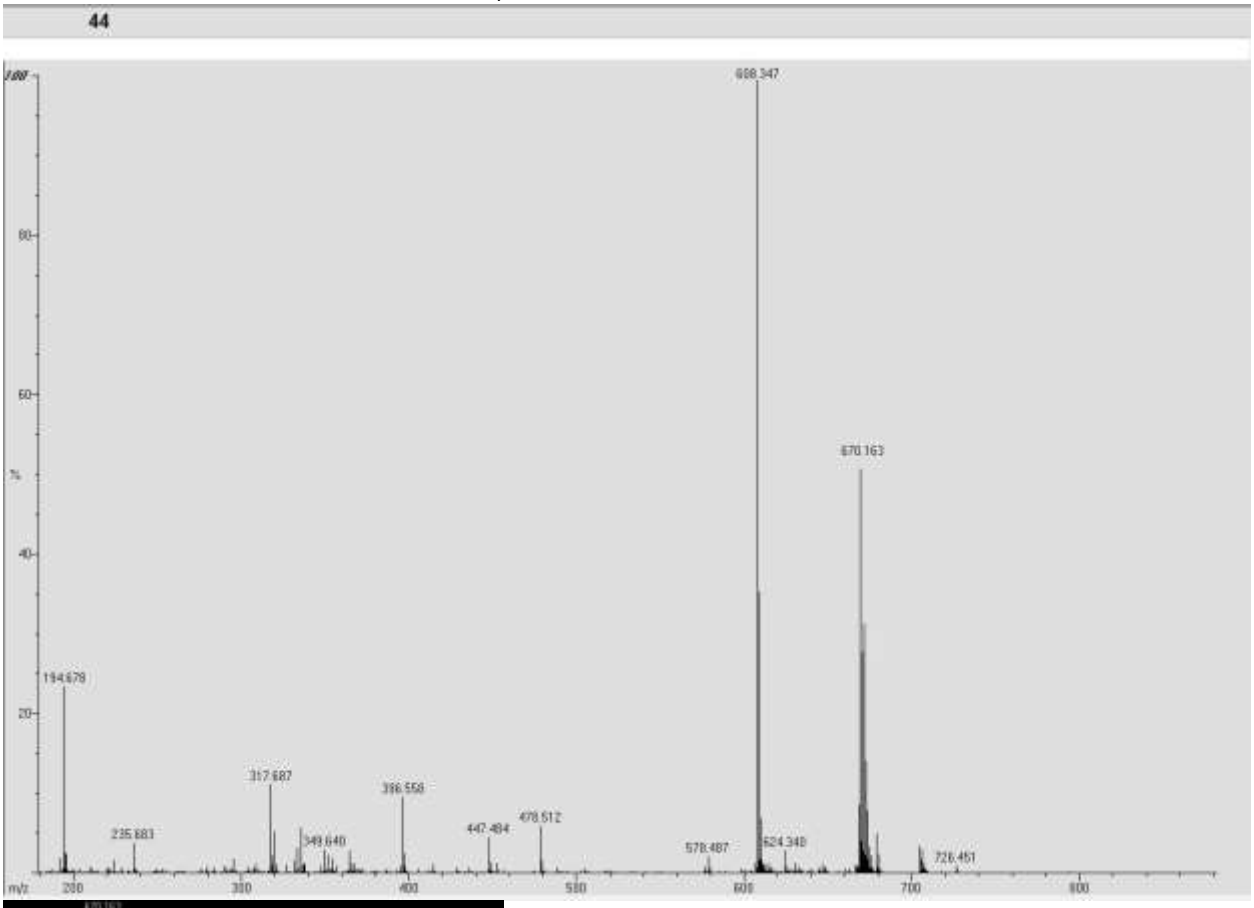

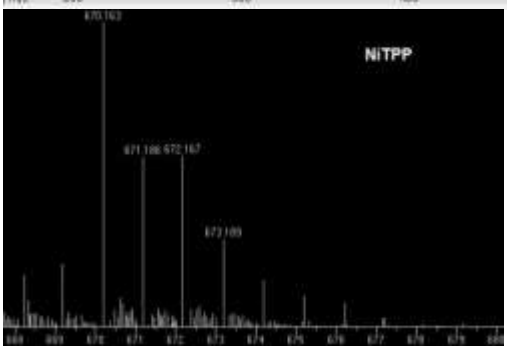

Vita

Olienka Patricia De la O Fernández was born in México City, México. The first daughter of Patricia Fernandez Pimentel, she graduated from completed a bachelors from Instituto Politécnico Nacional at México City in the Area of Physics and Mathematics. In the spring of 2003 she decided to immigrate to the United States in order to complete a Masters in Physics in The University of Texas at El Paso that she completed in summer 2004. Once she completed the Master's program she performed research in Spain at the Neuroscience Institute of Alicante in computational neuroscience. After acquiring the experience of working in Europe she decided to return to complete a PhD program in Material Science and Engineering. While studying for her doctoral program in the UTEP she also gathered professional teaching experience in the Physics Department at El Paso Community College as Physics and Astronomy Professor. Furthermore, she was also offered a position at The Shredded Company where she worked in the Engineering Department as Manager of Environmental and Safety and Senior Engineer. She then attended scientific conferences held in Tampa Bay, Kansas City, Salt Lake City, and Dallas.

Permanent address: 1057 Eagle Ridge
El Paso, Texas, 79912

odelaofernandez@miners.utep.edu

olienkadf@gmail.com

This thesis/dissertation was typed by Olienka Patricia De la O Fernandez